Model development and analysis techniques for epidemiological and neurobiological dynamics on networks

Timothy John Taylor

Submitted for the degree of Doctor of Philosophy
University of Sussex
September 2013

Declaration

I hereby declare that this thesis has not been, and will not be, submitted in whole or in part to another University for the award of any other degree. This thesis was composed by myself and the work contained therein is my own, except where explicitly stated otherwise in the text.

signature .....

Timothy John Taylor

University of Sussex

Timothy John Taylor

Thesis submitted for the degree of Doctor of Philosophy

Model development and analysis techniques for epidemiological and neurobiological dynamics on networks

Summary

The interaction of entities on a network structure is of significant importance to many disciplines. Network structures can have both physical (e.g. power grids, computer networks, the World Wide Web, networks of neurones) and non-physical (e.g. social networks of friends, links between communities, the movement of livestock) realisations that are all amenable to study. In this thesis work on dynamical processes and the networks on which they occur is presented from a viewpoint of both mathematical epidemiology and computational/theoretical neuroscience, with additional consideration of the intersection between the two.

I begin with a paper illustrating how different models of disease transmission are derivable from others and provide a framework for the development of approximate ODEs based on their derivation from exact Kolmogorov equations. This work is followed with two papers that use two such approximate models and consider how they perform when the interplay between both disease and network dynamics is taken into account. Whilst the work in these papers focusses on the modelling of the temporal evolution of the disease and network dynamics, papers four and five consider the recent viewpoint within neuroscience that the brain operates within a critical regime. Making use of models analogous to meanfield models in epidemiology I analyse the behaviour of the system when it is in a balanced state, characterised by the system operating at or near its critical bifurcation, and how this is relevant to the brain itself. Whilst models used within the two areas are analogous, the behavioural aspects of interest within them are quite different. I conclude with a discussion of these differences, the overlaps between both fields and suggest where future work in each area may benefit from incorporating methods and ideas of the other.

Acknowledgments

Firstly, I would like to thank my two supervisors, Dr Luc Berthouze and Dr Istvan Kiss, for both their guidance and support over the past three years. Without their contribution this thesis would not exist. I would also like to thank Peter Simon, Caroline Hartley, Simon Farmer and Michael Taylor, all of whom I have had the privilege to collaborate with.

Most importantly I thank my family; my parents who have always been there for me over the years and my amazing wife, Neisha, who has supported me immensely through both my undergraduate degree and postgraduate study at the University of Sussex, always reminding me what is really important in life. Again, without them this thesis would not be possible.

List of publications and author contributions

Interdependency and hierarchy of exact and approximate epidemic models on networks

Taylor, T.J. and Kiss, I.Z. (2013).
Journal of Mathematical Biology. ISSN 0303-6812 (In Press)

- T.J. Taylor conceived the overall goals of the study and the analysis, wrote most of the paper, derived the linkages between the lower-order models, derived and proved the general population level ODE for higher-order motifs from the Markovian master equations, implemented the numerical ODEs and performed all relevant simulations. I.Z. Kiss conceived the overall goals of the study, wrote some of the paper and supervised the work of T.J Taylor.

Modelling approaches for simple dynamic networks and applications to disease transmission models

Kiss, I.Z. Berthouze, L., Taylor, T.J., and Simon, P.L. (2012).
Proceedings A: Mathematical, Physical and Engineering Sciences , 468 (2141). pp. 1332-1355. ISSN 1471-2946.

- I.Z. Kiss conceived the overall goals of the study and the analysis, derived the equations and analytical results for the four different network dynamic scenarios, wrote most of the paper and supervised the work of T.J. Taylor. L. Berthouze helped write some of the paper. T.J. Taylor helped write some of the paper and performed simulations. P.L. Simon conceived the overall goals of the study and the analysis, derived the equations and analytical results for the four different network dynamic scenarios and helped write some of the paper.

Epidemic threshold and control in a dynamic network

Taylor, M. Taylor, T.J. and Kiss, I.Z. (2012).
Physical Review E, 85 (1). 016103-1-016103-6. ISSN 1539-3755

- M. Taylor helped derive the dynamic effective degree model, coded and performed the necessary simulations, derived the next generation R_0 calculations, produced the figures and wrote the text. T.J. Taylor helped derive the effective degree model, coded its implementation and helped develop the next generation R_0 calculations. I.Z. Kiss helped derive the effective degree model and supervised the work of both M. Taylor and T.J. Taylor.

Identification of criticality in neuronal avalanches: I. A theoretical investigation of the non-driven case

Taylor, T.J. Hartley, C. Simon, P.L. Kiss, I.Z. and Berthouze, L. (2013).
The Journal of Mathematical Neuroscience, 3 (4). p. 5. ISSN 2190-8567

- T.J. Taylor and L. Berthouze wrote the paper. T.J. Taylor carried out analysis and numerical simulations for tree approach, finite-size expansion, critical slowing, the comparison to Kessler's approximate solution and the origin of the distributions truncation. C. Hartley carried out additional calculations and numerical simulations. P.L. Simon and I.Z. Kiss contributed the tree approach, and the derivation of the power law in the limit of the system size. L. Berthouze conceived the analysis and overall goals of the study, participated in the implementation and analysis of the different simulations and supervised the work of T.J. Taylor and C. Hartley.

Identification of criticality in neuronal avalanches: II. A theoretical and empirical investigation of the driven case

Hartley, C. Taylor, T.J. Kiss, I.Z., Farmer, S.F. and Berthouze, L. (2013).
Submitted (September 2013) to The Journal of Mathematical Neuroscience.

- C. Hartley, T.J. Taylor and L. Berthouze wrote the paper. C. Hartley contributed the theoretical derivation of the distribution of waiting times, carried out analysis and numerical simulations for tree approach and the study of long-range temporal correlations. T.J. Taylor contributed to the theoretical derivation of waiting times and analysis of the results, derived the dynamic range and carried out additional calculations and numerical simulations. I.Z. Kiss contributed to the development of the tree approach. S.F. Farmer contributed to the physiological interpretation of the results and edited the manuscript. L. Berthouze conceived the analysis and overall goals of the study, participated in the implementation and analysis of the different simulations and supervised the work of C. Hartley and T.J. Taylor.

Contents

Chapter 1

Introduction

1.1 Motivation

The interaction of entities on a network structure is of significant importance to many disciplines. Network structures can have both physical (e.g. power grids, computer networks, the World Wide Web, networks of neurones) and non-physical (e.g. social networks of friends, links between households and communities, the movement of livestock) realisations that are all amenable to study (Albert and Barabási, 2002a; Newman, 2003a; Dorogovtsev, 2010; Newman, 2010).

In this thesis we consider the dynamics of transmission on networks from a viewpoint of both mathematical epidemiology and computational/theoretical neuroscience. Whilst generally treated as individual areas of study, they are remarkably similar with both having a focus on transmission, be it of a disease between people or information between neurones. To see the similarities we can consider the following compartmental model of a firing neurone and an individual exposed to a disease. We may characterise a neurone as initially quiescent (Q) before becoming active (A) and subsequently entering a period of refraction (R), and finally returning to its initial quiescent state (Q) (see Fig. 1.1(a)). In this way we can view this QARQ model as akin to a compartmental disease transmission model where an individual can begin as susceptible (S) prior to becoming infectious (I), before entering a none infectious recovery period (R) and finally becoming susceptible again (SIRS; see Fig. 1.1(b)). Thus where neurones exhibit on/off (firing or not/refractory) behaviour, analogously an individual may be susceptible/ infected (disease free or not). Although abstractly similar it is the intrinsic transmission dynamics between infectious and susceptible individuals, and between neurones that differentiates the two. Whereas mathematical epidemiology will generally consider a disease causing contract to occur at a given rate, within neuroscience it is common to consider one of the many variants of integrate-and-fire neuronal models (e.g. leaky integrate-and-fire, exponential integrate-and-fire, Hodgkin-Huxley, Morris-Lecar (Koch and Segev, 1998)). Here neurones receive both excitatory and inhibitory synaptic inputs and when the membrane potential reaches threshold the neurone spikes before entering a refractory period.

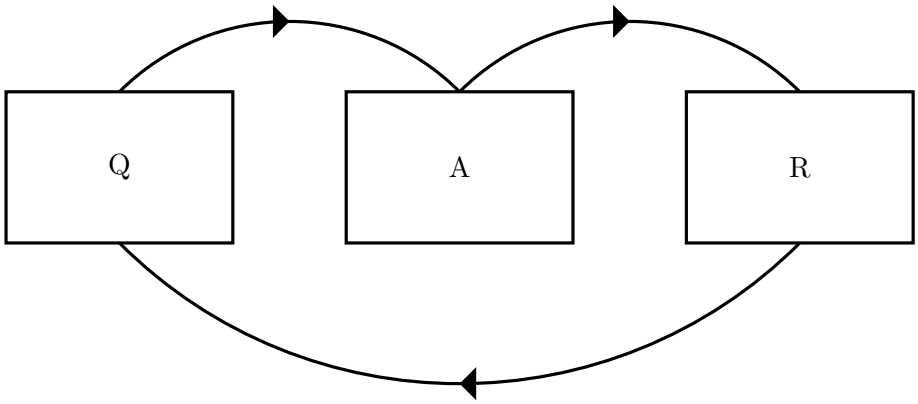

(a) QARQ

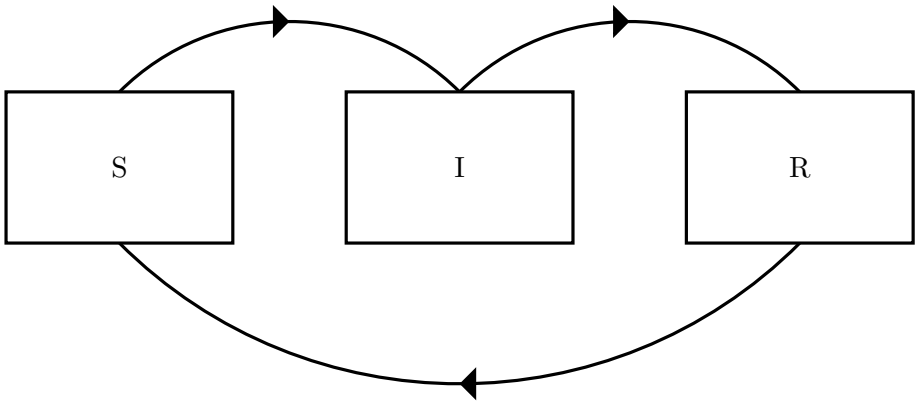

(b) SIRS

Figure 1.1: Compartmental model for QARQ and SIRS dynamics

In general, the behavioural aspects studied by the two disciplines also differ. Within epidemiology the focus is mainly on the two states, disease-free and endemic, that the system can be in and the analysis of their stability. Broadly speaking most research then focusses on the calculation of the temporal evolution of the disease (Lindquist et al., 2011), the final outbreak size or endemic state (House et al., 2013), the value of the basic reproduction ratio, R_0 (Diekmann et al., 1990), and the effect of strategies, such as vaccination and quarantine, used to reduce R_0 and the spread of the disease (Brauer et al., 2008). In contrast within neuroscience the focus is on balanced activity within the brain, an idea that can be traced back to the physiologist Walter Cannon (building on earlier ideas of Claude Bernard) who coined the term homeostasis for the self-regulation of the body (Cannon, 1932). Shadlen and Newsome (1994) hypothesised a balance of excitation and inhibition with the membrane potential of neurones hovering below the activation threshold and it is known that a lack of balance between excitation and inhibition can have serious consequences (for example see Dichter and Ayala (1987) who discuss how an increase in excitation and a blocking of inhibition occurs during epileptic activity). Even though the exact mechanisms are not fully understood, homeostatic plasticity (Turrigiano, 2011) is generally viewed as the way neurones are able to self-regulate by altering both intrinsic and synaptic properties, and allowing the necessary balancing to occur (see Williams et al. (2013) for examples of how neurones react to different perturbations of their environment). Whilst physiologists have long appreciated this need for a balance of activity within the brain, the influx of statistical physicists and mathematicians into the discipline over the last few decades (e.g. Jack Cowan, Larry Abbott, Eugene Izhikevich, ...), has led to an attempt at characterising this balance using tools and ideas motivated from the study of dynamical systems (the most obvious abstraction being the idea that the brain is poised at a steady state). Accepting that a thorough introduction to balanced activity within the brain is beyond the scope of this thesis, we restrict our attention to the recent idea that has developed from observations of neuronal activity, that is, that the brain is not only poised at a steady-state, but is also critical. Here it is hypothesised that the brain operates at, or near to, a critical bifurcation, akin to a model of epidemiology where $R_0 = 1$. The focus in this area is then not on the temporal evolution of the first moment of activity within the system but rather on cascades of neurones firing, the fluctuations they exhibit and how being poised at a critical bifurcation is beneficial for our brains.

To analyse disease dynamics on networks, mathematical epidemiology makes use of ordinary differential equation (ODE) models that allow calculation of both the temporal evolution and basic reproductive ratio of the disease. These models are built around network motifs such as individual nodes (meanfield (Allen, 2008)), pairs of nodes (pairwise (Keeling, 1999)), or even star-like structures (effective degree (Lindquist et al., 2011)). Inherently required within these models is the need to approximate higher-order structures by lower ones (e.g. approximating triples by pairs) in order to obtain a closed tractable model and we refer to these approximations as moment-closures. Whilst meanfield and moment closure based approaches

are used within neuroscience (e.g. Wilson and Cowan (1972) and Buice et al. (2009)), close to the critical bifurcation agreement can break down due to the dominance of fluctuations (Buice et al., 2009) and they are unable to provide results for important metrics such as the size distributions of consecutively firing neurones and long-range temporal correlations. Similarly the use of higher-order topologically orientated models such as pairwise and effective degree, that take in to account network structure, is rare with more attention given to sandpile-esque models (see Levina et al. (2007) for example) that self-organise to a critical regime (of exception is the attempt[1] of Droste et al. (2013) at a pairwise self-organising model).

In the papers of this thesis we try and shed light on the links and rigorous derivation of some of the more common ODE-based approaches used for studying disease dynamics on networks in epidemiology. We also consider more realistic scenarios where the networks are allowed to change dynamically both independent from and in conjunction with the simultaneous disease dynamics. Finally we consider a simple neuronal model and study how it behaves when it is tuned to operate both at and close to the critical regime. Contributory papers are included in chapters 3 to 7 and whilst each article contains a detailed introduction to the research contained within, in what follows we provide a brief overview of the relevant areas of study.

1.2 Mathematical epidemiology

Understanding the spread of a disease within a population requires not only an understanding of the characteristics of the disease-causing pathogen, but also an appreciation of the community on which it spreads. By gaining a thorough understanding of both, appropriate control and prevention strategies can be introduced that can help control or even eradicate a disease (Anderson et al., 1992).

1.2.1 Homogeneous random mixing

The early work of Kermack and McKendrick (1927) was hugely influential in bringing differential-equation models to the forefront of epidemiology and in turn forms the basis for much of the current endeavours in the area (Diekmann et al., 1995). A special case of Kermack and McKendrick (1927) is the well known susceptible $\rightarrow$ infected $\rightarrow$ recovered (SIR) model

$$\begin{aligned}\frac{dS}{dt} &= -\beta I\frac{S}{N}\\ \frac{dI}{dt} &= \beta I\frac{S}{N} - \lambda I\\ \frac{dR}{dt} &= \lambda I.\end{aligned}$$

[1] We have identified a flaw in the analysis of this paper and are currently in correspondence with Felix Droste regarding this.

Here $S + I + R = N$ and it is assumed infective individuals recover at a rate λ whilst making infectious contacts at a rate β. A key concept in epidemiology is that of the basic reproduction ratio R_0. R_0 is defined as the 'expected number of secondary cases produced, in a completely susceptible population, by a typical infected individual during its entire period of infectiousness' (Diekmann et al., 1990). For the above model R_0 can be calculated as β/λ. The calculation and interpretation of R_0 is not always straightforward (see Heffernan et al., 2005) but generally we say that if $R_0 < 1$ we would not expect the disease to spread within a population and if $R_0 > 1$ we would expect it to spread (see Roberts, 2007, for a discussion on this). Whilst early models may make mass-action assumptions and view subpopulations as infinite (Diekmann and Heesterbeek, 2000) they provide great understanding of the effect of vaccination and control strategies (Brauer and Castillo-Chavez, 2012) on the value of R_0 (and hence the spread of the disease). They are also highly adaptable in allowing varying disease dynamics (i.e. SIRS) and the study of other variables such as age structure (Li and Brauer, 2008) and demography (Diekmann and Heesterbeek, 2000) and the effect these can have on a disease. Whilst homogenous random mixing models are a good starting point for modelling infection, for many diseases to spread it is reasonable to assume that there is some form of contact between infected (or carrying) and susceptible entities (acknowledging this may not be the case for airborne disease). Therefore the contact structure within a population is of utmost importance and this needs incorporating within the model (Diekmann and Heesterbeek, 2000).

1.2.2 Contact structure and networks

In order to incorporate contact structure into mathematical models various approaches have been taken. Ball et al. (1997) considered a model with both global and local mixing of the population obtaining results for the final outbreak size of epidemics, threshold conditions and the effects of vaccination strategies. Newman (2002) used a percolation-based model and probability generating functions (PGF) to calculate threshold and final outbreak size results for epidemics occurring on random graphs with arbitrary degree distributions (Kenah and Robins (2007) corrects some of the incorrect assumptions of Newman (2002)). Volz (2008) and Miller (2011) provide a model that calculates the temporal evolution of a disease again making use of PGFs on random graphs. Whilst the aforementioned models provide significant results for scenarios exhibiting particular disease dynamics, the assumptions required mean they are restricted to operating on disease dynamics where reinfections do not occur. An alternative to these models is to use pairwise models that came to prominence in the work of Keeling et al. (1997) and Rand (1999), following earlier work on ecology models by Matsuda et al. (1992) and Satō et al. (1994). Whilst traditional models focussed on the interactions at the level of the individual, pairwise models also incorporate the interactions at the level of pairs and the effect an individual's neighbour has on their status. This information is then used to write differential equations for the epidemic time course. In Taylor et al. (2012a) it was shown shown that the pairwise equations for susceptible $\rightarrow$ infectious $\rightarrow$ susceptible

(SIS) dynamics on an arbitrary graph are 'exact' before a closure is applied, meaning that they can be derived directly from the forward Kolmogorov equations. To obtain a closed system of equations it is necessary to describe the effects of triples in terms of pairs and this necessitates the need for moment closures (Rand, 1999). The performance of these closures then determines the accuracy of the approximation. It is not necessary to truncate at the level of pairs and in theory the equations could be closed at any level (i.e. triples) but with added complexity required in the derivation of the equations (Bauch, 2005). Nor is it necessary to use pairs or simple structures as the basis for the differential equations as any graph motif can be utilised. In Eames and Keeling (2002) the status of individuals, pairs and the number of neighbours they have is taken into account. Similarly in Lindquist et al. (2011) the status of individuals and the status of all of their neighbours is considered. The benefit of these models over percolation and PGF-based models is that they can be applied to multiple types of disease dynamics including those that allow reinfections to occur. Interestingly it has recently been shown that for susceptible $\rightarrow$ infectious $\rightarrow$ recovered (SIR) dynamics the PGF based model of Volz (2008), under appropriate assumptions, can be derived directly from a pair based model (House and Keeling, 2011). Even though much progress has been made, many of these models still perform best on non-clustered (where an individual's neighbours are not connected) networks with connections created randomly using a configuration model approach (Newman, 2003a). Similarly, whilst networks allow us to incorporate greater heterogeneity into our models, the assumption of static links between individuals is not necessarily a good reflection of human behaviour and the contacts people make. In reality, over time (both long and short-term) an individual's contacts are likely to be highly dynamic in their nature and the development and adaption of models is needed to reflect this.

1.2.3 Dynamic network models

Read et al. (2008) discuss how people will have fewer but more regular and closer contacts within the home, whilst having more but less regular casual contacts within the workplace. Similarly sexual contacts are dynamic with consideration needed for the formation and breaking of partnerships (Liljeros et al., 2003). To this end it is natural to consider epidemics occurring on dynamic networks. In Gross et al. (2006) and Gross and Blasius (2008) the phrases "dynamics on networks" and "dynamics of networks" are used. "Dynamics on networks" relates to dynamical process occurring on networks (like the aforementioned epidemics) and the effect the topology has on these. "Dynamics of networks" refers to the dynamical evolution of the topology itself through processes such as preferential attachment (Barabási and Albert, 1999) and link rewiring (Watts and Strogatz, 1998) (for more of an overview see Albert and Barabási, 2002b; Dorogovtsev and Mendes, 2002). Saramäki and Kaski (2005) considered a dynamic small world network with fixed short-range (nearest neighbour) and random long-range links and using simple meanfield ODEs derive an analytic result for the disease threshold. In Volz and Meyers (2007) and Miller et al. (2012) PGF-based models are imple-

mented on a variety of dynamic networks (e.g. meanfield social heterogeneity (MFSH) and dynamic fixed degree with or without dormant contacts) combined with susceptible-infectious-recovered (SIR) dynamics, and obtained results for R_0, the final outbreak size of epidemics and the temporal evolution of the disease. Whilst the aforementioned models incorporate dynamic networks that effect the disease dynamics there is no effect of the disease dynamics on those of the network. As an initial assumption it seems reasonable that susceptible individuals would break contact with infected individuals (or vice-versa) as a disease progressed. To investigate this coupling of dynamics Gross et al. (2006) used pairwise differential equations to investigate a model based on SIS disease dynamics but allowed susceptible individuals to rewire a link to an infective, to a randomly chosen susceptible. The pairwise equations that modelled the dynamics also gave rise to not only disease free and endemic states but also more interesting dynamical features such as bistability and stable oscillations. Whilst the model of Gross et al. (2006) implicitly assumed global knowledge of infections (a susceptible never rewired to an infective), Zanette and Risau-Gusmán (2008) develops the model by allowing either the complete removal of links between susceptible and infected individuals or allowing susceptible individuals to rewire the links at random (thus making no assumption of global knowledge). Although there is a great wealth of models (both static and dynamic) based on different considerations and modelling choices, it is important to realise that not all are completely independent and distinct from one another. In order to direct future research in useful directions it is thus important to understand the links between different models and attempt to understand how these perform in relation to each other.

1.2.4 Thesis contribution

In this thesis the first paper helps to elucidate the links between some of the more popular approaches to modelling SIS dynamics, also analysing their performance against one another in an attempt to provide a better understanding of model performance hierarchy. In addition, we propose a heuristic differential equation for the expected value of an arbitrary motif and show how it can be derived directly from the exact Kolmogorov equations.

Whereas paper 1 formalised the links between popular models of disease dynamics, papers 2 and 3 take two such models (the pairwise (Keeling, 1999) and effective degree (Lindquist et al., 2011)), extending them to consider dynamically evolving networks. We develop the models to incorporate more realistic human behaviour where contacts change over time. Paper 2, making use of a pairwise model, focusses on the situation where the disease status of individuals is globally known and how type-dependent link deletion and creation alter the stability of the endemic state. In comparison, using a model based on effective degree, paper 3 models the situation where links are broken and created at random, and considers both the temporal evolution of the disease and the effect that the breaking and creation of links between individuals has on the value of R_0.

1.3 Criticality within the brain

In mathematical epidemiology the transition of the disease free state of a system from stable to unstable occurs when the basic reproduction ratio is equal to one ($R_0 = 1$). Operating at this point the system is said to be critical and the movement from the stable to unstable regime is known as a critical phase transition. Within statistical physics the classic example of a critical phase transition is the Ising model of the ferromagnetic-paramagnetic phase transition that occurs when a magnet is heated. Below a critical temperature the spin orientations are all in the same direction and the magnet is ferromagnetic. If the magnet is heated the spins begin to swap directions becoming more and more disordered, until above a critical point they appear to be directed at random. Most interesting is what occurs at the critical point, where there is neither total order nor disorder but the system exhibits scale invariant fluctuations and long-range correlations. Similarly the Kuramoto model (Kuramoto, 1984) of coupled oscillators exhibits a similar transition from desynchronous to synchronous behaviour with fluctuations in the number of synchronised pairs maximised at a critical coupling parameter. Motivated by this, in neuroscience a recent theory proposes that the brain is operating within a critical regime (Chialvo, 2010), between a very ordered and highly disordered state (Beggs and Timme, 2012). *In vitro* studies (Beggs and Plenz, 2003; Klaus et al., 2011) have shown that neuronal avalanches (cascades of neuronal firing) appear to exhibit power law statistics and subsequent work has found similar results for *in vivo* avalanches (Petermann et al., 2009; Hahn et al., 2010). These power law like statistics were used as initial evidence that the brain is critical. If the brain were in a critical state then, it is argued, this would enable it to respond and adapt optimally to the dynamics of the surrounding environment (Chialvo, 2010; Linkenkaer-Hansen et al., 2001) whilst also maintaining balanced neuronal activity (Meisel et al., 2012). One possibility as to how the brain becomes critical is that it may self-organise to a critical state (Bak et al., 1987), with an intrinsic mechanism driving the dynamics and without the dependence on external tuning. An illustration of how this may occur is given by Levina et al. (2007) where they created a simple model to show how activity-dependent depressive synapses can create parameter-independent criticality. It should be noted, however, that Bonachela et al. (2010) regard this as not true criticality and instead argue it should be referred to as a self-organised quasi-critical (SOqC) due to its non-conserving nature.

Before claiming the brain is indeed critical, caution must, however, be taken as it has been shown that apparent power laws may be explained by thresholding of stochastic process (Touboul and Destexhe, 2010) rather than a system being critical. Benayoun et al. (2010) argue that the avalanches are a necessary but not sufficient condition for criticality and that careful balancing of excitation and inhibition can generate similar distribution of avalanche sizes. Furthermore, recent work by Dehghani et al. (2012) has called into question whether *in vivo* avalanches are well approximated by power laws suggesting they are more likely to follow exponential distributions. Whilst the picture in regard to criticality is still not clear, it is helpful to understand what the functional benefits of criticality would be and whether they are

exhibited within the brain (Shew and Plenz, 2013). Theoretically, if the brain were operating in a critical regime it should benefit from an optimisation of dynamic range (Kinouchi and Copelli, 2006), as well as the maximisation of mutual information transmission (Greenfield and Lecar, 2001) and information capacity (Rämö et al., 2007). Importantly recent experimental work has confirmed the presence of these functional benefits (Shew et al., 2009, 2011).

1.3.1 Thesis contribution

Benayoun et al. (2010) consider the following stochastic model of inhibitory and excitatory neurones that in the limit of large N converges to the Wilson-Cowan equations (Wilson and Cowan, 1972). Both all-to-all and sparse networks are considered with the strength of connections fixed depending on the type (inhibitory or excitatory) of neurones being connected. Within the network, neurones are considered to be either quiescent (Q) or active (A). Taking a small time step dt and allowing $dt \to 0$ the transition probabilities between the two states are then given by:

$$P\left(Q \to A, \text{ in time } dt\right) = f\left(s_i(t)\right) dt$$
$$P\left(A \to Q, \text{ in time } dt\right) = \alpha dt$$

where $s_i(t) = \sum_j \frac{w_{ij}}{N} a_j(t) + h_i$ is the input to the neurone. Here f is an activation function, h_i is an external input, w_{ij} is the connection strength from neurone i to neurone j and $a_j(t) = 1$ if neurone j is active at time t and zero otherwise. α is the de-activation rate and therefore controls the refractory period of the neurone. In Benayoun et al. (2010), w_{ij} is set equal to a value w_E if neurone i is excitatory and w_I otherwise. The model is then analysed from a viewpoint of balanced excitation and inhibition.

In order to gain further analytic tractability, in papers 4 and 5 we consider a simplified version of this model where a fully connected population is comprised only of excitatory neurones. Making use of a meanfield ODE description of the temporal evolution of activity, we can then easily tune the model to be at or near the critical regime.

Paper 4 considers the behaviour of this system tuned to criticality in the absence of external input. We provide a numerical method for calculating the exact avalanche distribution and show that although this distribution is given by a summation of exponentials, over a limited range, shows characteristics of a power law distribution. We are also able to provide an analytic justification for the often exhibited finite-size cutoff and suggest other possible markers of criticality, such as the divergence of susceptibility and the critical slowing down of the system when exposed to a perturbation, that may be worthy of experimental exploration.

Paper 5 looks at the driven case (i.e. with a constant external input) and when the system is operating near to the critical regime (the critical regime only being reached in the absence of an external input). This is important as if a brain were tuned to the critical regime it would still be influenced by external inputs and should exhibit other functional benefits. We

show that one such functional benefit, the dynamic range, is indeed maximised when the network parameters are tuned to the critical regime (in the absence of external input). We also consider how the network behaves when the external input is reduced, thus moving the network to the critical regime, via two different routes. By scaling the external input h as $h = x/N$ we consider tuning to the critical regime by reducing x and secondly by increasing the network size N. Depending on the approach taken there is a notable difference in the resultant distribution of avalanche sizes with more a more scale-free like distribution obtained when x is decreased. We also consider the inter avalanche intervals (IAIs) obtained under both approaches proving that although the inter-avalanche intervals (IAIs) follow a weighted sum of hypoexponential distributions they are again well approximated by a power law (for a particular parameter). Interestingly we find that when the critical regime is approached by increasing the network size, another marker of criticality, long-range temporal correlations (LRTCs), increase but disappear when the critical regime is approached by decreasing x.

Chapter 2

Overview of contributory papers

Paper 1

Interdependency and hierarchy of exact and approximate epidemic models on networks. Taylor and Kiss (2013)

We begin with a paper discussing some of the different models proposed (meanfield (Allen, 2008), pairwise (Keeling, 1999), heterogeneous pairwise (Eames and Keeling, 2002), effective degree (Lindquist et al., 2011)) for the study of SIS disease dynamics unfolding on networks. We discuss the links between these models and formalise how they can be viewed as more general motif-based models. We illustrate how the different models can be derived from one another and, where this is not possible, discuss extensions to established models that enables this derivation. Building on the work of Simon et al. (2011) and Taylor et al. (2012a) we also derive a general result for the exact differential equation for the expected number of an arbitrary motif directly from the Kolmogorov/master equations and conclude with a comparison of the performance of the different closed systems of equations on networks of varying structure.

Paper 2

Modelling approaches for simple dynamic networks and applications to disease transmission models. Kiss et al. (2012)

The second paper considers a random link activation-deletion model that gives rise to a stochastically evolving network. Coupling this dynamic network with susceptible-infectious-susceptible (SIS) dynamics on the network, we explore the resulting model behaviour using both simulation and a dynamic version of a pairwise motif model. In this paper a random link activation-deletion (RLAD) model is proposed that gives rise to a stochastically evolving network. Exploration of behaviour is done systematically, first considering models with no disease dynamics and with both link independent and dependent network dynamics coupled

with globally constrained link creation. This is done rigorously with some analytical results and we highlight where such analysis can be performed and how these simpler models provide a benchmark to test and validate full simulations. The pairwise model is used to study the interplay between SIS-type dynamics on the network and link-type-dependent activation-deletion. Assumptions of the pairwise model are identified and their implications interpreted in a way that complements our current understanding. Furthermore, we also discuss how the strong assumptions of the closure relations can lead to disagreement between the simulation and pairwise model. Unlike on a static network, the resulting spectrum of behaviour is more complex with the prevalence of infections exhibiting not only a single steady state, but also bistability and oscillations.

Paper 3

Epidemic threshold and control in a dynamic network. Taylor et al. (2012b)

In the third paper we again consider a model of SIS disease dynamics spreading on a dynamic network with random link activation and deletion with the activation being locally constrained. This time we use an extension of the effective degree model proposed by Lindquist et al. (2011). The resulting set of ordinary differential equations (ODEs) is solved numerically, and results are compared to those obtained using individual-based stochastic network simulation. We show that the ODEs display excellent agreement with simulation for the evolution of both the disease and the network and are able to accurately capture the epidemic threshold for a wide range of parameters. In addition to this this evaluation of the temporal evolution of the system, using the next generation matrix approach (Diekmann and Heesterbeek, 2000) we also present an analytical calculation of R_0 for this dynamic network. We show that, depending on the relative time scales of the network evolution and disease transmission, two limiting cases are recovered: (i) the static network case when network evolution is slow and (ii) homogeneous random mixing when the network evolution is rapid. We also use our threshold calculation to highlight the dangers of relying on local stability analysis when predicting epidemic outbreaks on evolving networks.

Paper 4

Identification of Criticality in Neuronal Avalanches: I. A Theoretical Investigation of the Non-driven Case. Taylor et al. (2013)

In this paper, consideration is given to a simple model of a purely excitatory neural network with dynamics akin to the SIS disease dynamics of the previous papers. The simplicity of the dynamics means that we can tune the system to operate at a critical point. The model operates on a fully connected network under the assumption of no external input (paper 5, the companion paper, considers the driven case). This model allows us to consider various markers

of criticality and illustrate how they should perform in a finite-sized system. By calculating the exact distribution of avalanche sizes arising from the activation of an individual neurone in a quiescent network, we are able to show that, over a limited range of avalanche sizes which we precisely identify, the distribution has scale-free properties but is not a power law. This suggests that it would be inappropriate to dismiss a system as not being critical purely based on an inability to rigorously fit a power law distribution as has been recently advocated. We then stress that in assessing whether a system, especially a finite-sized one, is critical it is thus important to consider other possible markers. We illustrate one of these by showing the divergence of susceptibility as the critical point of the system is approached. Finally, we provide evidence that power laws may underlie other observables of the system that may be more amenable to robust experimental assessment.

Paper 5

Identification of Criticality in Neuronal Avalanches: II. A Theoretical and Empirical Investigation of the Driven Case. Hartley et al. (2013)

In the final paper we consider the same model as in the previous work but with the addition of the network being driven by an external input. We do this as within the framework of self-organised criticality a separation of timescales is thought to be crucial for the observation of power-law dynamics and computational models are often constructed with this property. However, this is not a characteristic of physiological neural networks - external input does not only occur when the network is at rest/a steady state. The external input present in our model prevents this separation of timescales and instead we tune the network to operate in the region of a critical state (it reaches the critical regime exactly in the absence of input - see the previous paper). The system displays avalanche dynamics in terms of cascades of neuronal firing separated by periods of silence. We observe an apparent power-law in the distribution of avalanche size for low levels of the external input. Considering waiting times we show that they can exhibit close to power-law dynamics coinciding with recent experimental findings. We further show that as the system approaches the critical state by two alternative routes, different markers of criticality (power-law distributions and long-range temporal correlations) are displayed. This suggests that signatures of criticality exhibited by a particular system in close proximity to a critical state are dependent on the region in parameter space at which the system (currently) resides. In addition to this we prove that by tuning the non-driven system to a critical bifurcation it will maximise its dynamic range when an external input is introduced and this leads to a consideration of external input in relation to the distribution of avalanche sizes, both *in vitro* and *in vivo*.

Chapter 3

Paper 1: Interdependency and hierarchy of exact and approximate epidemic models on networks

Timothy J. Taylor[1] and Istvan Z. Kiss[2]

[1]Centre for Computational Neuroscience and Robotics, University of Sussex, Brighton BN1 9QH, UK

[2]School of Mathematical and Physical Sciences, Department of Mathematics, University of Sussex, Brighton BN1 9QH, UK

Journal of Mathematical Biology. ISSN 0303-6812 (In Press)

3.1 Abstract

Over the years numerous models of SIS (susceptible $\rightarrow$ infected $\rightarrow$ susceptible) disease dynamics unfolding on networks have been proposed. Here, we discuss the links between many of these models and how they can be viewed as more general motif-based models. We illustrate how the different models can be derived from one another and, where this is not possible, discuss extensions to established models that enables this derivation. We also derive a general result for the exact differential equations for the expected number of an arbitrary motif directly from the Kolmogorov/master equations and conclude with a comparison of the performance of the different closed systems of equations on networks of varying structure.

3.2 Introduction

Modeling the spread of infectious diseases requires an understanding of not only disease characteristics but also an understanding of the community (be it a hospital, school, town, etc) in which it pervades. An important consideration in modelling the spread of diseases is thus the contact structure on which disease transmission happens. Whereas traditional approaches (Anderson et al., 1992; Diekmann and Heesterbeek, 2000) assume little or no topological structure, recent work (Keeling, 1999; Kenah and Miller, 2011; Lindquist et al., 2011) has tried to incorporate the underlying linkages between entities in the population and study how these links facilitate the spread of the disease. For a continuous-time stochastic disease transmission model on an arbitrary network it is possible (Simon et al., 2011), to write down the relevant Kolmogorov/master equations and thus model it as a continuous time Markov chain that fully describes the movement between all possible system states. Unfortunately the complexity of the model comes from the size of the state space and the number of equations scales exponentially as a^N, where a is the number of different states a node can be in and N is the network size. One widely used resolution to this complexity is to create individual-based simulation models and investigate the system behaviour directly. Even though increasing computational power makes simulations an increasingly attractive proposition they lack analytic tractability. Whilst this is not always a hindrance, when the system displays a rich range of behaviour (e.g. oscillations, bistability) it may not be feasible to obtain a global overview of the effects of different parameter values and thus the more analytic approach is needed. For this reason, low-dimensional systems of differential equations (Keeling, 1999; Eames and Keeling, 2002; Lindquist et al., 2011) are sought provided that these can approximate the exact solution. By reducing the problem to a smaller system of equations it is easier to study the bifurcation structure of the model and gain a greater understanding of the full spectrum of behaviour. The challenge is then finding the set of equations that best approximate the solution of the Kolmogorov equations.

Given that here we focus on epidemic models, usually such models are formulated in terms of the expected values of the number of infected and/or susceptible individuals or some other

motif in the network such as the expected number of infected and/or susceptible individuals of different degrees (the number of connections a node has). Such models range from classic meanfield (Allen, 2008) to pairwise (Keeling, 1999), heterogenous pairwise (Eames and Keeling, 2002), effective degree (Lindquist et al., 2011; Marceau et al., 2010) and individual-level models (Sharkey, 2008) to name a few. Whilst these models seem to use different approaches their derivation is based on the same conceptual framework, namely they begin by choosing a base-motif (e.g. a node, a link and the two nodes it connects, a node and all its links). These base-motifs are then used to formulate equations for the different possible states that they can achieve (e.g. for the expected number of motifs in different states or the probability that a specified motif in the network is in a certain state). These equations generally involve not only the base-motif itself, but larger or extended motifs of which they are usually part of. These larger motifs in turn depend on more complex motifs and a closure is needed in order to obtain a self-contained system of equations of reasonable size. Importantly the base-motif determines not only the complexity of the model (the larger the motif the greater the number of states it can be in) but also how much of the network topology can be captured. Interestingly differential equations for smaller motifs that are part of the base-motif should, in theory, be recoverable from the original differential equation. To this end the main focus of the paper is the consideration of various simple models of disease dynamics and the relations between them. We also consider which models are derivable directly (subject to a suitable closure) from the Kolmogorov/master equations and can thus be referred to as exact.

We begin in section 3.3 with an introduction of some of the more common approaches to modelling disease dynamics on networks, considering meanfield (Allen, 2008), pairwise (Keeling, 1999), heterogeneous pairwise (Eames and Keeling, 2002) and the effective degree (Lindquist et al., 2011) model formulations. In section 3.4 we formulate an exact version of the effective degree model and then illustrate how the pairwise model can then be recovered from this new set of equations. We are, however, unable to recover the heterogenous pairwise model from the exact effective degree and this motivates, in section 3.5, an extension of this which incorporates further network topology into the ODEs. From this extension we then show how it is then possible to recover the heterogeneous pairwise equations. Once the links between the models have been established, in section 3.6 we show how the unclosed version of the models can be derived directly from the Kolmogorov equations. This is done by proving that as long as the heuristic equations for any motif are written following a certain set of rules they will always be exact. We conclude, in section 3.7 with a brief comparison of the models and discuss under what circumstances they perform best, in the sense of being close to simulation results.

3.3 Models of disease dynamics

In this paper we focus on susceptible → infected → susceptible (SIS) disease dynamics on networks but note that all of the following models can be adapted for other disease (e.g. SIR and/or contact tracing) or non-disease (e.g. evolutionary (Hadjichrysanthou et al., 2012)) dynamics. With this in mind we use τ as the per-link transmission rate between susceptible and infected nodes and γ as the recovery rate of an infected individual. Both infection and recovery are modelled as independent poisson processes. As a starting point we give a short summary of ODE-based models that are either exact or an approximation of the true dynamics resulting from the full system based on the Kolmogorov/master equations, where these are solvable, or based on simulation.

3.3.1 Pairwise and the resulting simple compartmental model

In order to focus on the underlying network of contacts, we introduce the pairwise model first (Keeling, 1999; Rand, 1999). The main idea of this model is to develop the hierarchical dependence of lower order moments (e.g. expected number of susceptible $[S]$ and infected $[I]$ nodes) on higher ones (e.g. expected number of pairs with one susceptible and one infected node, $[SI]$) and to derive appropriate models that correctly account for these. As already suggested, the expected number of pairs will depend on larger motifs, in this case these being the expected number of triples denoted by $[ABC]$, where $A, B, C \in \{S, I\}$ and B is connected to A and C. Using this notation the equations governing the evolution of the disease dynamics at the level of singles and pairs are given by

$$\frac{d}{dt}[I] = -\gamma[I] + \tau[SI], \tag{3.1}$$

$$\frac{d}{dt}[SS] = -2\tau[ISS] + 2\gamma[SI], \tag{3.2}$$

$$\frac{d}{dt}[SI] = \tau([ISS] - [ISI] - [SI]) + \gamma([II] - [SI]), \tag{3.3}$$

$$\frac{d}{dt}[II] = 2\tau([ISI] + [SI]) - 2\gamma[II]. \tag{3.4}$$

Here we consider ordered pairs and triples, meaning they are counted in both directions. For pairs (with similar remarks for triples) this means $[IS] = [SI]$ and links of type $S - S$ and $I - I$ have a double contribution to the $[SS]$ and $[II]$ counts. Importantly we note that these equations are unclosed as no equations are given for the evolution of the triples. The standard closure (in the absence of clustering) makes the assumption that the status of pairs are statistically independent of one another and then

$$[ABC] \approx [AB](n-1)\frac{[BC]}{n[B]},$$

where n is the average degree of the network. When we use this closure we say we have closed "at the level of triples" . In order to derive the classic mean-field model a closure at the level of paris can be applied, namely, $[SI]$ can be approximated as

$$[SI] \approx n[S]\frac{[I]}{N}$$

and upon using Eq. (3.1), the classic mean-field model can be recovered

$$\frac{d}{dt}[I] = -\gamma[I] + \tau n[S]\frac{[I]}{N}, \tag{3.5}$$

where the widely used transmission rate from the compartmental model (Allen, 2008) is $\beta = \tau n$.

It is also important to note that the unclosed equations above (Eqs. (3.1-3.4)) can be derived directly from the state-based Kolmogorov equations and for this reason we refer to these equations as exact. Whilst a proof for the exactness of these equations was given in Taylor et al. (2012a), in section 3.6 we provide a more general proof that allows us to write down exact equations for, not just pairs, but any motif structure. We also note that an alternative approach was used by Sharkey (2008), to prove that the standard pairwise equations were exact for models with susceptible $\rightarrow$ infected $\rightarrow$ recovered (SIR) disease dynamics.

3.3.2 Heterogeneous pairwise model

Whilst the pairwise equations perform well in capturing disease dynamics on networks that are well described by their average degree, the closure assumption fails when greater heterogeneity is introduced. More precisely, whilst the pairwise equations above are exact for an arbitrary network before a closure, these do not guarantee that with the current choice of singles and pairs (i.e. $[S]$ could be further divided to account for heterogeneity in degree) a valid closure could be found for any network. Indeed, to account for greater heterogeneity Eames and Keeling (2002) further developed the pairwise model by taking into account not just the state of nodes and pairs but also the degrees of the nodes. By using $[A^n]$ to represent expected number of nodes of type A with degree n and with similar notation for pairs and triples, they

were able to formulate the following set of unclosed equations

$$\frac{d}{dt}[S^n] = \gamma[I^n] - \tau \sum_q [S^n I^q], \tag{3.6}$$

$$\frac{d}{dt}[I^n] = -\gamma[I^n] + \tau \sum_q [S^n I^q], \tag{3.7}$$

$$\frac{d}{dt}[S^n S^m] = -\tau \sum_q \left([S^n S^m I^q] + [I^q S^n S^m]\right) + \gamma\left([S^n I^m] + [I^n S^m]\right), \tag{3.8}$$

$$\frac{d}{dt}[S^n I^m] = \tau \sum_q \left([S^n S^m I^q] - [I^q S^n I^m]\right) - \tau[S^n I^m] - \gamma[S^n I^m] + \gamma[I^n I^m], \tag{3.9}$$

$$\frac{d}{dt}[I^n I^m] = \tau \sum_q \left([I^n S^m I^q] + [I^q S^n I^m]\right) + \tau[I^n S^m] + \tau[S^n I^m] - 2\gamma[I^n I^m]. \tag{3.10}$$

Again assuming the statistical independence of pairs and absence of clustering, Eames and Keeling (2002), suggest the following approximations of triples

$$[B^n C^m D^p] \approx [B^n C^m](m-1)\frac{[C^m D^p]}{m[C^m]}.$$

3.3.3 The effective degree model

Lindquist et al. (2011) introduced the effective degree model for SIS (and also SIR) dynamics on a network (an equivalent model formulation was also proposed by Marceau et al. (2010)). In this model they consider not only the state of a node (S or I), but also the number of the immediate neighbours in the various potential states. This is done by writing the following set of equations for all the possible star-like motifs in the network where $S_{s,i}$ ($I_{s,i}$) represents the expected number of susceptible (infected) nodes with s susceptible and i infected neighbours,

$$\begin{aligned}\dot{S}_{s,i} =& -\tau i S_{s,i} + \gamma I_{s,i} + \gamma[(i+1)S_{s-1,i+1} - iS_{s,i}] \\ &+ \tau \frac{\sum_{k=1}^{M}\sum_{j+l=k} jlS_{j,l}}{\sum_{k=1}^{M}\sum_{j+l=k} jS_{j,l}}[(s+1)S_{s+1,i-1} - sS_{s,i}],\end{aligned} \tag{3.11}$$

$$\begin{aligned}\dot{I}_{s,i} =& \tau i S_{s,i} - \gamma I_{s,i} + \gamma[(i+1)I_{s-1,i+1} - iI_{s,i}] \\ &+ \tau \frac{\sum_{k=1}^{M}\sum_{j+l=k} l^2 S_{j,l}}{\sum_{k=1}^{M}\sum_{j+l=k} jI_{j,l}}[(s+1)I_{s+1,i-1} - sI_{s,i}],\end{aligned} \tag{3.12}$$

with $1 \leq s+i \leq M$, where M is the maximum degree and the equations are suitably adjusted on the boundaries. It is important to note that this model is not exact as a closure has been already applied. Namely the infection of a node's susceptible neighbours is based on a

population-level approximation. To illustrate this more precisely we borrow the notation of the pairwise model and make two observations

$$\frac{\sum_{k=1}^{M}\sum_{j+l=k} jlS_{j,l}}{\sum_{k=1}^{M}\sum_{j+l=k} jS_{j,l}} = \frac{[ISS]}{[SS]},$$
$$\frac{\sum_{k=1}^{M}\sum_{j+l=k} l^2S_{j,l}}{\sum_{k=1}^{M}\sum_{j+l=k} jI_{j,l}} = \frac{\sum_{k=1}^{M}\sum_{j+l=k} l(l-1)S_{j,l} + lS_{j,l}}{\sum_{k=1}^{M}\sum_{j+l=k} jI_{j,l}} = \frac{[ISI]+[SI]}{[SI]} = \frac{[ISI]}{[SI]} + 1.$$

These means that the infection pressure on the susceptible neighbours of the central node is equal to the population level average taken from all the possible star-like configurations rather then from the extended star structures that would account exactly for these infections.

3.4 Recovering the pairwise model from the effective degree

Whilst the pairwise and effective degree models seem different they are based on a similar approach. Both models work on approximating the evolution of different motifs in the network; individuals and links in the pairwise model and star-like structures in the effective degree. For both models, but more clearly for the pairwise, the models begin with a starting or base motif (e.g. nodes) for which an evolution equation is required. This will of course depend on an extended motif, typically the base motif extended by the addition of an extra node (e.g. pairs). This dependency on higher order motifs continues, for example, with pairs depending on triples, and then triples depending on quadruplets (four nodes connected by a line, i.e. $A-B-C-D$, or a star with a centre and three spokes, i.e. $A-\overline{B-C \quad D}$). Hence, the models only differ in the choice of the base motif and then potentially in the way in which the systems are closed to curtail the dependency on higher order motifs. Since, here we are mainly interested in exact models, that is before a closure is applied, we begin by conjecturing an exact version of the effective degree model and show how starting from this the exact pairwise model can be derived.

3.4.1 Exact effective degree

Based on the ideas presented above, we extend the star-like base motif to reveal the dependence on higher order motifs and conjecture that this unclosed version of the effective degree model is exact. We begin by introducing a variable to count the expected number of infecteds connected to a node's susceptible neighbours. This is done by introducing two new terms, $[ISS_{s',i'}]$ and $[ISI_{s',i'}]$. For the term $[ISI_{s',i'}]$ (and similarly for $[ISS_{s',i'}]$) the S in the middle is actually used to represent the susceptible neighbours of the central I from the motif with composition $I_{s'i'}$ (i.e. the I node with neighbourhood (s',i') is the centre of the star, while S is a susceptible spoke). The I (on the left-hand side), in turn, represents the infective neighbours of these susceptibles' and within this count, in the case of $[ISI_{s',i'}]$, we also include the

originating central I. The exact effective degree model can then be written as

$$\begin{aligned}\dot{S}_{s,i} =& -\tau i S_{s,i} + \gamma I_{s,i} + \gamma[(i+1)S_{s-1,i+1} - iS_{s,i}] \\ &+ \tau\left[ISS_{s+1,i-1}\right] - \tau\left[ISS_{s,i}\right], \end{aligned} \tag{3.13}$$

$$\begin{aligned}\dot{I}_{s,i} =& \tau i S_{s,i} - \gamma I_{s,i} + \gamma[(i+1)I_{s-1,i+1} - iI_{s,i}] \\ &+ \tau\left[ISI_{s+1,i-1}\right] - \tau\left[ISI_{s,i}\right]. \end{aligned} \tag{3.14}$$

Figure 3.1 shows the possible transitions captured by this model.

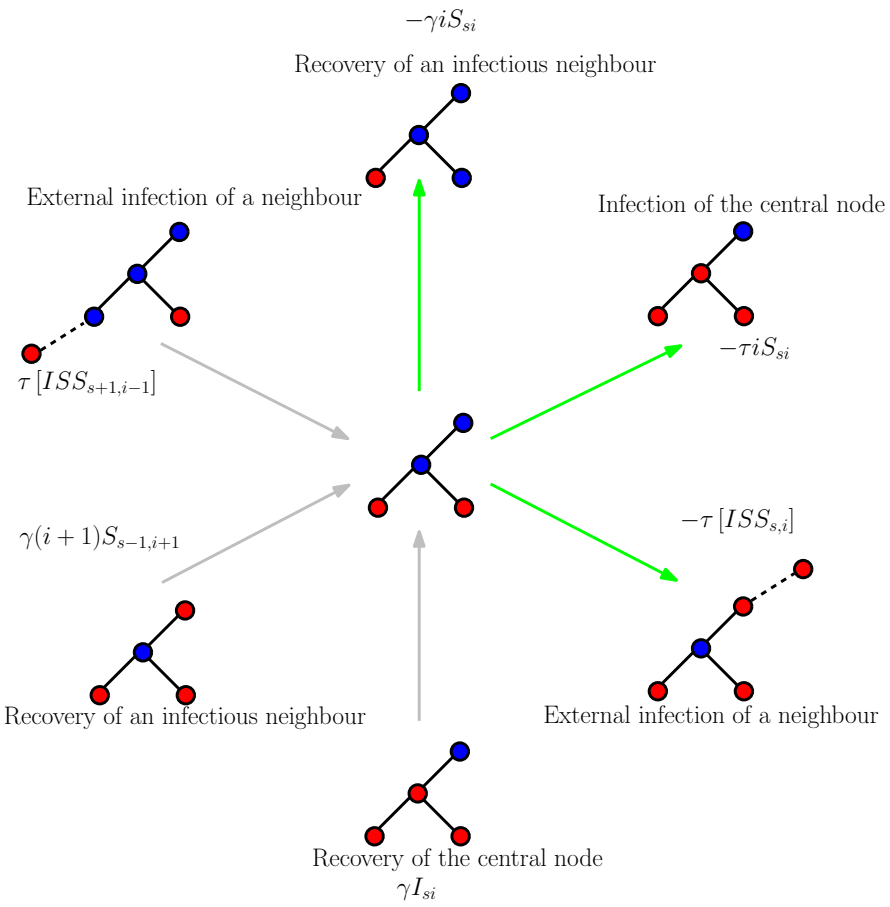

Figure 3.1: Illustration of the transitions into and out of the $S_{2,1}$ class. Susceptible nodes are given in blue and infective nodes in red. Transitions into and out of the class are shown in grey and green, respectively. The corresponding terms of the general equation are also given. In Appendix 1 a similar illustration is given for a configuration with a centrally infectious node.

3.4.2 Recovering the pairwise equations

The star-like composition of the effective degree model allows us to recover the pairwise equations via careful summations. The full derivation of the pairwise model is given in Appendix 2, whilst here we only illustrate the derivation of the individuals (trivial but given for completeness) and the $[II]$ pairs,

$$\frac{d}{dt}[S] = \sum_{s,i} \dot{S}_{s,i} = \gamma [I] - \tau [SI],$$
$$\frac{d}{dt}[I] = \sum_{s,i} \dot{I}_{s,i} = -\gamma [I] + \tau [SI],$$

where most terms from the original effective degree equations cancel and we have used that $\sum_{s,i} iS_{s,i} = [SI]$ and $\sum_{s,i} I_{s,i} = [I]$. For $[II]$ the following equality holds

$$\begin{aligned}
\frac{d}{dt}[II] =& \sum_{s,i} i\dot{I}_{s,i} \\
=& \tau \sum i^2 S_{s,i} - \gamma \sum i I_{s,i} + \gamma \sum i(i+1) I_{s-1,i+1} - \gamma \sum i^2 I_{s,i} \\
&+ \tau \sum i[ISI_{s+1,i-1}] - \tau \sum i[ISI_{s,i}] \\
=& \tau \sum i(i-1) S_{s,i} + \tau \sum i S_{s,i} - \gamma [II] \\
&+ \gamma [III] - \gamma \sum i(i-1) I_{s,i} - \gamma \sum i I_{s,i} \\
&+ \tau \sum (i-1)[ISI_{s+1,i-1}] + \tau \sum [ISI_{s+1,i-1}] - \tau \sum i[ISI_{s,i}] \\
=& \tau [ISI] + \tau [IS] - \gamma [II] + \gamma [III] - \gamma [III] - \gamma [II] + \tau [ISI] + \tau [IS] \\
=& 2\tau ([ISI] + [IS]) - 2\gamma [II],
\end{aligned}$$

where we have used that $\sum_{s,i} iI_{si} = [II]$, $\sum_{s,i} (i-1)[ISI_{s+1,i-1}] = \sum i[ISI_{s,i}]$ and that $\sum [ISI_{s+1,i-1}] = [ISI] + [SI]$. These all follow from the definition of the pairwise model and the definition of the new extended motifs from the exact effective degree model. We note that this result does indeed correspond to that of the given pairwise model.

3.5 Higher order models

Whilst we can recover the pairwise equations from the exact effective degree model we note that the same is not possible with the heterogeneous pairwise equations. This motivates an extension of the effective degree model where the degrees of neighbouring nodes are also taken in to account. Again we conjecture that this model can, in theory, be derived from the exact Kolmogorov equations and thus refer to it as exact.

3.5.1 Exact effective degree with neighbourhood composition

We extend the exact effective degree model to include the number of neighbours of the central nodes' neighbours. We begin by defining the following notation

$$\begin{aligned} s' &= (s_1, s_2, \ldots, s_M), \\ i' &= (i_1, i_2, \ldots, i_M), \\ |s'| &= s_1 + s_2 + \ldots + s_M, \\ |i'| &= i_1 + i_2 + \ldots + i_M, \end{aligned}$$

where s_j (i_j) represents the number of susceptible (infective) neighbours of degree j. We now define $S_{s'i'}$, ($I_{s'i'}$) as the number of susceptible (infective) nodes with neighbouring nodes whose own degrees are given by the entries in s' and i'. We can now write the extended ODEs in the following form

$$\begin{aligned} \dot{S}_{s,'i'} =& -\tau|i'|S_{s,'i'} + \gamma I_{s',i'} + \gamma \sum_{k=1}^{M} (i_k+1) S_{s'_{k-},i'_{k+}} - \gamma|i'|S_{s',i'} \\ &+ \tau \sum_{k=1}^{M} \left[IS^k S_{s'_{k+},i'_{k-}} \right] - \tau \left[ISS_{s',i'} \right], \end{aligned} \tag{3.15}$$

$$\begin{aligned} \dot{I}_{s',i'} =& \tau|i'|S_{s',i'} - \gamma I_{s',i'} + \gamma \sum_{k=1}^{M} (i_k+1) I_{s'_{k-},i'_{k+}} - \gamma|i'|I_{s',i'} \\ &+ \tau \sum_{k=1}^{M} \left[IS^k I_{s'_{k+},i'_{k-}} \right] - \tau \left[ISI_{s',i'} \right]. \end{aligned} \tag{3.16}$$

Here $s'_{k-} = (s_1, s_2, \ldots, s_k - 1, \ldots, s_M)$ and $s'_{k+} = (s_1, s_2, \ldots, s_k + 1, \ldots, s_M)$ with a similar definition for i'_{k-} and i'_{k+}. With a small modification to the exact effective degree notation terms such as $\left[IS^k S_{s'_{k+},i'_{k-}} \right]$ are taken to represent number of infectious contacts of the susceptible neighbours of degree k.

3.5.2 Model recovery

Here we show how, from the extended effective degree model, we can recover the heterogenous pairwise model. It is also straightforward to show, and thus omitted here, that the extended effective degree leads to the simpler exact effective degree. In turn, it also follows easily that both the exact effective degree and heterogenous pairwise models reduce to the standard pairwise model. This hierarchy of recovery is illustrated in Fig. 3.2.

Recovering the heterogeneous pairwise model from the extended effective degree

As earlier we make use of careful summation to recover the model. The full derivation is provided in Appendix 3 so here we just provide the derivation at the individual level and of

the $[I^l I^n]$ pairs. For singles the following identities hold,

$$\frac{d}{dt}\left[S^n\right] = \sum_{|s'|+|i'|=n} \dot{S}_{s',i'} = \gamma\left[I^n\right] - \tau\left[S^n I\right],$$
$$\frac{d}{dt}\left[I^n\right] = \sum_{|s'|+|i'|=n} \dot{I}_{s',i'} = -\gamma\left[I^n\right] + \tau\left[S^n I\right],$$

where most terms from the original effective degree cancel and we have used that

$$\sum_{|s'|+|i'|=n} I_{s',i'} = \left[I^n\right] \quad \text{and} \quad \sum_{|s'|+|i'|=n} |i'| S_{s',i'} = \left[S^n I\right].$$

For the $[I^l I^n]$ pair we obtain

$$\begin{aligned}
\frac{d}{dt}\left[I^l I^n\right] =& \sum_{|s'|+|i'|=n} i_l \dot{I}_{s',i'} \\
=& \tau \sum i_l |i'| S_{s',i'} - \gamma \sum i_l I_{s',i'} + \gamma \sum i_l \sum_{k=1}^{M} (i_k+1) I_{s'_{k-} i'_{k+}} \\
& - \gamma \sum i_l |i'| I_{s',i'} + \tau \sum i_l \sum_{k=1}^{M} \left[IS^k I_{s'_{k+},i'_{k-}}\right] - \tau \sum i_l \left[IS I_{s',i'}\right] \\
=& \tau \sum i_l \left(|i'|-1\right) S_{s',i'} + \tau \sum i_l S_{s',i'} - \gamma \left[I^l I^n\right] \\
& + \gamma \left[I^l I^n I\right] - \gamma \sum i_l \left(|i'|-1\right) I_{s',i'} - \gamma \sum i'_l I_{s',i'} \\
& + \tau \sum i_l \sum_{k\neq l} \left[IS^k I_{s'_{k+},i'_{k-}}\right] + \tau \sum \left(i_l - 1\right) \left[IS^l I_{s'_{l+},i'_{l-}}\right] \\
& + \tau \sum \left[IS^l I_{s'_{l+},i'_{l-}}\right] - \tau \sum i_l \left[IS I_{s',i'}\right] \\
=& \tau \left[I^l S^n I\right] + \tau \left[I^l S^n\right] - 2\gamma \left[I^l I^n\right] \\
& + \gamma \left[I^l I^n I\right] - \gamma \left[I^l I^n I\right] + \tau \left[IS^l I^n\right] + \tau \left[S^l I^n\right] \\
=& \tau \left[I^l S^n I\right] + \tau \left[I^l S^n\right] - 2\gamma \left[I^l I^n\right] + \tau \left[IS^l I^n\right] + \tau \left[S^l I^n\right] \\
=& \tau \sum_q \left(\left[I^l S^n I^q\right] + \left[I^q S^l I^n\right] \right) + \tau \left[I^l S^n\right] + \tau \left[S^l I^n\right] - 2\gamma \left[I^l I^n\right].
\end{aligned}$$

Again, we note that this result corresponds to previously given heterogenous pairwise model.

3.6 Exactness of the models

In the previous sections we have at times referred to a set of ODEs as being exact. This terminology implies that the ODEs can be derived directly from the Kolmogorov equations which describe the evolution of the epidemic through the full state space $\mathcal{S}$ (on a network of

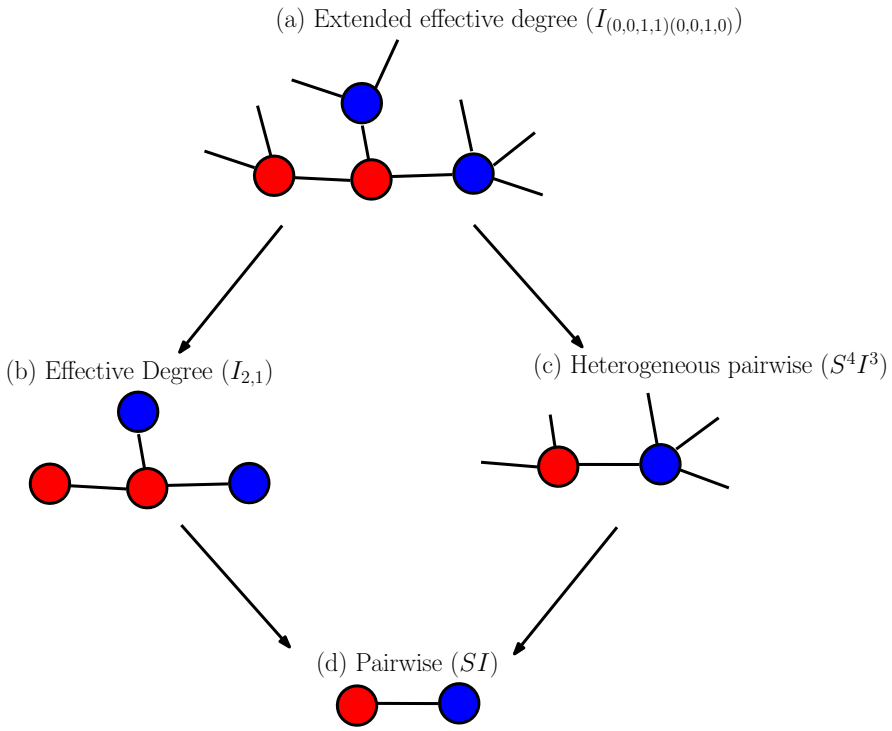

Figure 3.2: Illustration of the hierarchial structure of model recovery. Links that are known are given by lines and knowledge of a nodes status is given by circles. Susceptible and infective nodes are shown in blue and red respectively. The upper level (a) represents the extended effective degree ODEs. The status of the central node is known along with that of it's neighbours and also their degrees. The secondary level is given by (b), the effective degree model where there is no knowledge of neighbours' degrees and (c), the heterogenous pairwise model where the number of pairs of nodes and their relative degree is know. The final level shown, (d), is known as the standard pairwise model (Keeling, 1999) where the status of individual nodes and pairs is used.

size N, $\mathcal{S} = \{S, I\}^N$). In Taylor et al. (2012a) the exactness of the pairwise equations was rigorously proven but no other motif structures were considered. In section 3.4.1, we conjectured that the newly defined exact effective degree model is derivable from the Kolmogorov equations. Due to the structure of the motifs used in the effective degree model a mechanistic proof (as in Taylor et al. (2012a)) may be difficult and intricate to implement. Instead we will prove that a heuristic formulation of the ODEs for any motif structure is indeed exact providing they are written following rigorous bookkeeping. This derivation of the evolution equations for an arbitrary motif, directly from the Kolmogorv equations, will be based on an extension of ideas presented in Simon et al. (2011) and Taylor et al. (2012a) and using the notation defined in Tables 3.1 and 3.2.

We should note that in what follows a motif of connected nodes will only ever be counted once. In a network of size N and considering a motif, m, with k nodes this singular counting can be understood in the following way. We consider each of the $\binom{N}{k}$ unique sets of k nodes between 1 and N. Then for each set whose nodes are isomorphic in topological structure and status to the motif m, we simply increase the counter of such motifs by one. This formalism is unlike that used in the standard pairwise model where an SS link would contribute a value of two to the $[SS]$ count. However, the two resultant sets of equations are equivalent in the sense that the different ways of counting can easily be recovered by using a simple mapping between the two. For this reason, whilst we prove that the following theorem is correct, it's intricacy and generality means a certain amount of care is needed when interpreting the resultant terms. Using the notation defined in Table 3.2 the result for a general motif is then given in the following theorem.

Theorem 1. *The equation for the expected number ($|\mathcal{M}|$) of motifs of type $\hat{m}$, given by*

$$\begin{aligned} |\dot{\mathcal{M}}| =& \tau \mathcal{N}_{in}^{SI}(\hat{m}^-, \hat{m}) + \tau \mathcal{N}_{ex}^{SI}(\hat{m}^-, \hat{m}) - \tau |\mathcal{M}| N_{in}^{SI}(\hat{m}) - \tau \mathcal{N}_{ex}^{SI}(\hat{m}) \\ &+ \gamma \mathcal{N}^{I}(\hat{m}^+, \hat{m}) - \gamma |\mathcal{M}| N^{I}(\hat{m}) \end{aligned} \tag{3.17}$$

is derivable directly from the exact Kolmogorov equations.

3.6.1 Proof of Theorem 1

For a detailed description of writing the Kolmogorov equations for an arbitrary graph we refer the reader to Simon et al. (2011). Here we only provide a brief description making use of the notation defined in Table 3.1. The 2^N elements of the state space, $\mathcal{S} = \{S, I\}^N$, can be divided into $N + 1$ subsets where, for $0 \leq k \leq N$, $\mathcal{S}^k$ is the subset of all states with k infected nodes. Necessarily each subset contains $c_k = \binom{N}{k}$ distinct configurations, i.e. $\mathcal{S}^k = (\mathcal{S}_1^k, \mathcal{S}_2^k, \ldots, \mathcal{S}_{c_k}^k)$. The state of the system can only ever change in one of two ways, either via the infection of a node or via the recovery of a node. We can describe the evolution in the state space by a continuous time Markov-process. Setting $X_j^k(t)$ as the probability of the system being in state

Table 3.1: Notation for matrix representation of the Kolmogorov equations (Table from Taylor et al. (2012a)).

Variable	Definition
N	Number of nodes in the network
$G = (g_{ij}) \in \{0,1\}^{N^2}$, $i,j = 1,2,\ldots,N$	Adjacency matrix with $g_{ij} = 1$ if nodes i and j are connected and $g_{ij} = 0$ otherwise. The network is bi-directional and has no self loops such that $G = G^T$ and $G_{ii} = 0$, $\forall\ i$.
τ	Rate of infection per (S,I) edge.
γ	Rate of recovery.
$\mathcal{S} = \{S,I\}^N$	State space of the network, with nodes either susceptible, S, or infected, I and $\lvert S\rvert = 2^N$.
$\mathcal{S}^k = \{\mathcal{S}_1^k, \mathcal{S}_2^k, \ldots, \mathcal{S}_{c_k}^k\}$	The $c_k = \binom{N}{k}$ states with k infected individuals in all possible configurations, with $k = 0,1,\ldots,N$.
$X_j^k(t)$	Probability of being in state $\mathcal{S}_j^k$ at time t, where $k = 0,1,\ldots,N$ and $j = 1,2,\ldots,c_k$.
$X^k(t)$	$X^k(t) = \left(X_1^k(t), X_2^k(t), \ldots, X_{c_k}^k(t)\right)^T$.
$A_{i,j}^k$	Rate of transition from $\mathcal{S}_j^{k-1}$ to $\mathcal{S}_i^k$, where $k = 0,1,\ldots,N$, $i = 1,2,\ldots,c_k$ and $j = 1,2,\ldots,c_{k-1}$. Note that only one individual is changing (i.e. in this case an S node changes to an I through infection).
$C_{i,j}^k$	Rate of transition from $\mathcal{S}_j^{k+1}$ to $\mathcal{S}_i^k$, where $k = 0,1,\ldots,N$, $i = 1,2,\ldots,c_k$ and $j = 1,2,\ldots,c_{k+1}$. Note that only one individual is changing (i.e. in this case an I node changes to an S through recovery).
$B_{i,j}^k$	Rate of transition from $\mathcal{S}_j^k$ to $\mathcal{S}_i^k$, where $B_{i,j}^k = 0$ if $i \neq j$ with $k = 0,1,\ldots,N$ and $i,j = 1,2,\ldots,c_k$.

Table 3.2: Additional notation for matrix representation of the Kolmogorov equations

Variable	Definition
$\hat{m}$	An arbitrary motif encompassing both topology and status of nodes (e.g. an $S-I$ edge or a star like structure such as $I_{3,0}$). The arbitrary motif we are consdering which will encompass both topology and status of nodes.
$\hat{m}^+$	Represents the different motifs with the same structure as $\hat{m}$ but with a susceptible node of $\hat{m}$ having become infected.
$\hat{m}^-$	Represents the different motifs with the same structure as $\hat{m}$ but with with an infective node of $\hat{m}$ having become susceptible.
$M_{k,j}$	Set of $\hat{m}$ motifs in configuration state $\mathcal{S}_j^k$. Defining the i^{th} element of $M_{k,j}$ as $\hat{m}_{k,j}^i$ gives $M_{k,j} = \{\hat{m}_{k,j}^1, \hat{m}_{k,j}^2, \ldots, \hat{m}_{k,j}^{\lvert M\rvert}\}$.
$M_{k,j}^+$	The set of motifs, in configuration state $\mathcal{S}_j^k$, with the same topology as $\hat{m}$ but with 1 more infective and 1 less susceptible. Defining the i^{th} element of $M_{k,j}^+$ as $\hat{m}_{k,j}^{i+}$ gives $M_{k,j}^+ = \{\hat{m}_{k,j}^{1+}, \hat{m}_{k,j}^{2+}, \ldots, \hat{m}_{k,j}^{\lvert M_{k,j}^+\rvert +}\}$.
$M_{k,j}^-$	The set of motifs, in configuration state $\mathcal{S}_j^k$, with the same topology as $\hat{m}$ but with 1 less infective and 1 more susceptible. Defining the i^{th} element of $M_{k,j}^-$ as $\hat{m}_{k,j}^{i-}$ we have $M_{k,j}^- = \{\hat{m}_{k,j}^{1-}, \hat{m}_{k,j}^{2-}, \ldots, \hat{m}_{k,j}^{\lvert M_{k,j}^-\rvert -}\}$.
$N_{\hat{m}}(\mathcal{S}_j^k)$	Number of $\hat{m}$ motifs in state $\mathcal{S}_j^k$, with $k = 0, 1, \ldots, N$ and $j = 1, 2, \ldots, c_k$.
$N_{in}^{SI}(\hat{h})$	Number of SI links within the motif $\hat{h}$.
$\mathcal{N}_{in}^{SI}(\hat{h})$	Expected total number of SI links within all motifs of type $\hat{h}$
$N_{in}^{SI}(\hat{h}, k)$	Number of SI links within the motif $\hat{h}$, along which, were an infection to occur, would result in a motif of type k.
$\mathcal{N}_{in}^{SI}(\hat{h}, k)$	Expected total number of SI links within all motifs of type $\hat{h}$, along which, were an infection to occur, would result in a motif of type k.
$N_{ex}^{SI}(\hat{h})$	Number of SI links where the S is contained within the motif $\hat{h}$ and the I is external to it.
$\mathcal{N}_{ex}^{SI}(\hat{h})$	Expected total number of SI links to all motifs with structure $\hat{h}$, where the S is contained within the motif $\hat{h}$ and the I external to it.
$N_{ex}^{SI}(\hat{h}, k)$	Number of SI links where the S is contained within the motif $\hat{h}$ and the I is external to it, along which, were an infection to occur, would result in a motif of type k.
$\mathcal{N}_{ex}^{SI}(\hat{h}, k)$	Expected total number of SI links to all motifs with structure $\hat{h}$, where the S is contained within the motif $\hat{h}$ and the I external to it, along which, were an infection to occur, would result in a motif of type k.
$N^I(\hat{h})$	Number of I nodes within motif $\hat{h}$.
$N^I(\hat{h}, k)$	Number of I nodes within motif $\hat{h}$, whose recovery lead to a motif of type k.
$\mathcal{N}^I(\hat{h}, k)$	Expected total number of Is within motifs of type $\hat{h}$, whose recovery lead to a motif of type k.

$\mathcal{S}_j^k$ at time t and letting $X^k(t) = (X_2^k(t), X_2^k(t), \ldots, X_{c_k}^k(t)$ we can then write the Kolmogorov equations that capture the two possible transitions in the following matrix and vector form,

$$\dot{X}^k(t) = \begin{cases} B^0X^0 + C^0X^1 & \text{if } k = 0, \\ A^kX^{k-1} + B^kX^k + C^kX^{k+1} & \text{for } 1 \leq k \leq N-1, \\ A^NX^{N-1} + B^NX^N & \text{if } k = N \end{cases}$$

Here the matrices A^k capture the transitions into $\mathcal{S}^k$ via infection, C^k capture the transitions into $\mathcal{S}^k$ via recovery and B^k captures transitions within $\mathcal{S}^k$. Their entries are given as follows:

- $A_{i,j}^k$ is the rate of transition from $\mathcal{S}_j^{k-1}$ to $\mathcal{S}_i^k$, where $k = 0, 1, \ldots, N$, $i = 1, 2, \ldots, c_k$ and $j = 1, 2, \ldots, c_{k-1}$. Note that none-zero entries of the matrix represent the transitions where only one individual is changing from susceptible to infected and the corresponding entrance will then equal τ multiplied by the number of infectious neighbours of the susceptible. These matrices encode the topological structure of the network.
- $C_{i,j}^k$ is the rate of transition from $\mathcal{S}_j^{k+1}$ to $\mathcal{S}_i^k$, where $k = 0, 1, \ldots, N$, $i = 1, 2, \ldots, c_k$ and $j = 1, 2, \ldots, c_{k+1}$. Note that none-zero entries of the matrix represent the transitions where only one individual is changing from infected to susceptible and the corresponding entrance will then equal γ.
- $B_{i,j}^k$ is the rate of transition from $\mathcal{S}_j^k$ to $\mathcal{S}_i^k$ where $B_{i,j}^k = 0$ if $i \neq j$ with $k = 0, 1, \ldots, N$ and $i, j = 1, 2, \ldots, c_k$.

Letting $X(t) = (X^0(t), X^1(t), \ldots, X^N(t))^T$, we then write Kolmogorov equations in the following block tridiagonal form, $\dot{X} = PX$, where

$$P = \begin{pmatrix} B^0 & C^0 & 0 & 0 & 0 & 0 \\ A^1 & B^1 & C^1 & 0 & 0 & 0 \\ 0 & A^2 & B^2 & C^2 & 0 & 0 \\ 0 & 0 & A^3 & B^3 & C^3 & 0 \\ 0 & 0 & \ldots & \ldots & \ldots & 0 \\ 0 & 0 & 0 & 0 & A^N & B^N \end{pmatrix}.$$

From Simon et al. (2011), we also know that the entries of the matrix B are zero except on the diagonals, where we find that

$$\begin{aligned} B_{jj}^k &= -\sum_{i=1}^{c_{k+1}} A_{i,j}^{k+1} - \sum_{i=1}^{c_{k-1}} C_{i,j}^{k-1} \\ &= -\tau N_{SI}(S_j^k) - k\gamma. \end{aligned} \tag{3.18}$$

Where Simon et al. (2011) focussed on individual and edge motifs here we focus on the derivation of evolution equations for the expected number of an arbitrary motif, $\hat{m}$. We begin

by writing the exact equations for an arbitrary motif $\hat{m}$ based on the transition and recovery matrices. Using the notation from Table 3.2 this yields,

$$\begin{aligned}
|\dot{\mathcal{M}}| =& \sum_{k=0}^{N} N_{\hat{m}}(S^k)\dot{X}^k \\
=& N_{\hat{m}}(S^0)\left[B^0X^0 + C^0X^1\right] \\
&+ \sum_{k=1}^{N-1} N_{\hat{m}}(S^k)\left[A^kX^{k-1} + B^kX^k + C^kX^{k+1}\right] \\
&+ N_{\hat{m}}(S^N)\left[A^NX^{N-1} + B^NX^N\right] \\
=& \sum_{k=1}^{N} N_{\hat{m}}(S^k)A^kX^{k-1} + \sum_{k=0}^{N} N_{\hat{m}}(S^k)B^kX^k + \sum_{k=0}^{N-1} N_{\hat{m}}(S^k)C^kX^{k+1} \\
=& \sum_{k=0}^{N-1} N_{\hat{m}}(S^{k+1})A^{k+1}X^k + \sum_{k=0}^{N} N_{\hat{m}}(S^k)B^kX^k + \sum_{k=1}^{N} N_{\hat{m}}(S^{k-1})C^{k-1}X^k \\
=& \left[N_{\hat{m}}(S^1)A^1 + N_{\hat{m}}(S^0)B^0\right]X^0 \\
&+ \sum_{k=1}^{N-1}\left[N_{\hat{m}}(S^{k+1})A^{k+1} + N_{\hat{m}}(S^k)B^k + N_{\hat{m}}(S^{k-1})C^{k-1}\right]X^k \\
&+ \left[N_{\hat{m}}(S^N)B^N + N_{\hat{m}}(S^{N-1})C^{N-1}\right]X^N. \qquad (3.19)
\end{aligned}$$

Before continuing we note the following

$$B^N = B^N_{1,1} = -\sum_{i=1}^{N} C^{N-1}_{i,1} = -\gamma N,$$

$$B^0 = B^0_{1,1} = -\sum_{i=1}^{N} A^1_{i,1} = -\tau N_{SI}(S^0_1) = 0.$$

Taking these and (3.18) into account and using the fact that B is only none zero on it's diagonal, we then obtain the following equation,

$$\begin{aligned}
|\dot{\mathcal{M}}| =& N_{\hat{m}}(S^1)A^1X^0 \\
&+ \sum_{k=1}^{N-1}\left[N_{\hat{m}}(S^{k+1})A^{k+1} - \tau\left(N_{\hat{m}}(S^k) * N_{SI}(S^k)\right) - \gamma k N_{\hat{m}}(S^k) + N_{\hat{m}}(S^{k-1})C^{k-1}\right]X^k \\
&+ \left[N_{\hat{m}}(S^{N-1})C^{N-1} - \gamma N N_{\hat{m}}(S^N)\right]X^N \\
=& \sum_{k=1}^{N-1}\left[N_{\hat{m}}(S^{k+1})A^{k+1} - \tau\left(N_{\hat{m}}(S^k) * N_{SI}(S^k)\right)\right]X^k \\
&- \sum_{k=1}^{N}\left[\gamma k N_{\hat{m}}(S^k) - N_{\hat{m}}(S^{k-1})C^{k-1}\right]X^k, \qquad (3.20)
\end{aligned}$$

where $*$ denotes component-wise multiplication. We note that the term containing X^0 vanishes because A^1 is a column vector with all zero entries. We now consider the summations involving the A and C matrices and the state $\mathcal{S}_j^k$. In this state there are k infected and $N-k$ susceptible individuals. Without loss of generality the susceptible individuals are numbered 1 to $N-k$ and the infected numbered from $N-k+1$ to N. Defining r_t to be the number of

infective neighbours of the node numbered t we then obtain:

$$\begin{aligned}
\left[N_{\hat{m}}(S^{k+1})A^{k+1}\right]_j &= \sum_{i=1}^{c_{k+1}} N_{\hat{m}}(S_i^{k+1})A_{i,j}^{k+1} \\
&= r_1\tau \Big[N_{\hat{m}}(S_j^k) + (\text{number of } \hat{m} \text{ gained by node 1 becoming infected }) \\
&\quad -(\text{number of } \hat{m} \text{ lost by node 1 becoming infected })] \\
&\quad + r_2\tau \Big[N_{\hat{m}}(S_j^k) + (\text{number of } \hat{m} \text{ gained by node 2 becoming infected }) \\
&\quad -(\text{number of } \hat{m} \text{ lost by node 2 becoming infected })] \\
&\quad + \dots \\
&\quad + r_{N-k}\tau \Big[N_{\hat{m}}(S_j^k) + (\text{number of } \hat{m} \text{ gained by node } (N-k) \text{ becoming infected }) \\
&\quad -(\text{number of } \hat{m} \text{ lost by node } (N-k) \text{ becoming infected })] \\
&= r_1\tau \Big[N_{\hat{m}}(S_j^k) + (\text{number of elements of } M_{k,j}^- \text{ where node 1 is susceptible} \\
&\qquad \text{and where node } 1's \text{ infection would lead to a motif of type } \hat{m}) \\
&\quad -(\text{number of elements of } M_{k,j} \text{ where node 1 is susceptible })] \\
&\quad + r_2\tau \Big[N_{\hat{m}}(S_j^k) + (\text{number of elements of } M_{k,j}^- \text{ where node 2 is susceptible} \\
&\qquad \text{and where node } 2's \text{ infection would lead to a motif of type } \hat{m}) \\
&\quad -(\text{number of elements of } M_{k,j} \text{ where node 2 is susceptible })] \\
&\quad + \dots \\
&\quad + r_{N-k}\tau \Big[N_{\hat{m}}(S_j^k) + (\text{number of elements of } M_{k,j}^- \text{ where node } (N-k) \text{ is susceptible} \\
&\qquad \text{and where node } (N-k)'s \text{ infection would lead to a motif of type } \hat{m}) \\
&\quad -(\text{number of elements of } M_{k,j} \text{ where node } (N-k) \text{ is susceptible })]\,,
\end{aligned}$$

grouping the terms we obtain,

$$\begin{aligned}
\left[N_{\hat{m}}(S^{k+1})A^{k+1}\right]_j =& \tau N_{SI}(S_j^k)N_{\hat{m}}(S_j^k) + \tau \sum_{i=1}^{|M_{k,j}^-|} \left[N_{in}^{SI}(\hat{m}_{k,j}^{i-}, \hat{m}) + N_{ex}^{SI}(\hat{m}_{k,j}^{i-}, \hat{m})\right] \\
& -\tau |M_{k,j}| N_{in}^{SI}(\hat{m}) - \tau \sum_{i=1}^{|M_{k,j}|} \left[N_{ex}^{SI}(\hat{m}_{k,j}^{i})\right].
\end{aligned}$$

Similarly,

$$\begin{aligned}
\left[N_{\hat{m}}(S^{k-1})C^{k-1}\right]_j &= \sum_{i=1}^{c_{k-1}} N_{\hat{m}}(S_i^{k-1})C_{i,j}^{k-1} \\
&= \gamma \Big[N_{\hat{m}}(S_j^k) + (\text{number of } \hat{m} \text{ gained by node } (N-k+1) \text{ recovering }) \\
&\quad -(\text{number of } \hat{m} \text{ lost by node } (N-k+1) \text{ recovering })] \\
&\quad +\gamma \Big[N_{\hat{m}}(S_j^k) + (\text{number of } \hat{m} \text{ gained by node } (N-k+2) \text{ recovering }) \\
&\quad -(\text{number of } \hat{m} \text{ lost by node } (N-k+2) \text{ recovering })] \\
&\quad +\dots \\
&\quad +\gamma \Big[N_{\hat{m}}(S_j^k) + (\text{number of } \hat{m} \text{ gained by node } (N) \text{ recovering }) \\
&\quad -(\text{number of } \hat{m} \text{ lost by node } (N) \text{ recovering })] \\
&= \gamma \Big[N_{\hat{m}}(S_j^k) + (\text{number of elements of } M_{k,j}^+ \text{ where node } (N-k+1) \text{ is infective} \\
&\qquad \text{and where node } (N-k+1)'s \text{ recovery would lead to a motif of type } \hat{m}) \\
&\quad -(\text{number of elements of } M_{k,j} \text{ of which node } (N-k+1) \text{ belongs })] \\
&\quad +\gamma \Big[N_{\hat{m}}(S_j^k) + (\text{number of elements of } M_{k,j}^+ \text{ where node } (N-k+2) \text{ is infective} \\
&\qquad \text{and where node } (N-k+2)'s \text{ recovery lead to a motif of type } \hat{m}) \\
&\quad -(\text{number of elements of } M_{k,j} \text{ of which node } (N-k+2) \text{ belongs })] \\
&\quad +\dots \\
&\quad +\gamma \Big[N_{\hat{m}}(S_j^k) + (\text{number of elements of } M_{k,j}^+ \text{ where node } (N) \text{ is infective} \\
&\qquad \text{and where node } N's \text{ recovery would lead to a motif of type } \hat{m}) \\
&\quad -(\text{number of elements of } M_{k,j} \text{ of which node } (N) \text{ belongs })]\,,
\end{aligned}$$

grouping the terms we obtain

$$\left[N_{\hat{m}}(S^{k-1})C^{k-1}\right]_j = \gamma k N_{\hat{m}}(S_j^k) + \gamma \sum_{i=1}^{|M_{k,j}^+|} N^I(\hat{m}_{k,j}^{i+}, \hat{m}) - \gamma |M_{k,j}| \left(N^I(\hat{m})\right).$$

Defining

$$\begin{aligned}
\mathcal{A}_j^{k+1} &= \tau \sum_{i=1}^{|M_{k,j}^-|} \left[N_{in}^{SI}(\hat{m}_{k,j}^{i-}, \hat{m}) + N_{ex}^{SI}(\hat{m}_{k,j}^{i-}, \hat{m})\right] - \tau |M_{k,j}| N_{in}^{SI}(\hat{m}) - \tau \sum_{i=1}^{|M_{k,j}|} \left[N_{ex}^{SI}(\hat{m}_{k,j}^{i})\right] \\
\mathcal{C}_j^{k-1} &= \gamma \sum_{i=1}^{|M_{k,j}^+|} \left[N^I(\hat{m}_{k,j}^{i+}, \hat{m})\right] - \gamma |M_{k,j}| \left(N^I(\hat{m})\right)
\end{aligned}$$

and setting $\mathcal{A}^{k+1} = [A_1^{k+1}, A_j^{k+1}, \ldots, A_{c_k}^{k+1}]$ and $\mathcal{C}^{k-1} = [C_1^{k-1}, C_j^{k-1}, \ldots, C_{c_{k-1}}^{k-1}]$ yields,

$$
\begin{aligned}
|\dot{\mathcal{M}}| =& \sum_{k=1}^{N-1} \left[N_{\hat{m}}(S^{k+1}) A^{k+1} - \tau \left(N_{\hat{m}}(S^K) * N_{SI}(S^k) \right) \right] X^k - \sum_{k=1}^{N} \left[\gamma k N_{\hat{m}}(S^k) - N_{\hat{m}}(S^{k-1}) C^{k-1} \right] X^k \\
=& \sum_{k=1}^{N-1} \left[\tau \left(N_{\hat{m}}(S^K) * N_{SI}(S^k) \right) + \mathcal{A}^{k+1} - \tau \left(N_{\hat{m}}(S^K) * N_{SI}(S^k) \right) \right] X^k - \\
& \sum_{k=1}^{N} \left[\gamma k N_{\hat{m}}(S^k) - \left(k N_{\hat{m}}(S^k) + \mathcal{C}^{k-1} \right) \right] X^k \\
=& \sum_{k=1}^{N-1} \left[\mathcal{A}^{k+1} \right] X^k + \sum_{k=1}^{N} \left[\mathcal{C}^{k-1} \right] X^k \\
=& \sum_{k=1}^{N-1} \sum_{j=1}^{c_k} \mathcal{A}_j^{k+1} X_j^k + \sum_{k=1}^{N} \sum_{j=1}^{c_k} C_j^{k-1} X_j^k \\
=& \sum_{k=1}^{N-1} \sum_{j=1}^{c_k} \left\{ \tau \sum_{i=1}^{|M_{k,j}^-|} \left[N_{in}^{SI}(\hat{m}_{k,j}^{i-}, \hat{m}) + N_{ex}^{SI}(\hat{m}_{k,j}^{i-}, \hat{m}) \right] - \tau |M_{k,j}| N_{in}^{SI}(\hat{m}) - \tau \sum_{i=1}^{|M_{k,j}|} \left[N_{ex}^{SI}(\hat{m}_{k,j}^{i}) \right] \right\} X_j^k \\
& + \sum_{k=1}^{N} \sum_{j=1}^{c_k} \left\{ \gamma \sum_{i=1}^{|M_{k,j}^+|} \left[N^I(\hat{m}_{k,j}^{i+}, \hat{m}) \right] - \gamma |M_{k,j}| \left(N^I(\hat{m}) \right) \right\} X_j^k \\
=& \tau \mathcal{N}_{in}^{SI}(\hat{m}^-, \hat{m}) + \tau \mathcal{N}_{ex}^{SI}(\hat{m}^-, \hat{m}) - \tau |\mathcal{M}| N_{in}^{SI}(\hat{m}) - \tau \mathcal{N}_{ex}^{SI}(\hat{m}) \\
& + \gamma \mathcal{N}^I(\hat{m}^+, \hat{m}) - \gamma |\mathcal{M}| N^I(\hat{m}).
\end{aligned}
$$

Which matches equation 3.17 from Theorem 1. □

It is worth noting that our result is related to the equation for the "expectation of some average quantity" given in Rand (1999). However, whilst the result in Rand (1999) is very general here we provide a proof by construction that, for a given motif, pinpoints the events that influence these motif and their rates.

3.6.2 Using the Theorem to prove the conjectured exact effective degree model is derivable from the Kolmogorov equations

Letting $\hat{m}$ be an $S_{s,i}$-type motif from the effective degree model earlier and using Theorem 1, we find that the exact equations can be written as

$$\begin{aligned}
\frac{dS_{s,i}}{dt} =& \tau\mathcal{N}_{in}^{SI}(\hat{m}^-,\hat{m}) + \tau\mathcal{N}_{ex}^{SI}(\hat{m}^-,\hat{m}) - \tau|\mathcal{M}|N_{in}^{SI}(\hat{m}) - \tau\mathcal{N}_{ex}^{SI}(\hat{m}) \\
&+ \gamma\mathcal{N}^{I}(\hat{m}^+,\hat{m}) - \gamma|\mathcal{M}|N^{I}(\hat{m}) \\
=& \tau \times (\text{the total expected number of SI connections within } S_{s+1,i-1}\text{-type motifs} \\
&\quad \text{where if infection occurs we obtain a } S_{s,i}\text{-type motif }) \\
&+ \tau \times (\text{the total expected number of SI connections where S lies within} \\
&\quad S_{s+1,i-1}\text{-type motifs and the I is external to the given motif} \\
&\quad \text{and where, were an infection to occur, we obtain a } S_{s,i}\text{-type motif }) \\
&- \tau S_{s,i} \times (\text{number of SI connections within an individual } S_{s,i}\text{-type motifs}) \\
&- \tau \times (\text{the total expected number of SI connections where S belongs to} \\
&\quad S_{s,i}\text{-type motifs and the I is external to the given motif }) \\
&+ \gamma \times (\text{the total expected number I's within } S_{s-1,i+1}\text{-type and } I_{s,i}\text{-type motifs} \\
&\quad \text{where there recovery would give a } S_{s,i}\text{-type motif }) \\
&- \gamma S_{s,i} \times (\text{number of I within an individual } S_{s,i}\text{-type motif}) \\
=& \tau\left[ISS_{s+1,i-1}\right] - \tau i S_{s,i} - \tau\left[ISS_{s,i}\right] + \gamma I_{si} + \gamma(i+1)S_{s-1,i+1} - \gamma i S_{s,i}
\end{aligned}$$

which is indeed the conjectured exact equation for $S_{s,i}$ (similar derivation holds for $I_{s,i}$). To clarify the above derivation we note that a term such as $\tau\mathcal{N}_{in}^{SI}(\hat{m}^-,\hat{m})$ will make no contribution to the resultant equation as there are no internal SI connections within $S_{s-1,i+1}$-type motifs along which an infection would lead to an $S_{s,i}$-type motif. However other terms, such as $\tau\mathcal{N}_{ex}^{SI}(\hat{m}^-,\hat{m})$, have a direct correspondence with the resultant output (in this case the $\tau\left[ISS_{s+1,i-1}\right]$ term).

3.7 Comparison of the closed models

In comparing the models the obvious question to ask is when does one model perform better than another, i.e. which model approximates better or more accurately the simulation results or the solution of the Kolmogorov/master equations where solvable. As discussed earlier, the pairwise model is known to perform well on networks that are well characterised by the average degree (i.e. regular random and Erdős-Rényi graphs). What is less known is under what circumstances do the heterogenous pairwise and effective degree models outperform one another.

To assess the performance of the three closed models we compared individual simulations

to the solutions of the ODE's on four different types of undirected network. For each of the different types of networks we used the Gillespie algorithm (Gillespie, 1977) to run 500 simulations on networks of size $N = 500$ (1 simulation on 500 different randomly generated networks). The results of these simulations were then averaged to obtain an expected value to compare to the solution of the various ODE's. We began by considering regular random networks where all nodes have the same number of randomly chosen neighbours and then Erdős-Rényi random networks where the distribution of degrees converges to a Poisson distribution. Figure 3.3 plots simulation results against the different solutions of the ODEs for these two networks. On the regular network, whilst the two different pairwise models and the effective degree offer an improvement in performance over the standard meanfield equations, there is little to distinguish between the improved approaches. As expected, on the Erdős-Rényi random networks, the pairwise model improves on the meanfield model and, in turn, the effective degree and heterogeneous pairwise models improve even further on this. Again, however, there is little to distinguish between effective degree and the heterogeneous pairwise models.

To investigate further we ran simulations on networks exhibiting greater heterogeneity in their degree distribution. Firstly we considered networks with degrees between 1 and 25 chosen from a powerlaw degree distribution ($p(x) = Ax^{-1.5}$) and generated by the configuration model algorithm (Newman, 2003a). Networks with scale-free like degree distributions may be more closely related to those of real world networks (Barabási, 2009) and may thus be of greater use in understanding the applicability of more theoretical modelling approaches. Secondly we considered graphs with the same power law degree distributions as before but this time rewired based on the "greedy" assortativity algorithm (discussed in Winterbach et al. (2012)). This rewiring leads to an increase in the assortativity coefficient (Newman, 2003b) which measures the propensity of nodes of similar degrees to attach to one another. In theory, we should be able to capture this correlation with the heterogenous pairwise equations as they explicitly take the degree of connected nodes into account within the initial conditions. The results are illustrated in Fig. 3.4.

Whilst on the powerlaw network there is little difference between heterogeneous pairwise and effective degree when the assortativity is increased, there is a clear improvement in the performance of the heterogenous pairwise model over the effective degree. Any performance benefit must, however, be considered in terms of the model complexity given in table 3.3 (note that in this table M is the maximum possible degree in the network and we given the minimum number of equations needed to implement the ODEs).

A final comparison between the performance of the different closed models is to look at their rate of convergence to the solution of the Kolmogorov equations on a complete (fully connected) network. On a complete network it is possible (see Simon et al. (2011)) to reduce the full system of 2^N equations to just $N + 1$ equations. This allows us to compare the true solution to the approximate solution of the meanfield, pairwise (equivalent to heterogenous

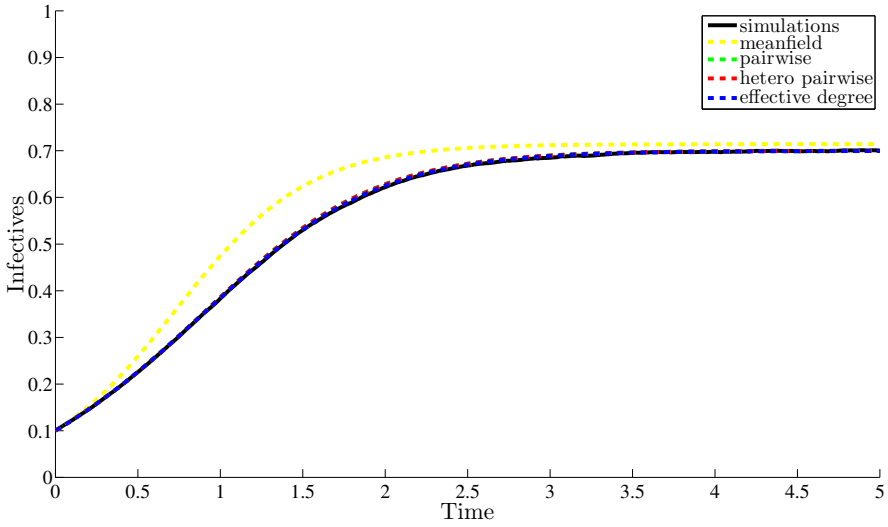

(a) Regular random

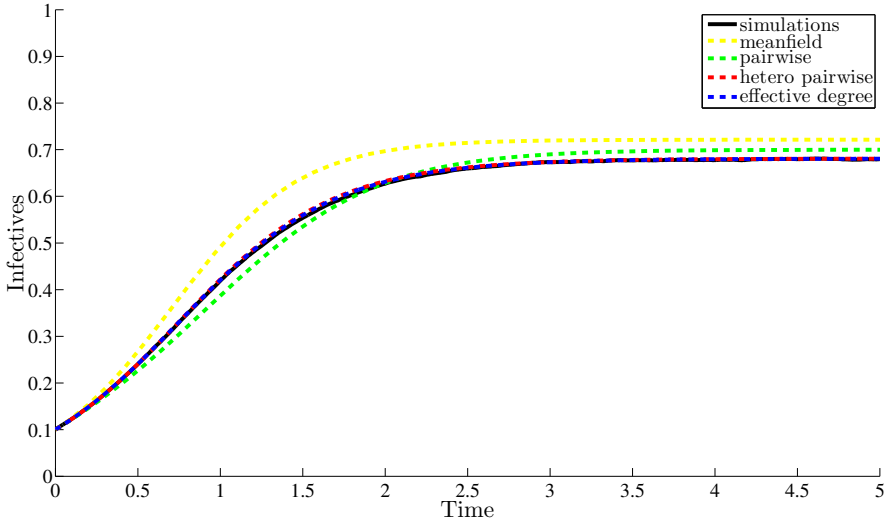

(b) Erdos-Renyi

Figure 3.3: **ODE performance on different networks** Each network is of size $N = 500$ and with disease parameters given by $\gamma = 1$ and $\tau = 0.5$. Average prevalence was calculated from individual simulations on 500 different networks. Initial conditions for the ODEs were obtained by averaging the initial conditions from each of the simulations. (a) Regular random network, each node having degree 7. (b) Erdős-Rényi random network with average degree 7.

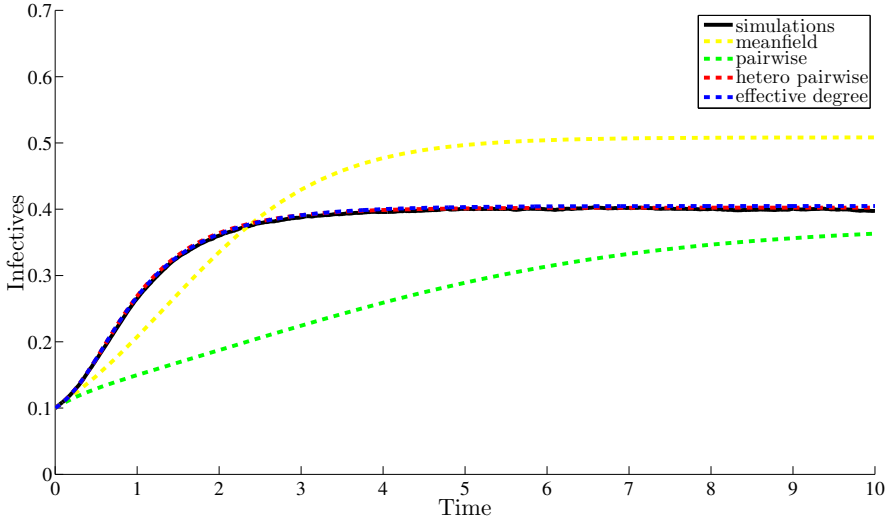

(a) Power-law

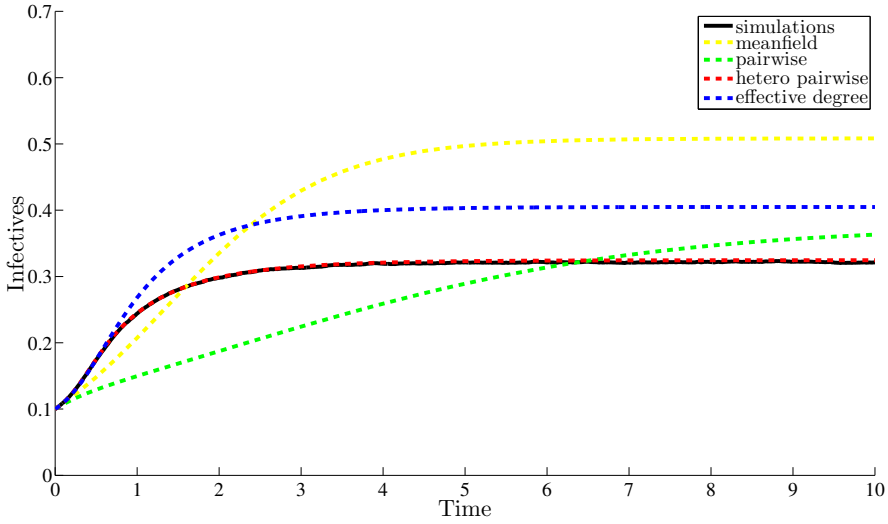

(b) Assortative power-law

Figure 3.4: **ODE performance on different networks.** Each network is of size $N = 500$ and with disease parameters given by $\gamma = 1$ and $\tau = 0.5$. Average prevalence was calculated from individual simulations on 500 different networks. Initial conditions for the ODEs were obtained by averaging the initial conditions from each of the simulations. (a) Network with degrees chosen from a power law distribution (b) Networks with degrees chosen from a powerlaw distribution but rewired to have assortativity coefficient $r \approx 0.49$.

Table 3.3: Complexity of closed ODEs

Model	# equations	complexity
meanfield	1	$\mathcal{O}(1)$
pairwise	3	$\mathcal{O}(1)$
effective degree	$M(M+3)-1$	$\mathcal{O}(M^2)$
heterogeneous pairwise	$2M(M+1)-1$	$\mathcal{O}(M^2)$
Kolmogorov equations	2^N	$\mathcal{O}(2^N)$

pairwise on a complete graph) and effective degree models. Interestingly we find that all three exhibit $O(1/N)$ convergence, where although both pairwise and effective degree bring an improvement on meanfield, the difference between the convergence of the two is neglible and almost indecernible (see Fig. 3.5).

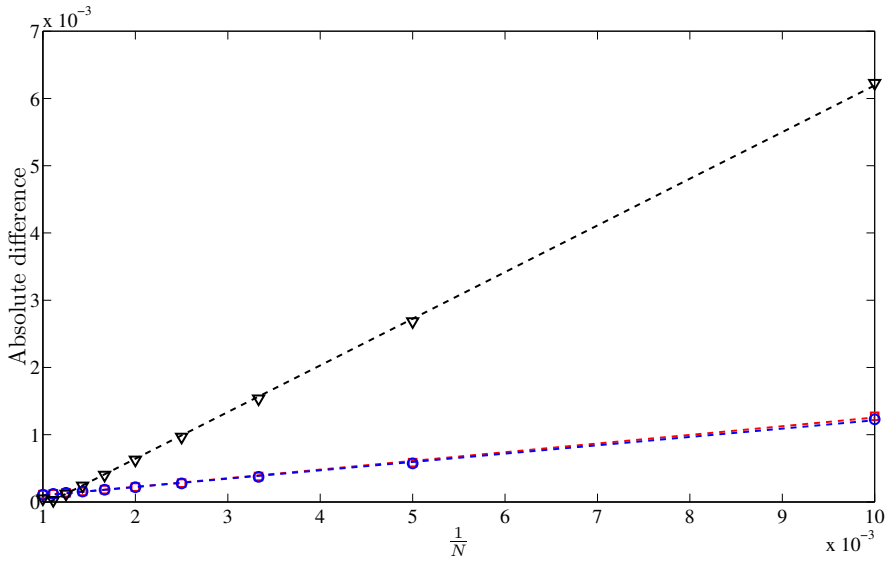

Figure 3.5: **Convergence to exact solution on a complete graph.** Absolute difference between the exact steady state solution of the percentage of infected individuals and those calculated from three different ODE models for 10 different network sizes and initial prevalence of 40 percent. Black triangles represent meanfield, blue circles effective degree and red squares the pairwise equations. Linear lines of best fit are also shown. This shows that the error(N) appears to be of O(1/N) as N tends to infinity.

3.8 Discussion

In this paper we set out to achieve a greater understanding of the relation between some of the more common approaches to modelling disease dynamics. In doing so we conjectured an exact version of the effective degree model (Lindquist et al., 2011) and showed how this model could be used to recover the pairwise model (Keeling, 1999). We then extended this

model to incorporate greater network structure and illustrated how, from this extension, we could then recover the heterogeneous pairwise model (Eames and Keeling, 2002). We then proved that the conjectured exact effective degree model was indeed exact by proving that a heuristic derivation of an ODE model for an arbitrary motif was derivable directly from the Kolmogorov equations and noting that the exact effective degree model was just a particular case of this heuristic model. Finally we considered the performance of the different models on four different type of networks and have analysed numerically the rate of convergence to the lumped Kolmogorov equations on a complete network. These comparisons suggest a performance hierarchy of models as illustrated in Fig. 3.6 and it is worth noting that the performance benefit of the heterogenous pairwise model on networks exhibiting susceptible $\rightarrow$ infectious $\rightarrow$ removed (SIR) disease dynamics was also touched upon in Danon et al. (2011).

Whilst we have shown how current models can be extended in a way that can capture more network topology, these extensions have a more theoretical rather than practical motivation as their added complexity makes them not only less tractable but also more resource intensive in their solving, thus making the use of simulations more of an attractive proposition. As the links between these models are better understood, future work will likely focus on the following three areas. Firstly, a more realistic network will have a more clique-like structure. For example an individual is likely a member of a household in which he has regular contacts within and less regular contacts outside. Being able to incorporate this household structure within epidemic models is thus important in understanding the outbreak and necessary curtailment of an infectious disease (see Ball et al. (2010); House and Keeling (2008); Volz et al. (2011)). Secondly, a network of individuals is not well represented by a static network. An individual may have regular contact with few individuals but may create or break contacts with others in ways that a static network representation cannot capture. For this reason it is important to take into consideration not only the dynamics of the disease but also the dynamics of the network and how the two impact on one another (see Gross et al. (2006); Kiss et al. (2012)). Thirdly, assuming we can write down exact differential equations we have to close them in some way. Understanding the performance of current, and also the derivation of new closures, is arguably the most important task ahead as it is the closures that limit the performance of any system of ODEs.

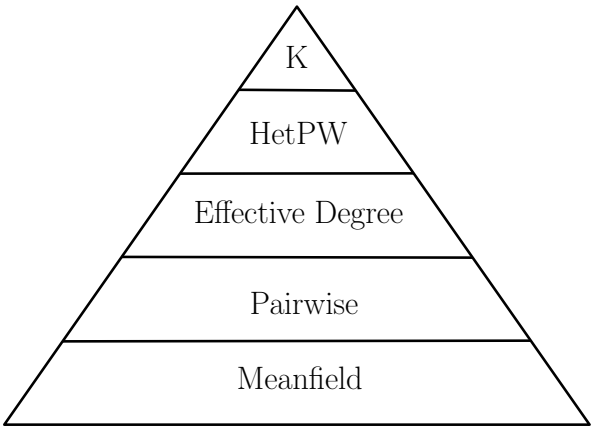

Figure 3.6: **Model performance hierarchy.** Model performance hierarchy based on our observations. Here K represents the Kolmogorov equations and HetPW the heterogeneous pairwise equations.

Acknowledgments We thank the two referees for their careful consideration of the manuscript and their suggestions that improved the clarity and presentation of the paper.

3.9 Appendices

3.9.1 Appendix 1

Illustration of the exact effective degree transitions where the central node is infective.

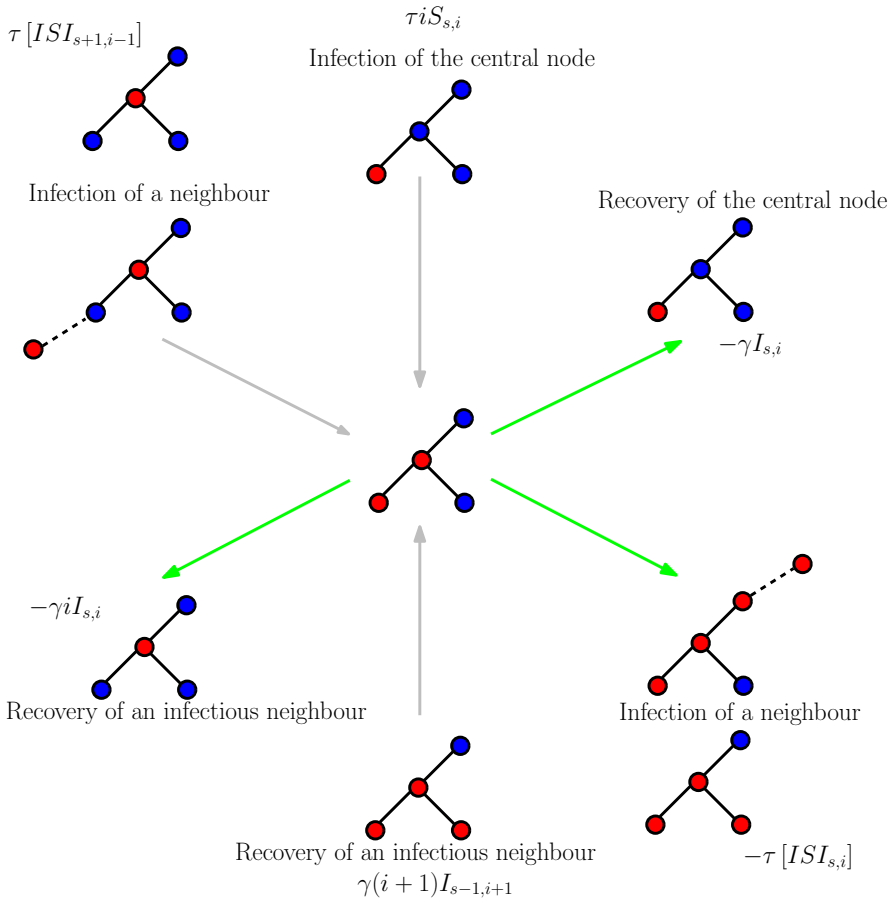

Figure 3.7: Illustration of the transitions into and out of the $I_{2,1}$ class. Susceptible nodes are given in blue and infective nodes in red. Transitions into and out of the class are shown in grey and green, respectively. The corresponding terms of the general equation are also given.

3.9.2 Appendix 2

Derivation of the pairwise equation from the exact effective degree model for singles and pairs are as follows,

$$\frac{d}{dt}[S] = \sum_{s,i} \dot{S}_{s,i} = \gamma[I] - \tau[SI],$$
$$\frac{d}{dt}[I] = \sum_{s,i} \dot{I}_{s,i} = -\gamma[I] + \tau[SI],$$

where most terms from the original effective degree equations cancel and we have used that $\sum_{s,i} iS_{s,i} = [SI]$ and $\sum_{s,i} I_{s,i} = [I]$. For the pairs the effective degree model yields,

$$\begin{aligned}
\frac{d}{dt}[SS] =& \sum_{s,i} s\dot{S}_{si} \\
=& -\tau \sum siS_{s,i} + \gamma \sum sI_{s,i} + \gamma \sum s(i+1)S_{s-1,i+1} - \gamma \sum isS_{s,i} \\
&+ \tau \sum s[ISS_{s+1,i-1}] - \tau \sum s[ISS_{s,i}] \\
=& -\tau[ISS] + \gamma[IS] + \gamma \sum (s-1)(i+1)S_{s-1,i+1} + \gamma \sum (i+1)S_{s-1,i+1} \\
&- \gamma[ISS] + \tau \sum (s+1)[ISS_{s+1,i-1}] - \tau \sum [ISS_{s+1,i-1}] - \tau \sum s[ISS_{s,i}] \\
=& -\tau[ISS] + \gamma[IS] + \gamma[ISS] + \gamma[IS] - \gamma[ISS] - \tau[ISS] \\
=& -2\tau[ISS] + 2\gamma[IS],
\end{aligned}$$

$$\begin{aligned}
\frac{d}{dt}[SI] =& \sum_{s,i} s\dot{I}_{si} \\
=& \tau \sum siS_{s,i} - \gamma \sum sI_{s,i} + \gamma \sum s(i+1)I_{s-1,i+1} - \gamma \sum siI_{s,i} \\
&+ \tau \sum s[ISI_{s+1,i-1}] - \tau \sum s[ISI_{s,i}] \\
=& \tau[ISS] - \gamma[IS] + \gamma \sum (s-1)(i+1)I_{s-1,i+1} + \gamma \sum (i+1)I_{s-1,i+1} \\
&- \gamma[IIS] + \tau \sum (s+1)[ISI_{s+1,i-1}] - \tau \sum [ISI_{s+1,i-1}] - \tau \sum s[ISI_{s,i}] \\
=& \tau[ISS] - \gamma[IS] + \gamma[IIS] + \gamma[II] - \gamma[IIS] - \tau([ISI] + [IS]) \\
=& \tau([ISS] - [ISI] - [IS]) + \gamma([II] - [IS]),
\end{aligned}$$

$$
\begin{aligned}
\frac{d}{dt}[II] =& \sum_{s,i} i\dot{I}_{si} \\
=& \tau \sum i^2 S_{s,i} - \gamma \sum i I_{s,i} + \gamma \sum i(i+1) I_{s-1,i+1} - \gamma \sum i^2 I_{s,i} \\
& + \tau \sum i[ISI_{s+1,i-1}] - \tau \sum i[ISI_{s,i}] \\
=& \tau \sum i(i-1) S_{s,i} + \tau \sum i S_{s,i} - \gamma[II] \\
& + \gamma[III] - \gamma \sum i(i-1) I_{s,i} - \gamma \sum i I_{s,i} \\
& + \tau \sum (i-1)[ISI_{s+1,i-1}] + \tau \sum [ISI_{s+1,i-1}] - \tau \sum i[ISI_{s,i}] \\
=& \tau[ISI] + \tau[IS] - \gamma[II] + \gamma[III] - \gamma[III] - \gamma[II] + \tau[ISI] + \tau[IS] \\
=& 2\tau([ISI] + [IS]) - 2\gamma[II].
\end{aligned}
$$

3.9.3 Appendix 3

Derivation of the heterogeneous pairwise equations from the effective degree with neighbourhood composition model. For singles and pairs the following identities hold,

$$\frac{d}{dt}\left[S^n\right] = \sum_{|s'|+|i'|=N} \dot{S}_{s',i'} = \gamma\left[I^n\right] - \tau\left[S^n I\right],$$
$$\frac{d}{dt}\left[I^n\right] = \sum_{|s'|+|i'|=N} \dot{I}_{s',i'} = -\gamma\left[I^n\right] + \tau\left[S^n I\right],$$

$$\begin{aligned}
\frac{d}{dt}\left[S^l S^n\right] &= \sum_{|s'|+|i'|=n} s_l \dot{S}_{s',i'} \\
&= -\tau \sum s_l |i'| S_{s',i'} + \gamma \sum s_l I_{s',i'} + \gamma \sum s_l \sum_{k=1}^{M} (i_k+1) S_{s'_{k-},i'_{k+}} \\
&\quad - \gamma \sum s_l |i'| S_{s',i'} + \tau \sum s_l \sum_{k=1}^{M} \left[IS^k S_{s'_{k+},i'_{k-}}\right] - \tau \sum s_l \left[IS S_{s',i'}\right] \\
&= -\tau \left[IS^n S^l\right] + \gamma \left[S^l I^n\right] + \gamma \sum s_l \sum_{k\neq l} (i_k+1) S_{s'_{k-},i'_{k+}} \\
&\quad + \gamma \sum (s_l-1)(i_l+1) S_{s'_{l-},i'_{l+}} + \gamma \sum (i_l+1) S_{s'_{l-},i'_{l+1}} - \gamma \left[IS^n S^l\right] \\
&\quad + \tau \sum s_l \sum_{k\neq l} \left[IS^k S_{s'_{k+},i'_{k-}}\right] + \tau \sum (s_l+1) \left[IS^l S_{s'_{l+},i'_{l-}}\right] \\
&\quad - \tau \sum \left[IS^l S_{s'_{l+},i'_{l-}}\right] - \tau \sum s_l \left[IS S_{s',i'}\right] \\
&= -\tau \left[IS^n S^l\right] + \gamma \left[S^l I^n\right] + \gamma \left[S^l S^n I\right] + \gamma \left[I^l S^n\right] \\
&\quad - \gamma \left[IS^n S^l\right] - \tau \left[IS^l S^n\right] \\
&= -\tau \left[IS^n S^l\right] - \tau \left[IS^l S^n\right] + \gamma \left[S^l I^n\right] + \gamma \left[I^l S^n\right],
\end{aligned}$$

$$
\begin{aligned}
\frac{d}{dt}\left[S^l I^n\right] =& \sum_{|s'|+|i'|=n} s_l \dot{I}_{s',i'} \\
=& \tau \sum s_l |i'| S_{s',i'} - \gamma \sum s_l I_{s',i'} + \gamma \sum s_l \sum_{k=1}^{M} (i_k+1) I_{s'_{k-},i'_{k+}} \\
& - \gamma \sum s_l |i'| I_{s',i'} + \tau \sum s_l \sum_{k=1}^{M} \left[IS^k I_{s'_{k+},i'_{k-}}\right] - \tau \sum s_l \left[IS I_{s',i'}\right] \\
=& \tau \left[IS^n S^l\right] - \gamma \left[S^l I^n\right] + \gamma \sum s_l \sum_{k\neq l} (i_k+1) I_{s'_{k-},i'_{k+}} \\
& + \gamma \sum (s_l - 1)(i_l+1) I_{s'_{l-},i'_{l+}} + \gamma \sum (i_l+1) I_{s'_{l-},i'_{l+1}} - \gamma \left[II^n S^l\right] \\
& + \tau \sum s_l \sum_{k\neq l} \left[IS^k I_{s'_{k+},i'_{k-}}\right] + \tau \sum (s_l+1) \left[IS^l I_{s'_{l+},i'_{l-}}\right] \\
& - \tau \sum \left[IS^l I_{s'_{l+},i'_{l-}}\right] - \tau \sum s_l \left[IS I_{s',i'}\right] \\
=& \tau \left[IS^n S^l\right] - \gamma \left[S^l I^n\right] + \gamma \left[S^l I^n I\right] + \gamma \left[I^l I^n\right] \\
& - \gamma \left[II^n S^l\right] - \tau \left[IS^l I^n\right] - \tau \left[S^l I^n\right] \\
=& \tau \left[IS^n S^l\right] - \tau \left[IS^l I^n\right] - \tau \left[S^l I^n\right] + \gamma \left[I^l I^n\right] - \gamma \left[S^l I^n\right],
\end{aligned}
$$

$$
\begin{aligned}
\frac{d}{dt}\left[I^l I^n\right] =& \sum_{|s'|+|i'|=n} i_l \dot{I}_{s',i'} \\
=& \tau \sum i_l |i'| S_{s',i'} - \gamma \sum i_l I_{s',i'} + \gamma \sum i_l \sum_{k=1}^{M} (i_k+1) I_{s'_{k-},i'_{k+}} \\
& - \gamma \sum i_l |i'| I_{s',i'} + \tau \sum i_l \sum_{k=1}^{M} \left[IS^k I_{s'_{k+},i'_{k-}}\right] - \tau \sum i_l \left[IS I_{s',i'}\right] \\
=& \tau \sum i_l \left(|i'|-1\right) S_{s',i'} + \tau \sum i_l S_{s',i'} - \gamma \left[I^l I^n\right] \\
& + \gamma \left[I^l I^n I\right] - \gamma \sum i_l \left(|i'|-1\right) I_{s',i'} - \gamma \sum i_l I_{s',i'} \\
& + \tau \sum i_l \sum_{k\neq l} \left[IS^k I_{s'_{k+},i'_{k-}}\right] + \tau \sum (i_l - 1) \left[IS^l I_{s'_{l+},i'_{l-}}\right] \\
& + \tau \sum \left[IS^l I_{s'_{l+},i'_{l-}}\right] - \tau \sum i_l \left[IS I_{s',i'}\right] \\
=& \tau \left[I^l S^n I\right] + \tau \left[I^l S^n\right] - 2\gamma \left[I^l I^n\right] \\
& + \gamma \left[I^l I^n I\right] - \gamma \left[I^l I^n I\right] + \tau \left[IS^l I^n\right] + \tau \left[S^l I^n\right] \\
=& \tau \left[I^l S^n I\right] + \tau \left[I^l S^n\right] - 2\gamma \left[I^l I^n\right] + \tau \left[IS^l I^n\right] + \tau \left[S^l I^n\right].
\end{aligned}
$$

Chapter 4

Paper 2: Modelling approaches for simple dynamic networks and applications to disease transmission models

Istvan Z. Kiss[1], Luc Berthouze[2], Timothy J. Taylor[1,2] and Péter L. Simon[3] [1]School of Mathematical and Physical Sciences, Department of Mathematics, University of Sussex, Brighton BN1 9QH, UK
[2]Centre for Computational Neuroscience and Robotics, University of Sussex, Brighton BN1 9QH, UK
[3]Institute of Mathematics, Eötvös Loránd University Budapest, Budapest, Hungary

Published in *Proceedings A: Mathematical, Physical and Engineering Sciences , 468 (2141). pp. 1332-1355. ISSN 1471-2946*

4.1 Abstract

In this paper a random link activation-deletion (RLAD) model is proposed that gives rise to a stochastically evolving network. This dynamic network is then coupled to a simple (SIS) dynamics on the network and the resulting spectrum of model behaviour is explored via simulation and a novel pairwise model for dynamic networks. First, the dynamic network model is systematically analysed by considering link-type independent and dependent network dynamics coupled with globally constrained link creation. This is done rigorously with some analytical results and we highlight where such analysis can be performed and how these simpler models provide a benchmark to test and validate full simulations. The pairwise model is used to study the interplay between SIS-type dynamics on the network and link-type dependent activation-deletion. Assumptions of the pairwise model are identified and their implications interpreted in a way that complements our current understanding. Furthermore, we also discuss how the strong assumptions of the closure relations can lead to disagreement between the simulation and pairwise model. Unlike on a static network, the resulting spectrum of behaviour is more complex with the prevalence of infections exhibiting not only a single steady-state but also bistability and oscillations.

4.2 Introduction

Many real-world systems ranging from neuroscience and epidemiology to computer sciences and socioeconomics can be represented as well-defined units interacting via a static or dynamic set of links or connections, e.g., Kossinets and Watts (2006); Vernon and Keeling (2009); Sporns (2011a); Broder et al. (2000). The wide applicability of networks as a modelling tool has captured the attention of many different research communities and has lead to the development of a large body of research at the interface of network/graph theory, stochastic processes, probability theory, discrete mathematics and computer sciences (Albert and Barabási, 2002b; Newman, 2003a). Initially, most of the research concentrated on the structure and properties of real-world networks and aimed to understand and uncover the laws that gave rise to the observed or empirical networks. In parallel a different research direction emerged, namely, the study of how the properties and structure of the network impact on the dynamical processes taking place on it (e.g. flow of information on the WWW, disease transmission on social networks, self organization of neurons). While earlier research focused on the dynamics or evolution of networks (Chan et al., 2003; Dorogovtsev and Mendes, 2002) without considering the dynamical processes they support, latter research considered fixed and static networks and mainly focused on the dynamics on networks. However, in many cases considering both the dynamics of the network and on the network is essential to understand the problem that is being modelled, but, doing so raises several challenges. Firstly, capturing and modelling the interaction between the two dynamics is non-trivial with little empirical evidence and second, the increased complexity reduces analytical tractability with

results mainly relying on simulation.

Over the last few years various simple classes of models have been proposed where both the dynamics of the network and on the network are considered (Gross and Blasius, 2008). For example, Saramäki and Kaski (2005) proposed a model where nodes are distributed on a ring and links are divided into short-range (SR) and long-range (LR) links. SR links are considered to be fixed and connect nodes to their nearest neighbours. LR links vary randomly, meaning that an infected node tries to infect with some probability a node chosen at random and succeeds to do so if the chosen individual is susceptible. The authors formulated a simple ODE model that is similar to pairwise models and used this to derive analytic results for disease transmission threshold and to validate simulation results.

Gross et al. (2006) proposed a network-based model where (SI) links are broken at a certain rate with susceptible nodes immediately re-wiring to other susceptible nodes chosen at random from the entire population. Again, a simple pairwise type model was used to derive a low dimensional dynamical system that describes the interaction of network and disease dynamics. This model operates on the strong assumption that the status of each node is globally available. Risau-Gusman and Zanette (2009) relaxed the assumptions of the model proposed by Gross et al. (2006) and considered the case when the susceptible node from an (SI) pair re-wires to a node chosen at random from the entire network regardless of its state. They generalised the model further and considered the case where not only susceptible nodes are allowed to change their contacts but also the infectious nodes can do so. In this model, when an SI link is cut, the I node will reconnect with probability q to a node chosen at random and independently of its state, and with probability $1-q$ the susceptible node will keep the contact and look to reconnect at random. Both papers use pair-approximation models to validate simulation results.

Grindrod and Higham (2010) proposed two simple models of undirected evolving graphs by starting from the complete state space $\mathcal{S}$ with $\mathcal{S} = 2^{N(N-1)/2}$ possible elements or different graphs over N nodes. With this in place, the evolution of a graph can be represented as a path in the state space $\mathcal{S}$ governed by some stochastic process $P(G_{i+1}|G_i, G_{i-1}, \dots)$, where G_i is the state of the graph, represented as a symmetric adjacency matrix, at discrete time step i. While this formulation is exact and can be extended to continuous time, the drawback of this approach comes from the large number of transition probabilities for time independent processes (i.e. $2^{N(N-1)}$) or the Kolmogorov transition equations (i.e. $2^{N(N-1)/2}$). The authors proposed an edge birth and death model where each edge can become activated or deleted at a fixed probability that is independent of all other edges or the current state of the graph. They extended this to a more sophisticated model where link activation and deletion depends on some form of proximity between edges as given by the initial setup of the nodes (e.g. fixed location on a line with nodes connected according to some connectivity kernel). The aim of their study was twofold: first to use such models to simulate a series of dynamic or evolving networks and second, to fit evolving network models to data and use likelihood-based

estimation of model parameters.

Miller et al. (2012) and Volz and Meyers (2007), using the probability generating function (PGF) formalism or edge-based compartmental modelling, have recently also studied a variety of dynamic network models (e.g. MFSH (mean-filed social heterogeneity) and dynamic fixed degree with or without dormant contacts) coupled with SIR (susceptible-infectious-recovered) dynamics. However, these network dynamics are not coupled with the epidemic and the authors propose low-dimensional ODEs that capture the time evolution of the epidemic well. Calculation of the basic reproductive number, R_0, are also presented with focus on the impact of partnership duration and social heterogeneity on epidemics.

In this paper, we consider a set of simple dynamic networks based on the link birth-and-death or activation-deletion model, and also a variant of this, where link birth/activation is globally constrained. In order to provide a succinct overview of different analytical methodologies and their limits when applied to such models, the paper considers four scenarios of increasing complexity: the impact of simple network dynamics on the structure of the network when node dynamic is absent (Section 3.3, unconstrained and globally constrained link creation), when the nodes are static but labeled (Section 3.4) and when the dynamic network is coupled with SIS (susceptible-infectious-suceptible) node dynamics (Section 3.5). To conclude we study in-depth the impact of network dynamics and its coupling with the disease transmission on the outcome of epidemics (Section 3.6). For the first three models, results are obtained by using the exact formulation in terms of Markov Chains and Kolmogorov equations and a mean-field type approach with further results from simulation. These methodologies cannot deal with the final scenario, however, the output of the analytical models can be used as a benchmark to test the validity of the full simulation model. The full simulation model is used in conjunction with a novel pairwise approximation to investigate and characterise the full spectrum of behaviour. The agreement between simulation and pairwise model is discussed in detail. This is done by providing some new insight into how the assumptions of the pairwise model can be interpreted and how the strong assumptions of the closure relation can lead to disagreement between the two models. Parameter regimes where agreement is excellent are identified, however, many open questions remain regarding the exact relation between simulation results and output from the pairwise model.

4.3 Simple models of stochastically evolving networks

In this Section, the impact of simple network dynamics on the structure and properties of the network is explored. We present different modelling techniques to derive exact or approximation models and compare these to simulation results. Two simple network dynamics are considered: (i) random Link Activation-Deletion (RLAD) whereby non-active or non-existing links are activated with a given rate (e.g. α) while existing ones are deleted with some other rate (e.g. ω) and (ii) globally-constrained RLAD whereby the above link creation process is

constrained globally, i.e. the higher the number of active links the lower the rate at which new links are activated. Initially, the simple *dynamics of the network* are studied without considering any *dynamics on the network* or any link activation or deletion that may depend on node labels.

4.3.1 Random link activation-deletion: probabilistic approach

Let us consider an undirected and unweighted network with N nodes where the maximum number of edges is $M = N(N-1)/2$. The dynamics of edges evolve according to the following two simple rules. Non-active or absent links are activated independently at random at rate α while existing links are broken independently at random at rate ω. Let $(X(t))_{t\geq 0}$ be an integer valued random variable that represents the number of edges/links in the network at time t. If $P(X(t) = k) = p_k(t)$ then the Kolmogorov equations for p_k are given by

$$\frac{dp_k(t)}{dt} = \alpha[M-(k-1)]p_{k-1}(t) - [\alpha(M-k)+\omega k]p_k(t) + \omega(k+1)p_{k+1}(t), \tag{4.1}$$

where $k = 0, 1, 2, \ldots, M$ with $p_{M+1}(t) = p_{-1}(t) = 0$ (no link activation when $k = M$ and no link deletion when $k = 0$). The average number of edges in the graph at time t can be defined as $K_1(t) = \sum_{k=0}^{M} kp_k(t)$. Upon using Eq. (4.1) and after some simple algebra, the equation for $K_1(t)$ follows easily and is given by

$$\dot{K}_1(t) = \sum_{k=0}^{M} k\dot{p}_k(t) = \alpha M - (\alpha+\omega)K_1(t). \tag{4.2}$$

Hence, at equilibrium

$$K_1^{eq} = \frac{\alpha M}{\alpha+\omega}.$$

The equilibrium value can also be found heuristically by determining the number of edges K_1^{eq} at which the total rate of link activation ($\alpha(M - K_1^{eq})$) is balanced by the total rate of link deletion (ωK_1^{eq}). For this setup, the average number of links per node or average node degree is given by

$$\langle k\rangle(t) = \frac{2\sum_{k=0}^{M} kp_k(t)}{N} = \frac{2K_1(t)}{N}.$$

A traditional and commonly used method to determine the probability distribution as given by the forward Kolmogorov equations above (Eq. (4.1)) is via the probability generating function (PGF) technique. This is defined as

$$G(t,s) = \sum_{k=0}^{M} p_k(t)s^k, \tag{4.3}$$

where s is a placeholder variable that allows to concentrate all the information about the probability distribution into one single function. Multiplying Eq. (4.1) by s^k, followed by

summation for $k = 0, 1, \ldots, M$ and some simple calculations gives rise to the following partial differential equation

$$\frac{\partial G(t,s)}{\partial t} = (1-s)(\alpha s + \omega)\frac{\partial G(t,s)}{\partial s} - \alpha M(s-1)G(t,s), \tag{4.4}$$

$$G(0,s) = s^{m_0} \quad \text{for} \quad (t,s) \in [0,\infty) \times (0,1), \tag{4.5}$$

where the initial condition corresponds to starting with m_0 edges (i.e. $p_{m_0}(0) = 1$ and $p_k(0) = 0$ for $\forall k \in \{0, 1, 2, \ldots, M\} \setminus \{m_0\}$). This is a first-order homogeneous partial differential equation that can be solved using the method of characteristics and its solution is given by

$$G(t,s) = \left(\frac{\omega + \alpha s + \omega(s-1)e^{-(\alpha+\omega)t}}{\omega + \alpha s + \alpha(1-s)e^{-(\alpha+\omega)t}}\right)^{m_0} \left(\frac{\omega + \alpha s + \alpha(1-s)e^{-(\alpha+\omega)t}}{\alpha + \omega}\right)^{M}. \tag{4.6}$$

From the equation above, $K_1(t)$, the expected number of edges in the network is given by $\frac{\partial G(t,1)}{\partial s}$, and in the limit of $t \to \infty$, $K_1(t)$ tends to its equilibrium value defined as

$$K_1^{eq} = \lim_{t\to\infty} \frac{\partial G(t,1)}{\partial s} = \frac{\alpha M}{\alpha + \omega}. \tag{4.7}$$

Moreover for $t \to \infty$

$$G(t,s) \to \left(\frac{\alpha}{\alpha+\omega}s + \frac{\omega}{\alpha+\omega}\right)^{M}, \tag{4.8}$$

which is the generating function of the binomial distribution with M trials and a per-trial probability of success $p = \alpha/(\alpha + \omega)$. The excellent agreement between the exact model and simulation is shown in Fig. 4.1(a), and confirms that the formulation of the two models is correct and consistent. The number of equations in the exact model scale as $O(N^2)$ which restricts its applicability to small networks.

4.3.2 Random link activation-deletion: mean-field approach

To overcome the limitations of the exact model and to gain more insight into the properties or structure of the network a different modelling approach is presented below. Here, the network is considered as a population of nodes where nodes can be classified according to their number of links/contacts and the rates of moving to either more highly or less well connected classes. Hence, the modelling relies on deriving evolution equations for the number of nodes with degree $0, 1, 2, \ldots, N-1$. Let n_k denote the number of nodes with k contacts where $0, 1, 2, \ldots, N-1$. Based on simple heuristic reasoning the evolution equations for n_ks

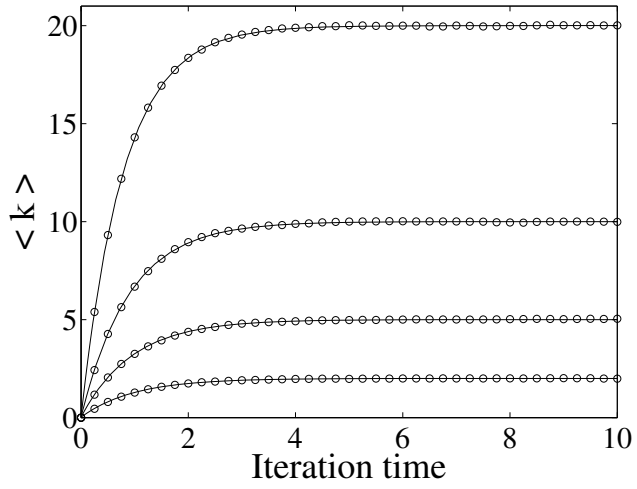

(a)

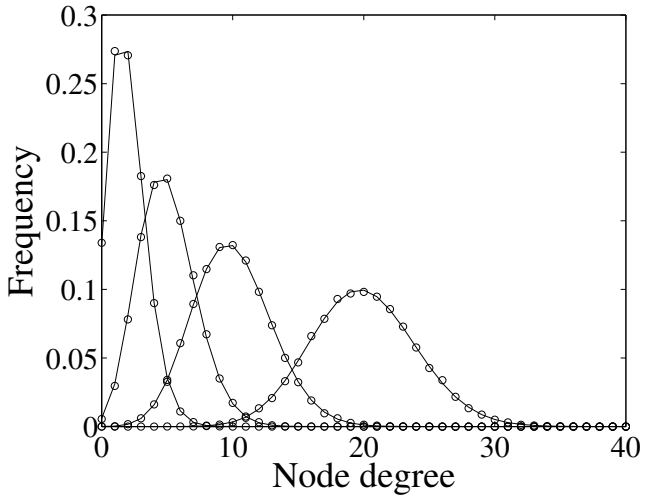

(b)

Figure 4.1: (a) Time evolution of $\langle k \rangle$ given by Eq. (4.2) (solid line, Kolmogorov model) compared to simulation ($\circ$). (b) Degree distribution at equilibrium as given by Eq. (4.9) (continuous, mean-field model) compared to simulation ($\circ$). Results from the mean-field model are identical to the binomial distribution Bin $\left(N-1, \frac{\langle k \rangle}{N-1} = \frac{\alpha}{\alpha+\omega}\right)$. For both (a) and (b), $\omega = 1$ and $\alpha = \left(\frac{\omega\langle k \rangle}{(N-1)-\langle k \rangle}\right)$ is set to obtain different values of the average degree at equilibrium (e.g. $\langle k \rangle = 2, 5, 10, 20$). All simulations start from a completely sparse graph with $N = 100$.

are given by

$$\frac{dn_k(t)}{dt} = \alpha[(N-1)-(k-1)]n_{k-1}(t) - \{\alpha[(N-1)-k] + \omega k\}n_k(t) + \omega(k+1)n_{k+1}(t). \tag{4.9}$$

This approach is similar to compartmental models where, in this case, transitions between compartments represent link gain or link loss. Solving the equations above provides information about the number of nodes with different connectivity but does not test whether such a network is realisable. This bears strong similarities to some modelling approaches where networks are simply considered in terms of nodes and their stubs but without being connected up in a coherent network (Ball and Neal, 2008; Lindquist et al., 2011). The linear system of ordinary differential equations lends itself to some simple analysis. The rates matrix is of particular interest as this determines the eigenvalues (λ_j) and the corresponding eigenvectors (s_j), where $j = 0, 1, \ldots N-1$, that are used to construct the solution of the system. The solution of the system in terms of these is given by

$$n(t) = \sum_{j=0}^{N-1} c_j s_j \exp(\lambda_j t),$$

where c_js are some arbitrary constants. Due to the special structure of the rates matrix, all eigenvalues but one have negative real parts. The single eigenvalue with a *non-negative real part* is in fact a zero eigenvalue. Hence, when $t \to \infty$, the solution of Eq. (4.9), $n(t) = (n_0(t), n_1(t), \ldots, n_{N-1}(t))$ tends to the eigenvector associated with the 0 eigenvalue times some constant, $n(t) \to Cs_0$ when $t \to \infty$. It is easy to show analytically that

$$s_0^j = \binom{N-1}{j} \left(\frac{\alpha}{\alpha+\omega}\right)^j \left(\frac{\omega}{\alpha+\omega}\right)^{N-1-j} \quad \text{for} \quad j = 0, 1, \ldots N-1.$$

This is equivalent to the binomial distribution with $N-1$ trials and a per trial probability of success given by $\alpha/(\alpha+\omega)$. This is further illustrated in Fig. 4.1(b) where the degree distribution, for large time, is plotted for different $\langle k \rangle$ values. Again, the agreement of the mean-field model with simulation is excellent, and confirms that, as expected, the simple RLAD model leads to simple Erdős-Rényi type networks.

4.3.3 Globally-constrained RLAD: probabilistic approach

Both real and theoretical networks are usually sparsely connected with $\langle k \rangle \ll N$ and thus it is natural to impose a limit on the total number of edges in the graph. To do this the simple RLAD model is extended to include a carrying capacity (K_1^{max}) that can limit link activation. This carrying capacity can be viewed as the maximum number of links allowable in the network. Of course this is not the only approach to limiting the number of edges in the network. It could be argued that a more realistic approach would be to introduce a local neighbourhood capacity to nodes in the network (see for instance, Taylor et al. (2012b)). Here, we continue with the global constraint and following the same notation as above, the

globally-constrained RLAD (GC-RLAD) model leads to the following equations

$$\frac{dp_k(t)}{dt} = \alpha[M-(k-1)]\left(1-\frac{k-1}{K_1^{max}}\right)p_{k-1}(t) - [\alpha(M-k)\Big(1-\frac{k}{K_1^{max}}\Big)+\omega k]p_k(t) + \omega(k+1)p_{k+1}(t), \tag{4.10}$$

where $k = 0, 1, 2, \ldots, M$ with obvious modifications for $k = 0$ and $k = M$. Using a similar approach as above, the equation for $K_1(t)$, the average number of edges in the graph at time t, is given by

$$\dot{K}_1(t) = \alpha M - \left(\alpha + \frac{\alpha}{K_1^{max}}M + \omega\right)K_1(t) + \frac{\alpha}{K_1^{max}}K_2(t), \tag{4.11}$$

where $K_2(t) = \sum_{k=0}^{M} k^2 p_k(t)$ is the second moment of the edge number distribution at time t. This equation cannot be solved directly since it involves the second moment of the edge distribution and an equation for this is needed. As an alternative to this exact approach, we consider the most obvious and simplest approximation whereby $K_2(t) = K_1^2(t)$. The following theorem shows that this approximation becomes exact in the limit of $M \to \infty$.

Theorem 2. *For the solution K_1^* of Eq. (4.11) upon substituting $K_2(t)$ by $K_1^2(t)$ the following statement holds. Provided that K_1^{max}/M remains constant as $M \to \infty$, then for any $T > 0$ there exists a constant $C > 0$ such that*

$$|K_1(t) - K_1^*(t)| \leq \frac{C}{M} \quad for \quad t \in [0, T],$$

where $K_1(t) = \sum_{k=0}^{M} k p_k(t)$.

The proof of the Theorem is rather technical and it will be presented in a more wider context as part of an additional paper. However, Fig. 4.2(a) confirms our statement and shows the excellent agreement between the exact and the approximation model even for small networks where M is also small. Using this result, a quadratic equation for the edge value at equilibrium ($K_1^{*,eq}$) follows easily,

$$K_1^{*,eq} = \frac{M}{2}\left[\left(1+\frac{K_1^{max}}{M}\left(1+\frac{\omega}{\alpha}\right)\right) \pm \sqrt{\left(1+\frac{K_1^{max}}{M}\left(1+\frac{\omega}{\alpha}\right)\right)^2 - 4\frac{K_1^{max}}{M}}\right]. \tag{4.12}$$

While both solutions are positive, the smaller of the two can be confirmed as the correct equilibrium value given that the number of edges in the network cannot be larger than the carrying capacity. In the case of $K_1^{max} = M$ our argument follows immediately.

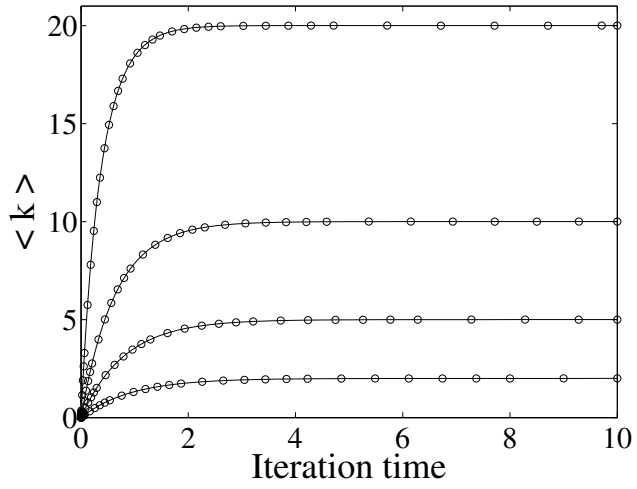

(a)

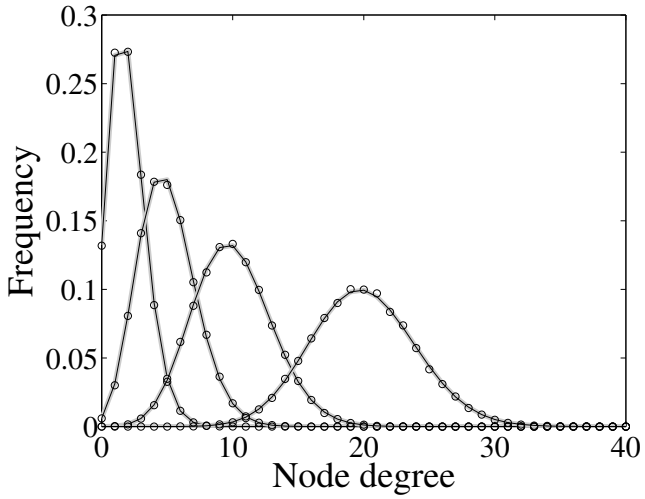

(b)

Figure 4.2: (a) Time evolution $\langle k \rangle$ given by Eq. (4.10)(solid line, Kolmogorov model) compared to the approximation obtained from Eq. (4.11)(∘). Here, $N = 50$. (b) Degree distribution at equilibrium based on Eq. 4.13 (thick grey line, mean-field model) compared to simulation (∘) and to the binomial distribution $\text{Bin}(N-1, \frac{\langle k \rangle}{N-1})$ (solid black line) with $N = 100$. For both (a) and (b), $\omega = 1$, $K_1^{max} = M$ and α is set to obtain different values of the average degree at equilibrium (e.g. $\langle k \rangle = 2, 5, 10, 20$). This can be done by assuming that all parameters in Eq. (4.12), except α, are known and solving a modified version of this ($2K_1^{*,eq} = \langle k \rangle N$) to obtain the desired α. All simulations start from a completely sparse graph.

4.3.4 Globally-constrained RLAD: mean-field approach

Following the same considerations as for the RLAD model and using the same notation, the globally-constrained RLAD at the node level is characterised by the following equations

$$\frac{dn_k(t)}{dt} = \alpha[(N-1)-(k-1)]\left(1-\frac{e(t)}{K_1^{max}}\right)n_{k-1}(t) - \{\alpha[(N-1)-k]\left(1-\frac{e(t)}{K_1^{max}}\right) + \omega k\}n_k(t) + \omega(k+1)n_{k+1}(t), \tag{4.13}$$

where $e(t)$ is given by

$$e(t) = \frac{1}{2}\sum_{k=0}^{N-1} kn_k(t).$$

In Fig. 4.2(b), for a given set of parameters, we show that the mean-field approach can again be used to predict the degree distribution of the network, and as before, the numerical results suggest that networks based on the GC-RLAD dynamics are also randomly connected with binomial distribution. However, in this case the good agreement with the binomial distribution could not be demonstrated analytically directly from Eq. (4.13).

4.4 Simple stochastically evolving networks in the presence of node labelling

The network dynamics so far has only been considered without the dynamics on the network and independently of node and/or link type. To explore the full impact of the dynamics on the network it is advisable that a step-by-step approach is taken as proposed by Gross et al. (2006). First, the impact of network dynamics can be investigated independently of node and/or link characteristics which could either be imposed externally and be static or be dynamic as a result of a separate dynamics running on the network. Second, the network dynamics based on static node/edge labelling can be investigated, and finally, the impact of coupling the dynamics of the network with the dynamics on the network needs to be considered. In the latter and most interesting case, the state of the nodes will have an impact on the network dynamics and vice versa (e.g. breaking susceptible-infected links impacts on the networks with the converse also being true; neuronal activation impacts on networks through experience-dependent plasticity and vice-versa).

4.4.1 *SI* labelling

Be it disease or information transmission, the manipulation of networks via preferential node/link addition and/or deletion provides a powerful mechanism to influence and optimise processes unfolding on the network. For example, disease transmission can be slowed or halted if links between susceptible and infected individuals are cut fast enough (Gross et al., 2006). Using the analogy of simple epidemic models, such as the susceptible-infected-

susceptible model, nodes are labelled at random as S or I. In the spirit of the network dynamics so far, all pair types can be activated or deleted at random with pair-type dependent rates. The rates at which SS, SI and II links are activated are denoted by α_{SS}, α_{SI} and α_{II}, respectively. Similarly, ω_{SS}, ω_{SI} and ω_{II} represent the rates at which SS, SI and II links are deleted. These labels are permanent and do not change during the evolution of the network. In this case, the Kolmogorov equations can be written down but are far more complicated compared to the previous cases. The state space is now given in terms of three variables, namely the counts of the various link types $\{SS\}$, $\{SI\}$ and $\{II\}$. These take values from 0 to $\{S\}(\{S\}-1)$, $\{S\}\{I\}$ and $\{I\}(\{I\}-1)$, respectively, where $\{S\}$ and $\{I\} = N - \{S\}$ are the initial number of nodes labelled S and I. It is more practical to use the mean-field approach and write down ODEs for the number of different pair types. For brevity, only the equations for the globally constrained case are given,

$$\frac{dn_{SS}(t)}{dt} = \alpha_{SS}[\{S\}(\{S\}-1) - n_{SS}(t)]\left(1 - \frac{e(t)}{K}\right) - \omega_{SS} n_{SS}(t), \tag{4.14}$$

$$\frac{dn_{SI}(t)}{dt} = \alpha_{SI}[\{S\}\{I\} - n_{SI}(t)]\left(1 - \frac{e(t)}{K}\right) - \omega_{SI} n_{SI}(t), \tag{4.15}$$

$$\frac{dn_{II}(t)}{dt} = \alpha_{II}[\{I\}(\{I\}-1) - n_{II}(t)]\left(1 - \frac{e(t)}{K}\right) - \omega_{II} n_{II}(t), \tag{4.16}$$

where now K is the carrying capacity, and $e(t)$ is given by

$$e(t) = n_{SS}(t) + 2n_{SI}(t) + n_{II}(t)$$

and represents the number of doubly counted edges. It is worth noting that here n_{AB} (where $A, B \in \{S, I\}$) stands for doubly counted edges (i.e. a single SS pair counts for two SS edges in n_{SS}). Similarly, the carrying capacity K needs to be understood as such. The expected number of pairs at equilibrium $(SS_{eq}, SI_{eq}, II_{eq})$ are given as the solutions of the following simple equations,

$$\alpha_{SS}[\{S\}(\{S\}-1) - SS_{eq}]\left(1 - \frac{e_{eq}}{K}\right) = \omega_{SS} SS_{eq}, \tag{4.17}$$

$$\alpha_{SI}(\{S\}\{I\} - SI_{eq})\left(1 - \frac{e_{eq}}{K}\right) = \omega_{SI} SI_{eq}, \tag{4.18}$$

$$\alpha_{II}[\{I\}(\{I\}-1) - II_{eq}]\left(1 - \frac{e_{eq}}{K}\right) = \omega_{II} II_{eq}, \tag{4.19}$$

where

$$e_{eq} = SS_{eq} + 2SI_{eq} + II_{eq}$$

and $\{S\}(\{S\}-1)$, $\{S\}\{I\}$ and $\{I\}(\{I\}-1)$ are constants determined by the initial number of S and Is. These equations allow us to find the equilibrium values at which the total rate of link activation equals the total rate of link deletion. The following Proposition shows that

the solution of Eqs. (4.17-4.19) is unique.

Proposition 1. *The system given by Eqs. (4.17-4.19) has a unique solution given as*

$$SS_{eq} = \frac{K_1 y}{A_1 + y}, \quad SI_{eq} = \frac{K_2 y}{A_2 + y}, \quad II_{eq} = \frac{K_3 y}{A_3 + y},$$

where

$$K_1 = \{S\}(\{S\} - 1), \quad K_2 = \{S\}\{I\}, \quad K_3 = \{I\}(\{I\} - 1),$$
$$A_1 = K\frac{\omega_{SS}}{\alpha_{SS}}, \quad A_2 = K\frac{\omega_{SI}}{\alpha_{SI}}, \quad A_3 = K\frac{\omega_{II}}{\alpha_{II}}$$

and y is the unique root of the function

$$h(y) = \frac{K_1 A_1}{A_1 + y} + \frac{2K_2 A_2}{A_2 + y} + \frac{K_3 A_3}{A_3 + y} - y + K - (K_1 + 2K_2 + K_3)$$

in the interval $[0, K]$. Finding the solution of the equation $h(y) = 0$ reduces easily to finding the root of a fourth degree polynomial.

Proof: Multiplying Eqs. (4.17-4.19) by K/α_{SS}, K/α_{SI} and K/α_{II}, respectively, and introducing the following new notation

$$x_1 = SS_{eq}, \quad x_2 = SI_{eq}, \quad x_2 = II_{eq}, \quad y = K - (x_1 + 2x_2 + x_3),$$

allows us to recast Eqs. (4.17-4.19) as follows,

$$x_1 = \frac{K_1 y}{A_1 + y}, \quad x_2 = \frac{K_2 y}{A_2 + y}, \quad x_3 = \frac{K_3 y}{A_3 + y}.$$

Substituting these expressions into the definition of y and using that

$$\frac{K_i y}{A_i + y} = K_i - \frac{K_i A_i}{A_i + y},$$

the following equation for y is obtained

$$\frac{K_1 A_1}{A_1 + y} + \frac{2K_2 A_2}{A_2 + y} + \frac{K_3 A_3}{A_3 + y} - y + K - (K_1 + 2K_2 + K_3) = 0.$$

This shows that y is a root of function h. It is easy to see that h is a decreasing function, hence it has at most one root. Moreover, $h(0) = K > 0$ and $h(K) < 0$, since $\frac{K_i A_i}{A_i + K} < K_i$. Therefore h has a unique root in the interval $[0, K]$.

□

It is important to note that if the network dynamics is not globally constrained, Eqs. (4.17-4.19) decouple and each equilibrium value can be found based on results from the non-constrained random link creation-deletion case. The excellent agreement between the theoretical equilibrium, as defined above, and simulation is illustrated in Fig. 4.3.

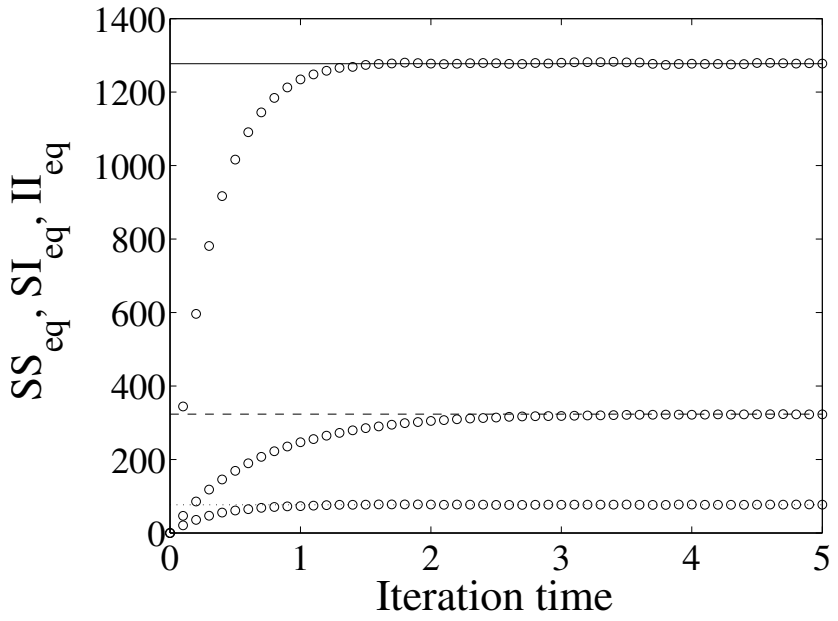

Figure 4.3: The time evolution of the number of (SS), (SI) and (II) pairs from simulation compared to analytic equilibrium values ((SS)-continuous, (SI)-dashed and (II) - dotted) predicted by the mean-field model. All simulations start from a completely sparse graph with $N = 100$ and with 80% of nodes labelled initially as S. The other parameters are $\alpha_{SS} = \alpha_{SI} = \alpha_{II} = 0.317$ and $\omega_{SS} = \omega_{SI} = \omega_{II} = 1.0$.

4.5 Interaction of network and disease dynamics: simulation and pairwise model

In this Section the dynamics of the network and the simple SIS (susceptible-infected-susceptible) model are studied concurrently using individual-based stochastic simulations and a low-dimensional, deterministic pairwise model which acts as an approximate model in the sense that, under appropriate conditions, output from the stochastic/exact model should tend to results based on the deterministic limit.

4.5.1 Simulation model and validity checks

The simulation is implemented on a network of fixed size with N nodes. Disease transmission (τ - transmission rate across an (SI) link), recovery (at rate γ), link creation (at rate α_{ab} with $a, b \in \{S, I\}$) and deletion (at rate ω_{cd} with $c, d \in \{S, I\}$) all act simultaneously and give rise to the coupled disease and network dynamics. The simulation is based on synchronous updating, where, to be in line with the Markovian framework, the simulation time-step (Δt) is kept small enough to try and ensure that not more than one event/update happens per single iteration. In a small time interval Δt, a susceptible node with k infectious neigbours becomes infected with probability $1 - \exp(-k\tau\Delta t)$, while an infectious node recovers with probability $1 - \exp(-\gamma\Delta t)$. The activation and cutting of links can be easily performed by considering

all pairs of nodes, independently of whether they are connected. If connected, an edge of type (ab) is cut with probability $1-\exp(-\omega_{ab}\Delta t)$, while a non-existing edge between nodes of type c and d is activated with probability $1-\exp(-\alpha_{cd}\Delta t)$. For globally constrained link creation, the unconstrained rate (α_{cd}) is simply multiplied by $(1-f)$, where f is the fraction of existing over allowable links given by the carrying capacity. All the above processes are modelled as simple Poisson processes that happen independently of each other.

The resulting simulation has an added level of complexity compared to simple disease transmission models, and it is therefore important that the simulation model be validated. In this case the checking and benchmarking of the simulation is possible due to the theoretical work developed in Sections 3.4 and 3,4. For example, to test the correctness of the implementation of the link-activation deletion mechanism the following checks have been performed and completed successfully: (a) comparison of simulation output, with no epidemic and link-type independent activation-deletion, to analytical results from Section 3.3, (b) comparison of simulation output, with no epidemics but with labelled nodes, to analytical results from Section 3.4. In both cases, the basis for comparison was the average number of links, and in the case of (b), the average number of different link types. While in this paper the globally-constrained RLAD was not coupled with epidemics, it was implemented and tested against analytical results from Section 3.3.

4.5.2 Pairwise model formulation for a dynamic network

In line with the standard pairwise models (Keeling, 1999; Simon et al., 2011) and the notations established above, we can now heuristically write down equations for the rate of change of individuals and pairs for the dynamic network as follows,

$$\frac{d[I]}{dt} = \tau[SI] - \gamma[I], \tag{4.20}$$

$$\begin{aligned}\frac{d[SI]}{dt} &= \gamma([II]-[SI]) + \tau([SSI]-[ISI]-[SI]) \\ &\quad - \omega_{SI}[SI] + \alpha_{SI}((N-[I])[I]-[SI]),\end{aligned} \tag{4.21}$$

$$\frac{d[II]}{dt} = -2\gamma[II] + 2\tau([ISI]+[SI]) - \omega_{II}[II] + \alpha_{II}(([I]-1)[I]-[II]), \tag{4.22}$$

$$\frac{d[SS]}{dt} = 2\gamma[SI] - 2\tau[SSI] - \omega_{SS}[SS] + \alpha_{SS}((N-[I])(N-[I]-1)-[SS]). \tag{4.23}$$

The system of equations is complemented by theoretical initial conditions or taken as expected counts from the simulation model. Triples are closed according to the simple closure given by

$$[ABC] = \frac{n-1}{n}\frac{[AB][BC]}{[B]},$$

where n is the average number of links per node. This closure implicitly assumes that the precise type of nodes (e.g. S or I) around a node in state B are independent. This type of

closure is widely used for homogeneous random graphs (House and Keeling, 2010; Keeling, 1999) with no clustering and also for unclustered random graphs with close to Poisson degree distribution (Taylor et al., 2012a). The equations above account for link activation-deletion and, without any further constraints, have been made dependent on the type of link being activated/deleted. For example, terms such as $\alpha_{SI}((N-[I])[I]-[SI])$ and $\omega_{SI}[SI]$ account for the activation and deletion of (SI) links, where $(N-[I])[I]-[SI]$ denotes the number of potential (SI)-type links that are not yet connected.

4.5.3 Comparison of pairwise model to simulation: a general consideration

In formulating such a low-dimensional model, the immediate key question is whether such a simple system can approximate, at least qualitatively, results obtained from the simulation model. The answer to this question depends strongly on the network structure, the type of dynamics and how the proposed closure performs when these factors combine. An important observation that is generally valid for all pairwise models with the known closures is that terms such as $-\tau[SI]$ are exact. Thus, the network structure and the formation of correlations as measured by $\mathcal{C}_{AB} = N[AB]/(n[A][B])$, where $A, B \in \{S, I\}$, should be conserved. However, the evolution equation for $[SI]$ relies on the exact expectation of triples which is approximated by the closure and thus is not exact. We note that values of the correlation measure close to one indicate that the true expected number of pairs is close to the value obtained in the case where nodes are labeled at random as S and I rather than as a result of the dynamics unfolding on the network. The strong assumption of independence in the closure leads to a closed ODE system that dissipates the true correlations to some degree but, not completely. This argument follows simply from considering a simpler closure at the pair level, i.e. $[SI]$ can be approximated by $[SI] = n[S][I]/N$. This obviously removes all correlations and gives rise to a system that is equivalent to the mean-field SIS model. Using the closure at the level of triples, rather than pairs, will conserve some of the correlations at pair level, however, a deviation from the simulation model is unavoidable. To shed some further light on the impact of closure it is important to make a distinction between whether nodes are labelled at random as S and I or whether (SS), (SI) and (II) links are placed at random to form a labelled graph (labelling is to be understood as carried out at random and fixed in time as opposed to being the result of an epidemic unfolding on the graph). Nodes labelled at random will lead to all pair correlation being close to one, $\mathcal{C}_{AB} = N[AB]/(n[A][B]) \simeq 1$, where $A, B \in \{S, I\}$, in which case the triples can be counted in terms of singles as follows

$$[ABC] = \frac{n(n-1)[A][B][C]}{N^2}.$$

This in turn is equivalent to the closure in terms of pairs. The main difference between the two closures is that the first, more realistic one, allows for pair correlations that are different from one, and thus not random, while keeping the distribution of links random. Thus, the

first closure can accommodate more realistic scenarios where non-random pair correlation and random link distribution can coexist. For the agreement between simulation and ODE (Eqs. (4.20)-(4.23)) to hold we can give the following sufficient conditions:

1. $\mathcal{C}_{AB} = N[AB]/(n[A][B]) \simeq 1$, where $A, B \in \{S, I\}$,
2. $[ABC] = \frac{(n-1)[AB][BC]}{n[B]}$ holds and the pair correlation can differ from one, $\mathcal{C}_{AB} \neq 1$, where $A, B, C \in \{S, I\}$,

where the first implies the second but not *vice-versa*.

The conditions above are rather strong and are easily violated even for simple static networks where the ODE model with an even more sophisticated closure (House and Keeling, 2010) will fail to match the outcome of simulation as shown by Taylor et al. (2012a). However, these conditions are not necessary to get good agreement. Even when the second condition is not fulfilled (i.e. $[ABC] \neq \frac{(n-1)[AB][BC]}{n[B]}$) it is still possible to get reasonably good agreement over time in the expected number of infecteds as illustrated in Fig. 4.4.

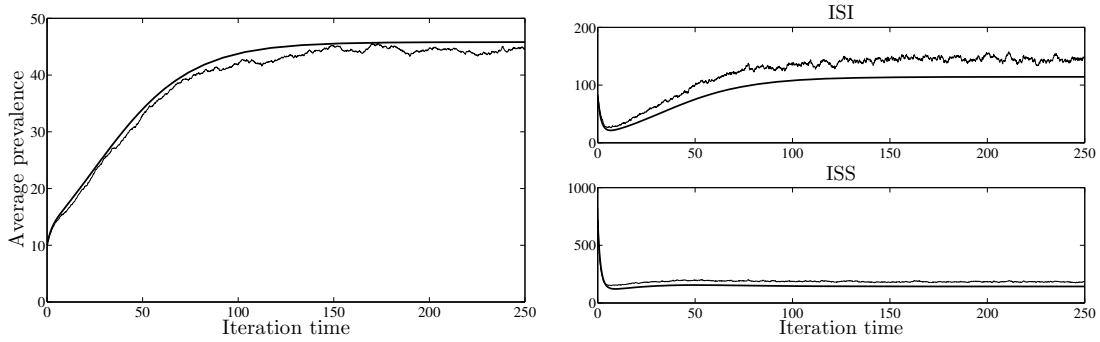

(a) Disease prevalence (b) Triple counts

Figure 4.4: Results from the average of 100 realisations on networks of size $N = 100$ with an initial average degree $\langle k \rangle = 10$, and corresponding output from the ODE model (simulation results, thin black lines; ODE - thick black lines). The other parameter values are $\gamma = 0.05$, $\tau = 0.025$, $\omega_{SI} = 0.5$, $\omega_{SS} = 0.5$, $\omega_{II} = 0.5$, $\alpha_{SI} = 0.02$, $\alpha_{SS} = 0.02$ and $\alpha_{II} = 0.02$. The networks were seeded with 10 infectious nodes. The prevalence of infection is plotted over time (a), and the true expected number of triples from the simulation is compared to the approximate value of triples from the closure with singles and pairs taken from the ODE (b).

Our discussion of the results and agreement between the two models will revolve around the arguments presented above and the concept of *preferential link or edge dynamics*. These will be used to underpin our explanation of results from model comparisons. Preferential link dynamics is a direct result of the model ingredients which allows us to tune link activation and deletion such that certain type of links can be over- or under-represented compared to a random link distribution scenario. Moreover, this means that nodes of certain type preferentially connect to nodes of similar or different nature leading to non-trivial correlation structures on the network. This alone can explain why the ODE with the triple approximation

cannot capture such type of correlation structures on the network. In extreme cases this can be easily illustrated by regimes where the graph breaks down into sub-graphs that are dominated by either S or I nodes and where these sub-graphs can be close to fully connected or with no edges. For example, if out of all link activation-deletion rates only ω_{SS} and α_{II} are non-zero, it is straightforward to obtain a regime where the network over time is such that S nodes are isolated and lose all their links while the I nodes tightly cluster into an almost completely connected graph. In cases such as these the ODE will fail to capture the true dynamics due to the isolation of susceptibles.

While correlations will not necessarily invalidate the agreement between the two models we identify them as an important factor in determining whether the two models will agree. Other important factors can contribute to whether good agreement is observed. For example, the parameter values could be such that an initially unclustered network may become clustered with higher link density and in this case the assumptions of the simple closure will break down. The effect of clustering however can be counteracted by the network becoming even more densely connected, at which point the mean-field limit can be approached.

4.6 Model behaviour: impact of network dynamics on epidemic

In this Section, the focus is on identifying possible system behaviours and understanding the coupled impact of disease and network dynamics on epidemics. The analysis starts with the consideration of the closed pairwise system which is four dimensional and lends itself to standard bifurcation analysis to determine all possible steady states and their stability as a function of the model parameters. Using the parametric representation method (PRM) (Simon et al., 1999), a more rigorous approach used to investigate global bifurcations, four different regimes are identified (see Fig. 4.5). The analysis shows that the interaction of network and disease dynamics leads to a spectrum of behaviours ranging from a single stable disease-free steady state to stable oscillations. More precisely there are three types of bifurcations. First, a transcritical bifurcation where the disease-free steady state loses stability with the disease becoming established and thus giving rise to a stable endemic equilibrium. Second, a saddle-node bifurcation which gives rise to the co-existence of two stable equilibria (one being disease-free and the other endemic) with an unstable equilibrium; and finally, a Hopf bifurcation, where the stable endemic equilibrium loses its stability and gives rise to a stable limit cycle. From a disease control viewpoint, of main interest is the region above the transcritical and saddle-node bifurcation curves. In this region, only the disease-free equilibrium is stable indicating that the deletion or breaking of (SI) edges curtails the spread of the epidemic and leads to a desirable disease-free steady state. As expected, the regions where different model behaviours are observed can vary and depend on model parameters. For example, in Fig. 4.5, the region of bistability is small compared to the Hopf island that covers a considerable part

of the parameter space. This case was chosen to illustrate a range of potential outcomes and the rich behaviour of a relatively simple model that can lead to outcomes other than a stable disease-free or stable endemic state, as in the case of the simple SIS model on a static network.

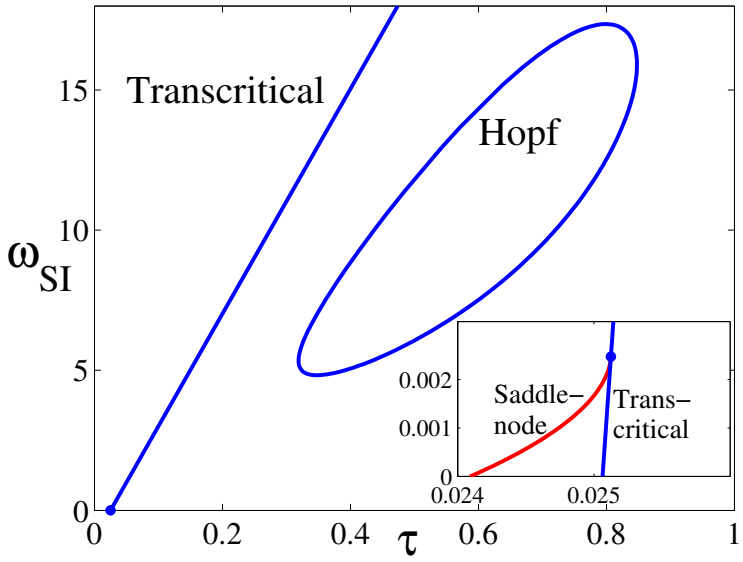

Figure 4.5: Bifurcation diagram showing the full possible spectrum of behaviour. The parameter space is divided into four distinct regions as follows: the disease-free is the only stable equilibrium (above the transcritical and saddle-node bifurcation curves), two stable (disease-free and endemic) and one unstable equilibria with non-zero infectious prevalence (between the transcritical and saddle-node bifurcation curves), one unstable (disease-free) and a stable endemic equilibria (below the transcritical curve and outside the Hopf bifurcation island), and finally, Hopf island with a stable limit cycle and unstable disease-free and endemic equilibria. Parameter values are as follows: $N = 100$, $n = 10$, $\alpha_{SS} = 0.004$, $\alpha_{SI} = 0.005$, $\alpha_{II} = 0$, $\omega_{SS} = 0.005$, $\omega_{II} = 0$ and $\gamma = 1.0$.

Owing to the dynamic nature of the network, the average degree of the nodes (i.e. n as given in the triple closure) is a variable itself and changes with time. Hence, the analysis above performed for a fixed n serves only as an indicator of possible system behaviours but can give good results if n is a slow variable where for example the network dynamics is much slower compared to the epidemic or if n does not vary considerably. We also note that n only enters via the $(n-1)/n$ term which for realistic networks that are well connected is close to one. For dynamic networks with type-dependent rates of link activation and deletion, the average degree of a susceptible node can be different to that of infective nodes. It is therefore more appropriate to use the following triple closure

$$[ABC] = \frac{n_B - 1}{n_B} \frac{[AB][BC]}{[B]},$$

where n_B is the average degree of a node of type B. Replacing n by $n_S(t) = ([SS]+[SI])(t)/S$ in the ODE prevents the straightforward derivation of analytical results but allows for fast numerical exploration of the parameter space to identify different possible model outcomes. If in good agreement with simulation, the ODE provides a simple and easy way to explore the full spectrum of behaviour for a large number of parameters, a problem that is extremely difficult to tackle via simulation alone.

The interplay between the two dynamics merits further scrutiny from the viewpoint of the relative timescale of the two processes. In particular, three different regimes can be identified: (i) fast network dynamics compared to the spread of the epidemic, (ii) comparable time scales, and (iii) slow network dynamics relative to disease transmission. As expected, in the limit of networks that mix fast (i.e. regime (i)), the simulation approaches the standard mean-field model, Fig. 4.6, given by

$$\frac{dI(t)}{dt} = \frac{\tau\langle k\rangle S(t)I(t)}{N} - \gamma I(t),$$

where $\langle k\rangle$ represents the average degree once the network has reached its equilibrium. For quick network dynamics, $\langle k\rangle$ is approached much faster compared to the timescale of the epidemic, and this value can be used as an input in the standard mean-field model above. This approach is in fact equivalent to decoupling the system of two ODEs composed of the simple mean-field model above and the evolution equation for $K_1(t)$ given by Eq. (4.2). For fast network dynamics, $\langle k\rangle$ quickly approaches $2K_1/N$, where $K_1 = \lim_{\alpha,\omega\to\infty} \frac{\alpha M}{\alpha+\omega}$ with creation and deletion rates chosen to obtain a plausible, positive value. Thus, the average degree of the network at the steady state serves as input to the mean-field epidemic model and the system decouples. The setup in the third regime leads to some interesting behaviour of the coupled system. A slow network dynamics, relative to the spread of the epidemic, may make the coupled process look like disease transmission on a static network. However, this will only hold initially as shown in Fig. 4.6 , where a well established epidemic can be brought to a halt by a slow but potent network dynamics that thins the networks sufficiently. The same figure also illustrates that when the thinned network can still support an epidemic, the slow network dynamics applies a delayed but severe correction to the steady state, i.e. reduced infection prevalence level. When the timescales are comparable the processes evolve hand-in-hand and this regime is explored further both from an application and model agreement viewpoint.

Good agreement between pairwise model and simulation would demonstrate that the ODE model can be used as an effective tool to investigate possible model outcomes. In what follows, we identify parameter sets where such agreement for the coupled dynamics case exists. The results are based on extensive individual-based stochastic network simulations for a large selection of different parameter combinations. The degree to which preferential link creation can be captured by the ODE depends on the parameter values. As expected when all link activation-deletion rates are not type dependent (i.e. $\alpha_{SS} = \alpha_{SI} = \alpha_{II}$ and $\omega_{SS} = \omega_{SI} = \omega_{II}$) the agreement between ODE and simulations is excellent as illustrated in Fig. 4.7 for a range of different parameter values. In this regime the assumption of independence of links of the triple

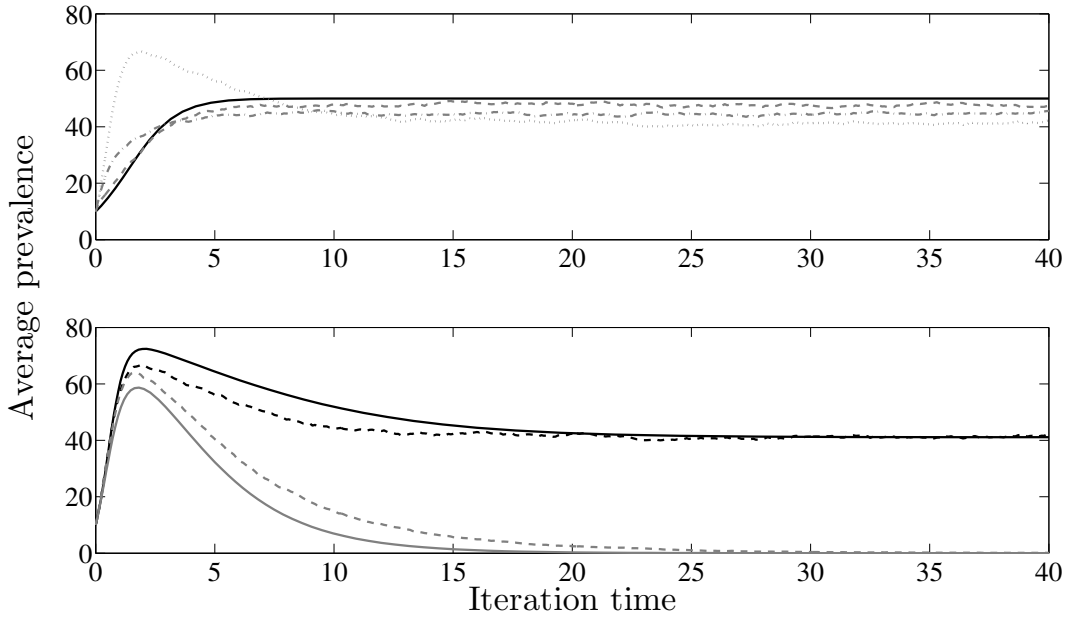

Figure 4.6: Results from the average of 200 simulations on networks with $N = 100$, $\gamma = 1$, $\tau = 0.5$ and an initial average degree of 10. Each run was initially seeded with 10 infectious nodes. (a) Time evolution of the infection prevalence for network dynamics of increasing magnitude. The grey lines represent simulation results for $\alpha = 0.01$ and $\omega = 0.2375$ (dotted), $\alpha = 0.1$ and $\omega = 2.375$ (dash-dotted), and $\alpha = 0.5$ and $\omega = 11.875$ (dashed). The solid black line represents the solution of the standard, mean-field epidemic model solved with $\langle k \rangle = 4$ which is equivalent to an epidemic with an infinitely fast dynamics but with an average degree of 4. (b) Time evolution of infection prevalence for different network dynamics with $\alpha = 0.01$ and $\omega = 0.2375$ (black lines), and $\alpha = 0.01$ and $\omega = 0.485$ (grey lines), and with an average degree at equilibrium given by $\langle k \rangle = 4$ and $\langle k \rangle = 2$, respectively . Output from the pairwise models (solid lines), with the same parameters, are plotted along with the simulation results (dashed lines).

closure performs even better than on a static network as the random breaking and creating of links helps to dissipate some of the high correlation in triplets (e.g. $[III]$) observed with SIS type dynamics. Random activation-deletion helps to decrease the building of correlation in the network that may otherwise invalidate the independence assumption. Good agreement between the two models also holds for parameter values that are much different from the equal activation and deletion rates scenario. Figure 4.8 shows that agreement can also be found for more realistic parameter values where for example, efforts to control a disease may require a higher ω_{SI} rate compared to other link deletion rates. In such situations however, care has to be taken since the agreement depends on whether the precise parameter values will lead to moderate correlations or correlations that can be captured by the ODE model. Finally, in Fig. 4.9 the bistability regime is illustrated for both simulation and the ODE model. We note that the networks resulting from the coupled dynamics on the upper branch have on average 6 nodes that become isolated. As expected, the ODE cannot capture this but, we can take this

into account by decreasing population size from $N = 100$ to $N = 94$. This results in excellent agreement between the two models. The plots in Fig. 4.9 have been obtained via continuation method where the steady state obtained at a value τ_0 of the transmission rate is used as the initial condition for a new set of simulations with a smaller value of the transmission rate, i.e. $\tau_0 - \delta\tau$. This approach has also been used with the full set of ODEs with time dependent average connectivity $n(t)$. The qualitative agreement is good and highlights that the pairwise model can be used as an exploratory tool when mapping out full system behaviour. This is especially useful where models with many parameters make this exploration almost impossible via simulations alone.

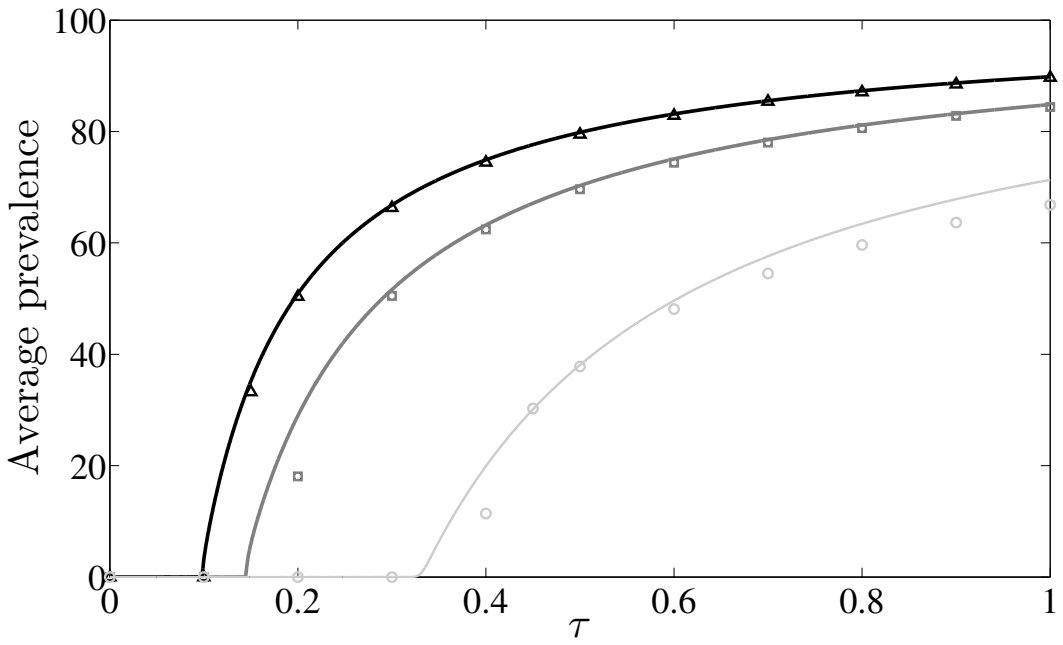

Figure 4.7: Results from the average of 50 realisations on networks of size $N = 100$ with an initial average degree $\langle k \rangle = 10$, and corresponding output from the ODE model for various values of τ (simulation results, open triangles, squares and circles; ODE, solid lines). The other parameter values are $\gamma = 1.0$, $\omega_{SS} = \omega_{SI} = \omega_{II} = 0.5$. The black, dark-grey and light-grey lines correspond to all αs being equal to 0.06, 0.04 and 0.02, respectively. The networks were seeded with 20 infectious nodes. The prevalence from the ODE is plotted after 200 time units and the simulation results are normalised from time 160 to 200, this is a region where the average prevalence settles to a steady state.

4.7 Discussion

The paper set out to carry out a systematic analysis of a model where network dynamics is coupled with a simple disease dynamics model. Network dynamics is based on link activation and deletion that can depend on link type. A step-by-step approach has been taken where the network dynamics has been modelled and studied in isolation, without disease dynamics,

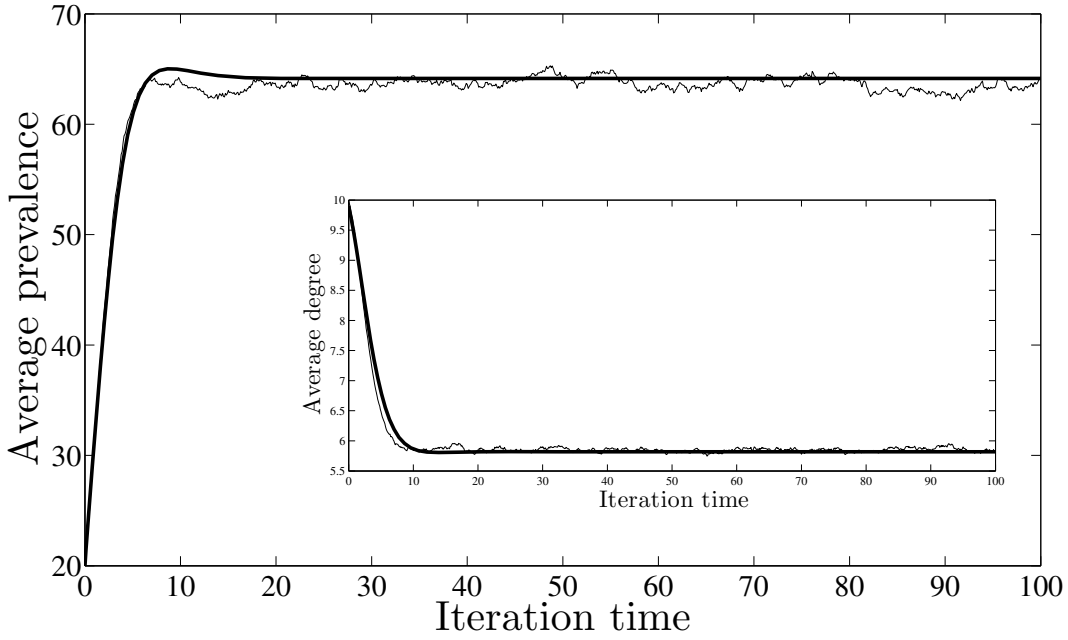

Figure 4.8: Results from the average of 100 realisations on networks of size $N = 100$ with an initial average degree $\langle k \rangle = 10$, and corresponding output form the ODE model (simulation results, thin black lines; ODE, thick black lines). The other parameter values are $\gamma = 0.2$, $\tau = 0.1$, $\omega_{SI} = 0.5$, $\omega_{SS} = 0.3$, $\omega_{II} = 0.6$, $\alpha_{SI} = 0.03$, $\alpha_{SS} = 0.04$ and $\alpha_{II} = 0.03$. The networks were seeded with 20 infectious nodes. The inset shows the good agreement in the average degree of the evolving network.

and then in presence of node labelling that was stationary in time. The key result is the analysis of the pairwise ODE model and its comparison to simulation where both network and disease dynamics act concurrently. Different modeling approaches have been proposed, discussed and their performance relative to each other has been investigated. The models studied have ranged from exact stochastic models based on Kolmogorov equations and simple low dimensional ODE models to simulation often with good agreement between complex simulations and ODE models. We have highlighted that approximate ODE models are desirable as they are more tractable compared to simulation and can be used as a more rigorous tool to investigate the full spectrum of behaviour, especially when faced with more complicated models with a large number of parameters.

Pairwise models have been developed in the context of static networks with applications in epidemiology and ecology (Keeling, 1999; Matsuda et al., 1992; Rand, 1999). This approach has been generalised to dynamic networks coupled with simple epidemics and have been shown to have the potential to be a useful modelling tool that complements simulation models and aids analysis. However, many open problems remain regarding the validity of these simple ODE models when compared to full simulation. To date there is no coherent framework with theoretical results where for example the convergence, in some appropriate limit, of

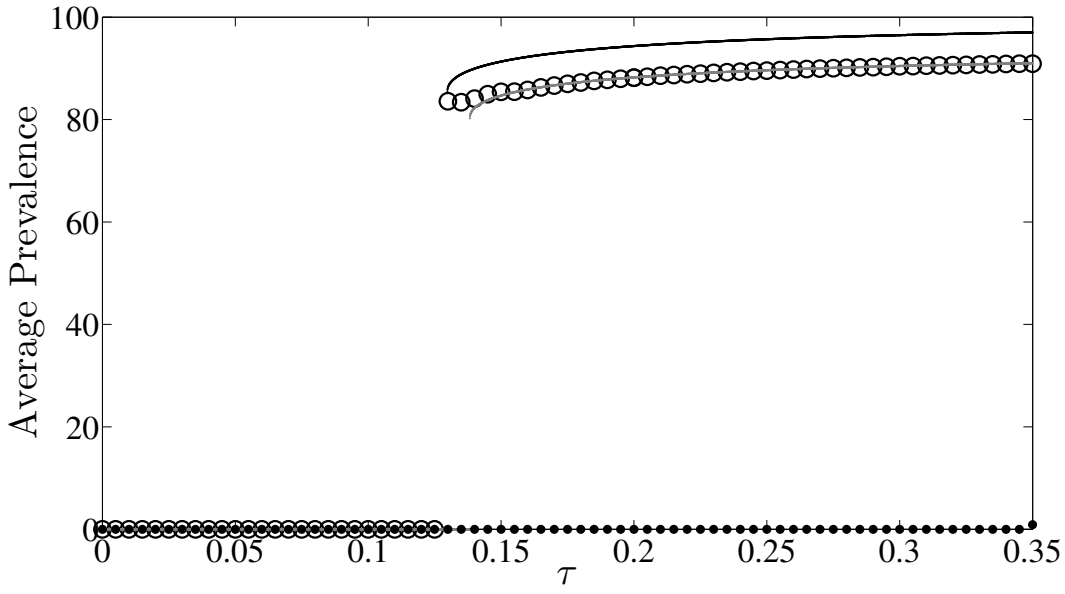

Figure 4.9: Results based on simulation and pairwise model showing bistability. The upper branch (open circles) obtained using the continuation method on networks of size $N = 100$ and 50 realisations. The solid black line and grey lines are the corresponding results based on the pairwise model for $N = 100$ and $N = 94$, respectively. The lower branch from the simulation (black dots) and the continuation from the upper branch (open circles) all show zero prevalence. Results from the ODE also predict zero prevalence and are omitted to increase clarity. When tracing out the upper branch via simulation, only epidemics that did not become extinct have been considered (unless all died out). For a large enough value of τ, the lower branch will eventually move away from the zero prevalence state. The parameter values are $\langle k \rangle = 10$ (for the starting network and on the lower branch), $\omega_{SS} = 2.0$, $\alpha_{II} = 0.06$, $\gamma = 1.0$ with all other rates set to zero. The upper and lower branches were seeded with 50 and 5 infectives, respectively.

a stochastic process to a deterministic model is formalised. This holds even for the static network case where the need for such developments has been highlighted (House and Keeling, 2011). In our particular case, there are many parameter regimes where agreement between the ODE model and simulation is good. These include for example regimes where either of the two dynamics is fast or slow compared to the other. This time-scale separation reflects that when considered separately, the ODE model tends to perform better. Furthermore, if the parameters are such that the system is dominated by nodes in either susceptible or infected state, then the agreement is again good given that many of the link activation and deletion processes are dormant. Hence, the dynamics of the network is predominantly governed by the creation and deletion of a unique link type, i.e., non-preferential link dynamics.

As previously highlighted, and also confirmed here, the interaction of the two dynamical process can lead to networks that are either highly clustered, display some specific structure or are fragmented in sub-networks dominated by S or I nodes even with some being completely

isolated. Obviously in such cases the current pairwise model will fail to approximate the simulation correctly but alternatives models, more sophisticated pairwise or other type of models that keep track of the number of links or even the type of neighbours a node has (Lindquist et al., 2011) may prove to give a more satisfactory result. Such models could better capture the correlations driven by preferential link dynamics, heterogeneity in node degree or other node, pair of larger scale property, that cannot be captured by the basic pairwise model.

The results of the paper also highlight the importance of coupling network and disease dynamics. This is easy to motivate from a practical viewpoint and our model illustrates that this is a worthwhile exercise with findings that complement the body of knowledge focusing on dynamics on static networks. As demonstrated in the paper, the network dynamics can be exploited as a control mechanism aimed at stopping or reducing the impact of an epidemic and there remains much work to understand how the link-type dependent cutting and creation as well the relative timescale of the two processes impact on the type and nature of observable system behaviour. The proposed network dynamic model is basic and, while it sheds light on some interesting and relevant behaviour, it needs to be adapted based on some empirical evidence of social interaction and perturbations to it by adversities such as epidemics. While the applications of the modelling framework was in terms of epidemic models, coupling network dynamics with dynamical processes unfolding on the network remains a very current topic in areas such as computational neuroscience (notably in developmental neuroscience, e.g. Hagmann et al. (2010) and more generally the problem is recognised in Bullmore and Sporns (2009)) and we foresee that this will lead to various network dynamics and coupling mechanisms with important contributions in the future on both the modelling and analysis front.

Acknowledgements

Istvan Z. Kiss acknowledges support from EPSRC (EP/H001085/1). Timothy Taylor is funded by a PGR studentship from MRC, and the Departments of Mathematics and Informatics at Sussex University. Péter L. Simon acknowledges support from OTKA (grant no. 81403) and from the European Union and the European Social Fund (financial support to the project under the grant agreement no. TÁMOP-4.2.1/B-09/1/KMR).

Chapter 5

Paper 3: Epidemic threshold and control in a dynamic network

Michael Taylor[1], Timothy J. Taylor[1,2] and Istvan Z. Kiss[1]

[1]School of Mathematical and Physical Sciences, Department of Mathematics, University of Sussex, Brighton BN1 9QH, UK
[2]Centre for Computational Neuroscience and Robotics, University of Sussex, Brighton BN1 9QH, UK

Published in *Physical Review E, 85 (1). 016103-1-016103-6. ISSN 1539-3755*

5.1 Abstract

In this paper we present a model describing Susceptible-Infected-Susceptible (SIS) type epidemics spreading on a dynamic contact network with random link activation and deletion where link activation can be locally constrained. We use and adapt an improved effective degree compartmental modelling framework recently proposed by Lindquist et al. (2011) and Marceau et al. (2010). The resulting set of ordinary differential equations (ODEs) is solved numerically and results are compared to those obtained using individual-based stochastic network simulation. We show that the ODEs display excellent agreement with simulation for the evolution of both the disease and the network, and is able to accurately capture the epidemic threshold for a wide range of parameters. We also present an analytical R_0 calculation for the dynamic network model and show that depending on the relative timescales of the network evolution and disease transmission two limiting cases are recovered: (i) the static network case when network evolution is slow and (ii) homogeneous random mixing when the network evolution is rapid. We also use our threshold calculation to highlight the dangers of relying on local stability analysis when predicting epidemic outbreaks on evolving networks.

5.2 Introduction

The rise in the popularity and relevance of networks as a tool for modelling complex systems is well illustrated by the ever increasing body of research concerned with the spread of diseases within host populations exhibiting non-trivial contact structures (Newman, 2003a; Albert and Barabási, 2002b). Networks offer an intuitive and relatively simple modelling framework which enables us to relax the strong implicit assumptions of more classical ordinary differential equations (ODE) based approaches and to account for complexities in the contact structure of the host population (Newman, 2002; Gross and Blasius, 2008; Strogatz, 2001; Bansal et al., 2007; Eames and Keeling, 2002). This approach has shown that epidemic thresholds not only depend upon the infectiousness of the pathogen, or even simply the mean number of contacts per individual, but also upon the exact structure of the host population (Trapman, 2007; Andersson, 1999). In addition to its inherent theoretical value, this paradigm has immediate practical benefits, as the primary role of public health services is to put measures in place to bring diseases below their epidemic threshold. These measures depend heavily upon disrupting the transmission of a disease through vaccination and also more directly through the closure of public services, or even quarantine and curfews in extreme cases. Hence the knowledge of how the structure of the host population is contributing to the spread of a disease would help to increase the efficacy of any intervention (Meyers et al., 2005).

Despite advances in both rigorous and non-rigorous analysis of networks, a key assumption in many network models is that contacts are fixed for the duration of an epidemic and that the disease propagates with a constant intensity across links. This will not be true for many diseases, especially those with long infectious periods, or diseases that become endemic.

Indeed human contact patterns are well described by short repeated events, with individuals having a number of contacts best described by some appropriate time dependent random variable (Read et al., 2008). Furthermore, individuals and the communities they belong to are likely to change their contact behaviour as a result of natural evolution and endogenous or exogenous perturbations such as a disease outbreak (Liljeros et al., 2001).

Recently a number of studies have attempted to relax this assumption by allowing the networks to evolve over time by either varying contacts independently of the status of individuals (Volz and Meyers, 2007, 2009) or by explicitly coupling contact activation and deletion to the disease status of individuals (Marceau et al., 2010; Gross et al., 2006; Van Segbroeck et al., 2010). Thus, in the latter case, the dynamics of the disease is coupled with the dynamics of the network itself, with both acting as a feedback mechanism for the other (Van Segbroeck et al., 2010; Zanette and Risau-Gusmán, 2008; Grindrod and Higham, 2010). Many of these studies have built macro ODE-based models that describe the coevolution of networks and the diseases that spread along them (Marceau et al., 2010; Gross et al., 2006; Van Segbroeck et al., 2010; Schwarzkopf et al., 2010). All these studies confirm that dynamic networks and the coupling between the two dynamics lead to a richer spectrum of behaviour than is found for epidemics on static networks.

A crucial feature of allowing the co-evolution of disease and network is the interplay and feedback between both dynamics, however this interdependence is difficult to measure empirically. The models developed so far mainly use rewiring rules that intuitively make sense given that individuals would have knowledge of the disease states of the rest of the population. However in this paper we move away from these assumptions and we propose a dynamic network model that is based on random link activation-deletion, which would be more relevant for asymptomatic diseases, such as Chlamydia (Low et al., 2009). Furthermore our dynamic network model is refined by introducing a local constraint on link activation to account for the difference in the magnitude of the number of contacts of a node relative to system size. This dynamic network coupled with the simple Susceptible-Infected-Susceptible (SIS) disease dynamics leads to the full model that will be analysed and discussed. We study this system and explore to what extent a macro ODE-based compartmental model proposed for static networks is flexible enough to be adapted to a dynamic network case. Specifically, we focus on the SIS effective degree model as described in detail by Lindquist et al. (2011) and also, to our knowledge, proposed by Marceau et al. (2010) in close succession. Gleeson (2011) later uses this same modelling framework and demonstrates that the effective degree formulation can be used to model other binary-state dynamics such as Glauber spin dynamics and shows that the ODE model can be used to carry out linear stability type analysis.

Whereas both Lindquist et al. (2011) and Gleeson (2011) confine themselves to modelling on static contact networks, Marceau et al. (2010) uses this same improved effective degree formalism to explore SIS disease dynamics on adaptive networks. In this model the number of links in the network is fixed but the susceptible individuals can replace links to infectious

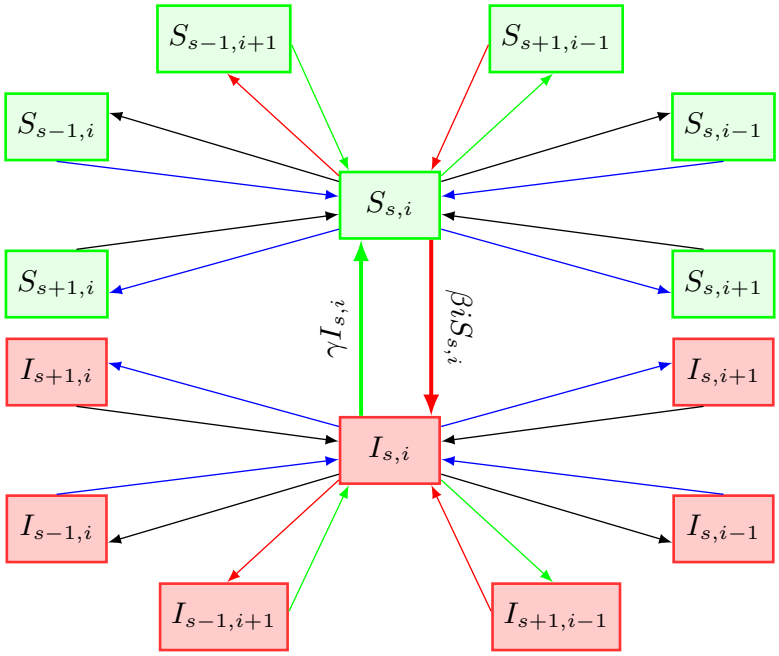

Figure 5.1: Flow chart showing transitions in the dynamic SIS effective degree model. The directed red (gray), green (light gray), blue (dark gray) and black lines represent changes in state of an individual via infection, recovery, link creation and link deletion respectively. The thick lines represent changes to the individual, and thin lines represent changes to that individual's immediate neighbourhood. In relation to nodes of type $X_{si}, X \in \{S, I\}$, infection of neighbours occurs at rate sG_X, recovery of neighbours at rate γi, creation of a susceptible (infectious) link at rate $\alpha(M-(s+i))P_{S(I)}$ and deletion of a susceptible (infectious) link at rate $\omega s(i)$, where:
$G_S = \beta\frac{\sum_{k=1}^{M}\sum_{j+l=k} jlS_{jl}}{\sum_{k=1}^{M}\sum_{j+l=k} jS_{jl}}$, $G_I = \beta\frac{\sum_{k=1}^{M}\sum_{j+l=k} l^2S_{jl}}{\sum_{k=1}^{M}\sum_{j+l=k} jI_{jl}}$
and $P_X = \frac{\sum_{k=0}^{M}\sum_{j+l=k}(M-(j+l))X_{jl}}{\sum_{k=0}^{M}\sum_{j+l=k}(M-(j+l))(S_{jl}+I_{jl})}$.

neighbours with links to other randomly chosen susceptible individuals, as originally proposed by Gross et al. (2006). Our proposed model also uses SIS type epidemics on dynamic networks, but unlike Marceau et al. (2010) our model allows for the random activation and deletion of links over time. As such not only the network topology will evolve and change over time, but also the number of links. This modified dynamic effective degree model is also governed by a closed set of ODEs, which is then solved and compared to results from individual based simulations and its ability to accurately predict the epidemic threshold over a range of parameters is investigated. We also derive an analytical R_0 calculation that describes the stability of the disease-free equilibrium and we discuss the limitations of such a calculation in the light of having a dynamically active and evolving contact network.

5.3 The model

Lindquist et al. (2011) and Marceau et al. (2010) use different notation to describe the same modelling framework. For consistency, in this paper we follow the notation used by the former throughout. The effective degree modelling approach for SIS type disease dynamics (Lindquist et al., 2011) not only categorizes the disease state of each individual as susceptible (S) or infected (I) but also describes the state of their immediate neighbourhood. This is achieved by keeping track of the number of susceptible and infected neighbours that belongs to a given node. For example, S_{si} represents the number of susceptible individuals that have s susceptible and i infected neighbours. This gives rise to more states and equations than would be seen in a standard pairwise model, where equations are given at the population level for all types of singles and pairs (Keeling and Eames, 2005). For example if a S_{si} type node became infected via one of its i infectious neighbours, this individual would move to state I_{si} as only the status of the node itself is changing. However, if one of the i infected neighbours of an S_{si} type node recovered then the node would enter the $S_{s+1,i-1}$ class, whereas infection of one of the s neighbouring susceptible nodes moves the S_{si} type node into the $S_{s-1,i+1}$ class.

Lindquist et al. (2011) defined γ to be the per node recovery rate, β the per link infection rate and M the maximum nodal degree of a network with N nodes. They then derived the following system of $\sum_{k=1}^{M} 2(k+1) = M(M+3)$ equations:

$$\begin{aligned}
\dot{S_{si}} &= -\beta i S_{si} + \gamma I_{si} + \gamma[(i+1)S_{s-1,i+1} - iS_{si}] \\
&\quad + \beta \frac{\sum_{k=1}^{M}\sum_{j+l=k} jlS_{jl}}{\sum_{k=1}^{M}\sum_{j+l=k} jS_{jl}}[(s+1)S_{s+1,i-1} - sS_{si}], \qquad (5.1)\\
\dot{I_{si}} &= \beta i S_{si} - \gamma I_{si} + \gamma[(i+1)I_{s-1,i+1} - iI_{si}]] \\
&\quad + \beta \frac{\sum_{k=1}^{M}\sum_{j+l=k} l^2 S_{jl}}{\sum_{k=1}^{M}\sum_{j+l=k} jI_{jl}}[(s+1)I_{s+1,i-1} - sI_{si}], \qquad (5.2)
\end{aligned}$$

for $\{(s,i) : s,i \geq 0, 1 \leq k = s+i \leq M\}$. This is the SIS effective degree model for a *static* contact network.

In oder to adapt this model to describe SIS dynamics on a *dynamic* contact network, we introduce two new parameters: ω, the per link deletion rate and α, the per non-link, or more precisely the per *potential* link creation rate. These rates could also be made to be link-type dependent, i.e. ω_{SI} would be the per SI link deletion rate. For the dynamic network cae, the system size will increase slightly from $M(M+3)$ to $\sum_{k=0}^{M} 2(k+1) = (M+1)(M+2)$ equations to account for nodes of the type $X_{0,0}$ where $X \in \{S, I\}$. In the static case, these nodes were dynamically unimportant as they could neither infect nor become infected by other nodes. However in the dynamic model, they could connect to other nodes in the system and so enter states $X_{1,0}$ or $X_{0,1}$ depending on the state of the node with which they have just formed a new link.

The total number of links in the system at time t, $\Lambda(t)$, and potential links, $\Phi(t)$ can easily be calculated from the effective degree formulation as

$$\begin{aligned}\Lambda(t) &= \sum_{k=0}^{M}\sum_{j+l=k}(j+l)(S_{jl}+I_{jl}),\\ \Phi(t) &= \sum_{k=0}^{M}\sum_{j+l=k}(M-(j+l))\,(S_{jl}+I_{jl})],\end{aligned}$$

with the mean nodal degree given by $\langle k(t)\rangle = \frac{\Lambda(t)}{N}$. At the equilibrium, $\alpha\Phi = \omega\Lambda$ which gives us the mean nodal degree:

$$\langle k\rangle^* = \frac{\alpha}{\alpha+\omega}M. \tag{5.3}$$

Note that Eq. (5.3) does not depend on the system size, N, but rather on the maximum nodal degree, M. This is important because in the static model, M is simply given by the node or nodes with the highest degree whilst in the dynamic case, however, M can be considered as a carrying capacity, whereby no node can have more than M links. This subtle but important difference means that in the dynamic case, M itself can be regarded as a parameter which controls the potential level of network saturation.

When adding the terms that govern link creation and deletion to Eqs. (5.1) and (5.2) it is far simpler to construct the terms that govern deletion of existing links than those for the creation of new links. Links to nodes of type X_{si} where $X \in \{S, I\}$ are cut at a rate proportional to their degree, so individuals will leave X_{si} through link deletion at a rate $\omega(s+i)$ and will either enter the $X_{s-1,i}$ or $X_{s,i-1}$ classes depending on the state of the nodes to which they were previously connected. Similarly individuals can enter state X_{si} if they were in states $X_{s,i+1}$ or $X_{s+1,i}$ and a link to an infected or susceptible node was deleted respectively.

When creating new links to nodes of type X_{si}, there are $M-(s+i)$ stubs remaining, so nodes will transition out of this state at a rate $\alpha(M-(s+i))$ and will either enter the $X_{s+1,i}$ or $X_{s,i+1}$ classes depending on the state of the node to which they have just connected. The rate at which nodes enter the X_{si} class from either $X_{s-1,i}$ or $X_{s,i-1}$ depends not only on the number of stubs still available in the node in question, but also on the probability that the newly created link attaches to a node of state S or I respectively. So nodes enter X_{si} from $X_{s-1,i}$ at the rate $\alpha P_S(M-(s-1+i))$, and nodes enter X_{si} from $X_{s,i-1}$ at rate $\alpha P_I(M-(s+i-1))$, where $P_X = \frac{\sum_{k=0}^{M}\sum_{j+l=k}(M-(j+l))X_{jl}}{\sum_{k=0}^{M}\sum_{j+l=k}(M-(j+l))(S_{jl}+I_{jl})}, X \in \{S, I\}$ is the probability of picking an available stub belonging to nodes of type X where $X \in \{S, I\}$. The full set of transitions captured by this model is shown in Fig. 5.1.

The addition of these terms to Eqs. (5.1) and (5.2) transforms the SIS effective degree model for a static network into one that captures the spread of SIS type diseases on a dynamic

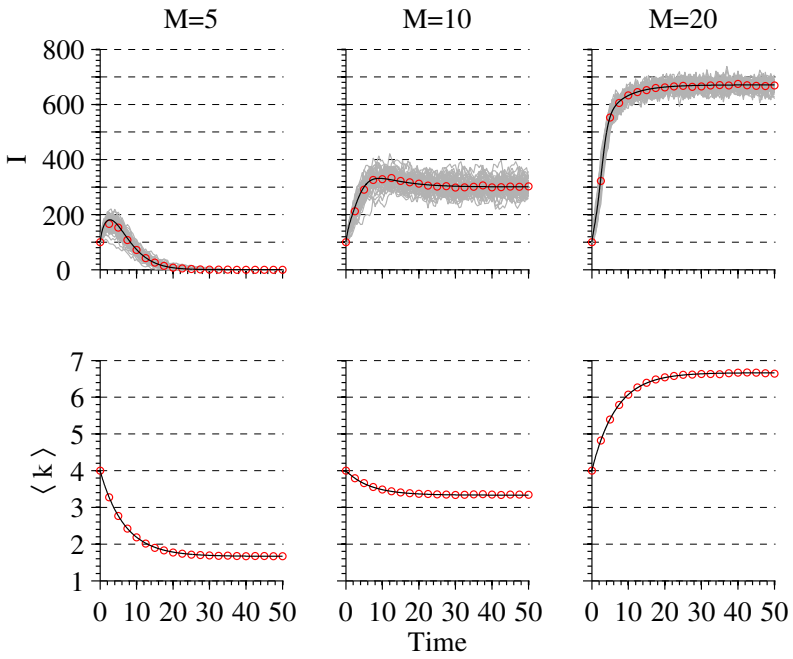

Figure 5.2: Time evolution of $I(t) = \sum_{k=0}^{M} \sum_{j+l=k} I_{jl}(t)$ and $\langle k \rangle(t) = \frac{\Lambda(t)}{N}$ for three different values of M. Results from the ODE are given by solid lines and those from simulation by points. In all cases $N = 1000$, $I_0 = 100$, $\alpha = 0.05$, $\omega = 0.1$, $\beta = 0.5$ and $\gamma = 1$. The initial network is a regular random graph with $k = 4$. In each case, mean values from the stochastic simulations were found by averaging over 100 repetitions, with the individual realisations plotted in grey.

contact network and is described by the following system of $(M+1)(M+2)$ equations:

$$\begin{aligned}
\dot{S_{si}} &= -\beta i S_{si} + \gamma I_{si} + \gamma[(i+1)S_{s-1,i+1} - iS_{si}] \qquad (5.4)\\
&\quad + \beta \frac{\sum_{k=0}^{M} \sum_{j+l=k} jl S_{jl}}{\sum_{k=0}^{M} \sum_{j+l=k} j S_{jl}} [(s+1)S_{s+1,i-1} - sS_{si}]\\
&\quad - \omega[(s+i)S_{si} - (i+1)S_{s,i+1} - (s+1)S_{s+1,i}]\\
&\quad - \alpha(M-(s+i))S_{si} + \alpha(M-(s-1+i))P_S S_{s-1,i},\\
&\quad + \alpha(M-(s+i-1))P_I S_{s,i-1}\\
\dot{I_{si}} &= \beta i S_{si} - \gamma I_{si} + \gamma[(i+1)I_{s-1,i+1} - iI_{si}] \qquad (5.5)\\
&\quad + \beta \frac{\sum_{k=1}^{M} \sum_{j+l=k} l^2 S_{jl}}{\sum_{k=1}^{M} \sum_{j+l=k} j I_{jl}} [(s+1)I_{s+1,i-1} - sI_{si}]\\
&\quad - \omega[(s+i)I_{si} - (i+1)I_{s,i+1} - (s+1)I_{s+1,i}]\\
&\quad - \alpha(M-(s+i))I_{si} + \alpha(M-(s-1+i))P_S I_{s-1,i}\\
&\quad + \alpha(M-(s+i-1))P_I I_{s,i-1},
\end{aligned}$$

for $\{(s,i) : s,i \geq 0, 0 \leq k = s+i \leq M\}$. This system is the *dynamic* SIS effective degree model.

5.4 Calculating the disease threshold

For the static case, Lindquist et al. (2011) used the next generation matrix approach (Diekmann and Heesterbeek, 2000) to calculate the disease threshold to be

$$\mathcal{R}_0 = \rho(FV^{-1}) = \frac{\beta}{\sum_{k=1}^{M} kS_{k,0}} \sum_{k=1}^{M} v_k^T V_k^{-1} u_k. \tag{5.6}$$

In this approach, Eqs. (5.4) and (5.5) are linearized at the disease-free equilibrium (DFE) and the Jacobian at the DFE is written as $F - V$. In this formulation, F accounts for transitions from disease-free states to disease states (in the static case only the transition from $S_{s,0}$ to $S_{s-1,1}$ needs to be considered) and V accounts for transitions between different disease states. The spectral radius, ρ, the leading eigenvalue of FV^{-1}, gives R_0 and describes the stability of the DFE. If $R_0 < 1$ the DFE is stable and no epidemic will occur, but if $R_0 > 1$ the DFE is unstable and the infectious agent can spread through the population.

We can calculate F in the dynamic case by noting that the same $S_{s,0}$ to $S_{s-1,1}$ type transitions can still occur, but in addition nodes can enter the disease states by linking to an infected node, namely $S_{s,0}$ to $S_{s,1}$ transitions. If we introduce a subscript s to denote the static version of the next generation matrix, so the static version of F is called F_s and so on, we have

$$F_s = \frac{\beta}{\sum_{k=0}^{M} kS_{k,0}} \begin{bmatrix} u_{s_0} \\ u_{s_1} \\ \vdots \\ u_{s_M} \end{bmatrix} \begin{bmatrix} v_{s_0}^T & v_{s_1}^T & \dots & v_{s_M}^T \end{bmatrix}, \tag{5.7}$$

where u_{s_k} and v_{s_k} are $(2k+1)$ x 1 vectors. The u_{s_k} vectors have $kS_{k,0}$ as their first entry and zeros elsewhere and the v_{s_k} vectors have their first $(k-1)$ entries equal to $(k-1), 2(k-2), \dots, s(k-s), \dots, (k-1)$ and zeros elsewhere. This is almost identical to the F matrix constructed by Lindquist et al., but is augmented by u_{s_0} and v_{s_0} to account for the new disease state, $I_{0,0}$, and the summation starts at $k = 0$ rather than $k = 1$,

We now introduce a new subscript d to describe the new transitions that are only possible in the dynamic model. Hence a new F matrix, F_d, is created, which has exactly the same dimensions as F_s, and is given by

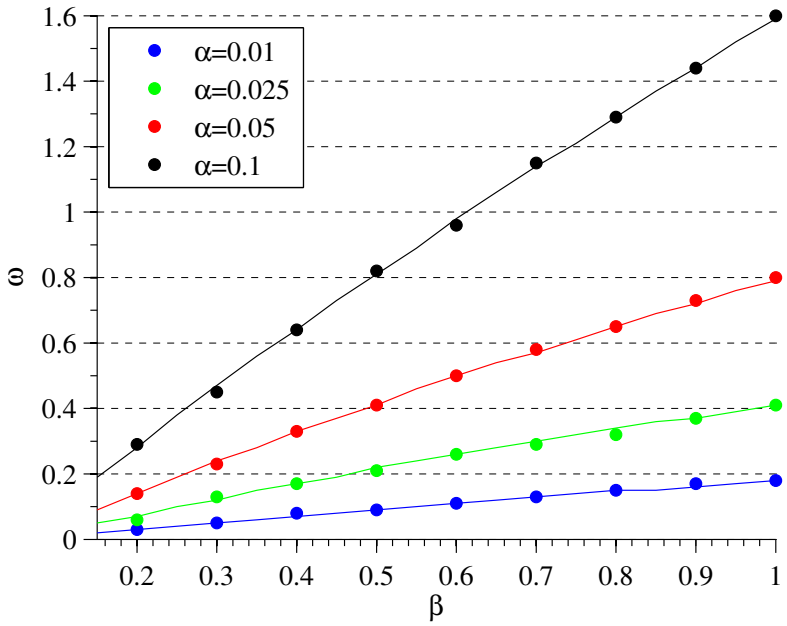

Figure 5.3: Epidemic threshold plot in the (β, ω) parameter space for four distinct values of α. Results from the ODE are given by solid lines and those from simulation by solid points. In each case, $N = 1000$, $I_0 = 10$, $M = 20$ and $\gamma = 1$. The initial network is a regular random graph with $k = 4$.

$$F_d = \frac{\alpha}{\sum_{k=0}^{M}(M-k)S_{k,0}} \begin{bmatrix} u_{d_0} \\ u_{d_1} \\ \vdots \\ u_{d_M} \end{bmatrix} \begin{bmatrix} v_{d_0}^T & v_{d_1}^T & \dots & v_{d_M}^T \end{bmatrix}. \tag{5.8}$$

.

Here, u_{d_k} is again a $(2k+1)$ x 1 vector with the first entry equal to $(M-(k-1))S_{k-1,0}$ and all other entries equal to zero. In the case where $k = 0$, $u_{d_0} = (0)$. In addition, v_{d_k} is the same size as u_{d_k} and the first k entries are equal to zero, with the remaining $k+1$ entries equal to $M-k$. The final F matrix that captures all the possible transitions in the dynamic effective degree model is found by taking a linear sum of the two, namely $F = F_s + F_d$.

As with the static case, the V matrix is constructed through careful book-keeping, which can be done through iterative routines. In the static case, as the nodes have fixed degree, V_s is a block diagonal matrix with $V_s = V_{s_1} \oplus V_{s_2} \oplus ... \oplus V_{s_M}$. For the dynamic model, V_d will be a block tri-diagonal matrix, as state transitions can now also occur by nodes gaining or loosing a link. In addition, the extra disease state $I_{0,0}$ needs to be considered, and V will now also depend upon α and ω as well as β and γ. Once $F = F_s + F_d$ and $V = V_d$ are constructed, the leading eigenvalue or R_0 is computed numerically.

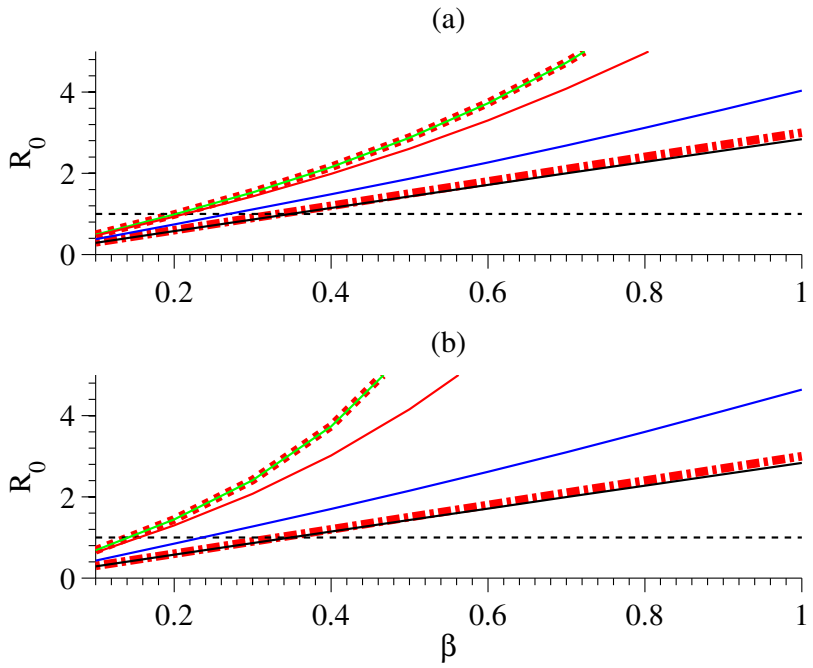

Figure 5.4: Threshold stability in the (β, R_0) space with $\gamma = 1$, $M = 20$ and $\langle k \rangle^* = 3$ for (thin solid lines, in order from top to bottom) $\alpha = 10^{-4}$ (green), $\alpha = 10^{-2}$ (red), $\alpha = 10^{-1}$ (blue) and $\alpha = 10$ (black). In (a) the initial network is a regular random graph with $k = 6$ and in (b) the initial degree distribution is negative binomial with $\langle k \rangle = 6$ and $\sigma^2 = 12$. In each case, $\omega = \alpha \frac{M - \langle k \rangle^*}{\langle k \rangle^*}$. The thick short-dashed red line is the theoretical value of R_0 for a static network, and the thick red dash-dotted line is the mean field limit $R_0 = \frac{\beta}{\gamma} \langle k \rangle^*$.

5.5 Results and discussion

As shown in Fig. 5.2, the ODEs given by Eqs. (5.4) and (5.5) closely capture the time evolution of an epidemic as predicted by stochastic simulations. The only parameter that is varied in Fig. 5.2 is M, and it is interesting to note the effect it has on the evolution of the disease. As per Eq. (5.3), the mean nodal degree at equilibrium is dependent on M, and hence, given the same initial network configuration and values of α and ω, the network either loses or gains links as the system evolves. Thus varying the carrying capacity alone leads to different outcomes depending on whether the network can reach a level of connectedness that allows an epidemic to spread and become established. Allowing M to become an active model parameter that is able to control the outcome of an epidemic has potentially interesting real world implications. The number of contacts per person is a natural, countable property unlike the other model parameters, such as ω, which are more difficult to infer. Therefore local constraints that limit the maximum number of contacts per person could be potentially used as a metric when promoting safe behaviour at a population level in the event of an outbreak or other public health crisis.

In Fig. 5.3, for a given value of α, M and β, the epidemic threshold has been calculated

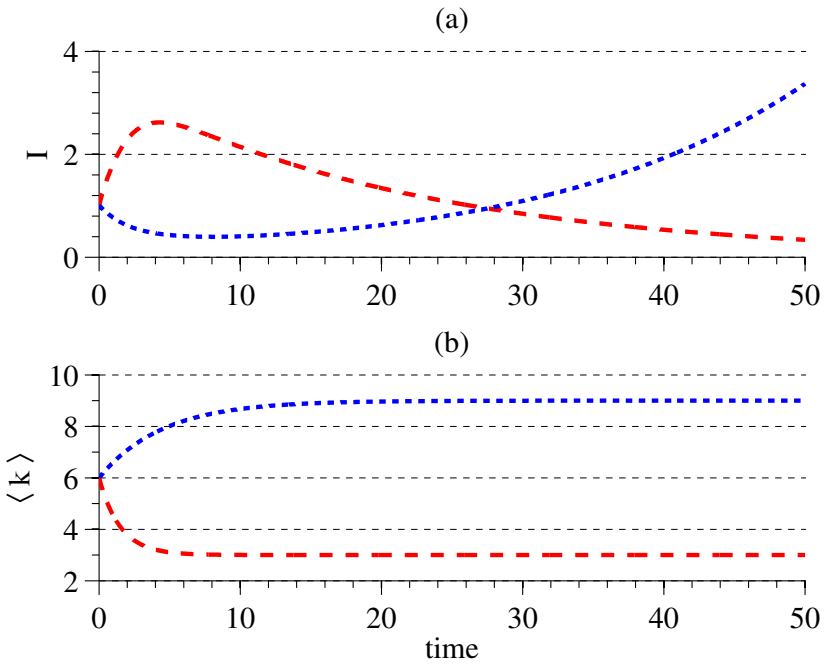

Figure 5.5: Time evolution of I and $\langle k \rangle$ with $\gamma = 1$, $M = 20$, $\alpha = 0.1$, $\omega = \alpha \frac{M - \langle k \rangle^*}{\langle k \rangle^*}$ and an initial regular random network with $k = 6$. The two cases illustrated above correspond to: $\langle k \rangle^* = 3$ and $\beta = 0.35$, giving $R_0 \approx 1.29$ (red long-dashed line) and $\langle k \rangle^* = 9$ and $\beta = 0.125$, giving $R_0 \approx 0.77$ (blue short-dashed line).

from the ODEs in terms of ω and compared to that predicted by simulations. The agreement is excellent and this is strong evidence that the dynamic effective degree model accurately captures the evolution of an epidemic on a network with random link creation and deletion. When considering the (β, ω) parameter space used for the threshold plot in Fig. 5.3, there are three distinct regions that are worth noting. Firstly, given an initial starting network, it is possible to calculate the threshold value of β in the static network case. For the regular random graph with $k = 4$ used here, that value is $\beta^* \approx 0.36$. For values of $\beta < 0.36$, the relative time scales of disease and network evolution are crucial in determining whether or not an epidemic will occur. In this situation, the network needs to quickly evolve to become more densely connected in order for there to be an outbreak. The second area of interest is when the disease is highly infectious and as a result requires a high value of ω to drive the epidemic below threshold. Indeed, if the disease parameters β and γ are fixed then the only way of affecting the outcome of an epidemic is through changing the network structure, i.e. reducing the number of links or the variance. Hence, for a fixed α and M, a value of β can be chosen large enough so that the minimum value of ω needed to reduce the connectivity of the network sufficiently to stop an outbreak (see Fig. 5.3), gives $\langle k \rangle^* < 2$ as can be calculated from Eq. 5.3. If a network has $\langle k \rangle^* < 2$ then it becomes fragmented, with many nodes becoming unconnected. In these situations, the value ω needed to prevent an epidemic virtually destroys the network. In terms of real world implications, a large value of ω could correspond to a

situation of strict quarantine and curfew whereby links between individuals are kept to a minimum. In between these two cases lies a region within which an epidemic would take hold naturally, given the initial network, but which can be prevented by a value of ω that leaves the network well connected.

In Fig. 5.4, we show analytical values of R_0 for a range of values of β and α. It is worth noting that two limiting cases are recovered when the timescale of the network dynamics is fast and slow relative to the timescale of the disease dynamics. The thick short-dashed red line shows R_0 calculated for a static network, as proposed by Lindquist et al. (2011) and given in Eq. 5.6, and this is exactly followed by results from our dynamic R_0 calculation when the network dynamics are set to be much slower than the disease dynamics. The other extreme is shown by the thick dash-dotted red line, and is the value of R_0 that results form the classic mean-field calculation $R_0 = \frac{\langle k \rangle \beta}{\gamma}$. The time evolution of $\langle k \rangle$ is given by $\langle \dot{k} \rangle = \alpha(M - \langle k \rangle) - \omega \langle k \rangle$ but, when the network dynamics is fast, the equilibrium network distribution, and hence $\langle k \rangle^*$, is approached much quicker than the epidemic timescale and hence a value of $\langle k \rangle = \langle k \rangle^*$ as given by Eq. 5.3 can be used. This limit is closely matched by results from our dynamic R_0 calculation when the network dynamics are rapid compared to disease transmission as shown in Fig. 5.4.

Although Fig. 5.4 demonstrates the accuracy of our analytical R_0 calculation, Fig. 5.5 highlights two example cases where the long term epidemic outcomes are the opposite of what is predicted by R_0. In the cases $R_0 < 1$ (blue short-dashed curve) and $R_0 > 1$ (red long-dashed curve) the system settles to an endemic and to a disease free equilibrium respectively, due to the different ways the networks evolve. Given that R_0 is based on a local stability analysis, it can only incorporate the immediate next-generation effects of random link activation and deletion, and cannot account for long term changes to the network structure. It is well established in the literature (see, for example Li et al. (2011)) that R_0 is of limited value when used as a predictor, and even for static networks needs to be used with care. Our results add weight to this argument, and we show that when dealing with disease spreading through dynamic contact networks the use of R_0 as any kind of predictor on long term disease evolution should be met with some degree of caution.

In summary, this paper has proposed an effective degree model for epidemics on dynamic networks with random link activation and deletion, where activation is locally constrained. We have shown that this model agrees extremely well with results obtained from stochastic simulations, and as such can reliably be used for the analytical and semi-analytical study of coupled disease and network dynamics. We have shown how a local constraint limiting the number of contacts per individual can be used to control and prevent the outbreak of an epidemic in this dynamic model. We have also proposed an analytical calculation of R_0, but also demonstrated the limited value of threshold stability analysis in predicting the evolution of a disease in a dynamic contact network. In future work, this model can be adapted and extended to account for individuals cutting and creating links with knowledge of the state of

others in the population, i.e., link-type dependent network dynamics. This two-way feedback will lead to more sophisticated network properties such as degree correlations, high clustering or even network fragmentation. In such cases ODE models need to be used with care, making sure that the agreement with simulations remains valid. Besides modelling epidemics, this framework could also be used to study the spread of information, beliefs and new ideas within populations, and as such could have implications across a wide range of disciplines beyond the mathematical biology and physics communities.

Acknowledgments Michael Taylor acknowledges support from EPSRC (DTA grant). Timothy J. Taylor acknowledges support from MRC and Sussex University.

Chapter 6

Paper 4: Identification of criticality in neuronal avalanches: I. A theoretical investigation of the non-driven case

Timothy J. Taylor[1], Caroline Hartley[2,3], Péter L. Simon[4], Istvan Z. Kiss[5] and Luc Berthouze[1,2]

[1]Centre for Computational Neuroscience and Robotics, University of Sussex, Brighton BN1 9QH, UK

[2]Institute of Child Health, London, University College London, London WC1E 6BT, UK

[3]Centre for Mathematics and Physics in the Life Sciences and Experimental Biology, University College London, London, WC1E 6BT, UK

[4]Institute of Mathematics, Eötvös Loránd University Budapest, Budapest, Hungary

[5]School of Mathematical and Physical Sciences, Department of Mathematics, University of Sussex, Brighton BN1 9QH, UK

Published in *The Journal of Mathematical Neuroscience, 3 (4). p. 5. ISSN 2190-8567*

6.1 Abstract

In this paper we study a simple model of a purely excitatory neural network that, by construction, operates at a critical point. This model allows us to consider various markers of criticality and illustrate how they should perform in a finite-size system. By calculating the exact distribution of avalanche sizes we are able to show that, over a limited range of avalanche sizes which we precisely identify, the distribution has scale free properties but is not a power law. This suggests that it would be inappropriate to dismiss a system as not being critical purely based on an inability to rigorously fit a power law distribution as has been recently advocated. In assessing whether a system, especially a finite-size one, is critical it is thus important to consider other possible markers. We illustrate one of these by showing the divergence of susceptibility as the critical point of the system is approached. Finally, we provide evidence that power laws may underlie other observables of the system, that may be more amenable to robust experimental assessment.

6.2 Introduction

A number of *in vitro* and *in vivo* studies (Beggs and Plenz, 2003, 2004; Petermann et al., 2009; Hahn et al., 2010) have shown neuronal avalanches – cascades of neuronal firing – that may exhibit power law statistics in the relationship between avalanche size and occurrence. This has been used as *prima facie* evidence that the brain may be operating near, or at, criticality (Chialvo, 2010; Sethna et al., 2001). In turn, these results have generated considerable interest because a brain at or near criticality would have maximum dynamic range (Kinouchi and Copelli, 2006; Shew et al., 2009; Buckley and Nowotny, 2011; Larremore et al., 2011) enabling it to optimally react and adapt to the dynamics of the surrounding environment (Chialvo, 2010; Linkenkaer-Hansen et al., 2001) whilst maintaining balanced neuronal activity (Benayoun et al., 2010; Magnasco et al., 2009; Meisel et al., 2012). Neuropathological states (e.g., epileptic seizures) could then be conceptualised as a breakdown of, or deviation from, the critical state, see Milton (2012), for example. Furthermore, these findings have led to the notion that the brain may self-organise to a critical state (Bak et al., 1987), i.e., its dynamics would be driven towards the critical regime by some intrinsic mechanism and not be dependent on external tuning. In support of this view, Levina et al. (2007) showed analytically and numerically that activity-dependent depressive synapses could lead to parameter-independent criticality.

The interpretation that neuronal activity is poised at a critical state appears to be mostly phenomenological whereby an analogy has been developed between the propagation of spikes in a neuronal network and models of percolation dynamics (Essam, 1980) or branching processes (Beggs, 2006; Harris, 1963). Remarkable qualitative similarities between the statistical properties of neuronal activity and the above models have given credence to this analogy, however, the question remains as to whether it is justified. Indeed, various key assumptions

underlying percolation dynamics and branching processes are typically violated in the neuroscience domain. For example, full sampling, which is required in order to assess *self-organised* criticality, is unattainable even in the most simple *in vitro* scenario and yet it has been shown that sub-sampling can have profound effects on the distribution of the resulting observations (Priesemann et al., 2009). On a related note, and more generally, the formal definition of a critical system as one operating at, or near, a second order (continuous) phase transition is problematic since the concept of phase transition applies to systems with infinite degrees of freedom (Deco et al., 2012). Many neuroscience authors address this by appealing to the concept of finite size scaling and many published reports implicitly assume that distributions are power law with truncation to account for the so-called finite size effect. Typically, such reports adopt an approach whereby (a) scale invariance is assessed through finite size scaling analysis, confirming that upon rescaling the event size, the curves collapse to a power law with truncation at system size (but see below regarding the definition of system size); (b) the parameters of statistical models are estimated, typically over a range of event size values that are rarely justified; and (c) the best model is determined by model selection, in which power law and exponentially truncated power law are compared to alternatives such as exponential, lognormal and gamma distributions, see Klaus et al. (2011) for a typical example. Whilst greater rigour in the statistical treatment of the assessment of the presence of power laws has been attained following the influential paper of Clauset et al. (2009), what seems to be lacking is a rigorous treatment as to why a power law should be assumed to begin with. Although this question is particularly pertinent to the neurosciences, it should be noted that similar questions remain open in the field of percolation theory (e.g., Ziff (2011); Borgs et al. (2001)), namely: (i) how does the critical transition behaviour emerge from the behaviour of large finite systems and what are the features of the transition? (ii) what is the location of the scaling window in which to determine the critical parameters?

This paper specifically seeks to address the following questions:

1. Assuming that the whole brain, or indeed a region of interest defined by where data can be obtained, is operating at criticality, can we reasonably expect power law statistics in neural data coming from a very small (possibly sub-sampled) subset of the system? If not, what would be the expected distribution? Sornette (2006) states that the Gamma distribution is "found in critical phenomena in the presence of a finite size effect or at a finite distance from the critical point". Jensen (1998) claims that finite-size systems often show an exponential cut-off below the system size. However, we are not aware of any study in which the distribution of event sizes in a finite-size system set to operate at a critical regime has been investigated.

2. In a finite-size system, is it reasonable/possible to perform a robust statistical assessment of power law statistics? Even the application of a rigorous model selection approach will lead to different results depending on the choice of the range of event sizes and the number of samples being considered (Touboul and Destexhe, 2010). The issue of

range selection is of particular interest. Whilst the notion of system size is clear in models of criticality such as the Abelian sandpile where (i) there is full sampling, (ii) the number of sites is finite, and (iii) there is dissipation at the edges, system size is much less obvious where re-entrant connections exist, making it possible, in principle, for avalanches to be of infinite size. Here, the counting measure which leads to the definition of an avalanche is important. Counting the number of neurones involved in an avalanche will lead to a clearly defined system size, whereas counting the total number of activations – the *de facto* standard, e.g., Beggs and Plenz (2003); Levina et al. (2007); Benayoun et al. (2010) – will not. Furthermore, it should also be noted that the presence of re-entrant connections invalidates the standard theory of branching processes (Harris, 1963), and makes a rigorous determination of the branching parameter σ problematic if not impossible, e.g., in the presence of avalanches merging.

3. Are there other markers of criticality that may be more amenable to characterisation and that should be considered instead of, or in addition to, the statistics of event sizes? The need for such markers in neuroscience has been recognised (see Touboul and Destexhe (2010) for example) and a number of studies have investigated long-range temporal correlations (power-law decay of the autocorrelation function) in amplitude fluctuations (Linkenkaer-Hansen et al., 2001) and in inter-burst intervals (Hartley et al., 2012; Segev et al., 2002). However, a theoretical account of how those may relate to one another is lacking (although see the recent work in Poil et al. (2012)). Other markers of criticality (or markers of transitions) have been associated with critical physical systems, e.g., divergence of susceptibility and slowing of the recovery from perturbations near the critical point (Sornette, 2006), however, we are not aware of any theoretical or empirical study investigating them in a neuroscience context.

One way to address these questions more rigorously is to use simplified but therefore more tractable conceptual models (e.g., Droste et al. (2013)). In this paper, we use a model of a purely excitatory neuronal system with simple stochastic neuronal dynamics that can be tuned to operate at, or near, a second order phase transition (specifically, a transcritical bifurcation). The simplicity of the model allows us to analytically calculate the exact distribution of avalanche sizes, which we confirm through simulations of the system's dynamics. We study our model at the critical point and compare our exact distribution to the explicit but approximate solution proposed by Kessler (2008) in an analogous problem of modelling disease dynamics. We confirm that Kessler's approximate solution converges to our exact result. Importantly, we show that, in the proposed finite-size system, this distribution is not a power law, thus highlighting the necessity of considering other markers of criticality. We thus analyse two potential markers of criticality: (i) the divergence of susceptibility that arises in the model as we approach the critical point, (ii) the slowing down of the recovery time from small disturbances as the system approaches the critical point. Finally, we speculate on a sufficient but not necessary condition under which our exact distribution could converge to a

true power law in the limit of the system size.

6.3 The stochastic model

We start from the stochastic model of Benayoun et al. (2010) which we simplify to the most trivial of models. A fully connected network of N neurones is considered with purely excitatory connections (as opposed to the excitatory and inhibitory networks considered in Benayoun et al. (2010)). Within the network, neurones are considered to be either quiescent (Q) or active (A). Taking a small time step dt and allowing $dt \to 0$ the transition probabilities between the two states are then given by:

$$P\left(Q \to A, \text{ in time } dt\right) = f\left(s_i(t)\right) dt$$
$$P\left(A \to Q, \text{ in time } dt\right) = \alpha dt$$

where $s_i(t) = \sum_j \frac{w_{ij}}{N} a_j(t) + h_i$ is the input to the neurone. Here f is an activation function, h_i is an optional external input, w_{ij} is the connection strength from neurone i to neurone j and $a_j(t) = 1$ if neurone j is active at time t and zero otherwise. α is the de-activation rate and therefore controls the refractory period of the neurone.

To allow tractability, we further make the following simplifications:

1. We assume that all synaptic weightings are equal ($w_{ij} = w$).
2. We assume there is no external input. The driven case will be explored theoretically and empirically in a companion manuscript.
3. We assume the linear identity activation function $f(x) = x$. Although it is more common to use sigmoid activation functions we note that the identity function can just be thought of as a suitably scaled *tanh* function over the desired range.

As the network is fully connected we can write the following mean field equation for active neurones:

$$\frac{dA}{dt} = \frac{wA}{N}Q - \alpha A = \frac{wA}{N}(N - A) - \alpha A,$$

where we have appealed to the fact that the system is closed and thus $A + Q = N$. This ODE is analogous to the much studied (Allen, 2008) susceptible $\to$ infectious $\to$ susceptible (SIS) model used in mathematical epidemiology and we can appeal to some of the known results in studying its behaviour. Primarily we can use simple stability analysis. The non-zero steady state is given by $A^* = N(1 - \alpha/w)$. Setting $g(A) = \frac{dA}{dt}$, this equilibrium point is stable if $g'(A^*) < 0$. Thus

$$g'(A) = (w - \alpha) - 2w\frac{A}{N} \Rightarrow g'(A^*) = (w - \alpha) - 2w\frac{N(1 - \alpha/w)}{N} = \alpha - w.$$

Borrowing from epidemiology we define the threshold $R_0 = \frac{w}{\alpha}$. If $R_0 > 1$ we see that $g'(A^*) = \alpha - w < 0$ and the non-zero steady state is stable. Figure 6.1 illustrates the differing behaviour of the solution to the above ODE for $R_0 < 1$ (sub-critical), $R_0 = 1$ (critical) and $R_0 > 1$ (super-critical).

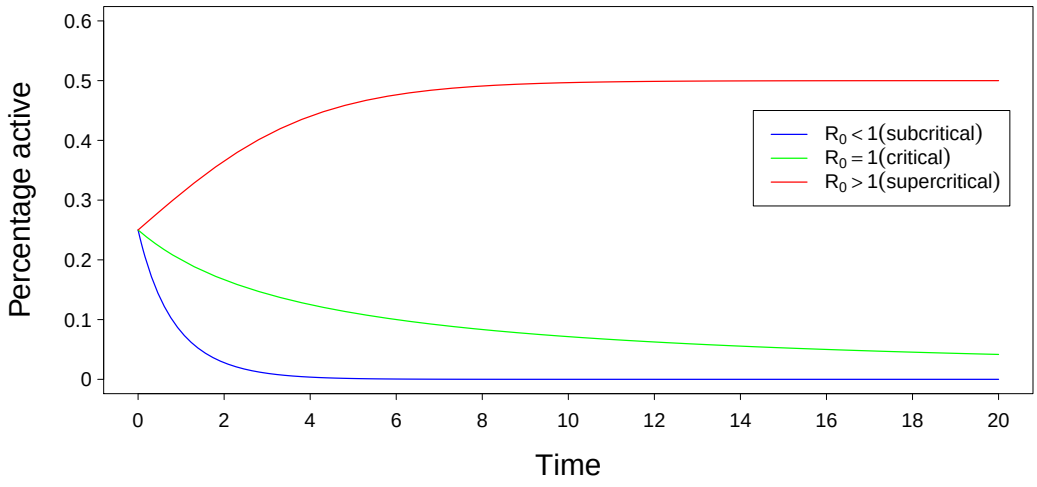

Figure 6.1: **Activity in the different regimes.** Plot of the solution to the ODE for $N = 800$ and three different regimes where R_0 was set to 0.5 (blue), 1.0 (green) and 2.0 (red). Initially we activated 25% of the network.

6.3.1 Firing neurones and avalanches

Instead of focussing on the average activity level across the network we will instead look at the size distribution of firing neurones following one firing event. To do this we begin with a fully quiescent network and initially activate just one neurone. We then record the total number of neurones that fire (the number of quiescent to active transitions) until the network returns to the fully quiescent state. We use this process of sequential activation as our definition of an avalanche and our main interest is the distribution of the avalanche sizes. Unfortunately, the simple ODE approach will not provide us with this distribution. To calculate this distribution, we use the semi-analytic approach described in the following section.

6.3.2 Tree approach to the avalanche distribution

We begin by defining q_i as the probability the next transition is a recovery (from A to Q) given i active neurones ($i > 0$). The probability the next transition is an activation is then

$1 - q_i$ and we have:

$$q_i = \frac{\alpha N}{w(N-i) + \alpha N} = \frac{N}{R_0(N-i) + N},$$
$$1 - q_i = \frac{w(N-i)}{w(N-i) + \alpha N} = \frac{R_0(N-i)}{R_0(N-i) + N}.$$

In order to calculate the avalanche size distribution we adopt a recursive approach. We begin by considering the process unfolding in a tree like manner with 1 initially active neurone. The tree can be divided into levels based on the number of transitions that have occurred and how the process is unfolding. Let level j contain the possible number of active neurones after j transitions. The recursive tree approach relates the probability of transition between levels to the final avalanche size. Figure 6.2 illustrates the initial levels of this process.

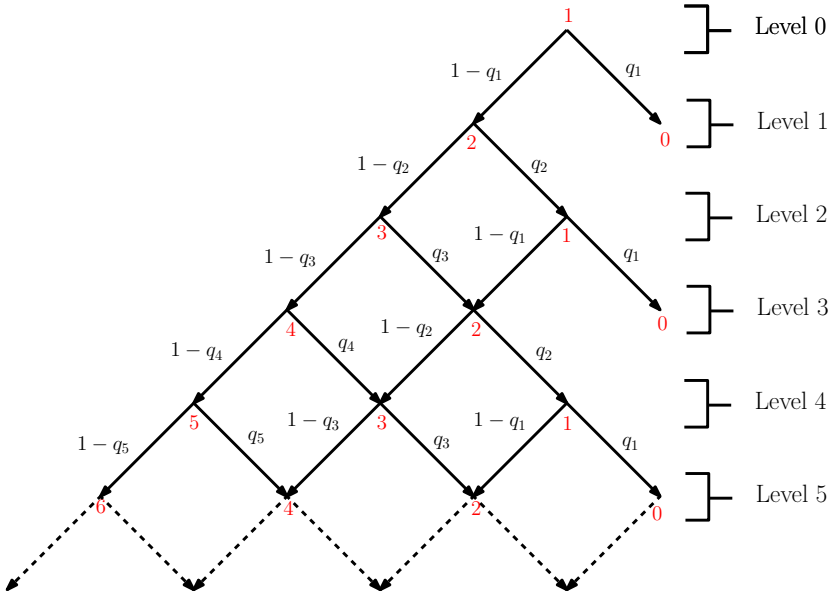

Figure 6.2: **First six levels of the probability tree.** Red numbers are the number of active neurones, black values are the probability of transitions between levels and sub levels.

To continue we define p_j^i as the probability of having i active neurones on level j with $i = 0, 1, 2, \ldots, N$ and $j \in \mathbb{N}_0$. Assuming initially only one active neurone, we immediately see that $p_0^1 = 1$, $p_1^2 = 1 - q_1$ and $p_1^0 = q_1$. To proceed we will consider the probability of having a particular number of active neurones on an arbitrary level. First we note the following

relation between levels

$$p_j^i = \begin{cases} p_{j-1}^2 q_2, & \text{if } i = 1, \\ p_{j-1}^{i-1}\left(1 - q_{i-1}\right) + p_{j-1}^{i+1} q_{i+1}, & \text{for } 1 < i < N, \\ p_{j-1}^{N-1}\left(1 - q_{N-1}\right), & \text{if } i = N. \end{cases}$$

We now define:

$$\mathbf{p}(l) = \begin{pmatrix} p_l^1 \\ . \\ . \\ . \\ . \\ . \\ p_l^N \end{pmatrix}.$$

We can now write $\mathbf{p}(l+1) = \mathbf{A} \cdot \mathbf{p}(l)$ where matrix $\mathbf{A}$ is given by the following tridiagonal matrix:

$$\mathbf{A} = \begin{pmatrix} 0 & c_1 & & & & & & \\ \ddots & \ddots & \ddots & & & & & \\ & \ddots & \ddots & \ddots & & & & \\ & & b_i & 0 & c_i & & & \\ & & & \ddots & \ddots & \ddots & & \\ & & & & \ddots & \ddots & \ddots & \\ & & & & & b_N & 0 \end{pmatrix}$$

with $b_i = (1 - q_{i-1})$ and $c_i = q_{i+1}$.

On the j^{th} level of the tree, the probability of only 1 neurone being active is given by p_j^1. As on level 0 we began with only a single active neurone then for j odd, p_j^1 is always equal to zero. For j even, say $j = 2k$, then as we began with only one active neurone on level 0, to have only one active neurone on level j means that k firings must have occured. We can then calculate the probability of zero active neurones after k firings as $q_1 p_{2k}^1$; this is thus the probability, $P(k+1)$, of having an avalanche of size $k+1$ (or size k if we were not to include the initial active neurone). Setting $e = (1, 0, 0, \ldots, 0)^T$ and noting that $p_{2k}^1 = e^T A^{2k} e$ we have $P(k+1) = q_1 e^T A^{2k} e$. To calculate the distribution we implemented this recursive method of calculation in the MATLAB® environment. Whilst this result is exact, and will be referred to as such henceforth, it can only be calculated numerically via recursion and cannot be given

in the form of a closed expression.

6.3.3 Simulations of neuronal avalanches

In order to check the validity of our method, we performed simulations of the firing neurones using the Gillespie algorithm (Gillespie, 1977). Due to the network being fully connected the algorithm is relatively straightforward:

- As earlier let A be the number of active neurones in the network (Q the number of quiescent). Given that an individual neurone becomes quiescent at rate α then the total rate of (Active $\rightarrow$ Quiescent) transitions is given by $r_{aq} = A\alpha$. Similarly the total rate of (Quiescent $\rightarrow$ Active) transitions is given by $r_{qa} = f(s_i)Q = f(s_i)(N - A)$.
- Let $r = r_{aq} + r_{qa}$ and generate a timestep dt from an exponential distribution of rate r.
- Generate a random number n between 0 and 1. If $n < \frac{r_{aq}}{r}$ an active neurone turns quiescent, otherwise a quiescent neurone is activated (fires). This event is said to occur at time $t + dt$ and the network is updated accordingly.

6.3.4 Exact solution compared to simulation

Values of the threshold, R_0, were chosen less than, equal to and finally above 1. We will refer to these regimes as subcritical, critical and supercritical respectively. Figure 6.3 illustrates the, as expected, good agreement between the simulations and the exact result for the three different regimes of R_0.

6.3.5 Comparing the exact solution to a closed form approximation

In Kessler (2008), Kessler proposed a closed solution to the analogous susceptible-infected-susceptible (SIS) problem where he was interested in the number of infections (including reinfections) occurring over the course of an epidemic. For small avalanche sizes where the number of infectives is negligible compared to the network size the transition probabilities can be approximated as

$$\begin{aligned} q_i &= \frac{N}{R_0(N-i)+N} \approx \frac{1}{R_0+1}, \\ 1-q_i &= \frac{R_0(N-i)}{R_0(N-i)+N} \approx \frac{R_0}{R_0+1}. \end{aligned}$$

In the critical regime $R_0 = 1$, the problem reduces to calculating the distribution of first passage times of a random walk with equal transition probabilities. Thus for avalanche sizes in the range, $1 \ll n \ll \sqrt{N}$, Kessler (2008) gave the following distribution based on Stirling's

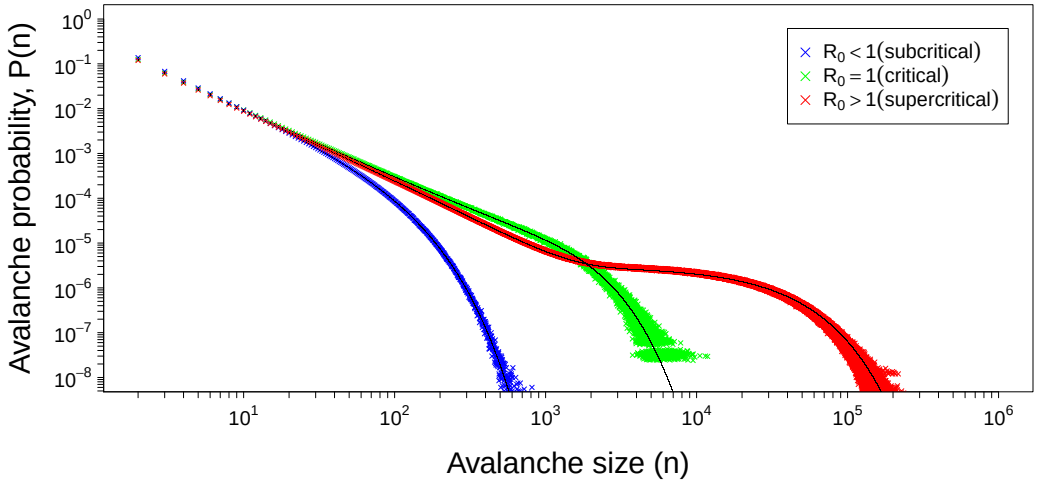

Figure 6.3: **Avalanche distributions.** Results from the simulations of the avalanche distributions for the subcritical ($R_0 < 1$, blue), critical ($R_0 = 1$, green) and supercritical ($R_0 > 1$, red) regimes for a network of size $N = 800$. For each regime $2,000,000,000$ avalanches were simulated. The corresponding exact solutions are shown in black.

approximation

$$P(n) = \frac{1}{2^{2n-1}}\left[\binom{2n-2}{n-1} - \binom{2n-2}{n}\right] \approx \frac{1}{\sqrt{4\pi n^3}}. \tag{6.1}$$

We note however that the range over which the distribution can be shown to be a power law is rather limited and for small networks will not hold. Using the theory of random walks and a Fokker-Planck approximation Kessler also derived the following closed solution to the probability distribution of infections in the critical regime ($R_0 = 1$) for larger sizes:

$$P(n) = \frac{1}{\sqrt{4\pi N^3}} \exp(n/2N) \sinh^{-\frac{3}{2}}(n/N) \quad (n \gg 1) \tag{6.2}$$

Figure 6.4 plots this approximation against our exact solution for a network of size $N = 800$. To more formally assess the convergence of the approximate solution to that of our exact solution we considered the probabilities of avalanches from size $N/10$ to $20N$ and measured the difference between the distributions using two different metrics. Letting $P_e(n)$ be the exact probability of an avalanche of size n and $P_k(n)$ be the Kessler approximation to this we first considered the standard mean-square error given by

$$Error(N) = \frac{1}{R}\sum_{n=N/10}^{20N} (P_e(n) - P_k(n))^2 \quad \text{where } R = 20N - N/10 + 1.$$

Secondly we considered a more stringent measure of the error by looking at the supremum of difference between the same range of avalanches

$$Error(N) = \sup_n |P_e(n) - P_k(n)|.$$

Figure 6.5 illustrates the two errors for increasing network size and both show how the proposed closed solution is indeed converging to that of the exact.

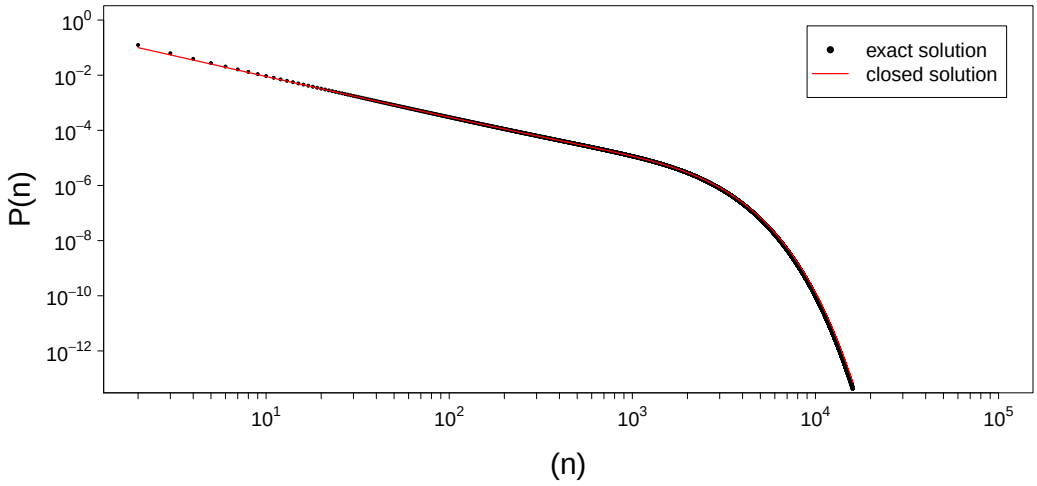

Figure 6.4: **Closed solution versus exact.** Plot of the closed solution (red solid line) versus the exact solution (black dots) for a network of size $N = 800$ operating in the critical regime.

6.4 Scale-free behaviour in the $R_0 = 1$ regime

Whilst Equation 6.1 gives a power law, this equation only holds over a limited range. Equation 6.2, in turn, is neither a power law nor a truncated power law. Here, we assess the range over which the distribution of sizes can be said to exhibit scale-free behaviour. For a rigorous assessment of this range, we employ a subset of the model selection approach described by Clauset et al. (2009). Specifically, we consider 100,000 of the simulated avalanches described earlier and fit a truncated power law distribution of the form $P(x) = Cx^{-\alpha}$ to avalanches up to size $x_{max} = \frac{9}{10}N$ (the choice of this upper bound will be justified in the following section) by using the maximum likelihood method (here C is a normalising constant to keep the sum of the distribution between $[x_{min}, x_{max}]$ equal to 1). We do this by finding values of α and x_{min} that maximise the probability of obtaining our simulated avalanches given the fitted distribution. Next we randomly generate 1000 data sets from the fitted distribution and compute the difference between these synthetic data sets and the fitted form (using the

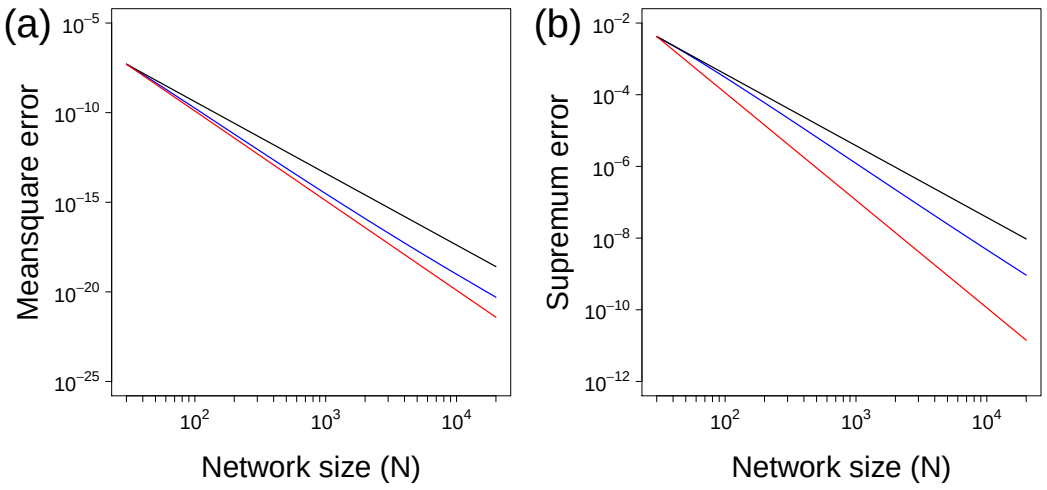

Figure 6.5: **Convergence of closed solution to exact.** (a) Here the mean square error is given by the blue line and $O(N^2)$ and $O(N^3)$ convergence represented by the black and red lines respectively. (b) Here the supremum error is given by the blue line and $O(N^4)$ and $O(N^5)$ convergence represented by the black and red lines respectively.

Kolmogorov-Smirnov statistic). Similarly we compute the difference between our simulations and the fitted power law. The p-value is then calculated as the proportion of synthetic data sets that are further away from the theoretical distributions than our simulations. As per Clauset et al. (2009), the hypothesis (that the data comes from a power law) is rejected if the p-value is less than 0.1. Note that in the model selection approach, should the hypothesis not be rejected, then one should test alternative models and use an information criterion to identify the best model. However, our focus here is purely on assessing whether our distribution can be said to behave like a power law distribution (we know it is not actually a power law) and therefore alternative models were not tested. With $100,000$ avalanches we obtained a p-value of 0.382 leading us not to reject the hypothesis that the distribution was power law (see Fig. 6.6). Since the distribution is not a power law, we would expect that upon considering a larger number of avalanches, this hypothesis should be rejected (Klaus et al., 2011). Indeed, using data from $1,000,000$ avalanches yielded a p-value of 0, i.e., the truncated power law is not an appropriate model for the distribution.

The fact that the truncated power law was a plausible fit for the fewer number of avalanches (note that $100,000$ is of the same order of magnitude as the number of avalanches typically reported in *in vitro* or *in vivo* studies of neuronal avalanches) is indicative of the partial scale-free behaviour the model exhibits. The appeal of the concept of a critical brain is that the critical regime is the one in which long-range correlations keep the system poised between too highly correlated states of no behavioural value and too weakly correlated states that prevent information flow (Chialvo, 2004). Thus, the actual nature of the distribution of the

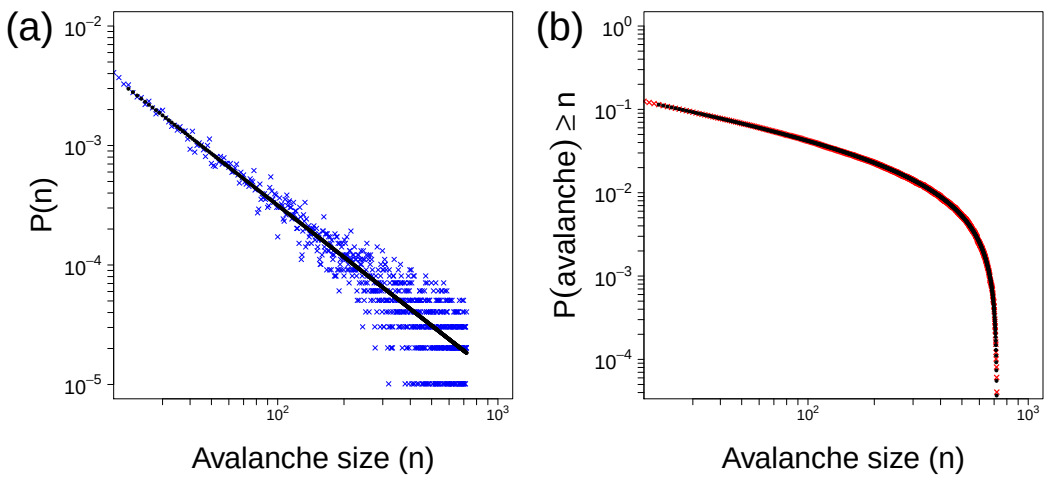

Figure 6.6: **Fitted distributions.** Out of 100,000 of the observed avalanches we fit the 98,833 whose size was less than $\frac{9}{10}N$. (a) The fitted probability distribution function (black line) fitted over the simulated avalanche distribution (blue dots). (b) The fitted cumulative distribution function (black line) fitted over the simulated avalanche distribution (red dots).

avalanche size matters less than any indication of the presence of long range correlations. In other words, neuronal avalanches need not precisely follow a power law, they just need to exhibit similar behaviour. It is important to appreciate this distinction. As the exact solution to the distribution of avalanche sizes is known, we can then compare it visually with a fit of a truncated power law over avalanche sizes from $\frac{1}{10}N$ to $\frac{9}{10}N$. This is done in Fig. 6.7 which confirms that over a limited range of sizes the distribution is well approximated by a power law.

6.5 Origin of the distribution's truncation

The fact that we have an exact form for the distribution allows us to make further important observations about some of its characteristics. Here, we explore the origin of the distribution's truncation. Let λ_1, λ_2, ..., λ_N be the eigenvalues of $\mathbf{A}$ with the corresponding eigenvectors u_1, u_2, ..., u_N. The initial condition can then be given as $\mathbf{p}(0) = c_1u_1 + c_2u_2 + ... + c_Nu_N$. As the matrix $\mathbf{A}$ is similar to a symmetric tridiagonal matrix with real entries (consider the diagonal similarity transformation matrix D, with $D_1 = 1$ and $D_j = \sqrt{(b_jb_{j-1}\dots b_2)/(c_{j-1}c_{j-2}\dots c_1)}$), we know that its eigenvalues are real.

Using the property $\mathbf{A}u_j = \lambda_j u_j$ we then obtain $\mathbf{p}(k) = c_1\lambda_1^k u_1 + c_2\lambda_2^k u_2 + ... + c_N\lambda_N^k u_N$. This calculation leads to the probability of an avalanche being of size n being:

$$P(n) = q_1 \sum_{i=1}^{N} d_i \lambda_i^{2n}, \tag{6.3}$$

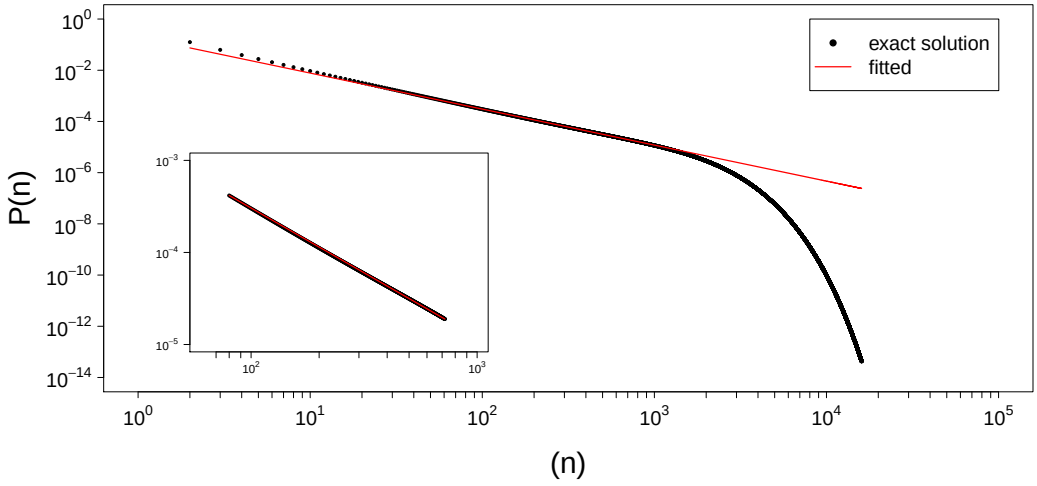

Figure 6.7: **Power law fit of the exact solution.** Main: plot of the truncated power law (red line) fitted over the entire range of the exact distribution (black dots). Inset: Fitted power law and exact distribution in the range $[\frac{1}{10}N, \frac{9}{10}N]$.

where q_1 is the probability that the next transition is a recovery (from A to Q) given 1 active neurone (as defined earlier), λ_i are the eigenvalues of the transition matrix $\mathbf{A}$ and d_i are specified by the eigenvectors of the transition matrix and the initial conditions. We note that the earlier equation, $\mathbf{p}(0) = c_1u_1 + c_1u_1 + \ldots\ldots + c_Nu_N$, can be solved to obtain c_i. Using this, we can then calculate d_i as the first entry of the vector c_iu_i. Equation 6.3, which is exact, thus demonstrates that the distribution of avalanche sizes is a linear combination of exponentials.

The structure of $\mathbf{A}$ (namely the all zero diagonal) means that if $u = (u_1, u_2, \ldots, u_{N-1}, u_N)$ is an eigenvector with corresponding eigenvalue λ_u, then $v = (u_1, -u_2, \ldots, (-1)^N u_{N-1}, (-1)^{N+1}u_N)$ is an independent eigenvector with corresponding eigenvalue $-\lambda_u$ (here, and in all that follows, we are assuming N is even; for N odd there is an additional zero eigenvalue). Setting $\tilde{N} = \frac{N}{2}$ and $e_i = d_i + d_{N-i+1}$ allows us to rewrite equation 6.3 as

$$P(n) = q_1 \sum_{i=1}^{\tilde{N}} e_i \lambda_i^{2n}. \tag{6.4}$$

Assuming the lead eigenvalue is denoted by λ_1, then for all i, $\lambda_i < \lambda_1$ and we have

$$\begin{aligned}\frac{P(n)}{q_1 e_1 \lambda_1^{2n}} &= \sum_{i=1}^{\tilde{N}} \frac{e_i \lambda_i^{2n}}{e_1 \lambda_1^{2n}} \\ &= \frac{e_1}{e_1}\left(\frac{\lambda_1}{\lambda_1}\right)^{2n} + \frac{e_2}{e_1}\left(\frac{\lambda_2}{\lambda_1}\right)^{2n} + \ldots + \frac{e_{\tilde{N}}}{e_1}\left(\frac{\lambda_{\tilde{N}}}{\lambda_1}\right)^{2n}\end{aligned}$$

Taking the limit as n increases we find

$$\lim_{n\to\infty} \frac{P(n)}{q_1 e_1 \lambda_1^{2n}} = 1$$

Hence $P(n) \sim q_1 e_1 \lambda_1^{2n}$ and for larger avalanche sizes we have the leading eigenvalue dominating thus giving the exponential cutoff observed. We illustrate this convergence in Fig. 6.8 where we plot the exact avalanche distribution, $P(n)$, against $q_1 e_1 \lambda_1^{2n}$. This figure also illustrates that the leading eigenvalue begins to dominate for avalanches just over the system size. It is for this reason that we chose an upper bound of $\frac{9N}{10}$ when fitting a power law to the distribution of avalanche sizes in the previous section.

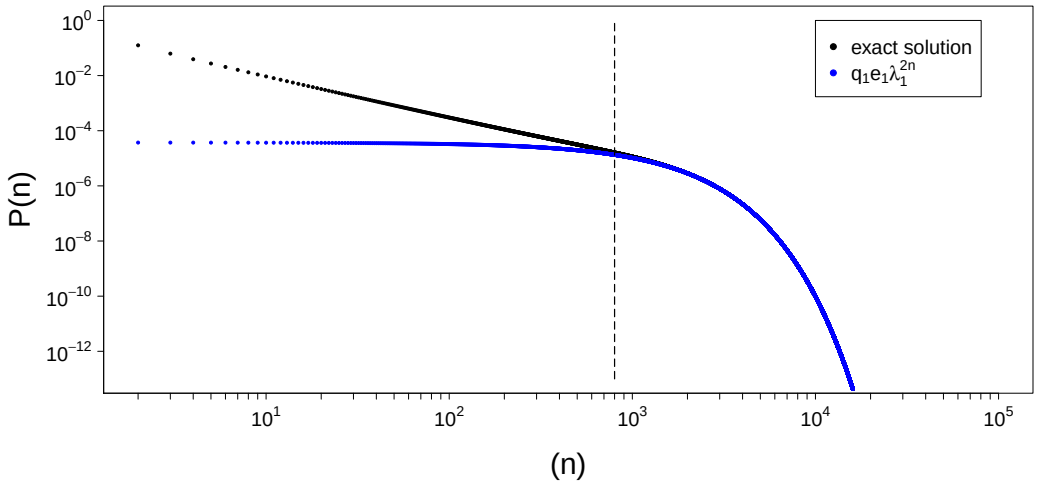

Figure 6.8: **Exponential cutoff.** Exact avalanche distribution (black dots), plotted against a distribution assuming only the leading eigenvalue is non-zero (blue dots). Avalanches greater than the system size, $N = 800$, appear after the dashed line.

Such a distribution as (6.4) could converge to a true power law under two important conditions:

1. the eigenvalues are well approximated by a geometric distribution, i.e. they are in the form $\lambda_i = Ke^{-\frac{\mu}{2}i}$,

2. the constants, e_i, are well approximated by $e_i = Li^q$,

where K, μ, L and q can be inferred via a numerical fitting procedure. In such a scenario, Equation 6.4 can be rewritten to give

$$P(n) = C \sum_{i=1}^{\tilde{N}} i^q (e^{\mu n})^{-i}, \tag{6.5}$$

where C is a given constant. In the limit of an infinite network size we then have

$$P(n) = C \sum_{i=1}^{\infty} i^q (e^{\mu n})^{-i}. \tag{6.6}$$

While $P(n)$ can be found based on standard mathematical arguments, we have chosen to use results derived in the context of the **Z**-transform. The standard results for integer values of q give

$$\sum_{i=1}^{\infty} i^q z^{-i} = (-1)^q D^q (\frac{z}{z-1}), \tag{6.7}$$

where D is an operator such that $D(f(z)) = z\frac{d(f(z))}{dz}$. For a fixed integer value of q, an approximation for $P(n)$ can be obtained by simply applying the operator as many times as necessary and then substituting $z = e^{\mu n}$. For $q = 1$ for example, $P(n) \propto \frac{e^{\mu n}}{(e^{\mu n}-1)^2}$ which for small values of μ is well approximated by $\frac{1}{\mu^2}\frac{1}{n^2}$.

These results only hold for integer values of q so an alternative approach is to approximate the sum for $P(n)$ in terms of an integral. Taking into account the special form for the eigenvalues and constants, $P(n)$ can be approximated as follows:

$$P(n) = C \sum_{i=1}^{\infty} i^q (e^{\mu n})^{-i} \simeq C \int_0^{\infty} x^q e^{-\mu n x} dx. \tag{6.8}$$

The latter integral can be interpreted as a Laplace transform of x^q and thus yields

$$P(n) \simeq C \frac{\Gamma(q+1)}{\mu^{q+1}} \frac{1}{n^{q+1}}. \tag{6.9}$$

It is worth noting that this result is consistent with that obtained for integer values of q.

For a simple empirical verification of this conjecture, we determined the values of K, μ, L and q in the above conditions through numerical fitting of the first 23 eigenvalues and e constants of the exact distribution for a network of size $N = 800$ (see Fig. 6.9(a,b)) and compared the resulting probability distribution with the exact distribution. Whilst the lesser valued eigenvalues and larger e values were not fitted well, Fig. 6.9(c) shows there is still remarkable agreement between both curves over a broad range of values, including the range $[\frac{1}{10}N, \frac{9}{10}N]$ over which a power law like behaviour was established earlier (see Fig. 6.7). This result clearly illustrates the dominance of the larger eigenvalues and, given that the fitted dis-

tribution converges to a power law, gives support to the conjecture that the exact distribution would do so in the limit of an infinite network.

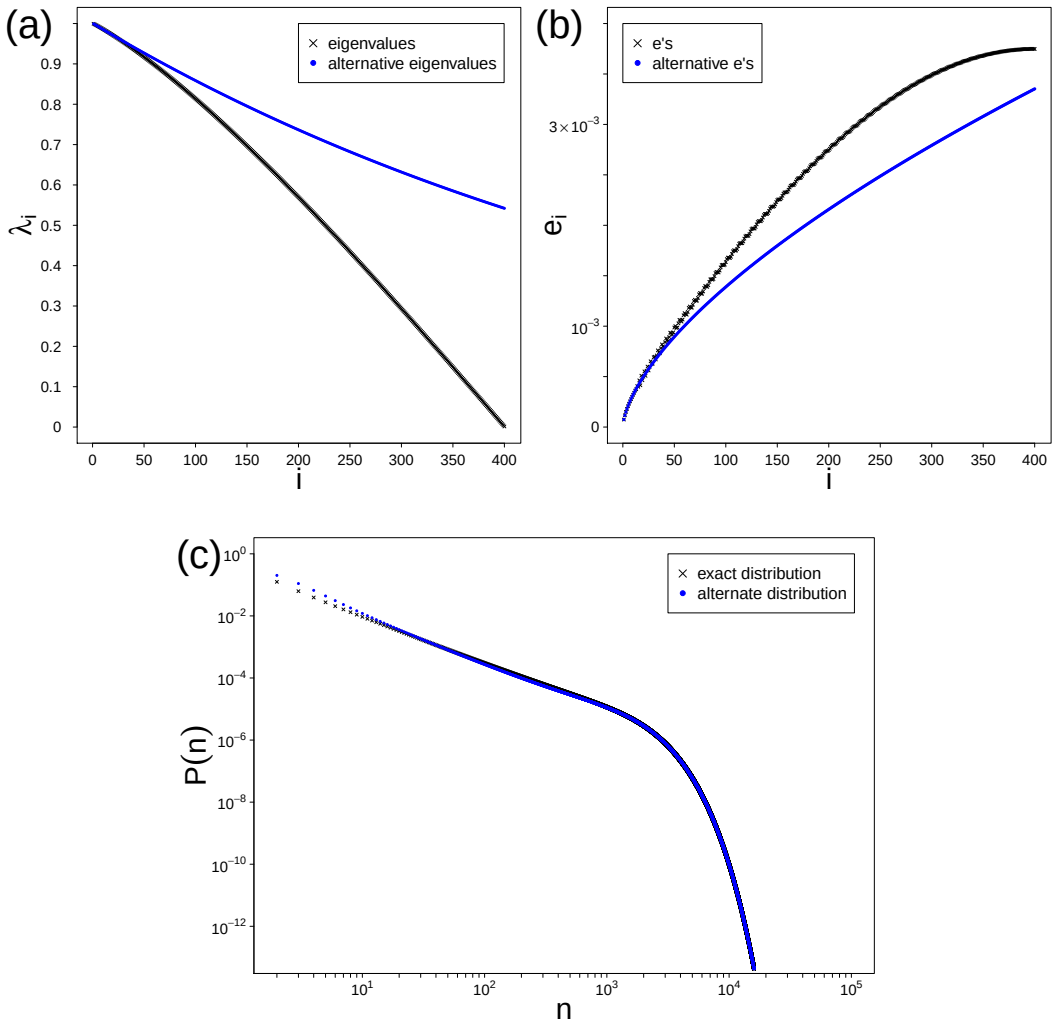

Figure 6.9: **Possible origin of the power law for large systems.** (a) Actual distribution of eigenvalues λ_i (black crosses) along with fitted distribution (blue dots). (b) Actual distribution of constants d_i (black crosses) along with fitted distribution (blue dots). (c) Exact distribution of avalanche sizes (black crosses) along with distribution resulting from fitted distributions of λ_i and d_i (blue dots). All plots are for a network of size $N = 800$ operating at criticality.

6.6 Other markers of criticality

Since the distribution of avalanche sizes in the finite-size critical system does not necessarily follow a true power law, the application of robust statistical testing in experimental conditions could well lead to rejecting the hypothesis that the data may come from a system

operating in the critical regime. Therefore, in this section, we consider two experimentally testable markers of criticality: critical slowing down and divergence of susceptibility. We will define those concepts below but first we briefly summarise Van Kampen's system size expansion (Van Kampen, 2007) which we use to illustrate those markers on our system.

6.6.1 System size expansion

For generality we now assume that each neurone receives a constant external input and that the activation function can take forms other than the simple identity function. We define the probability that the number of neurones active at time t is n as $P_n(t)$. Then the master equation can be given as

$$\begin{aligned}\frac{dP_n(t)}{dt} =& \alpha(n+1)P_{n+1}(t) - \\ & \alpha n P_n(t) + \\ & f\left(\frac{w(n-1)}{N} + h\right)(N-(n-1))P_{n-1}(t) - \\ & f\left(\frac{wn}{N} + h\right)(N-n)P_n(t).\end{aligned}$$

The idea of the system size expansion is to now model the number of active neurones as the sum of a deterministic component scaled by N and a stochastic perturbation scaled by $\sqrt{N}$, i.e.,

$$n(t) = N\mu(t) + N^{\frac{1}{2}}\xi(t).$$

A more detailed explanation of this can be found in Benayoun et al. (2010) and Van Kampen (2007), but importantly what is obtained is the following set of equations for μ (which is the solution to the mean field equation of the proportion of active neurones), $\langle\xi\rangle$ (the expected value of the fluctuations) and $\sigma^2 = \langle\xi^2\rangle - \langle\xi\rangle^2$ (the variance of the fluctuations)

$$\frac{\partial\mu}{\partial t} = -\alpha\mu + (1-\mu)\hat{f}, \tag{6.10}$$

$$\frac{\partial\langle\xi\rangle}{\partial t} = -\left(\alpha + \hat{f} - w\hat{f}'(1-\mu)\right)\langle\xi\rangle, \tag{6.11}$$

$$\frac{\partial\langle\sigma^2\rangle}{\partial t} = -2\left(\alpha + \hat{f} - w\hat{f}'(1-\mu)\right)\langle\sigma^2\rangle + \left(\alpha\mu + (1-\mu)\hat{f}\right). \tag{6.12}$$

Here $\hat{f} = f(w\mu + h)$ and $\hat{f}' = f'(w\mu + h)$. These equations, in turn, give the following equations for the mean, A, and variance, A_σ, of the number of active neurones

$$A = N\mu + N^{-\frac{1}{2}} \langle \xi \rangle = N\mu \quad \text{(assuming we know the initial number of active neurones)}, \tag{6.13}$$

$$A_\sigma = N \left\langle \sigma^2 \right\rangle . \tag{6.14}$$

We make use of these equations in the following two sections.

Critical slowing down

In dynamical systems theory, a number of bifurcations, including the transcritical bifurcation in our system, involve the dominant eigenvalue characterising the rates of changes around the equilibrium crossing zero. As a consequence, the characteristic return time to the equilibrium following a perturbation increases when the threshold is approached (Wissel, 1984). This increases has led to the notion of critical slowing down as a marker of critical transitions (Scheffer et al., 2009). Here, we illustrate the critical slowing down of our model with the analytic derivation of the rate of convergence to the steady state (this derivation has been previously shown by Stollenwerk and Jansen (2007)). We first begin by calculating the analytic solution to Equation 6.10 for the percentage of active neurones. We again consider the case where f is the identity function and can thus write

$$\frac{\partial \mu}{\partial t} = -\alpha\mu + (1-\mu)f(w\mu + h) = -\alpha\mu + (1-\mu)(w\mu + h). \tag{6.15}$$

Assuming zero external input ($h = 0$), we have

$$\frac{\partial \mu}{\partial t} = -\alpha\mu + (1-\mu)(w\mu + h) = -\alpha\mu + (1-\mu)w\mu. \tag{6.16}$$

We are interested in the solution of this equation and consider the result for different values of α. Firstly we consider $\alpha \neq w$. In this case we have

$$\frac{\partial \mu}{\partial t} = -\alpha\mu + (1-\mu)w\mu = \mu(w - w\mu - \alpha). \tag{6.17}$$

Integrating this using separation of variables and the initial condition $\mu(0) = \mu_0$, we find

$$\mu(t) = \frac{w - \alpha}{Ae^{(\alpha - w)t} + w} \quad \text{where } A = \frac{\mu_0}{w - w\mu_0 - \alpha}. \tag{6.18}$$

The solution to this depends on whether $\alpha < w$ or $\alpha > w$ ($R_0 > 1$ and $R_0 < 1$ respectively). If $\alpha < w$ then as $t \to \infty$, $\mu \to \frac{w-\alpha}{w}$. If $\alpha > w$ then as $t \to \infty$, $\mu \to 0$. Note that in both cases, convergence of the number of active neurones to the steady state solution is exponential.

Now we consider the solution when $\alpha = w$, i.e., the critical regime.

$$\frac{\partial \mu}{\partial t} = -\alpha\mu + (1-\mu)\alpha\mu = -\alpha\mu^2 \Rightarrow \mu(t) = \frac{1}{\alpha t + \mu_0^{-1}}.$$

Thus as $t \to \infty$ we find $\mu(t) \to 0$. However, unlike for $R_0 \neq 1$, convergence to the steady state exhibits a power law dependence on time (Stollenwerk and Jansen, 2007).

Divergence of susceptibility

A correlate of the phenomenon of critical slowing down is that of the divergence of susceptibility of the system as the system approaches the bifurcation (Scheffer et al., 2009). In this section, we investigate the behaviour of the equation for the variance. For simplicity, we consider again the case of the identity activation function and a non-driven system $h = 0$. First we use Equation 6.12 to calculate the variance in the percentage of active neurones:

$$\begin{aligned}
\frac{\partial \sigma^2}{\partial t} &= -2\left(\alpha + \hat{f} - w\hat{f}'(1-\mu)\right)\sigma^2 + \left(\alpha\mu + (1-\mu)\hat{f}\right) \\
&= -2\left(\alpha + w\mu + h - w^2(1-\mu)\right)\sigma^2 + \left(\alpha\mu + (1-\mu)(w\mu + h)\right) \\
&= -2\left(\alpha + w\mu - w^2(1-\mu)\right)\sigma^2 + \left(\alpha\mu + (1-\mu)w\mu\right)
\end{aligned}$$

Setting this equal to zero and rearranging we obtain

$$\sigma^2 = \frac{\left(\alpha\mu + (1-\mu)w\mu\right)}{2\left(\alpha + w\mu - w^2(1-\mu)\right)} = \frac{\left(\mu + (1-\mu)R_0\mu\right)}{2\left(1 + R_0\mu - R_0 w(1-\mu)\right)}.$$

Here we note that unlike the equation for μ where there was only the single bifurcation parameter R_0, we now have the additional dependence on w. To maintain consistency with earlier results, we now set $w = 1$ to obtain

$$\lim_{t\to\infty} \sigma^2(t) = \begin{cases} \alpha & \text{if } \alpha < 1 \quad (R_0 > 1), \\ \frac{1}{2} & \text{if } \alpha = 1 \quad (R_0 = 1), \\ 0 & \text{otherwise} \quad (R_0 < 1). \end{cases}.$$

Using Equation 6.14 we obtain

$$\lim_{t\to\infty} \langle A \rangle_\sigma = \lim_{t\to\infty} N\langle \sigma^2 \rangle = \begin{cases} \frac{N}{R_0} & \text{if } R_0 > 1, \\ \frac{N}{2} & \text{if } R_0 = 1, \\ 0 & \text{otherwise } (R_0 < 1). \end{cases}$$

Fig. 6.10 illustrates the jump to a non-zero steady state when the critical value $R_0 = 1$ is approached from below, and the divergence in variance when it is approached from above.

Here it should be noted that any finite-size network has a zero absorbing state so that

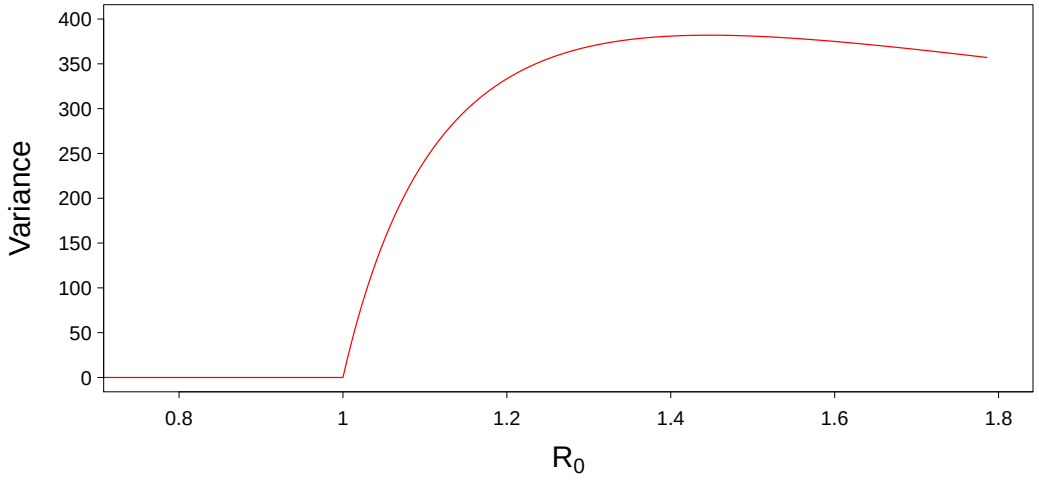

Figure 6.10: **Divergence of susceptibility.** Analytic result for the steady state of the variance as R_0 approaches 1 in a network of size $N = 800$. Results only provided down to $\alpha = 2/3$ for clarity.

eventually all activity will die out irrespective of the value of R_0. However, it has been shown that the ODE limit is a valid approximation to the solution of the master equation for reasonably sized systems with values of R_0 greater than 1 and only over a finite time horizon (see Nåsell (1996) for further discussion). Defining the true (i.e., calculated directly from the master equation for $P(n)$) expected value of active neurones at time t as $\tilde{A}(t)$, the convergence of the ODE approximation for $A(t)$ given by Equation 6.13 is such that for any $t \geq 0 \lim_{N\to\infty} |A(t) - \tilde{A}(t)| = 0$ (Simon et al., 2011).

6.7 Discussion

Over the last decade or so, the search for evidence that the brain may be a critical system has been the focus of much research. This is because it is thought that a critical brain would benefit from maximised dynamic range of processing, fidelity of information transmission and information capacity (Shew and Plenz, 2013). Whilst support for the critical brain hypothesis has emerged from comparing brain dynamics at various scales with the dynamics of physical systems at criticality (e.g., Plenz and Chialvo (2009); Expert et al. (2010); Linkenkaer-Hansen et al. (2001); Poil et al. (2012); Friedman et al. (2012); Ribeiro et al. (2010)), in this paper, we focus on the important body of work that has relied on characterising power laws in the distributions of size of neuronal avalanches (Beggs and Plenz, 2003; Shew et al., 2009). Our focus on this scale is motivated by empirical considerations regarding how one can go about demonstrating the above functional properties. Shew and Plenz (2013) remark that any research strategy to test whether these properties are optimal near criticality will have to

achieve two criteria: a means of altering the overall balance of interactions between neurones and a means of assessing how close to criticality the cortex is operating. As argued by these authors, the study of neuronal avalanches offers the greatest likelihood of achieving those two criteria.

The importance of a robust assessment of the statistical properties of the avalanche size is therefore two-fold: on the one hand, it is about ascertaining the extent to which the system being studied has the statistical properties expected of a system operating at, or near, criticality; on the other hand, it is about being able to confirm that a manipulation/perturbation of the system aimed to push the system away from this critical regime has been effective. This consideration therefore puts a lot of importance on the description of the statistics one should expect in such a system. In the current literature, the assumption of the distribution of avalanche sizes taking a power law functional form relies on an analogy between the propagation of spikes in a neuronal network and models of percolation dynamics or branching processes for which exact power laws have been demonstrated *in the limit of system size*. As a result of the importance of having a robust assessment of the expected presence of a power law, greater emphasis has recently been put on using a sound statistical testing framework, e.g., Clauset et al. (2009). Whilst we are unaware of any study in which the criticality hypothesis was rejected due to failure of rigorous statistical testing (which we suspect is due to the necessarily small number of observations, as we will argue below), there is clear evidence that many authors are now using the methods of Clauset et al. (2009) to confirm the criticality of their experimental findings, e.g., Klaus et al. (2011); Touboul and Destexhe (2010); Benayoun et al. (2010). As a result, we feel that it is all the more important to confirm that the assumed power law functional form is indeed a sensible representation of what one should expect in *in vivo* and *in vitro* recordings, which, unlike the physical systems considered when deriving the power law statistics, are finite-size systems. The aim of the paper was therefore to consider a model of neuronal dynamics that would be simple enough to allow the derivation of analytical or semi-analytical results whilst (i) giving us a handle on the parameter controlling the fundamental principle thought to underlie criticality in the brain, namely, the *balancing* between processes that enhance and suppress activity (note that we are intentionally not referring to excitation and/or inhibition – we will return to this below) and (ii) allowing us to determine its distribution of avalanche sizes when operating in the critical regime. Note that because we are using a finite-size system, we are appealing to a normal form of standard bifurcation, here, a transcritical bifurcation, because it embodies all that needs to be known about the 'critical' transition (Sornette, private communication).

Our semi-analytic derivation of the true distribution of avalanche sizes in a finite-size system suggests that, even though it is approximately scale free over a limited range, the distribution is not a true power law. First, this has important implications for the interpretation of results from a robust statistical assessment of the distribution. Indeed, as has been discussed by Klaus et al. (2011), with a large number of samples, any distribution that deviates

from the expected distribution by more than noise due to sampling, will eventually yield a p-value such that the power law hypothesis will be rejected, thus leading to the potentially incorrect conclusion that the system is not critical. This is the case in our scenario where using 10^6 avalanches lead to a rejection of the criticality hypothesis even though the system is tuned to the critical regime. In contrast, with 10^5 avalanches (which is consistent with empirical observations), a p-value above threshold leads to not rejecting the hypothesis that the distribution is a power law even though we established it is not one[1]. This finding therefore provides an important counterpart to the analytical results of Touboul and Destexhe (2010) who showed that thresholded stochastic processes could generically yield apparent power laws that only stringent statistical testing will reject. Whilst the stringent testing will reject the hypothesis of criticality for a system that is not necessarily critical, it may also reject the hypothesis of criticality for a system that is critical only because the actual distribution is not actually a power law. This ambiguity of the avalanche distribution in the finite-size system therefore requires that one should carefully consider to what fundamental property the idea of a critical brain actually appeals to. We suggest that the key appeal is that the brain can exhibit long-range correlations between neurones without it ever experiencing an over saturation of activity or long periods of inactivity. It then follows that the importance is not in the exact distribution obtained but in the approximately scale-free behaviour it exhibits. In turn, this highlights the importance of looking at other markers of criticality (which we will discuss below).

Another important result of this work is to provide the beginning of a mechanistic explanation for an often alluded to (e.g., Rubinov et al. (2011)) but never properly treated (as far as we are aware) observation that whereas avalanches in a critical system with re-entrant connections could in principle be arbitrarily long, and certainly, exceeding the number of recording sites, neuronal avalanches in *in vitro* or *in vivo* systems (and many computational models of self-organised criticality) often show a cut-off at the number of sites. Our work suggests that the lead eigenvalue of the transition matrix between states fully determine the location of this cut-off which turns out indeed to be at about the system size, even if avalanches of up to 20 times the system size can be observed. This finding therefore provides some justification for setting, or accepting, a bound within which to apply a Clauset-type methodology (we note that various reports use different ranges, e.g., 80% of system size in Levina et al. (2007), roughly system size in Rubinov et al. (2011)). It is worth remembering that the number of recording sites can have profound implications on the nature of the distribution observed (Priesemann et al., 2009).

In addition to providing results on the distribution of avalanche sizes, we also sought to explore other potential markers of criticality. We provided results on two other markers of criticality – critical slowing down and divergence of susceptibility – both of which again follow from a dynamical systems appreciation of a critical bifurcation, i.e., the behaviour of a system

[1] As the power law is not a sufficient condition of criticality, one should not infer from this that the system is indeed critical, however, this step is commonly taken in published reports and that is worth mentioning here.

whose lead eigenvalue crosses zero. The appeal of those markers, which have been documented in many other natural processes, e.g., Scheffer et al. (2009); Kelso (2008), but seldom at the mesoscopic brain level[2] (see Steyn-Ross et al. (2003) for a rare example) is that (a) they strengthen the assessment of the system being critical and (b) may contribute to achieving the second criterion of Shew and Plenz (2013). Although the authors are not in a position to provide explicit recommendations for an experimental design, we believe that these markers are amenable to robust experimentation, e.g., through pharmacological manipulation.

Whilst we hope we have convinced the reader of the potential importance of these findings, we also need to recognise that the very simplicity that makes analytical work possible does also raise questions regarding how physiologically plausible such a model is and therefore whether its conclusions should be expected to hold. Below, we address a few of the points worthy of further consideration.

6.7.1 Validity of inferring criticality in a finite network

In using the meanfield equations it is important to understand how well they capture the behaviour and bifurcation structure of the stochastic process they are approximating. Whilst it is known that on the complete graph (see Simon and Kiss (2012) for instance) and in the limit $N \to \infty$ the steady state solution of the ODE will converge to the expected value of the comparable stochastic process, it is unclear whether the critical point of the infinite system corresponds to that in the finite system. Furthermore it is unclear whether a finite system can truly have a critical point and we must be cautious in claiming one exists. Importantly, however, it has been shown in Ganesh et al. (2005) that for a complete graph, $R_0 \approx 1$ (the paper proves the result for α fixed as 1 but the result is generalisable for any α) is the threshold below which the disease will die out quickly (expected time to extinction $O(log(n))$), and above which it dies out slowly (expected time to extinction $O(n^a)$ for some a). Simulating the steady state of the network for increasing R_0 also shows (see Fig. 6.11) the characteristic feature of a second-order phase transition found at a critical point. For these reasons, whilst acknowledging the problem of inferring criticality in a finite regime, we feel justified in claiming $R_0 = 1$ as the critical point for the process unfolding on our finite network.

6.7.2 Validity of a purely excitatory network

In this paper, we have used a purely excitatory neuronal model. This not only simplifies the system but is also an important characteristic of the brain during early development. Experimental results have shown that during early development, before birth, GABAergic neurones (i.e. neurones which will later be inhibitory) have a depolarising effect on their post-synaptic neighbours (Cherubini et al., 1991; Rivera et al., 1999; Ben-Ari, 2002). Thus, our model might be considered as representative of early development. Power law statistics have been observed

[2]Strictly speaking the notion of critical slowing in neurones firing near firing threshold appeals to the same notion.

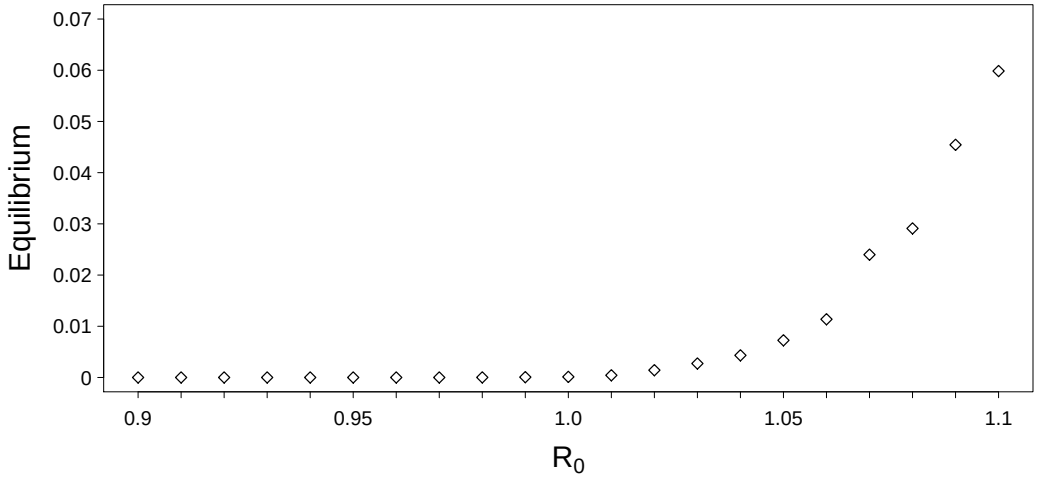

Figure 6.11: **Steady state versus R_0.** Plot of the steady state (averaged over 500 simulations at time $t = 150$) obtained at R_0 values around the putative critical value of 1.

in early development at a time when networks are thought to be purely excitatory (Gireesh and Plenz, 2008; Hartley et al., 2012). It should be noted that this approach has the benefit of casting a new light on the question of what is the minimum requirement for a neuronal system to show criticality. To a large extent, the current literature has been focused on a form of homeostasis resulting from either a fine balance between excitation and inhibition, e.g., Benayoun et al. (2010); Magnasco et al. (2009) or some relatively complex dynamical processes at synaptic level, e.g., Levina et al. (2007). Our results show that a purely excitatory system can show the exact same behaviour such that on average each active neurone only activates one postsynaptic neurone. Here, this balanced state is achieved through a trade-off between the rates at which neurones become active and quiescent. It should be noted that this formulation of the problem leads to interesting parallels with classical models of mathematical epidemiology which the authors intend to continue exploring.

6.7.3 Spatial structure

To make use of the analytic tractability of the mean field equation it was necessary to consider a fully connected network. While this is not true of the whole brain, it *may* be closer to the reality of the kind of in vitro systems typically considered in studies of neuronal avalanches. For example, Hellwig (2000) report up to 80% connection probability in local connectivity between pyramidal neurones in layers 2/3 of the rat visual cortex. Extending the work presented here to consider the effect of network topology on the system's dynamics and the resulting distribution of event sizes would be of particular interest from a developmental viewpoint (see, for instance, Larremore et al. (2012), who have considered the avalanche distribution of general tree-like networks with discrete dynamics). As networks mature, there is not only a

switch to inhibition by a proportion of the neurones (the so-called GABA switch), but also a subsequent pruning of synaptic connections (Huttenlocher and Dabholkar, 1997). The level of pruning is high, with a 40% reduction in the number of synaptic connections between early childhood and adulthood (Huttenlocher and Dabholkar, 1997). Thus, a developing network may be more readily approximated by a fully connected network than an adult neural network would be.

The lack of a spatial embedding of our model is in contrast with many classical models of criticality, and also with physiological systems. Accordingly, our model cannot display another important marker of criticality, namely, the divergence of correlation lengths in space. A spatial embedding is not needed for our system to be critical and to exhibit a distribution of avalanche size similar to that observed in physiological neuronal avalanches. It therefore begs the question of the exact role of spatial embedding in the dynamics of neuronal avalanches. It may well be that, just like balanced activity in our model comes about from a trade-off between excitation and refractoriness rather than between excitation and inhibition, specific spatial embeddings may enable balanced activity without the need for plastic mechanisms. Kaiser and Hilgetag (2010) showed that hierarchical modular networks can lead to limited sustained activity whereby the activity of neural populations in the network persists between the extremes of either quickly dying out or activating the whole network. Roxin et al. (2004) observed self-sustained activity in excitable integrate-and-fire neurones in a small-world network, whose dynamics depends sensitively on the propagation velocity of the excitation.

6.7.4 Non-driven case

Finally, in this paper, we have focused on the non-driven case $h = 0$. Whilst this constraint allowed the derivation of analytical results, it obviously contrasts with the reality of a physiological system unless one considers that any 'external' input operates at such a slower timescale that one could assume separation of time scales (an important assumption in the self-organised criticality framework). However, the fact that binning is required for identifying avalanches in physiological recordings suggests that this separation of time scales is unlikely. Whilst the introduction of a non-zero h in our model does not affect the results obtained using finite size expansion, it does effectively make it impossible for the system to operate at $R_0 = 1$. A thorough investigation of the driven case ($h > 0$) will be the subject of the companion paper.

Acknowledgments Timothy Taylor is funded by a PGR studentship from MRC, and the Departments of Informatics and Mathematics at University of Sussex. Caroline Hartley is funded through CoMPLEX (Centre for Mathematics and Physics in the Life Sciences and Experimental Biology), University College London. Istvan Z. Kiss acknowledges support from EPSRC (EP/H001085/1). Péter L. Simon acknowledges support from OTKA (grant no. 81403) and from the European Union and the European Social Fund (financial support to the project under the grant agreement no. TÁMOP-4.2.1/B-09/1/KMR).

Chapter 7

Paper 5: Identification of criticality in neuronal avalanches: II. A theoretical and empirical investigation of the driven case

Caroline Hartley[1,2], Timothy J. Taylor[3], Istvan Z. Kiss[4], Simon F. Farmer[5,6] and Luc Berthouze[2,3]

[1]Centre for Mathematics and Physics in the Life Sciences and Experimental Biology, University College London, London, WC1E 6BT, UK
[2]Institute of Child Health, London, University College London, London WC1E 6BT, UK
[3]Centre for Computational Neuroscience and Robotics, University of Sussex, Brighton BN1 9QH, UK
[4]School of Mathematical and Physical Sciences, Department of Mathematics, University of Sussex, Brighton BN1 9QH, UK
[5]National Hospital of Neurology and Neurosurgery, London, UK.
[6]Institute of Neurology, University College London, London, UK.

Submitted (September 2013) to *The Journal of Mathematical Neuroscience*

7.1 Abstract

The observation of apparent power-laws in neuronal systems has led to the suggestion that the brain is at, or close to, a critical state and may be a self-organised critical system. Within the framework of self-organised criticality a separation of timescales is thought to be crucial for the observation of power-law dynamics and computational models are often constructed with this property. However, this is not necessarily a characteristic of physiological neural networks - external input does not only occur when the network is at rest/a steady state. In this paper we study a simple neuronal network model driven by a continuous external input (i.e. the model does not have a separation of timescales) and analytically tuned to operate in the region of a critical state (it reaches the critical regime exactly in the absence of input - the case studied in the companion paper to this article). The system displays avalanche dynamics in the form of cascades of neuronal firing separated by periods of silence. We observe partial scale-free behaviour in the distribution of avalanche size for low levels of external input. We analytically derive the distributions of waiting times and investigate their temporal behaviour in relation to different levels of external input, showing that the system's dynamics can exhibit partial long-range temporal correlations. We further show that as the system approaches the critical state by two alternative 'routes', different markers of criticality (partial scale-free behaviour and long-range temporal correlations) are displayed. This suggests that signatures of criticality exhibited by a particular system in close proximity to a critical state are dependent on the region in parameter space at which the system (currently) resides.

7.2 Introduction

In recent years, apparent power-laws (i.e. where a power-law is the best model for the data using a model selection approach (Clauset et al., 2009; Klaus et al., 2011)) have been observed experimentally in neurophysiological data leading to the suggestion that the brain is a critical system (Chialvo, 2010; Linkenkaer-Hansen et al., 2001). These observations have included that of neuronal avalanches - cascades of neuronal firing recorded *in vivo* and *in vitro* whose size and duration appear to follow power-law distributions (Beggs and Plenz, 2003, 2004; Gireesh and Plenz, 2008; Hahn et al., 2010; Petermann et al., 2009). Recently it has been claimed that equivalent neuronal avalanche behaviour with the same power-law relationship can be identified in human MEG (magnetoencephalography) recordings (Shriki et al., 2013). On a wider scale, fluctuations in oscillation amplitude in human (adult and child) EEG (electroencephalography) and MEG exhibit a power-law decay of the autocorrelation function of the signal - a property known as long-range temporal correlations (LRTCs) (Linkenkaer-Hansen et al., 2001, 2004; Nikulin and Brismar, 2004, 2005; Smit et al., 2011; Berthouze et al., 2010). These observations and the idea that the brain is a critical system have drawn much attention as critical systems have been shown to exhibit optimal dynamic range and optimal information processing (Kinouchi and Copelli, 2006; Shew and Plenz, 2013). Moreover, it

has led to the hypothesis that brain dynamics may fit within the framework of self-organised criticality (SOC), i.e. a system that does not require external tuning of parameters to reach the critical state (Bak et al., 1987; Jensen, 1998; Linkenkaer-Hansen et al., 2001).

While the observation of power-laws within neuronal activity may be attractive we must address the issue of whether (specifically) a neuronal system in the region of a critical state can produce this type of dynamics. Propagation of the spiking of neurons within a network has been interpreted within the context of percolation dynamics and the theory of branching processes (Essam, 1980; Harris, 1963). A critical branching process is a process such that one active node will activate on average one other node at the next time-step and so one can discern how this would relate to neuronal systems whereby the system is critical if one active neuron on average activates one other neuron at the next time-step. A critical branching process will display power-law dynamics, however, a number of assumptions underlying branching processes do not hold true in neurophysiological systems. Firstly, the theoretical analysis of branching processes relies on full-sampling of the system. Full-sampling is unlikely to occur in the experimental setting and this can have a profound effect on the observed distributions (Priesemann et al., 2009). Additionally, re-entrant connections invalidate the standard theory of branching processes (Harris, 1963) which brings into question the idea that neuronal systems can be modelled as critical branching processes. Moreover, the strict definition of a critical system is one that operates at a second order phase transition which applies only to systems with infinite degrees of freedom. Therefore, we may expect a critical system to exhibit an exact power-law distribution in the case of infinite size but what should we expect if the system is finite? As neuronal systems are necessarily finite this is an important question in the field but one that has yet to be fully addressed. Within experimental results this fact has been accounted for by the concept of finite-size effects - where a power-law is observed up to a cut-off value (Jensen, 1998; Beggs and Plenz, 2003, 2004; Klaus et al., 2011). This cut-off value has been suggested to coincide with the size of the system and distributions from networks of different sizes have been shown to exhibit an exact scaling relationship - a phenomenon known as finite-size scaling (Klaus et al., 2011; Bonachela and Muñoz, 2009). However, the finite-size effect with a cut-off value at system size has been assumed without analytical derivation (though, see the companion paper to this article (Taylor et al., 2013), as described below) and the question of how a finite critical system behaves and the types of dynamics possible from such a system remains open in the field. Whether a finite-size system should display the same signatures of criticality as the system in the limit of system size is not known.

In the companion paper to this article (Taylor et al., 2013) we examined a computational model of a finite neuronal system analytically tuned to its critical state, defined as a transcritical bifurcation. There we showed that the dynamics of the system, which by analogy with experimental neuronal avalanches could be termed avalanches (discrete cascades of neuronal firing), exhibited scaling which does not follow an exact power-law but does exhibit

partial scale-free behaviour. We were able to show that the cut-off value is approximately the system size, as suggested experimentally by the finite-size effect, but is analytically related to the lead eigenvalue of the transition matrix (the matrix of all possible transitions at each simulation step). This is an important observation given that avalanches in systems with re-entrant connections could in principle be of infinite size and yet experimental observations have suggested that neuronal avalanches exhibit a finite-size cut-off (Beggs and Plenz, 2003; Klaus et al., 2011). Overall, the results suggested that finite systems at criticality exhibit signatures of critical systems dynamics but do not (at least in this instance) exhibit exact power-laws as had previously been suggested.

While the system studied in the companion paper leads us to a greater understanding of the dynamics displayed by a finite neuronal system, there is still an important difference between the system studied there and physiological neuronal systems. In the companion paper the system was seeded by setting a single neuron in the network into the active state and an avalanche was defined as the firing that occurred until the network returned to a stable state (the fully quiescent state). After this point no more firing could occur until the system was reseeded. This imposed a strict separation of timescales, with all avalanches and neuronal firing occurring on a much faster timescale than the timescale of the 'external input' reseeding the system. Many other computational models have also taken this approach (Levina et al., 2007; Bak et al., 1987; Olami et al., 1992), with a separation of timescales thought to be necessary for the observation of self-organised critical dynamics (Bonachela and Muñoz, 2009). While a separation of timescales is likely to occur in some natural systems such as earthquakes, where friction in the Earth's plates build up over the course of years but energy is released in a matter of minutes, this is not a physiologically realistic assumption for a neuronal system. External input (be it from the environment or other areas of the nervous system) will not arrive only once the neuronal population has returned to a set state. Before physiological recordings can be interpreted within the field of critical systems we must address the question of the types of dynamics that should be expected by not only a finite-size system but also a system that is driven by a physiologically realistic external input. Can a finite-size system without an explicit separation of timescales in the region of a critical regime exhibit markers of criticality? How might the external input to the system affect these markers?

Previous authors examining computational neuronal networks with continuous driving (i.e. no explicit separation of timescales) have observed power-law dynamics (Kinouchi and Copelli, 2006; Ribeiro and Copelli, 2008; Rubinov et al., 2011; Larremore et al., 2011). In particular, Kinouchi and Copelli (2006) and Larremore et al. (2011) analytically determined the parameters required such that the model they studied was at criticality and displayed peak dynamic range, in fully connected networks and networks with a range of topologies, respectively. However, these authors did not explicitly examine the firing dynamics of the system in the region of the critical regime, concentrating on average activity levels. In a SOC system such as the sandpile model (Bak et al., 1987) the waiting times (periods of inactivity

between avalanches) have been shown to follow an exponential distribution (Boffetta et al., 1999). However, these waiting times are related to the reseeding of the system - sand is added to cells chosen at random and the next avalanche begins when a cell exceeds the threshold. In contrast, recent experimental work has shown that waiting times between neuronal avalanches in cultures have a distribution with two trends - a (short) initial power-law region thought to relate to neuronal up-states and a bump in the distribution at longer waiting times thought to relate to neuronal down-states (Lombardi et al., 2012). Could this difference in these waiting time distributions (between the SOC sandpile model and the neuronal avalanches in culture) be explained by the fact that physiological neuronal systems do not have a separation of timescales?

As mentioned previously, another signature of criticality that has been reported in neural systems is the presence of LRTCs. In the majority of cases they have been observed in large scale neuronal signals such as human brain oscillations. Recent endeavours have been made to link these observations of scale-free behaviour on large scales with neuronal avalanches (Poil et al., 2012; Palva et al., 2013). Poil and colleagues demonstrated in a computational neuronal network that power-law distributed avalanches and LRTCs in oscillations emerge concurrently. In addition, LRTCs have also been detected in the waiting times of bursts of activity in cultures (Segev et al., 2002) and the discontinuous burst activity recorded from extremely preterm human neonates (Hartley et al., 2012). Thus, LRTCs have been demonstrated in discrete neuronal activity yet they have not been examined in the waiting times of neuronal avalanches themselves. While LRTCs in avalanche activity would not be possible in a seeded computational system (where the activity is initiated 'by hand' and there is no memory within the system's dynamics) it is conceivable that a driven system, which is more akin to physiological networks which can display LRTCs, might display this type of dynamics in the waiting times of neuronal avalanches.

In summary, in this paper we aim to address the following questions:

1. Assuming that the brain, or population of neurons under study, operates in the region of a critical regime can it be expected to display power-law statistics given that it is a finite-size system? If not what distribution should we expect? As discussed, this question was also addressed in the companion paper (Taylor et al., 2013), where we studied a system without an external input. However, here we specifically consider this question in the context of a driven system, i.e. with a non-zero external input and no explicit separation of timescales.

2. Can we expect a finite-size neuronal system in the region of a critical regime to exhibit other markers of criticality, and specifically the presence of LRTCs? Does the presence of LRTCs relate to that of power-law distributions? As described above, LRTCs have been observed in neurophysiological data sets. However, a systematic examination of how LRTCs may relate to other markers of criticality in neuronal systems is lacking.

3. How are signatures of criticality (power-law distributions and LRTCs) affected by proximity to the critical regime? One might assume that a system which is closer to a critical regime may exhibit signatures of criticality, whereas a system that is further from the critical regime will not. Importantly, our analysis shows that this assumption is in fact not (always) true.

In this paper, as in the companion paper, we examine a purely excitatory stochastic neuronal model. As in the companion paper, a number of assumptions are made to simplify the model with the outcome that it is analytically tractable and therefore can be tuned to operate in the region of a critical regime. This approach is taken as it allows direct exploration of the above questions, which would not be possible with a more complex system. We begin by examining the distributions of avalanche size and duration, investigating the presence of scale-free behaviour. We also show that as the system approaches the theoretical critical regime by decreasing the external input, there is a change in the distributions of avalanche characteristics with the appearance of partial scale-free behaviour in avalanche size. It is important to note that the definition of avalanches strongly depends on the choice of binning method. In the literature different definitions of avalanches are used in models with seeded systems and with systems where the dynamics are continuous (including physiological recordings). We will return to this in the discussion.

Unlike in the companion paper where the system was seeded after each avalanche, the system studied here does not have an explicit separation of timescales. This allows us to additionally assess the waiting times, which are intrinsic to the system, and we are able to analytically derive the distribution of waiting times. We then investigate the presence of partial LRTCs in the empirically derived waiting times. Finally, we show that as the system size increases (and the system approaches the theoretical critical regime from a different route) the range over which the correlations extend also increases. Overall we find that the system displays different signatures of criticality depending on the region of the parameter space around the critical regime.

7.3 The model

As in the companion paper, we study a stochastic model based on that of Benayoun et al. (2010). Though greatly simplified from a physiological neural network, the model is chosen as it is analytically tractable and thus enables direct derivation of the parameters such that there is a critical regime. With this approach it is therefore possible to assess the dynamics of a neuronal system in the region of (or at) a critical regime. While Benayoun et al. considered a network with both excitatory and inhibitory connections, we simplify the system further (as in the companion paper), considering a network with purely excitatory synaptic connections. As will be discussed later, this type of network can be set within the context of early brain development.

We consider a system of N fully connected neurons, with each neuron in one of two states - active (A) or quiescent (Q). For a small time step $dt \to 0$ the probability of transition for a neuron between the two states is given by:

$$P(Q \to A, \text{ in time } dt) = f(s_i(t))dt,$$

$$P(A \to Q, \text{ in time } dt) = \alpha dt,$$

where $s_i(t) = \sum_j \frac{w_{ij}}{N} a_j(t) + h_i(t)$ is the input to neuron i, f is an activation function, $h_i(t)$ is the external input to neuron i, w_{ij} is the connection strength from neuron i to neuron j and $a_j(t) = 1$ if neuron j is active at time t and zero otherwise. Finally, α is a constant rate at which neurons change from the active to inactive (quiescent) state.

For analytical tractability and characterisation of the critical state we make the following additional simplifications:

1. The synaptic connection strengths are the same for all connections with $w_{ij} = w > 0$.
2. The external input is constant to all neurons and at all simulation steps so that $h_i(t) = h > 0$.
3. The activation function is linear with $f(x) = x$.

While the first and third assumptions are the same as in the companion paper, we make the additional assumption of constant positive external input here as opposed to the companion paper where we examined the system with no external input ($h = 0$). As the network is fully connected, and the system is closed so that $A + Q = N$ (where A is the number of active neurons and Q is the number of quiescent neurons), the system can be described by the mean field equation:

$$\frac{dA}{dt} = \left(\frac{wA}{N} + h\right)(N - A) - \alpha A.$$

As stated in the companion paper, we can use this equation to analyse the stability of the system about the fixed point and determine the parameters for which the system is at the threshold of stability, i.e. when the fixed point is critical. This threshold occurs when the eigenvalue (λ) of the fixed point is zero, which can alternatively be stated, borrowing terms from the epidemiology literature, as $R_0 = 1$ (the basic reproductive ratio). Moreover, this is also equivalent to a branching parameter of one. In the companion paper it was shown that with $h = 0$, $R_0 = \frac{w}{\alpha}$ and so for $R_0 = \frac{w}{\alpha} = 1 \Rightarrow \alpha = w$ the system is critical.

Here we study the system in the presence of a positive external input, $h > 0$. In this case the fixed point of the system is given by:

$$-\frac{w}{N}A^2 + wA + h(N - A) - \alpha A = 0,$$

and the eigenvalue at the fixed point is:

$$\lambda = -2\frac{w}{N}A + w - h - \alpha.$$

For a fixed point to be critical we require that both these equations be satisfied. However, solving them simultaneously we find that there are no real roots when $w,\ h,\ N > 0$. This implies that there is no parameter region such that the system (with this activation function and positive external input) has a critical fixed point. However, considering again the case with no external input ($h = 0$) for which the critical state occurred with parameters $\alpha = w$, if this system is driven by a 'sufficiently low' level of external input it should still be within the region of the critical state. There has been some suggestion that the brain is not directly at a critical point but is in fact just very close to the critical regime and it has been speculated that the brain may actually be slightly supercritical (Poil et al., 2012). Additionally, it been shown that a computational model of neuronal avalanches which follows a SOC approach (Levina et al., 2007) is actually a system that 'hovers' close to the critical state (Bonachela and Muñoz, 2009). Therefore, the question of how a finite driven system behaves in the region of a critical regime is pertinent to the neuroscience field.

An additional motivation for considering a non-zero external input is the dynamic range (Δ) of the system. Larremore et al. (2011) describe the dynamic range as "the range of stimuli over which there is significant variation in the collective response of the network". Kinouchi and Copelli (2006) examined dynamic range in models of networks with uniform connectivity operating with *discrete* time dynamics where multiple firings can occur within each time step. They found that the dynamic range was maximised when the local branching ratio was equal to one. Larremore et al. (2011) considered a version of this model but with the introduction of heterogeneity in connections, showing that it is the lead eigenvalue, λ, of the connectivity matrix that governs the dynamic range and that the dynamic range is maximised when $\lambda = 1$. In Appendix 1 we provide an analytic calculation for the dynamic range of our *continuous* model. Analogous to the results described above (Kinouchi and Copelli, 2006; Larremore et al., 2011) the dynamic range is maximised when $R_0 = 1$ ($w/\alpha = 1$ when $h = 0$). This is illustrated in Fig. 7.1 where results from simulations are compared with the analytic solution. It is important to emphasise that the parameterisation of the dynamic range is in terms of the value R_0 calculated for networks when there is no external input. When this parameterisation is such that $R_0 = 1 \Rightarrow \alpha = w$ (and therefore when the system is tuned to the critical state) external input to the system will give rise to dynamics for which the dynamic range is maximised. This point will be considered further in the discussion.

Throughout this study we will examine the system in the presence of an external input of $h = 1/N$ or less. This level of the external input is equivalent to setting a single neuron to the active state and so corresponds to seeding the system in the zero input case. We therefore deem this level of external input to be sufficiently low such that we could expect the system to remain within the region of the critical regime. As in the companion paper we set $w = \alpha = 1$.

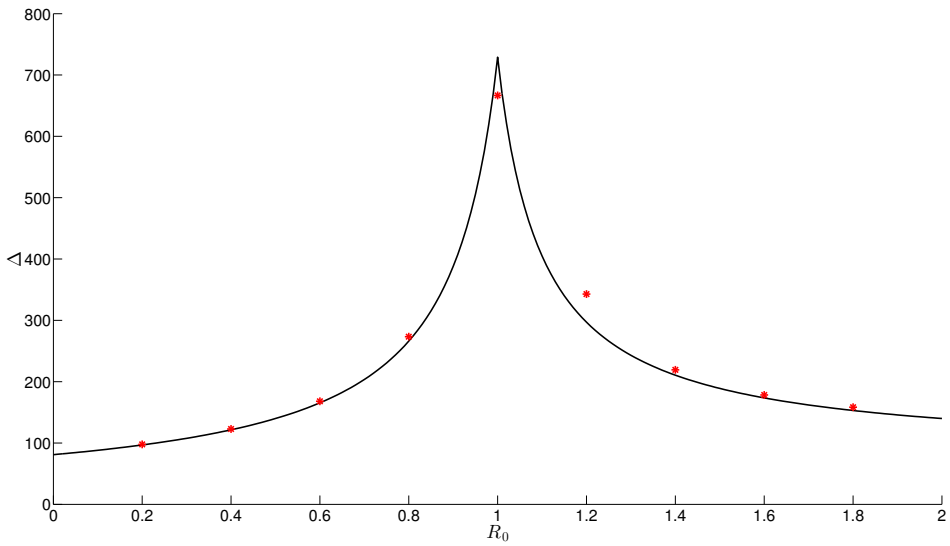

Figure 7.1: R_0 **versus** Δ**.** Plot of R_0 versus Δ (the dynamic range - see Appendix 1) for both the analytic result (black line) and simulations (red dots). For the comparable simulated result we average $10,000$ realisations that have run until time $t = 200$. To obtain a reasonable spread of h we used the conjugation of the intervals $[0 : 0.002 : 0.2]$ and $[0.4 : 0.2 : 18]$.

With these parameters and with positive external input we find that the fixed point of the system is given by

$$A = -\frac{hN}{2} \pm \sqrt{\frac{N^2h^2}{4} + N^2h},$$

and the eigenvalue of this fixed point is given by

$$\lambda = -\sqrt{h^2 + 4h}.$$

With lower levels of external input the system approaches the critical regime (see Fig. 7.2). Note that this approach is in fact from a slightly subcritical state given these values of α and w and with positive external input. Under these conditions it is not possible to consider an approach from a supercritical regime with a positive eigenvalue.

As described above, we (initially) set $h = 1/N$. With this level of external input:

$$A = -\frac{1}{2} \pm \sqrt{\frac{1}{4} + N},$$

and the eigenvalue of the fixed point is given by

$$\lambda = -\sqrt{\frac{1}{N^2} + \frac{4}{N}}.$$

As $N \to \infty$, $\lambda \to 0$ (see Fig. 7.2). Thus, for this level of the external input ($h = 1/N$), as the system size (N) increases the system approaches the critical state (as the system reaches the

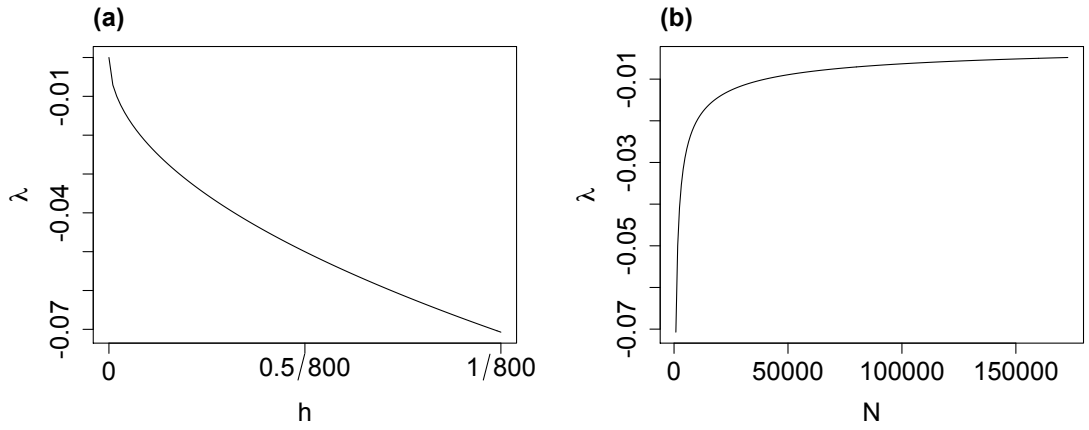

Figure 7.2: **The eigenvalue of the system compared with the level of external input and system size.** (a) With $w = \alpha$ the eigenvalue decreases with lower levels of external input h, with the system reaching the critical regime in the absence of external input ($\lambda = 0$ i.e. $R_0 = 1$, the case studied in the companion paper). (b) With $h = 1/N$ and $w = \alpha$ the eigenvalue of the fixed point $\lambda \to 0$ as $N \to \infty$. Thus, the system approaches the critical state as the system size increases.

critical state exactly when the eigenvalue $\lambda = 0$). We will examine the effect on the dynamics of decreasing the external input, thereby allowing the system to approach the critical regime. We will also investigate an alternative route to the critical regime by increasing system size at constant (overall) level of external input.

7.3.1 Model simulations and burst analysis

As in the companion paper and in Benayoun et al. (2010), simulations of the network dynamics were carried out using the Gillespie algorithm for stochastic simulations (Gillespie, 1977). Briefly, at each step in the simulation

- The total transition rate r for all the neurons within the network is calculated, with $r = r_{aq} + r_{qa}$ where r_{aq} is the total rate of active $\to$ quiescent transitions and is given by $r_{aq} = \alpha A$ and r_{qa} is the total rate of all quiescent $\to$ active transitions which is given by $r_{qa} = f(s_i)(N - A)$.
- The time to the next transition dt is selected at random from an exponential distribution of rate r.
- The type of transition is selected by generating a random number $n \in [0, 1]$. If $n < \frac{r_{aq}}{r}$ then a randomly chosen active neuron becomes quiescent, otherwise a (randomly chosen) quiescent neuron switches to the active state.

At each step in the simulation a single neuron makes a transition, though the rate at which transitions occur changes and so the simulation step changes. If the network is in a fully

quiescent state ($Q = N$) then, with positive external input, $r_{aq} = 0$ but $r_{qa} = hN$ and consequently there will necessarily be a transition of a neuron from the quiescent to the active state. Similarly, when the network is in the fully active state ($A = N$) $r_{qa} = 0$ but $r_{aq} = \alpha N$ and so there will necessarily be a transition of a randomly chosen neuron from the active to the quiescent state. From all other starting points transitions from the active to the quiescent or from the quiescent to the active state are possible. Thus, from all network states one neuron will change state. This is unlike the companion paper where with no external input the network must be seeded when in the fully quiescent state. Instead in this case network dynamics are continuous (i.e. no re-seeding is required) and are of finite length only in-so-far as they are restricted by simulation lengths.

We define a neuron as firing at the first time step at which the neuron switches from the quiescent to the active state. Fig. 7.3 shows raster plots of network firings for the first 1 second of simulations with three different levels of the external input. As was described above, unlike in the companion paper where there was no external input, the dynamics continue even if the system reaches the fully quiescent state. Interestingly, we can also notice that the network dynamics appear to exhibit burst-like behaviour, with periods of high neuronal firing interspersed with periods without network firing. It is important to realise that these bursts are intrinsic to the system and are not directly related to the dynamics of the external input (the input is constant to all neurons in each of the simulations) nor due to a saturation of the network - the bursts themselves consist of different numbers of neuronal firing. In all three cases the parameters are set to the critical state (with no external input). With lower levels of the external input the system approaches the critical regime and we see that the bursts become further apart and more distinct. We will characterise these dynamics below. (See also Appendix 2 where we examine driving the system from subcritical and supercritical states.)

These burst dynamics are analogous to the neuronal avalanches observed experimentally in that they are discrete cascades of firing. Neuronal avalanches observed experimentally in physiological networks are so called because they have sizes which are distributed according to a power-law and while the size distribution of the burst activity in this network has yet to be presented we will refer to the activity throughout the rest of this paper as avalanches due to their discrete burst behaviour. To determine the distribution of the avalanches we divided the activity into individual avalanches using the approach of Benayoun et al. (2010). This method divides consecutive neuronal spiking between any two neurons within the network into separate avalanches if the time difference between the spikes is greater than the average difference (δt) between consecutive spikes within the simulation. This approach (referred to later in the text as the binning method) is similar to the method used to define neuronal avalanches within physiological data (Beggs and Plenz, 2003, 2004) - though the choice of binning method will be discussed later in the paper. It is important to note that no binning approach was needed in the companion paper since an avalanche was naturally defined as all firing that occurred before the network reached the fully quiescent state and was reseeded.

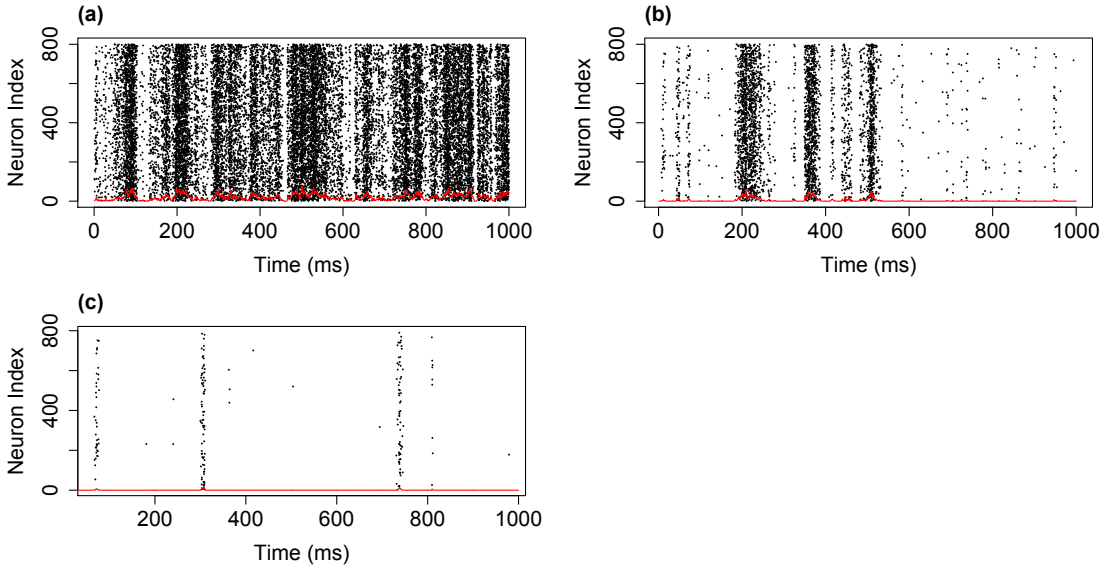

Figure 7.3: **Raster plots of the network dynamics for different levels of the external input.** Neuronal firing across 1 second of a simulation with an external input of (a) $h = 1/N$, (b) $h = 0.1/N$ and (c) $h = 0.01/N$. For all three simulations $N = 800$, $\alpha = w = 1$ and the red line indicates the rate of firing in 1 ms bins. As can be observed, as the level of the external input decreases the firing rate decreases and the time between avalanches increases.

This has been used as a standard classification for discontinuous data, stemming from the sandpile model of criticality (Bak et al., 1987). However, as the firing dynamics here continue for the entire simulation it was instead appropriate to use an approach that had been used previously for continuous dynamics.

Throughout the remainder of this paper we examine characteristics of these avalanches: namely the size and duration of avalanches as well as the inter-avalanche intervals (IAIs). The size of an avalanche is defined (in the standard way) as the number of firings within the avalanche. If a single neuron fires more than once within a single avalanche it is also counted more than once. The duration of an avalanche is defined as the time between the start of the avalanche (the first neuron firing) and the end of the avalanche. Note that if the avalanche consists of a single neuron firing then the duration of the avalanche is 0 (and the size of the avalanche is 1). Similarly, an IAI is defined as the time between the end of one avalanche and the start of the next avalanche, i.e. the waiting time between avalanches. Note that the minimum IAI is bounded below by δt as a separation between two consecutive spikes of greater than δt defines separate avalanches.

7.3.2 Distributions of avalanche size and duration

Fig. 7.4 shows the distributions of avalanche size and duration from example simulations for the three different levels of external input investigated – this can be compared with Fig. 3 of the companion paper (Taylor et al., 2013) which shows the avalanche size distribution in

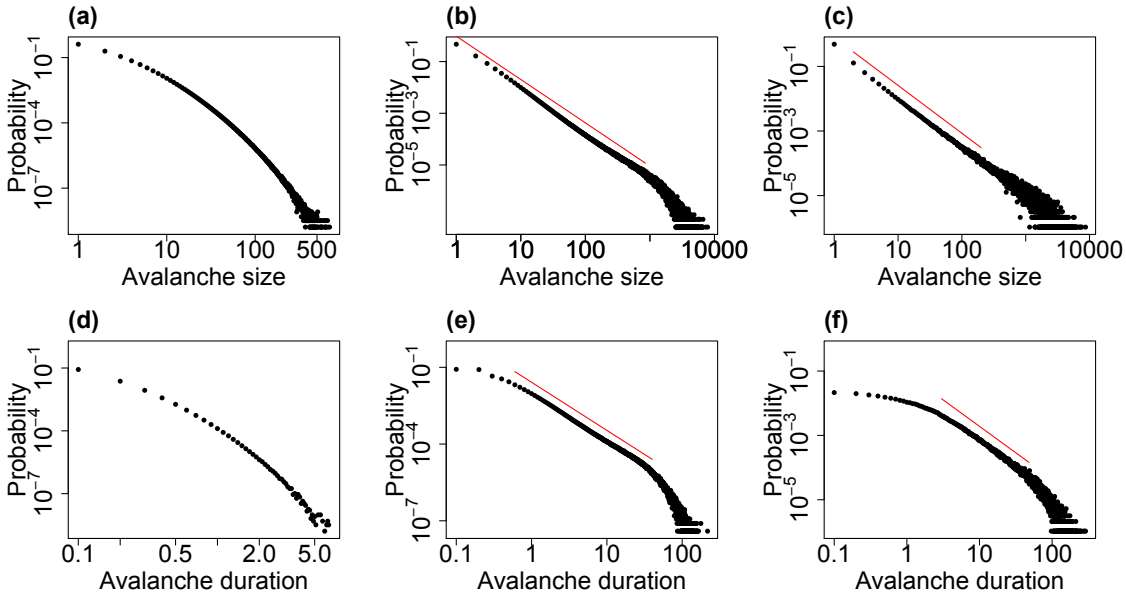

Figure 7.4: **Distributions of avalanche size and duration for varying levels of the external input.** The distributions of avalanche size (a,b,c) and duration (d,e,f) from simulations with $h = 1/N$ (a,d), $h = 0.1/N$ (b,e) and $h = 0.01/N$ (c,f). As the level of the external input is decreased the system approaches the critical regime. For all simulations $N = 800$, $\alpha = w = 1$ and the distributions are pooled from 10 simulations each of length 10^4 seconds. The red lines indicates linear fits on the double logarithmic scale (where appropriate), i.e. fitted power-laws with exponents of (b) 1.68, (c) 1.48, (e) 1.88 and (f) 1.64.

the absence of external input. With lower levels of external input the system approaches the critical regime and the distributions of avalanche size appear scale-free across a range of scales. The distribution approaches the distribution found in the companion paper for the system exactly tuned to the critical state. With $h = 0.01/N$ (i.e. the lowest level of eternal input) the exponent of the fitted power-law is approximately 1.5, see Fig. 7.4(c), which is consistent with experimentally observed neuronal avalanche sizes (Beggs and Plenz, 2003, 2004). However, for higher levels of the external input this scale-freeness of the distribution is lost which coincides with moving away from the critical regime. In the case of avalanche duration a similar relationship with the critical regime is seen with a scale-free portion in the middle ranges of the distribution (between approximately 2 and 50 ms) with lower levels of external input. Thus, for lower levels of external input, when the system approaches the critical regime, the distributions, in particular that of avalanche size, exhibit partial scale-free behaviour.

It is worth considering what leads to the changes seen in the distributions as the level of external input is varied. As stated, as the level of external input decreases, the system approaches the critical regime and so it is perhaps not surprising that signatures of criticality (i.e. scale-free behaviour) emerge in the distribution of avalanche size. Examining the raster plots of firing for the different levels of external input, see Fig. 7.3, we see that at lower

levels the avalanches are further apart and more distinct. While the external input itself is continuous, at lower levels of external input there is a separation of timescales, where one avalanche always finishes well before the next avalanche begins. The distribution therefore appears to follow similar characteristics to a system with a built-in separation of timescales and we confirm that the distribution is similar to that found in the companion paper (in which the model had an explicit separation of timescales) where an exponent close to 1.5 was also observed for the distribution of avalanche size. As the external input is increased there are no longer such distinct periods between avalanches. This leads to a superposition effect, with the next (actual) avalanche starting before the previous avalanche has finished (i.e. a new network cascade is initiated before the previous one has finished). This leads to these 'avalanches' being defined using the binning approach as a single avalanche (see discussion). The scale-free behaviour in the distributions of avalanche size and duration is therefore lost.

7.3.3 Theoretical derivation of the distribution of the IAIs and comparison with simulated data

The temporal patterning of activity within networks of neurons has long been investigated as a property of key importance, with rate and temporal coding suggested as potential substrates for information propagation. As it remains to be fully determined how different neuronal firing properties may lead to information transfer we suggest that in addition to the distribution of avalanches sizes the intervals between avalanches need to be considered as a functional entity in their own right. In this section we derive the theoretical distribution of IAIs and compare it with results from simulations.

We begin by noting that a single IAI is a period during which there is no neuronal firing, i.e. neurons can only be switching from the active to the quiescent states or an IAI may be a period with a single quiescent to active transition which is preceded by another quiescent to active transition. Let us initially ignore the fact that there is a minimum duration (δt) of an IAI and first consider the distribution of all consecutive active to quiescent transitions (we will return to the distribution of single quiescent to active transitions later).

Distribution of consecutive active to quiescent transitions

Let N_0 be the number of *active* neurons at a time point in the simulation. After a single simulation step the number of active neurons will be $N_0 + 1$ or $N_0 - 1$, as at every simulation step only one neuron makes a transition. Let q_i be the probability that an active neuron goes back to the quiescent state given that there are i active neurons. Note that from the transition rates:

$$q_i = \frac{\alpha i}{(\frac{w}{N} i + h)(N - i) + \alpha i} = \frac{\alpha i N}{(wi + hN)(N - i) + \alpha i N}.$$

Starting with N_0 active neurons the probability that there are $N_0 - 1$ active neurons after a single simulation step is q_{N_0} and the probability that there are N_0+1 active neurons is $1-q_{N_0}$. Given these probabilities we can construct a probability tree, shown in Fig. 7.5, particularly concentrating on the portion of the tree corresponding to active to quiescent transitions, i.e. those transitions that form a period of consecutive active to quiescent transitions. (Note that this probability tree focuses on different aspects of the model to that of the probability tree in the companion paper.)

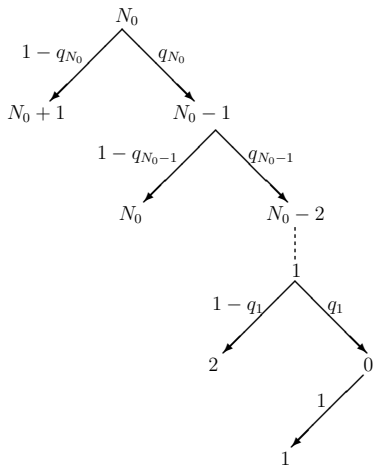

Figure 7.5: **Probability tree of consecutive active to quiescent transitions.** Starting from a state with N_0 active neurons the probability tree diagram indicates the possible transitions from each state specifically concentrating on the active to quiescent transitions. The probability q_i of each transition is as indicated in the main text and is dependent on the number of active neurons, i.

From this tree approach we can calculate that the probability of *exactly* k consecutive active to quiescent transitions (note that to consist of *exactly* k active to quiescent transitions the transition sequence must be ended by a quiescent to active transition):

$$P(IAI_k) = p(N_0, k) = (1 - q_{N_0-k}) \prod_{j=0}^{k-1} q_{N_0-j}. \tag{7.1}$$

The duration of this period of consecutive active to quiescent transitions is given by the sum of the times for each of these k transitions (plus the time for the quiescent to active transition). As the Gillespie algorithm is used for simulations, at each simulation step the time to the next transition is drawn randomly from an exponential distribution with rate r (see above), where r is dependent on the number of active neurons and so changes at each simulation step. The duration of consecutive active to quiescent transitions is therefore the sum of exponentially distributed variables drawn from distributions of different rates, i.e. the distribution of consecutive active to quiescent transitions is a hypoexponential. Thus, the duration distribution, $f(x, N_0, k)$, of consecutive active to quiescent transitions of length

x, consisting of k transitions, ending with an additional quiescent to active transition and starting from N_0 active neurons is (Ross, 2010):

$$f(x, N_0, k) = \sum_{j=0}^{k} r_{N_0-j} e^{-r_{N_0-j}x} \left(\prod_{i=0, i\neq j}^{k} \frac{r_{N_0-i}}{r_{N_0-i} - r_{N_0-j}} \right), \tag{7.2}$$

when $r_{N_0-i} \neq r_{N_0-j}$ and where r_m is the total transition rate for all neurons within a network with m active neurons and is the rate of the exponential distribution from which the time to the next transition is randomly drawn. This equation holds provided that $r_{N_0-i} \neq r_{N_0-j}\ \forall i, j$. If this is not the case and there exists $A, B \in \{1, \ldots N\}$ such that $(\alpha + w - h)/w = A + B \Rightarrow r_A = r_B$ then we use the more general form – assuming there are a distinct rates, which we label $\beta_1,\ \beta_2, \ldots, \beta_a$ that occur $c_1, c_2, \ldots, c_a$ times respectively (i.e. $c_1 + c_2 + \ldots c_a = k + 1$) – given by Scheuer (1988):

$$f(x, N_0, k) = B \sum_{k=1}^{a} \sum_{l=1}^{c_k} \frac{\phi_{k,l}(-\beta_k) x^{c_k - l} e^{-\beta_k x}}{(c_k - l)!(l-1)!}, \tag{7.3}$$

where

$$B = \prod_{j=1}^{a} \beta_j^{c_j} \text{ and } \phi_{k,l}(t) = \frac{d^{t-1}}{dt^{t-1}} \prod_{j=1, j\neq k}^{a} (\beta_j + t)^{-c_j}.$$

Whilst this involves higher order derivatives a closed-form solution is provided by Amari and Misra (1997).

From equation 7.1 we know the probability of k consecutive active to quiescent transitions. This equation holds true for any k up to $k = N_0$, which is the maximum number of consecutive active to quiescent transitions as the fully quiescent state is then reached. Therefore, the distribution, $F(x, N_0)$, of consecutive active to quiescent transitions of duration x starting with N_0 active neurons but consisting of any number of transitions is a weighted sum of hypoexponentials:

$$F(x, N_0) = \sum_{k=1}^{N_0} f(x, N_0, k) p(N_0, k). \tag{7.4}$$

Probability distribution of the initial number of active neurons

Finally, to calculate the full probability distribution of consecutive active to quiescent transitions for a network of set system size, N, we must combine equation 7.4 with the probability of the initial number of active neurons being equal to $N_0 \in \{1, 2, ...N\}$ (note that $N_0 = 0$ is not considered as the next transition will necessarily be an activation). To determine this probability, let us first consider the simple case of $N = 3$. We assume that the simulation starts from a state with no active neurons. Fig. 7.6 shows all possible transitions between the

number of active neurons in a network of this size.

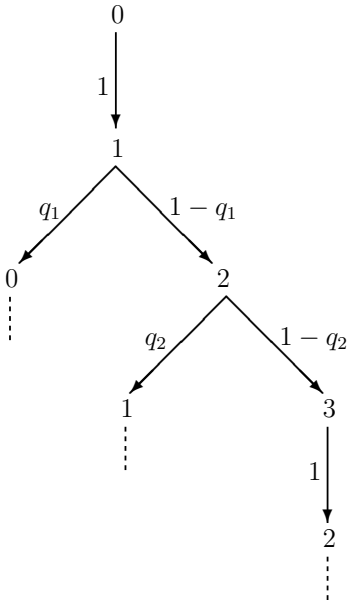

Figure 7.6: **Probability tree of all possible transitions in a network of size N = 3.** Simulations start from a state with no active neurons: $N_0 = 0$. The diagram shows the possible transitions at each step, along with the probability of making that transition. The probabilities are as defined in the main text with q_i being the probability of a neuron switching from the active to the quiescent state given i initially active neurons. Dotted lines indicate transitions that are already shown elsewhere in the tree and so the tree shown here completely describes all possible transitions in a network of this size.

From this probability tree the probabilities, $P(i)$, of the number of active neurons being equal to i, where $i \in \{0, 1, 2, 3\}$ are given by:

$$\begin{aligned} P(0) &= q_1 P(1), \\ P(1) &= P(0) + q_2 P(2), \\ P(2) &= (1 - q_1) P(1) + P(3), \\ P(3) &= (1 - q_2) P(2), \end{aligned} \tag{7.5}$$

(assuming a steady state has been reached such that the probabilities are time independent). Rearranging and substituting to write the equations in terms of $P(1)$:

$$\begin{aligned} P(0) &= q_1 P(1), \\ P(2) &= \frac{(1 - q_1)}{q_2} P(1), \\ P(3) &= \frac{(1 - q_1)(1 - q_2)}{q_2} P(1). \end{aligned} \tag{7.6}$$

Furthermore, the sum of all the probabilities must equal 1 and so

$$\left(q_1 + 1 + \frac{(1-q_1)}{q_2} + \frac{(1-q_1)(1-q_2)}{q_2}\right) P(1) = 1. \tag{7.7}$$

Therefore,

$$P(1) = \frac{q_2}{q_1 q_2 + q_2 + (1-q_1) + (1-q_1)(1-q_2)}. \tag{7.8}$$

By substituting this value back into the set of equations 6 the probabilities for the full system can be calculated.

Generalisation to a system of any size N

From considering this simple example we can generalise to derive the probabilities of the number of active neurons for a system of any size N. Firstly, as in equation 4 the probabilities can be written as (again assuming a steady state):

$$\begin{aligned}
P(0) &= q_1 P(1), \\
P(1) &= P(0) + q_2 P(2), \\
P(2) &= (1-q_1)P(1) + q_3 P(3), \\
&\vdots \\
P(k) &= (1-q_{k-1})P(k-1) + q_{k+1}P(k+1), \\
&\vdots \\
P(N-1) &= (1-q_{N-2})P(N-2) + q_N P(N), \\
P(N) &= (1-q_{N-1})P(N-1),
\end{aligned} \tag{7.9}$$

where $q_N = 1$ but it will remain in the equations so as to aid notation. Rearranging gives

$$P(2) = \frac{(1-q_1)}{q_2} P(1),$$

and by induction:

$$\begin{aligned}
P(k+1) &= \frac{1}{q_{k+1}} \left(P(k) - (1-q_{k-1})P(k-1)\right) \\
&= \frac{(1-q_1)(1-q_2)\ldots(1-q_k)}{q_2 q_3 \cdots q_{k+1}} P(1).
\end{aligned} \tag{7.10}$$

Summing all the probabilities and setting this equal to 1:

$$P(1) = \frac{q_2 q_3 \dots q_N}{q_1 q_2 \dots q_N + q_2 q_3 \dots q_N + (1-q_1) q_3 \dots q_N + \dots + (1-q_1)(1-q_2)\dots(1-q_N)}. \tag{7.11}$$

Having determined these probabilities we then need to take into account the fact that the consecutive active to quiescent transitions must be preceded by a quiescent to active transition, i.e. they must be preceded by a neuron firing (otherwise they would be a chain of $k+1$ consecutive active to quiescent transitions and so included elsewhere in the distribution). We are therefore only interested in the probability $P_A(N_0)$ of the number of active neurons being equal to N_0 given that a quiescent to active transition has just occurred. Considering again the probability tree, Fig 7.6, we find that these probabilities, are given by:

$$\begin{aligned} P_A(0) &= 0, \\ P_A(1) &= P(0), \\ &\vdots \\ P_A(k) &= (1-q_{k-1})P(k-1), \\ &\vdots \\ P_A(N) &= (1-q_{N-1})P(N-1), \end{aligned} \tag{7.12}$$

where we make use of the previously defined probabilities $P(k)$. From these probabilities the full probability distribution of the duration of consecutive active to quiescent transitions can be calculated. As was shown above, for a set initial number of active neurons N_0, the probability distribution of consecutive active to quiescent transitions is given by a weighted sum of hypoexponentials, see equation 7.4. This can then be further weighted by the probability $P_A(N_0)$ that the initial (at the start of the sequence of transitions) number of active neurons is equal to N_0 and the previous transition was quiescent to active. Thus, the overall probability distribution of consecutive active to quiescent transitions is given by:

$$\wp(x) = \sum_{i=0}^{N} \left(P_A(i) \sum_{m=1}^{i} f(x,i,m) p(i,m) \right). \tag{7.13}$$

To confirm that this theoretically derived distribution compares with results from simulations, we determined the distribution of the lengths of periods of any consecutive active to quiescent transitions from simulations. Fig. 7.7 shows the good agreement between the distribution of consecutive active to quiescent transitions from a simulation with $N = 50$ and the theoretical distribution.

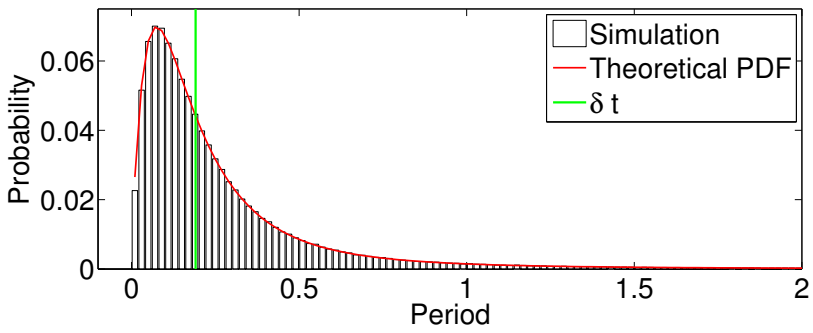

Figure 7.7: **Theoretical and simulated distributions of periods of consecutive active to quiescent transitions.** The simulated distribution (black) is compared with the theoretically derived probability density function (shown in red, see equation 7.13). For both distributions $\alpha = 1,\ w = 1,\ N = 50$ and $h = 1/N$. The mean difference between consecutive spikes (δt) within the simulation (green) is used to define avalanches through the binning approach described in the main text. Thus, the portion of the distribution for which the length of active to quiescent transitions are greater than this average time between consecutive spikes form the distribution of IAIs when combined with the distribution of single quiescent to active transitions.

Distribution of single quiescent to active transitions

As was described above, a single period in between two neurons firing can also be an IAI, provided that the duration of this IAI is longer than the average time between spikes as accounted for below. Note, however, that only single periods are considered, as consecutive periods necessarily include neurons switching to the active state and therefore cannot form part of an IAI. Thus, the distribution of IAIs should also take into account the distribution of single quiescent to active transitions. As we make use of the Gillespie algorithm, the duration distribution of these single transitions is an exponential with rate given by the total transition rate, which is dependent on the number of active neurons, N_0. This is then weighted by the probability of a quiescent to active transition given N_0 active neurons (i.e. by $1 - q_{N_0}$) and additionally weighted by the probability of starting with N_0 active neurons following a quiescent to active transition as calculated above. Thus, the probability distribution of single quiescent to active transitions of length x is given by:

$$\rho = \sum_{i=0}^{N} \left(P_A(i)(1 - q_i) r_i e^{-r_i x} \right). \tag{7.14}$$

Fig. 7.8(a) shows the good agreement between simulated distribution of single quiescent to active transitions and theoretical distribution.

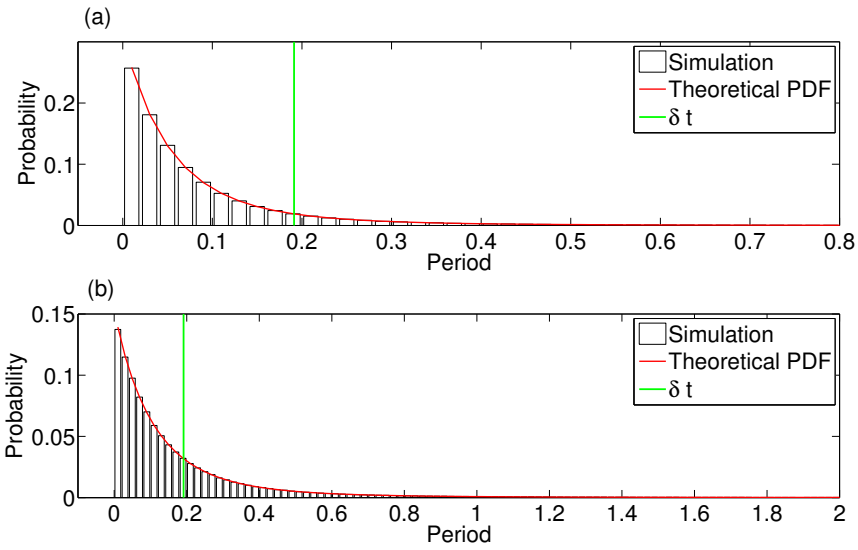

Figure 7.8: **Theoretical distributions of single quiescent to active transitions and the combined distributions.** Theoretical (red) and simulated (black) probability distributions for (a) single quiescent to active transitions and (b) this distribution combined with the distribution of consecutive active to quiescent transitions (see Fig. 7.7). In both cases $\alpha = 1$, $w = 1$, $N = 50$ and $h = 1/N$. The green line indicates the average time between consecutive spikes (δt) within the simulations. Thresholding the combined distribution (b) at this level determines the IAI distribution.

The IAI distribution

As discussed above, the IAI distribution combines these two distributions - the distribution of consecutive active to quiescent transitions and the distribution of single quiescent to active transitions. This combined distribution, along with simulated values, is shown in Fig. 7.8(b). As was described above, avalanches are defined from the network firing pattern as consecutive spikes where the time difference between them is no greater than the average time difference between consecutive spikes, δt, within the network. Thus, the minimum IAI is bounded below by δt and all consecutive active to quiescent transitions or single quiescent to active transitions whose total duration is greater than δt will be an IAI. Thresholding the combined distribution at δt determines the IAI distribution. Fig. 7.9(a) shows theoretical and simulated IAI distributions displayed on a double logarithmic scale. Despite the fact that the distribution is not a power-law (theoretically we know that it is a weighted sum of hypoexponentials), it appears scale-free over a range of scales on this double logarithmic scaling. As we will show below, the distribution can also pass statistical tests for power-law distributions, suggesting partial scale-free behaviour of the system close to the critical regime.

Fig. 7.9 also shows the theoretical and simulated distributions for lower levels of external input. With lower levels of external input (as the system approaches the critical regime) the average IAI increases and the distribution changes, no longer exhibiting scale-free behaviour.

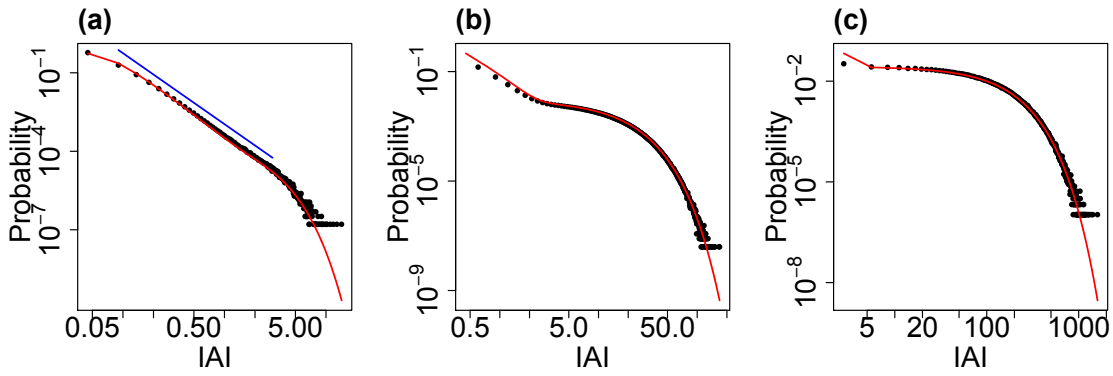

Figure 7.9: **Distribution of IAIs for varying levels of the external input.** The theoretical (red) and simulated (black) IAI distributions with (a) $h = 1/N$, (b) $h = 0.1/N$ and (c) $h = 0.01/N$. These distributions were for $N = 800$ with $\alpha = w = 1$, with a simulation length of 10^4 seconds. The distributions from the simulated data are pooled from 10 simulations. The theoretical distributions were calculated up to the level of active neurons which occur with a cumulative probability of 0.9 (see main text). The blue line in plot (a) indicates a linear fit, i.e. a fitted power-law with an exponent of 2.71.

Even when considering the same scale for all levels of the external input (IAIs in the region of 0.05-5 ms) it is only for $h = 1/N$ that the distribution is scale-free. Indeed, at the lowest level of input $h = 0.01/N$ the distribution is in fact best fit by an exponential, in this case $y = 0.028e^{-0.01x}$ as seen in Fig. 7.10, indicating the loss of the scale-free behaviour in the distribution. Thus, scale-free behaviour in the case of the IAI distribution does not increase with proximity to the critical regime.

As an aside, note that due to the product in the hypoexponential (see equation 7.2) determination of the probabilities for large N can become computationally intractable. For simulations larger than with $N = 50$ we therefore only determined the theoretical distribution up to a set level of the number of active neurons. We set the threshold level of the number of active neurons according to the probability distribution of starting from a particular number of active neurons (calculating the cumulative probability from zero active neurons), and sufficiently low so that the calculations were computationally viable. However, the theoretical distributions calculated using this threshold are still a good fit to the simulated data - Fig. 7.9.

Distributions of avalanche size and duration

As we have shown, the theoretical distribution of IAIs can be calculated by assessing periods of consecutive active to quiescent transitions and single quiescent to active transitions. It is also possible to derive the distribution of consecutive quiescent to active transitions. However, if a period of active to quiescent transitions (a period without firing) has a duration less than the average time difference between two spikes then this interval does not separate an avalanche into two. Therefore, the distributions of number and length of consecutive quiescent to active transitions does not describe the distributions of avalanche size and duration -

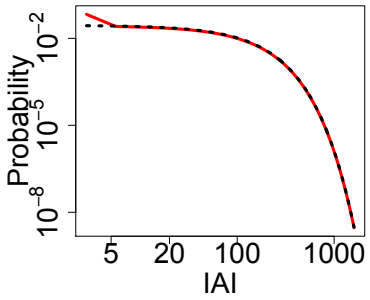

Figure 7.10: **The IAI distribution with $h = 0.01/N$ is well fitted by an exponential distribution.** The theoretical IAI distribution at the lowest level of the external input (shown in red, see also Fig. 7.9c) compared with the fitted exponential distribution (black dashed). The exponential is given by $y = 0.028e^{-0.01x}$. This indicates that as the external input is decreased and the system approaches the critical regime the IAI distribution loses the scale-free behaviour seen at higher levels of the external input and is dominated by an exponential.

these distributions can also contain periods of active to quiescent transitions within two or more periods of quiescent to active transitions. Note that a period of active to quiescent transitions having a duration less than the average difference between consecutive spikes is not dependent on the number of active to quiescent transitions within the interval, as the length of each transition is drawn at random from an exponential distribution. It was therefore not possible for us to determine a theoretical distribution of avalanche size and duration using this approach.

7.3.4 Statistical comparison with a power-law distribution

The influential paper by Clauset et al. (2009) developed a model selection based methodology to determine whether empirical data are likely to be power-law distributed. This method has been used to assess physiological neuronal avalanches and the results have shown that the power-law hypothesis is not rejected for this data (Klaus et al., 2011). It is therefore of interest to determine whether this is also the case for the data from the model studied here. Briefly, this method finds the best fit to a power-law of the distribution under study. The empirical data are then compared to distributions of the same size that are generated by randomly drawing values to follow the best-fit power-law distribution. A p-value is calculated as the proportion of times that the empirical data are a better fit to the power-law than the generated data (using the Kolmogorov-Smirnov test). As per Clauset et al. (2009) the hypothesis (that the data come from a power-law) is rejected if the p-value is less than 0.1. As we have observed (Figs. 7.4, 7.9), the distribution of avalanche sizes appears to exhibit partial scale-free behaviour for low levels of external input ($h = 0.1/N,\ 0.01/N$) and the IAI distribution appears scale-free over a range of scales for $h = 1/N$. As in the companion paper (Taylor et al., 2013), we fit a truncated power-law distribution up to an avalanche size

of $x_{max} = \frac{9}{10}N$ in the case of avalanche size distributions. We fit a power-law distribution without truncation to the IAI distribution. Testing the entire avalanche size distributions (consisting of over 900,000 avalanches) yielded $p = 0$ indicating that the hypothesis that the distribution follows a power-law should be rejected. Similarly, taking the IAI distribution for $h = 1/N$, testing the whole distribution of over 6,000,000 IAIs (note that there are more avalanches and therefore IAIs with larger h due to the higher firing rate) yielded $p = 0$. Testing instead the first 100,000 avalanches (a similar order of magnitude to the number of neuronal avalanches tested experimentally) with $h = 0.1/N$ yielded $p = 0.46$ indicating instead that the power-law hypothesis should not be rejected. Similarly, for $h = 0.01/N$ testing the first 10,000 avalanches yielded $p = 0.13$. These results are similar to those of the companion paper, where the power-law hypothesis was not rejected when the number of avalanches included in the distribution was of the same order as those tested experimentally, and are indicative of the partial scale-free behaviour of the system in proximity of the critical regime.

In the case of the IAI distribution testing the first 100,000 IAIs yielded $p = 0.44$ indicating that a power-law is a good fit to the data. Given that in this case we know that the IAI distribution is not a power-law (but is in fact a weighted sum of hypoexponentials), it is interesting to note that the hypothesis that the data follow a power-law is not rejected when the number of data points is of the same order as that which have been tested experimentally, an observation that will be explained in the discussion. When the power-law hypothesis is not rejected, Clauset et al. (2009) employ a model selection process to determine the best model for the data. We did not carry out this testing here (as, at least in the case of the IAI distribution, we already know what the distribution is) and it may be that such a process would suggest that a power-law is not the best fit to the data. However, the results here (and those of the companion paper) are indicative of the partial scale-free behaviour exhibited by the system in the region of the critical regime.

7.3.5 Long-range temporal correlations

As mentioned in the introduction, long-range temporal correlations are another possible signature of a system at (or near) a critical state and have also been observed in neurophysiological data (Linkenkaer-Hansen et al., 2001, 2004; Nikulin and Brismar, 2004, 2005; Berthouze et al., 2010; Smit et al., 2011). It is therefore of interest to determine whether this finite-size neuronal system with external input displays LRTCs - given that it is in the region of a critical regime - and whether LRTCs relate to other signatures of criticality, i.e. the presence of partial scale-free behaviour in the data distributions themselves. The latter is of particular interest given that we have seen a change in distributions as the system approaches the critical regime. As with all simulations the level of external input is constant, i.e., it does not itself display LRTCs, and therefore we stress at the outset that any LRTCs present in the dynamics of the system would have to be intrinsic to the system. Furthermore, it is useful to remember that a power-law distribution of any data set does not imply that the data will exhibit LRTCs and

vice-versa – consider points drawn at random from a power-law distribution - such a data set would not exhibit LRTCs.

In neurophysiological data, LRTCs have been observed in fluctuations of oscillation amplitude (i.e. within continuous data) (Linkenkaer-Hansen et al., 2001, 2004; Nikulin and Brismar, 2004, 2005; Berthouze et al., 2010; Smit et al., 2011) and also in discrete burst activity in our recent analysis of the inter-event intervals of bursts of nested oscillations in EEG recordings of extremely preterm human neonates (Hartley et al., 2012). Moreover, LRTCs in discrete data have previously been investigated by Peng et al. (1995) and a number of other authors, for example Toweill et al. (2003); Castiglioni et al. (2011); Ho et al. (1997), in their analysis of inter-heartbeat intervals. As the data from the model analysed here result in discrete avalanche activity, we adopt the approach used in these previous studies of LRTCs in discrete data and examine LRTCs in waiting times, i.e. in IAIs.

We assessed the presence of LRTCs in IAIs through estimating the Hurst exponent, H, which describes the degree of self-similarity within the data. A Hurst exponent of $H \approx 0.5$ indicates that there are no correlations in the data or short-range correlations only, for example a white noise process, whereas a Hurst exponent of $0.5 < H < 1.0$ indicates LRTCs in the data. Additionally, an exponent of 1 corresponds to $1/f$ noise (Peng et al., 1995). We estimated the Hurst exponent using detrended fluctuation analysis (DFA) – an approach that has been shown to produce more accurate estimates of the Hurst exponent than some other approaches (Taqqu et al., 1995) and has been used previously to assess the presence of LRTCs in neurophysiological data sets (Linkenkaer-Hansen et al., 2001, 2004; Berthouze et al., 2010; Hartley et al., 2012). DFA is a graphical method whereby the average root mean square fluctuations at a given box size are compared across different box sizes and the gradient of the line of best-fit is the estimate of the Hurst exponent (for more detail see Peng et al. (1995, 1994)). We used a minimum box size of 5, with 50 box sizes linearly spaced on a logarithmic scale up to a maximum box size of 1/10 of the length of the IAI sequence (Hu et al., 2001). Calculations were carried out using the MATLAB code of McSharry (McSharry, 2011).

Fig. 7.11 shows example DFA plots for IAIs from three simulations with $\alpha = w = 1$, $h = 1/N$. It is important to notice from these plots that there is not a single linear trend across all box sizes. Hu et al. (2001) discussed the importance of identifying crossover points - box sizes at which there is a change in the linear fit of the data - within DFA plots. Failure to examine these trends leads to erroneous estimates of the Hurst exponents. A single linear fit across all the points would give an estimate of the Hurst exponent for that sequence. However, crossover points indicate that the same correlations (i.e. temporal behaviour) do not extend across the whole sequence. In the DFA plots here there are in fact three regions, each with a different linear trend, between two crossover points. The best-fit to the data by three linear regions was found using the nonlinear regression function 'nlinfit' in the MATLAB environment, therefore determining the crossover points. In Fig. 7.11(a), the Hurst exponent (slope of the line) of the first two regions (at smaller box sizes) are 0.83 and 0.62 respectively - exponents which

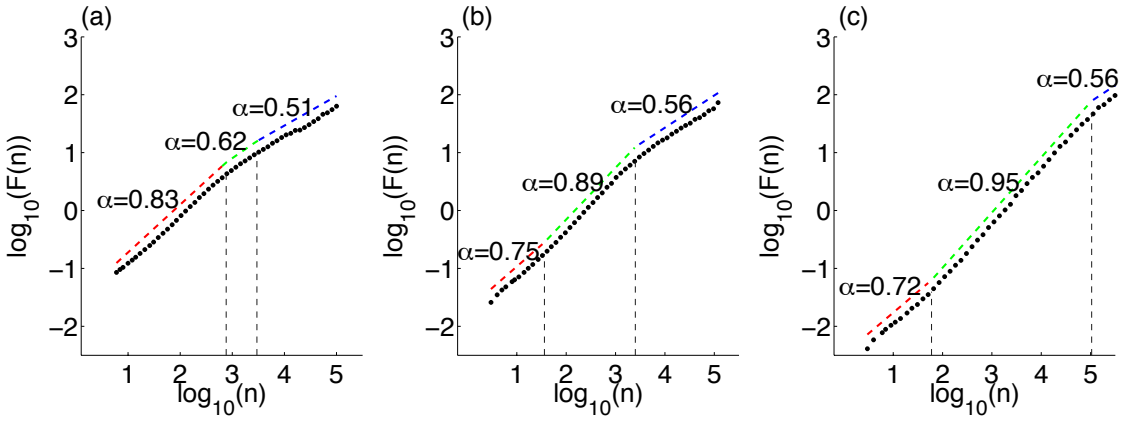

Figure 7.11: **DFA plot examining the presence of temporal correlations in IAIs.** Plot of the average fluctuations $F(n)$ against box size n for IAIs from simulations with $\alpha = w = 1$, $h = 1/N$ and (a) $N = 800$, (b) $N = 3200$ and (c) $N = 172800$. The data is best fit not by a single linear trend but by three lines (red, green, blue) between two crossover points (dashed black lines). For smaller box sizes the Hurst exponents (slope of the line - as annotated next to the individual lines: the DFA exponent α) indicates that correlations extend across these regions. However, for larger box sizes the exponents are closer to 0.5 suggesting that the correlations do not extend across these larger box sizes. With a larger system size (c) the upper crossover point increases to larger box sizes. With increasing system size the system approaches the critical regime - (a) $\lambda = -0.07$, (b) $\lambda = -0.04$ and (c) $\lambda = -0.005$.

indicate the presence of LRTCs within the data. However, the third region across the largest box sizes has an exponent of 0.51 indicating that there are no correlations in the data. This change in the exponents therefore suggests that the correlations observed in the data at small box sizes do not extend across the entire sequence length.

When examining the presence of LRTCs it is standard practice to compare the exponent of the actual data to the exponent of the data randomly shuffled (Linkenkaer-Hansen et al., 2001). Shuffling the data should destroy any correlations present and therefore the exponent of the shuffled data is expected to be approximately 0.5. We compared the original sequence (whose DFA plot is shown in Fig. 7.11) with 500 shuffled sequences. As expected, the DFA plots for the shuffled sequences (data not shown) did not exhibit crossover points and showed a mean exponent for the shuffled sequences of 0.50 with a range of 0.48-0.52. The fact that the exponents of the original sequence (at smaller box sizes) do not fall within the distribution of exponents for the shuffled sequences therefore demonstrates that the original sequence exhibits complex temporal ordering with correlations that extend across a range of box sizes (up to the upper crossover).

Increasing the system size

As noted previously (see Fig. 7.2), as $N \to \infty$ the eigenvalue of the system $\lambda \to 0$, i.e., the system approaches the critical regime with increasing system size. We might expect that as

the system approaches the critical regime it is more likely to exhibit signatures of criticality and therefore that LRTCs would extend to larger box sizes as the system size is increased. We therefore investigated whether there was a change in the temporal correlations of the IAIs with system size, while maintaining all other parameters including $h = 1/N$. For all system sizes investigated the DFA plots displayed three regions with different linear trends, as was discussed above. Fig. 7.11 shows example DFA plots for the IAIs of three simulations with the smallest and largest system sizes examined. It was observed that the pattern of the exponents in each of the cases remained the same - with the two lower regions having exponents indicative of LRTCs, while the exponent across the largest box sizes is closer to 0.5. Additionally, we found that the location of the upper crossover increased with system size. Fig. 7.12 shows the location of the upper crossover (the crossover at the higher box regions) for different system sizes (from N=3200 to N=172800) normalised with respect to the largest box size. We did not find a change, other than small fluctuations, in the exponents themselves for any of the three regions for all system sizes. Namely, across all system sizes considered, the mean exponent across the smallest box sizes (up to the first crossover point) was 0.73 with a range of 0.70 - 0.76. It was 0.95 with a range of 0.89 - 0.99 (close to an exponent of 1 which would indicate 1/f noise) between the first and second crossover points. The largest variation in exponents was for the region above the upper crossover point with an average exponent of 0.59 and a range of 0.46 - 0.73; on average this indicates that temporal correlations do not extend beyond the upper crossover. Thus, overall, as the system size is increased the temporal correlations extend across larger box sizes. This is consistent with the idea that, when the system reaches the critical regime, LRTCs could extend to infinite length (i.e., all possible box sizes) in the limit of system size.

Next we considered whether the distributions of IAIs and avalanche size themselves changed with system size and whether the change in the correlation length observed above was reflected in a change in the distributions. Fig. 7.12 also shows the IAI and avalanche size distributions for different network sizes. In both cases, the distributions for different system sizes show only small changes which can be accounted for by noise. Thus, as the system approaches the critical regime through increasing the system size there does not appear to be a change in the distributions despite the change in the temporal correlations. Moreover, LRTCs are present in the data but the distribution of avalanche sizes does not exhibit scale-free behaviour, i.e., these markers of criticality do not occur simultaneously in this case. By contrast, through approaching the critical regime by lowering the external input we have shown that the avalanches are more distinct and the distribution of avalanche sizes exhibits partial scale-free behaviour.

The effect on LRTCs of decreasing the level of external input

We also examined the DFA exponents at lower levels of external input ($h = 0.1/N$ and $h = 0.01/N$). In both cases there were no crossover points with a single linear trend across all box sizes (data not shown). The exponents were 0.50 (range 0.49-0.51, across 10 simulations

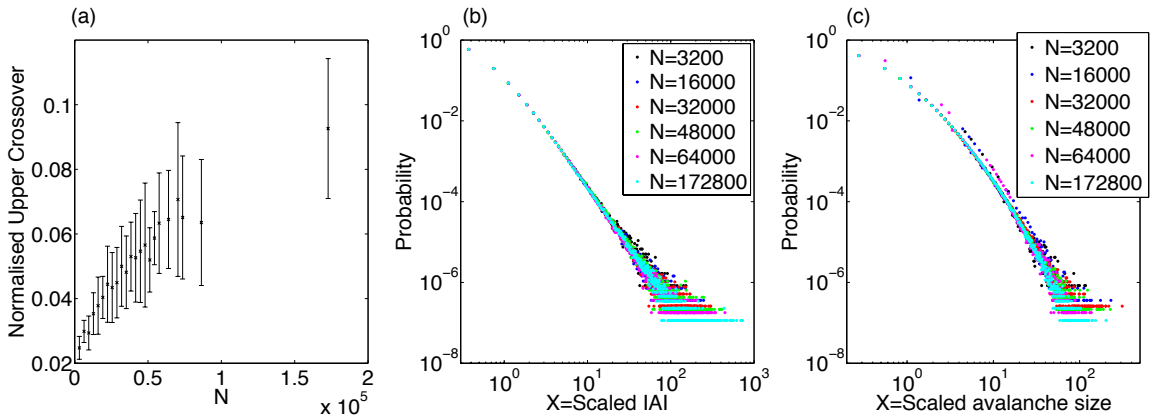

Figure 7.12: **Changes with increasing system size.** (a) The normalised (with respect to the largest box size) upper crossover box size increases with system size. The plot shows the average value across 10 simulations at the same system size and error bars indicate the standard deviation. (b) The IAI distributions and (c) the distributions of avalanche size for 6 different system sizes, scaled with respect to the mean IAI or avalanche size of each distribution respectively. For all simulations $\alpha = w = 1,\ h = 1/N$.

with $N = 800$) and 0.56 (range 0.55-0.57) for $h = 0.01/N$ and $h = 0.1/N$ respectively. Thus, at the lowest level of external input the IAIs do not exhibit LRTCs and there is a slight increase in the exponent as the external input increases. This suggests that as the system approaches the critical regime through a decrease in the external input the temporal correlations are lost. Thus, the existence of LRTCs as the system approaches the critical regime is dependent on how the critical regime is approached, namely, approaching the critical regime through increasing the system size extends the temporal correlations whereas decreasing the external input leads to a loss of long-range correlations. In addition, this signature of criticality is independent from the other marker we investigated – the presence of scale-free behaviour in the avalanche size distribution. Considering avalanche size and duration, scale-free behaviour is present at the lowest level of external input, when LRTCs are lost. Thus, we find that markers of criticality are not only dependent on the region around the critical regime but also may not be present for the same parameter set.

7.4 Discussion

This paper specifically examined a finite-size neuronal system without a separation of timescales between external input and the avalanches themselves. By analytically tuning the system to be in the region of a critical regime we were able to examine the type of dynamics displayed by such a system and to investigate whether the dynamics display signatures of criticality. In summary, we have shown that:

1. As the system approaches the critical regime through a reduction in the external input

the avalanches become more distinct and the distribution of avalanche sizes displays scale-free behaviour.

2. With $h = 1/N$ the IAIs exhibit temporal correlations which extend across a range of bin sizes to an upper crossover. As the system approaches the critical regime through increasing the system size the length of the temporal correlations is extended across a wider range of bin widths. These correlations (one noted signature of a critical system) are observed despite the fact that the distribution of avalanche sizes does not exhibit scale-free behaviour and does not change with the increase in system size. These temporal correlations are lost if the critical regime is instead approached through reducing the external input.

3. The distribution of IAIs was theoretically derived and was shown to be a weighted sum of hypoexponentials. However, for $h = 1/N$ (when the number of avalanches considered was of the same order as those tested experimentally) the hypothesis that the IAI distribution follows a power-law was not rejected by statistical testing indicating the scale-free nature of the distribution at this level of the external input.

7.4.1 Validity of the model

The model considered in this paper was a highly simplified neuronal system with a number of assumptions, such as equally weighted synapses and continuous constant external input. These assumptions were necessary in order to analytically tune the system to be in the region of a critical regime. Therefore, while this should not be taken as an accurate model of a real neuronal system it is important that we first consider models such as this, examining markers of criticality, which will then aid our understanding when building on this work with more complex models. This paper opens the way for future work examining the role of external input on signatures of criticality and the importance of the region of parameter space on network dynamics. Future work should also investigate the effect of topology on the dynamics (Larremore et al., 2011; Sporns, 2011b) and the effect of external input with different temporal and spatial characteristics.

A purely excitatory network

The synaptic connections investigated in this model were purely excitatory. This not only simplifies the model for analytical investigations but is also of interest from a neurological perspective in terms of early brain development. Before birth, GABA is thought to have a depolarising effect on postsynaptic neurons and it is not until the nervous system reaches a more mature state that this neurotransmitter becomes inhibitory (Cherubini et al., 1991; Ben-Ari, 2002). While *presynaptic* inhibition is thought to be present at all developmental stages (Holmes et al., 2002) this effect can be considered to be taken into account in the model by the fact that neurons cannot re-fire until they have returned to the quiescent state.

We have recently shown that EEG recordings from very preterm infants (when GABA is still thought to be purely excitatory) exhibit LRTCs in the temporal occurrence of bursts of activity (Hartley et al., 2012). The model studied here may be a candidate mechanism for the generation of this temporal patterning in the discontinuous activity of the developing brain. Moreover, it is interesting to note that despite the fact that the system has purely excitatory postsynaptic connections and input, for these parameter regions, the model does not exhibit runaway excitation (saturation) but is able to maintain stable dynamics through the 'balance' of individual neuronal dynamics resulting from a trade-off between the rates at which neurons become active and quiescent. Indeed, while a number of authors have suggested that a balance of excitation and inhibition in neuronal networks leads to critical behaviour (Shew et al., 2009), the work here and in the companion paper shows that excitatory networks can display the same behaviour. It can be speculated that this type of balanced activity in the region of a critical regime might be a way in which the brain avoids (for the most part) epileptic behaviour during early development.

The activation function

Here we used a linear activation function for the transition of neurons from the quiescent to the active states. However, physiologically neurons behave more like a saturating function. The linear activation function used here was chosen so as to be analytically tractable and is also equivalent to a saturating function at low input levels. However, considering instead a saturating function (see Appendix 3) we found the dynamics in the region of the critical regime to show similar behaviour to the system with the linear activation function.

With both the linear and saturating activation functions, the critical regime can only be reached exactly in the absence of external input. A positive external input therefore drives the system away from the critical regime. However, with a quadratic activation function (see Appendix 3) the system does have a critical fixed point even with a positive external input and it can be tuned directly to this regime. With such an activation function the dynamics do not appear to exhibit burst like behaviour, however, analysis shows that the activity fluctuates about the critical regime in an 'avalanche-like' manner. Thus, while a quadratic function does not best describe activation in a neuronal network, we can emphasise our conclusion that signatures of criticality are not universal and can be examined only in relation to the specific critical regime of the system (see Appendix 3).

The binning approach

As described previously, the binning method separated avalanches where the time difference between consecutive spikes was greater than the average time difference between consecutive spikes across the entire simulation. This was the approach taken by Benayoun et al. (2010). However, it is worth noting that this is a slightly different approach to the method first proposed by Beggs and Plenz (2003, 2004) to separate neuronal avalanches. In their analysis

neuronal firing is distributed into bins of width of the average time difference between consecutive spikes (δt) and firing is separated into avalanches by bins in which no firing occurs. Thus, two spikes may be separated by more than the average time difference δt but still be considered part of the same avalanche if they fell within consecutive bins. Our theoretical derivation of the IAI distribution relied on the fact that all consecutive active to quiescent transitions or single quiescent to active transitions with a length greater than the average time between two spikes is an IAI. This would not be the case if the alternative (Beggs and Plenz) binning approach was used to determine avalanches. If this alternative approach was used the distributions of consecutive active to quiescent transitions and single quiescent to active transitions would be the same, but transitions of length slightly greater than or equal to the average time between consecutive spikes (in fact up to twice this average) may or may not form part of the IAI distribution depending on the exact binning. It is also important to note that with the binning method used here, even with dense neuronal firing (which occurs if the external input is increased from the levels studied here), it is always possible to separate the dynamics into 'avalanches' since there is always an average time between consecutive spikes.

Additionally, both these binning approaches differ from that used in non-driven systems such as the classical sand-pile model (Bak et al., 1987) and the system investigated in the companion paper to this article (Taylor et al., 2013). In those models an avalanche consists of all firings until the system returns to the fully quiescent state. This means that although the system may have a long period without firing – during which neurons switch to the inactive state – activity before and after this period will not be considered as separate avalanches even if the period in-between exceeds the average difference between consecutive spikes. Future work is needed to fully investigate how differences in the definitions of avalanche affect the distributions of size, duration and IAIs and care needs to be taken when interpreting the results from these different approaches.

Validity of DFA and the investigation of LRTCs

DFA is one method by which to estimate the Hurst exponent and was chosen here as it has been shown to be an accurate estimate (Taqqu et al., 1995). Moreover, it is a graphical approach and so can be used to check for crossover points (Hu et al., 2001) – see also the recently proposed ML-DFA (Botcharova et al., 2013) whereby the existence of crossover behaviour can be rigorously tested. As the Hurst exponent can only be estimated it is is considered best practice to check the consistency of the exponents using two methods (Gao et al., 2006). However, as non-graphical methods only give single numerical values they cannot be interpreted when crossover behaviour exists. Given that there were crossover points we only considered DFA with this analysis.

Crossover points within a DFA plot have been shown to exist when the same correlations do not extend across the whole data sequence in analytically constructed data (Hu et al., 2001). It is important to correctly interpret these crossover points. Being box sizes, they

define sequence lengths, e.g., a box size of 10 indicates detrending across a sequence of 10 consecutive IAIs. Note that as the IAIs are of variable length the box size does not specify a particular simulation time but merely a number of events. Future investigation is therefore needed to determine the relationship between the model and its crossover points.

Correlations extended only across a range of box sizes, with this range extending as the system size increased and the system approached the critical regime. It appears that correlations could potentially extend across an arbitrarily large box size in the limit of system size. Thus, as the critical regime is approached in this way, this signature of a critical system emerges. LRTCs have been demonstrated previously in discrete neurophysiological data, in the waiting times of burst activity in cultures (Segev et al., 2002) and in the bursts of activity recorded using EEG in very preterm human neonates (Hartley et al., 2012). To our knowledge, waiting times of neuronal avalanches have yet to be examined in this manner. However, such a study would provide an additional link between studies on the neuronal scale and studies on a wider network scale for which LRTCs have been observed in the fluctuations of oscillation amplitude. Palva and colleagues demonstrated strong correlations between power-law exponents of avalanche size distributions and exponents of LRTCs in fluctuations of oscillation amplitude in human MEG recordings (Palva et al., 2013). Recent computational work also demonstrated a link between neuronal avalanches on the one scale and LRTCs on a wider temporal scale and the authors called for future work in this area (Poil et al., 2012). However, these authors did not investigate LRTCs in the waiting times of the avalanches themselves. Interestingly, in our model, LRTCs were observed when $h = 1/N$ but not for lower levels of external input. Thus, they were not observed when the avalanche size distribution exhibited scale-free behaviour – the type of distribution observed for avalanches recorded *in vivo* and *in vitro* (Beggs and Plenz, 2003, 2004; Petermann et al., 2009). It would therefore also be interesting to assess whether altering the driving force experimentally *in vitro* would lead to the types of dynamics (LRTCs) observed here.

7.4.2 Partial scale-free behaviour in avalanche size

Statistical testing of the avalanche size distribution (with $h = 0.1/N,\ 0.01/N$) did not reject the hypothesis that the distribution followed a power-law when the number of points within the distribution was of the order of the number of avalanches recorded in the experimental setting. Only with larger numbers of avalanches was the hypothesis that the distribution is a power-law rejected. This is to be expected, as has been discussed by Klaus et al. (2011). When a distribution deviates from the expected distribution by more than noise from sampling then given a large enough number of samples the power-law hypothesis will eventually be rejected. The fact that the power-law hypothesis was not rejected for lower numbers of avalanches demonstrates the partial scale-free behaviour of the system in the region of the critical regime. Further, it highlights the fact that stringent statistical testing, such as this, with high sampling may lead to rejecting the power-law hypothesis and so rejecting the criticality hypothesis even

when the system is critical.

7.4.3 Waiting times

In addition to increasing the physiological realism of the model, investigating the system with continuous external input also has the advantage of producing waiting times (termed IAIs throughout). In the companion paper the simple reseeding of the network with a neuron set to the active state implied that there was no waiting times between avalanches. Other authors have reseeded by increasing the membrane potential but stipulated that neurons must reach a threshold for them to become active (and a new avalanche to start) (Bak et al., 1987; Levina et al., 2007). This does lead to waiting times, however, these are not the same as the waiting times investigated in this model which are intrinsic to the network dynamics rather than as a result of an explicit separation of timescales.

Recent work by Lombardi et al. (2012) showed that the waiting times between neuronal avalanches recorded *in vitro* have a distribution with an initial power-law regime. The authors suggest that the shape of the distribution relates to up and down states within the network (which exhibit critical and subcritical dynamics respectively) and are able to reproduce the non-monotonic waiting time distribution in a computational model in which neurons switch between up and down states depending on short-term firing history. Interestingly, the distribution they observe is similar to the IAI distribution for the system with $h = 0.1/N$, see Fig. 7.9(b), which also has a scale-free initial regime albeit over a shorter range to that presented by Lombardi et al. It is therefore possible that the waiting time distribution observed experimentally fits with the model constructed here. It would be interesting to investigate whether a change in input to the network *in vitro* alters the distribution in a similar way to those distributions seen in Fig. 7.9.

Additionally, for different parameter ranges different distributions were observed, in the IAI distribution as well as the distributions of avalanche size and duration. This leads us to the important conclusion that power-law distributions will not necessarily be displayed by systems in the region of a critical regime. Therefore, this work suggests that the absence of a power-law in experimental data should not necessarily be taken to conclude that the system does not lie in the region of a critical regime. This was also seen in the companion paper where it was shown that despite being analytically tuned to the critical state (in absence of external input) the avalanche size distribution was not a power-law although it did exhibit partial scale-free behaviour. The fact that the system may not exhibit power-laws when close to (or at) the critical regime is an important finding given that the system is finite-size as will be the case in an experimental setting. This highlights the necessity of examining other markers of criticality before conclusions about the critical nature of a system can be drawn.

7.4.4 Dynamic range and power-laws

Coinciding with results from previous authors (Kinouchi and Copelli, 2006; Larremore et al., 2011) we showed that the system exhibits optimal dynamic range when the branching parameter is equal to one. When calculating the dynamic range of a system, we emphasised that this value was dependent on the critical state of the system calculated when there was no external input. We have shown that tuning a system to this critical point but then driving it with different levels of external input has considerable effect on the distribution of avalanche sizes. For non-zero h the corresponding ODE would, in the strictest sense, not be considered critical. Importantly, however, tuning to the critical point of the system with zero external input, maximises the dynamic range.

Dehghani et al. (2012) showed that *in vivo* (against the results of Petermann et al. (2009) and Hahn et al. (2010)) avalanches were not well approximated by power-laws, but were more likely to approach exponential distributions. They contrast this with the evidence that the brain is operating at criticality from *in vitro* studies (Beggs and Plenz, 2003; Friedman et al., 2012) where avalanches are well approximated by power-laws. Here we argue that external input and functional benefits (Shew and Plenz, 2013) such as dynamic range, information transmission and information capacity, provide an interesting possibility as to the reason why *in vivo* and *in vitro* studies could potentially give different results. The critical brain hypothesis demands that in isolation from its natural surroundings (*in vitro*) and whilst having no external influences acting upon it (akin to the model with $h = 0$ we studied in the companion paper (Taylor et al., 2013)), a culture should exhibit signs that it is tuned to criticality (i.e. avalanches that are well approximated by power-laws). However, when observed *in vivo*, and thus with external inputs acting upon it, a critical brain may no longer exhibit avalanches approximated by power-laws but still optimise functional benefits such as the dynamic range and information transmission (Shew and Plenz, 2013). In our model we have shown that tuning the parameters to the critical regime does indeed maximise the dynamic range, but it is the level of external input that dictates whether the avalanche distributions exhibit partial scale-free behaviour. For this reason, avalanches recorded *in vivo* that lacked a power-law distribution would not be in contradiction with the criticality hypothesis but rather an expected result. This further supports our suggestion in the companion paper (Taylor et al., 2013) that future work should shift its focus away from characterising avalanche distributions and towards more appropriate metrics.

7.4.5 Two routes to criticality

In this paper we examined two different parameter changes such that the system approaches the critical state: increasing the system size and lowering the overall level of the external input. Despite the fact that in both cases the critical regime is approached, the dynamics and the signatures of criticality observed are different. With increasing system size the temporal correlations extend across a wider range. However, the distributions of the avalanche

characteristics remain the same and the distribution of avalanche size does not exhibit scale-free behaviour. By contrast, for lower overall levels of the external input the distributions of avalanche size and duration do exhibit partial scale-free behaviour. However, in this case as the critical regime is approached the temporal correlations in the avalanches are lost. At these lower levels of the external input we also observe a greater separation of the avalanches suggesting that the avalanches have less of an influence on each other which would explain this loss of LRTCs. Thus, as the system approaches the critical state in two different regions of the parameter space the dynamical properties of the system are very different. Significantly, this implies that not just the critical state alone but the region around the critical regime is an important factor in the system's dynamics.

In conclusion, we have shown here and in the companion paper that in a finite-size neuronal system in the region of a critical regime the distributions of avalanche attributes need not be a power-law. The current assumption in the literature is that power-law dynamics imply criticality and vice versa that systems without power-law dynamics are not in the region of a critical regime, however, the results here suggest that this assumption need not be true. Moreover, we found that long-range temporal correlations and scale-free distributions are not dependent on proximity to the critical regime alone but on the region of the parameter space. The results further highlight the need for future work examining the type of dynamics we might expect from such systems.

7.5 Appendices

7.5.1 Appendix 1: Dynamic range

Whilst Kinouchi and Copelli (2006) and Larremore et al. (2011) consider a discrete model where multiple events can happen per time step, here we show analytically that our continuous model will exhibit the same maximisation of the dynamic range when $R_0 = 1$. We use the calculation of R_0 for a system where there is no external input ($h = 0$) and thus $R_0 = w/\alpha$.

We begin by defining (as in Kinouchi and Copelli (2006)) $F_{max}(R_0)$ as the saturation level of neurons in a network assuming a large external input h. For our model $F_{max}(R_0) = N$ for all R_0. Similarly we define $F_0(R_0)$ as the steady state solution of the mean field ODE for the system when there is zero external input, i.e.

$$\begin{aligned}\frac{dA}{dt} &= \left(\frac{wA}{N} + h\right)(N - A) - \alpha A \\ &= \frac{wA}{N}(N - A) - \alpha A.\end{aligned}$$

Therefore, solving this we have that

$$F_0(R_0) = \begin{cases} 0 & \text{if } R_0 \leq 1 \\ N\left(1 - \frac{\alpha}{w}\right) & \text{if } R_0 > 1. \end{cases}$$

Additionally let $F_x(R_0) = F_0(R_0) + x\left[F_{max}(R_0) - F_0(R_0)\right]$ giving

$$F_x(R_0) = \begin{cases} Nx & \text{if } R_0 \leq 1 \\ N\left[1 - \frac{\alpha}{w}(1-x)\right] & \text{if } R_0 > 1. \end{cases}$$

Finally, let $A(\sigma, y)$ be the number of active neurons at the steady state in a regime where $R_0 = \sigma$ and $h = y$ (where σ and y are dummy variables and h is the external input), then the dynamic range $\Delta(R_0)$ is defined (similarly to Kinouchi and Copelli (2006)) as:

$$\Delta(R_0) = \frac{h_{0.9}}{h_{0.1}},$$

where

$$h_{0.1} \text{ is the level of external input such that } A(R_0, h_{0.1}) = F_{0.1}(R_0) = F_{0.1}$$
$$\text{and } h_{0.9} \text{ is the level of the external input such that } A(R_0, h_{0.9}) = F_{0.9}(R_0) = F_{0.9}.$$

We note that in Kinouchi and Copelli (2006); Larremore et al. (2011), the logarithm of this is taken but as the logarithm is an increasing function it is unnecessary to scale in this way for the result we obtain. Whilst using $F_{0.1}$ and $F_{0.9}$ is the standard for calculating the dynamic range these values are somewhat arbitrary (Kinouchi and Copelli, 2006) and can be generalised to k_1 and k_2 respectively. To calculate the dynamic range analytically we consider the two regimes of R_0, firstly $R_0 \leq 1$ and secondly $R_0 > 1$.

$R_0 \leq 1$

Here the steady state is given by

$$\left(\frac{wF_k}{N} + h_k\right)(N - F_k) - \alpha F_k = 0$$
$$\Rightarrow (wk + h_k)(N - Nk) - \alpha Nk = 0$$
$$\Rightarrow h_k = \frac{\alpha k}{1-k} - wk,$$

thus

$$\Delta = \frac{h_{k_2}}{h_{k_1}} = \frac{[\alpha k_2 - w k_2(1-k_2)]\,(1-k_1)}{[\alpha k_1 - w k_1(1-k_1)]\,(1-k_2)} = \frac{k_2(1-k_1)\,[1-R_0(1-k_2)]}{k_1(1-k_2)\,[1-R_0(1-k_1)]}$$

$R_0 > 1$

Here the steady state is given by

$$\left(\frac{wF_k}{N} + h_k\right)(N - F_k) - \alpha F_k = 0$$
$$\Rightarrow \left[w\left(1 - \frac{\alpha}{w}(1-k)\right) + h_k\right]\left[\frac{N\alpha}{w}(1-k)\right] - \alpha N\left[1 - \frac{\alpha}{w}(1-k)\right] = 0$$
$$\Rightarrow h_k = \frac{k}{1-k}(w - \alpha + \alpha k)$$

thus

$$\Delta = \frac{h_{k_2}}{h_{k_1}} = \frac{k_2(1-k_1)(w-\alpha+\alpha k_2)}{k_1(1-k_2)(w-\alpha+\alpha k_1)} = \frac{k_2(1-k_1)(R_0-1+k_2)}{k_1(1-k_2)(R_0-1+k_1)}$$

Maximum of $\Delta(R_0)$

Calculating the derivative of $\Delta(R_0)$ we find that if $0 < k_1 < k_2 < 1$, then for $R_0 \leq 1$, $\frac{d\Delta}{dR_0} > 0$, whilst for $R_0 > 1$, $\frac{d\Delta}{dR_0} < 0$. Thus the maximum of $\Delta(R_0)$ is achieved for $R_0 = 1$. It is worth noting that $\Delta(R_0)$ is independent of N and only depends on the choice of k_1 and k_2.

7.5.2 Appendix 2: Driving the system from a subcritical and supercritical state

Throughout the paper we have examined parameters such that the system is critical when there is no external input. In the presence of a small external input we therefore investigate driving the system in the region of this critical state. In the companion paper (Taylor et al., 2013), with no external input, we also investigated the system with subcritical and supercritical parameters. In this appendix we briefly examine the dynamics of the system as it is driven from these states by an external input.

Fig. 7.13 shows raster plots of network firings when the system is driven from a subcritical and supercritical state with $h = 1/N$. Compared with the critical case, see Fig. 7.3(a), with the subcritical parameter set the bursts appear to be shorter and consist of fewer neurons firing. Conversely, in the supercritical case the bursts appear longer and consist of denser network firing. Fig. 7.14 shows the IAI distributions for the subcritical and supercritical parameters.

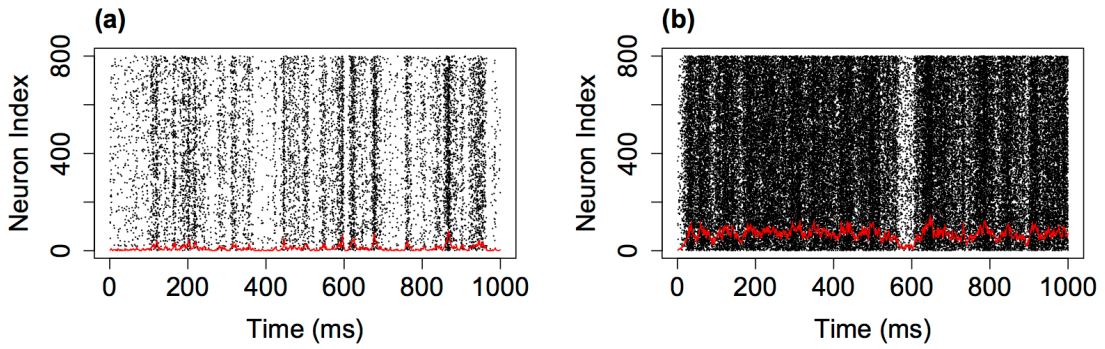

Figure 7.13: **Raster plots of neuronal firing for the network driven from subcritical and supercritical states.** The network firing for (a) subcritical, $\alpha = 1.1,\ w = 1 \ \Rightarrow \ \lambda < 0$ and (b) supercritical, $\alpha = 0.9,\ w = 1 \ \Rightarrow \ \lambda > 0$ parameter sets. Here we investigate the system with a small external input ($h = 1/N$) which drives the system slightly away from these fixed points. The red line indicates the level of firing in 1 ms bins. The subcritical case appears to give rise to smaller bursts and the supercritical case leads to a greater level of firing and longer burst activity compared with the critical system (see Fig. 7.3).

As expected from the raster plots, the IAIs are longer in the subcritical case compared with the critical (Fig. 7.9(a)) and the supercritical. While the subcritical distribution appears to exhibit partial scale-free behaviour similar to the critical case, the supercritical distribution loses this appearance. The distributions from simulations are shown with the theoretical distribution calculated as previously described as a weighted sum of hypoexpontials.

Fig. 7.15 shows the distributions of avalanche size and duration in the subcritical and supercritical cases. Contradicting what we would expect from the raster plots we find that the avalanche sizes are smaller (on average) in the supercritical system. In the companion paper we showed that the supercritical distribution (without the presence of external input) had an increased number of large avalanches compared with the distribution for the system at criticality. However, we do not find this here. As the firing with the supercritical parameters is relatively dense we believe that this highlights a limitation with the binning method in this case. We suggest that future research should focus on how binning can influence avalanche distributions.

7.5.3 Appendix 3: Altering the activation function

Throughout this paper we considered a linear activation function. What happens if a different activation function is chosen? Do we observe the same type of dynamics? In this appendix we briefly investigate two other activation functions: an exponential and a quadratic.

First let us consider the system with an exponential activation function such that:

$$\frac{dA}{dt} = \left(\frac{1}{1 + e^{-(\frac{w}{N}A + h)}} - \frac{1}{2} \right) (N - A) - \alpha A.$$

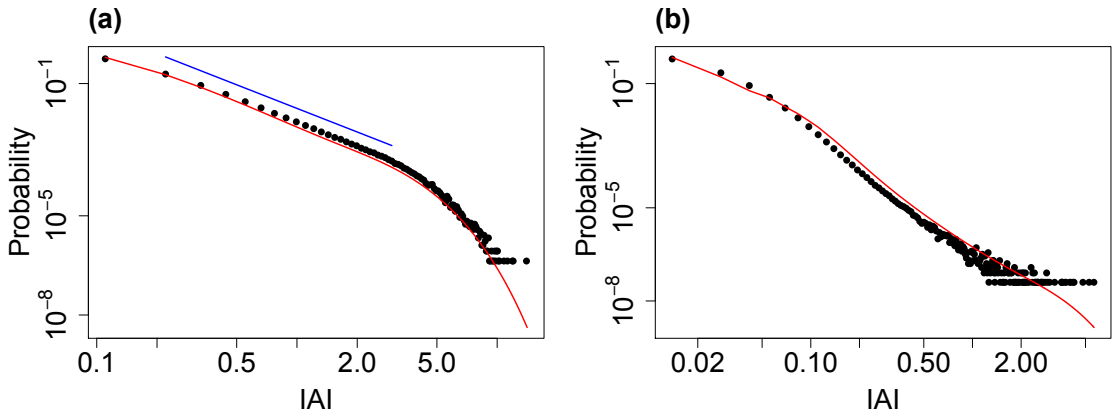

Figure 7.14: **Distribution of IAIs for the system driven from subcritical and supercritical states.** The theoretical (red) and simulated (black) IAI distributions with (a) $\alpha = 1.1$ (subcritical) and (b) $\alpha = 0.9$ (supercritical) parameters. The blue line in (a) indicates a linear fit, i.e. a fitted power-law with an exponent of 2.37. These distributions are with $N = 800,\ w = 1,\ h = 1/N$ and the theoretical distributions were calculated up to a level of initial active neurons which occur with a cumulative probability of 0.9 and 0.13 respectively (see main text).

This function saturates and so is somewhat more realistic than the linear function considered previously. Also, note that the function is set such that when A and h are both zero we also have $f(x) = 0$, i.e. without any external input and with no active neurons the network will remain in this state. With this activation function the eigenvalues of the fixed points are given by:

$$\lambda = f'(x)(N - A) - f(x) - \alpha.$$

We have that

$$f'(x) = \frac{\frac{w}{N}e^{-(\frac{w}{N}A+h)}}{(1+e^{-(\frac{w}{N}A+h)})^2} = \frac{w}{N}\left(f(x)+\frac{1}{2}\right)\left(\frac{1}{2}-f(x)\right) = \frac{w}{N}\left(\frac{1}{4}-f^2(x)\right),$$

and so this could be used to find a critical fixed point along with the fact that at the fixed point of the system we have that:

$$f(x) = \frac{\alpha A}{(N-A)},$$

which defines the level of the external input at the critical fixed point.

As before, consider initially the case where there is no external input ($h = 0$). In this case $A = 0$ is a fixed point, which is critical (with $\lambda = 0$) if and only if $\alpha = w/4$ by the above equations. What happens to this system in the presence of small external input? Fig. 7.16 shows the raster plot for the three different levels of the external input considered previously: $h = 0.01/N,\ 0.1/N,\ 1/N$. Comparing with Fig. 7.3, the firing rate is lower with the saturating

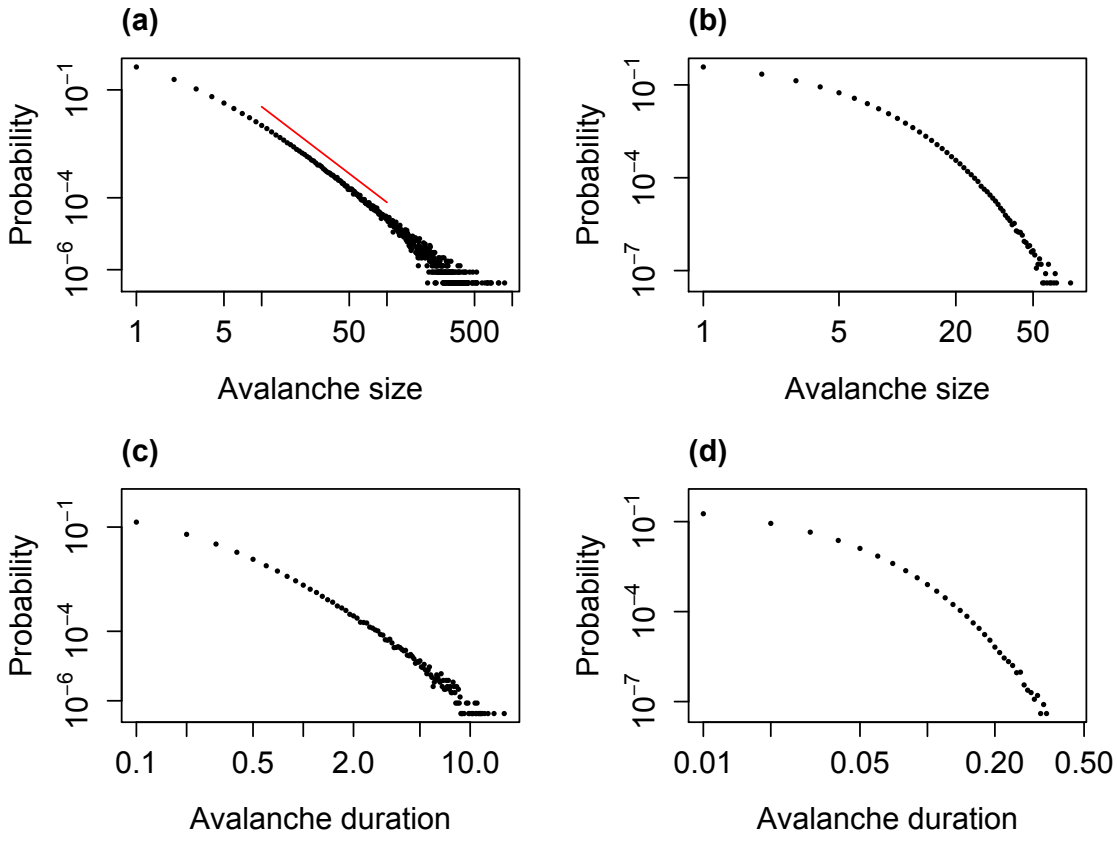

Figure 7.15: **Distributions of avalanche size and duration for the system driven from subcritical and supercritical regimes.** Avalanche size and duration distributions for the system driven from (a,c) subcritical ($\alpha = 1.1$) and (b,d) supercritical ($\alpha = 0.9$) states. Simulations were run with $N = 800,\ w = 1,\ h = 1/N$. The red line in (a) shows the linear fit with a slope of -2.66.

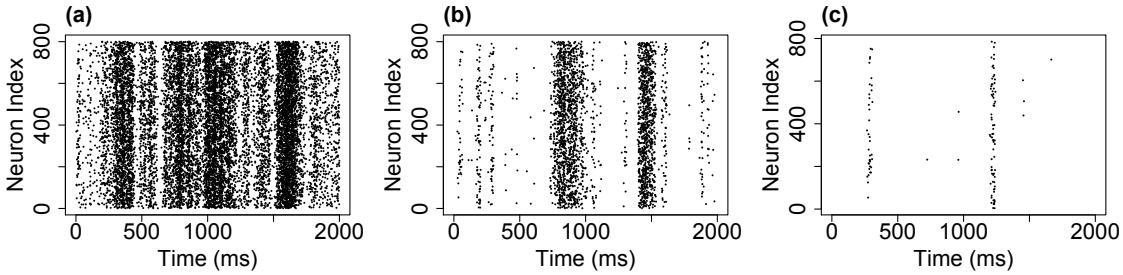

Figure 7.16: **Raster plots for different levels of the external input with the saturating activation function.** Neuronal firing during the first 2 seconds of example simulations with (a) $h = 1/N$, (b) $h = 0.1/N$ and (c) $h = 0.01/N$. For all three simulations $w = 1, \alpha = 0.25$ and $N = 800$. Comparing with Figure 7.3 we find that while in this case the firing rate is lower (note the longer time scale over which the raster plot is displayed) the overall pattern is the same, with the avalanches becoming more distinct with lower levels of the external input.

function studied here, however, the overall pattern of firing is the same. For all three levels of the external input we continue to observe avalanche dynamics and for lower levels of the external input (as the system approaches the critical regime) these avalanches become more distinct. Fig. 7.17 shows the avalanche size, duration and IAI distributions for each of these three levels of the external input. Comparing with Figures 7.4 and 7.9 we find that a similar relationship with the critical regime emerges. With $h = 1/N$ the IAI distribution shows scale-free behaviour (note that by the same derivation as previously, theoretically the distribution is a weighted sum of hypoexponentials). For lower levels of the external input the scale-free behaviour in the IAI distribution is lost but the distribution of avalanche sizes appears scale-free. As was shown previously for the system with a linear activation function, we also found that when $h = 1/N$ the IAIs exhibited LRTCs up to a crossover point (data not shown). For lower levels of the external input these correlations were lost.

With both the linear and saturating activation function we considered the system in the region of the critical regime, with the system driven from the critical regime by the positive external input. Consider the system instead with a quadratic activation function:

$$\frac{dA}{dt} = \left(\frac{w}{N}A^2 + h\right)(N - A) - \alpha A,$$

With this activation function the fixed points are given by:

$$g(A) = \frac{dA}{dt} = -\frac{w}{N} + wA^2 - (h + \alpha)A + hN = 0,$$

with eigenvalues:

$$\lambda = g'(A) = -3\frac{w}{N}A^2 + 2wA - h - \alpha.$$

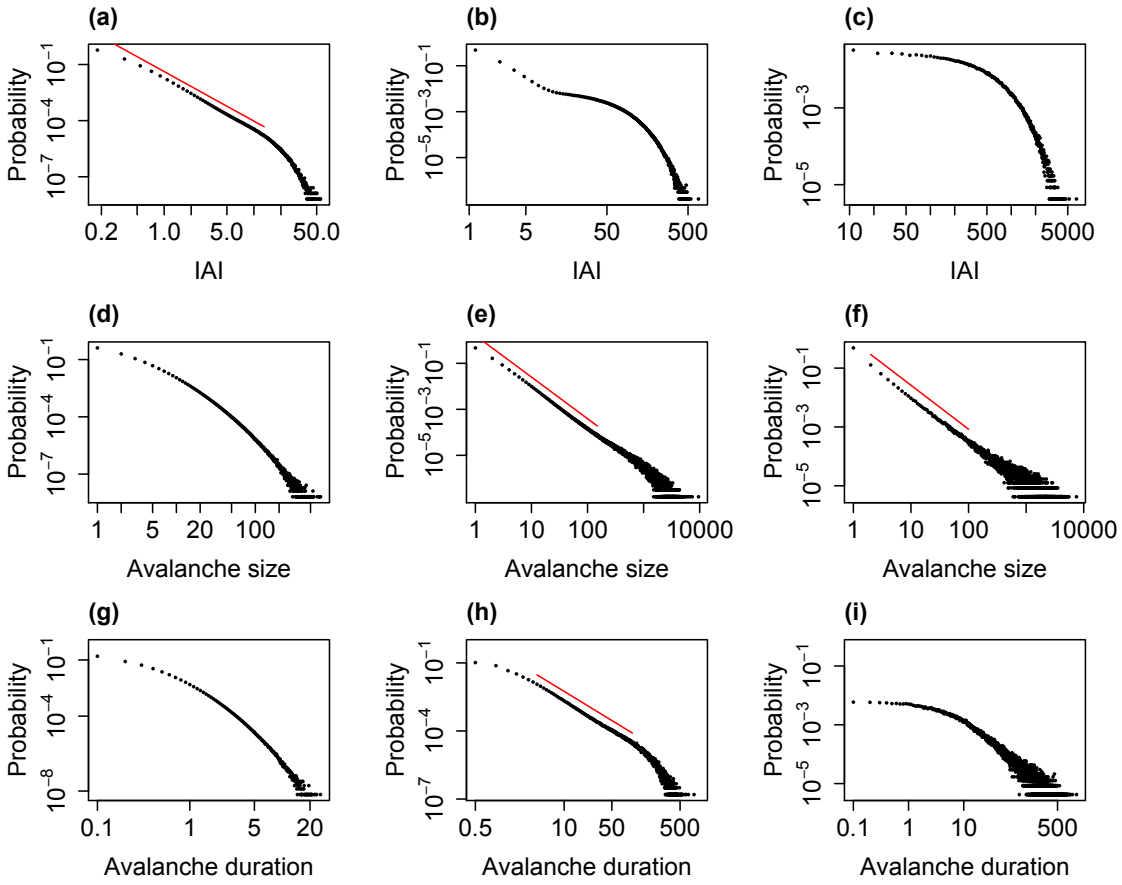

Figure 7.17: **IAI, avalanche size and duration distributions for the system with the saturating activation function.** The distributions are for simulations with $h = 1/N$ (a,d,g), $h = 0.1/N$ (b,e,h) and $h = 0.01/N$ (c,f,i). For all simulations $N = 800, \alpha = 0.25, w = 1$ and the distributions are pooled from 10 simulations each of length 10^4 seconds. The red lines indicates linear fits on the double logarithmic scale, i.e. fitted power-laws with exponents of (a) 2.65, (e) 1.81, (f) 1.49 and (h) 1.84.

Solving these simultaneously we find:

$$\alpha = -3\frac{w}{N}A^2 + 2wA - h,$$

$$2wA^3 - wNA^2 + hN^2 = 0,$$

which define the parameter space and the value of the fixed point for which a critical fixed point can be obtained. Thus, we find that unlike the model with the linear (and saturating) activation function, here with a non-zero external input it is possible to tune the system so that it is directly at the critical regime.

Upon examining this parameter space one can note that in many cases there also exists a stable (positive) fixed point as well as the critical fixed point. From simulating such a system we found (data not shown) that the dynamics of the system are quickly attracted to the stable fixed point and so the critical fixed point has little affect on the dynamics. Therefore, to have a system which is affected by a critical fixed point in the presence of a non-zero external input (in the case of this activation function and where positive parameters are required) the critical regime must be the only fixed point of the system. Given that $g(A)$ is a cubic equation, to achieve a single fixed point which is critical this point must be an inflection point with $g'(A) = 0$ and $g''(A) = 0$. From these equalities we find that the critical fixed point is $A = N/3$ and we must also have $h = \frac{wN}{27}$ and $\alpha = \frac{8wN}{27}$.

Fig. 7.18 shows a raster firing plot and the number of active neurons throughout a simulation for the system with a single critical fixed point. As would be expected, the number of active neurons fluctuates about the critical point. Previously when considering avalanche dynamics we have binned the firing. However, as noted in the discussion the binning method will always separate firing into avalanches and as there are no clear periods of inactivity this does not seem appropriate here. Recall that in the zero input case (see the companion paper) we seeded the system so perturbing it away from the fully quiescent state (which was the critical fixed point) and defined an avalanche as the firing that occurred before the system returned to the fully quiescent state. In a similar approach here it is possible to define an avalanche as the number of neurons that fire in a single excursion from the critical fixed point. We therefore counted the number of neurons that fired from when the system was deflected (either in a positive or negative direction) from the fixed point ($A = N/3$) until the next time at which the system had exactly $N/3$ active neurons. Fig. 7.18 shows the probability distribution of the size of the avalanches defined in this way. The distribution appears to be scale-free over a range of scales.

Thus, while critical dynamics may not be apparent initially when examining data (for example if we were to look at the overall dynamics from the simulations with quadratic activation function), we can observe signatures of criticality when the dynamics are examined in relation to the known critical regime. Here we can note that the network firing fluctuates about the critical regime - that is the number of active neurons fluctuates about this regime

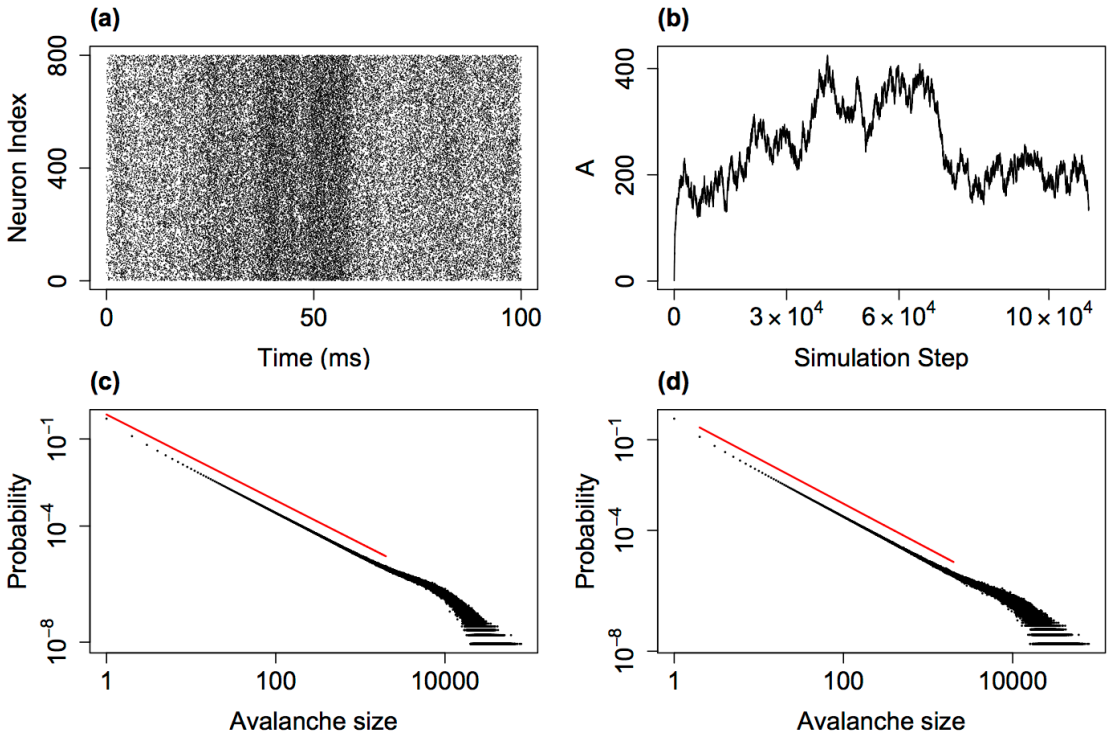

Figure 7.18: **Dynamics of the network with a quadratic activation function.** (a) Raster plot of network firing for simulation with $N = 800$, $h = \frac{wN}{27}$, $\alpha = \frac{8wN}{27}$, $w = 0.01$. (b) For the same simulation this plot shows the number of active neurons (A) at each simulation step. The distribution of avalanches (c) and positive avalanches only (d) - as described in the main text - pooled from 20 simulations of 1000 seconds in length. The red lines indicate linear fits, i.e. fitted power-laws, both with exponents of 1.48.

and so the average number of active neurons across the course of a simulation is approximately equal to the critical state of $N/3$. It might therefore be interesting to examine the fluctuations about the mean activity level in experimental settings where activity is continuous (i.e. cannot be described as intermittent avalanche-like activity) to determine whether signatures of criticality are present. Indeed, such an approach has been taken previously to examine MEG data, thresholding at the median level (Poil et al., 2008).

Acknowledgments Caroline Hartley is funded through CoMPLEX (Centre for Mathematics and Physics in the Life Sciences and Experimental Biology), University College London. Timothy Taylor is funded by a PGR studentship from MRC, and the Departments of Informatics and Mathematics at University of Sussex. Istvan Z. Kiss acknowledges support from EPSRC (EP/H001085/1). Simon Farmer acknowledges support from the National Institute for Health Research University College London Hospitals Biomedical Research Centre.

Chapter 8

Discussion

In this thesis we have presented work on dynamical processes occurring on networks across the disciplines of mathematical epidemiology and theoretical neuroscience. In paper 1, we illustrated the links between some of the more common ordinary differential equation (ODE) models for the temporal evolution of a disease. We were able to provide a precise derivation of lower-order motif-based models from higher-order ones and were also able to provide a rigorous proof of a heuristic formulation for the exact ODE model of an arbitrary motif. Whilst neither results are surprising in their nature, both help provide a more rigorous framework for models based on Markovian dynamics. Although our work focussed purely on the SIS disease dynamics occurring on static networks future work should consider providing a proof of the exact ODE models for arbitrary dynamics of both the disease and the network (i.e. proving that the unclosed dynamic pairwise and effective models of Kiss et al. (2012) and Taylor et al. (2012b), respectively, are exact). In the discussion within paper 1 (section 3.8), we tentatively proposed a hierarchy of the common models (Fig. 3.6). Already other research by Demirel et al. (2013) shows that this hierarchy will not necessarily carry over when different dynamics of and on a network are considered (in this case an adaptive voter model). Future work should therefore try to understand the criterion under which one approach will perform better than another. Intertwined with this is the performance of the moment closures within each model. Typically these operate by assuming the independence of higher-order moments and agreement breaks down when this assumption does not hold. Future work may therefore also consider whether there are more appropriate closures (see for instance work by Demirel et al. (2013)) that could be utilised for more heterogeneous network topologies and transmission dynamics.

Whilst paper 1 focussed on the links between models, paper 2 considered the development of a pairwise model that incorporated type-dependent random link activation and deletion. Following Gross et al. (2006) a step by step approach was taken to investigating the *dynamics of the network* and *dynamics on the network*. We began studying network dynamics independent of the states of individuals, then the dynamics where there was dependence on an individuals state but these states themselves did not change and finally a coupling of both the disease and network dynamics. We obtained a model that performed well for a range

of parameter regimes and also exhibited bifurcation behaviour not found for similar disease dynamics on a static network. Whilst type-dependent link deletion requires only local knowledge of the state of your connections type-dependent activation requires a global knowledge of the states of nodes in the network, which is not necessarily a realistic assumption. In paper 3 we thus considered a model where link deletion and creation happen where neither local nor global knowledge is available. We also incorporated a greater knowledge of the network structure by extending the effective degree model of Lindquist et al. (2011). Here we not only obtained a model with good agreement for a range of parameters but were also able to calculate the basic reproductive ratio for disease dynamics on a dynamic graph. Specific to the content of these papers, future work should follow two lines. Firstly a simple comparison of the two models (with the effective degree model being adapted to consider type-dependent link creation and deletion) should be made, determining whether the performance benefit of effective degree over pairwise in static network models, carries through when dynamic models are considered. Secondly, as effective degree assumes more local knowledge (the disease state of a nodes neighbours) it would be interesting to consider a situation with locally led link deletion (isolating yourself from infectious contacts with your neighbours) but global link creation.

It can be argued that the requirement for analytic tractability means more realistic, non-markovian transmission dynamics are overlooked. For the field to flourish it is vitally important in both static and dynamic network models of epidemiology that greater consideration be given to non-markovian processes. Spreading processes do not necessarily have exponential waiting times (Vergu et al., 2010) and recent work by Van Mieghem and van de Bovenkamp (2013) illustrates the dramatic effect that non-exponential infection rates (in this case a Weibull distribution is used) can have on the epidemic threshold. Cator et al. (2013) builds on this, proposing a model that makes use of general transition distributions and provides a set of resulting meanfield equations. Future work should examine models such as these and their possible extensions with a view to incorporate network dynamics and to further develop our understanding of both the qualitative and quantitative differences between these and models with Markovian dynamics.

Although not considered in this paper (but motivated by our work in papers 4 and 5), it is interesting to note how the behaviour of a system at criticality may explain some characteristics of disease outbreaks evidenced in real life. Stollenwerk and Jansen (2007) gives an overview of current work. In particular they highlight how a decline in uptake of the combined measles, mumps and rubella (MMR) vaccinations may have pushed the unvaccinated population towards a critical regime (from a subcritical when vaccinations were higher) evidenced by outbreak distributions moving towards power laws (Jansen et al., 2003). They also discuss how self-organised criticality may occur within a model of meningococcal disease (Stollenwerk and Jansen, 2003). As the aforementioned work indicates, the role of criticality within epidemiology is not overlooked, it is arguably, however, not as popular a concept as in other

areas and future work may endeavour to explore further its role within an epidemiological framework.

Papers 4 and 5 considered a simple network of firing neurones tuned to operate at and near a transcritical bifurcation. In paper 4, with no external input into the system (bar the initial seeding of the network), we analytically calculate the avalanche distribution as a linear combination of exponentials that appears approximately scale-free over a limited range of sizes. We utilise the methodology of Clauset et al. (2009) to fit a power-law to a critical avalanche distribution generated via simulations of our model. Continuing with the methodology of Clauset et al. (2009) we found that for a sufficient number of avalanches we, correctly, reject the hypothesis that the distribution is a power law. Thus we advice caution when using robust statistical methods to confirm power-laws that are unlikely to be present in their pure form. Whilst we are unaware of studies rejecting a criticality hypothesis due to robust statistical testing, the fact that many authors are utilising these methods to confirm the presence of power-laws and in turn criticality in their findings (Klaus et al., 2011; Touboul and Destexhe, 2010; Benayoun et al., 2010), suggest the potential for some to erroneously dismiss criticality based on a failure to rigourously fit this distribution. Often considered, but not justified, is why there is a cut-off at system size in the apparent scale-free like behaviour of the avalanche distribution even when reentrant connections are present. We illustrate that it is the dominance of the lead eigenvalue of the transition matrix above system size, that fully determines the location of this exponential cut-off. Due to the possible ambiguity in the distribution of avalanche sizes in a critical system we conclude with the suggestion that other markers of criticality should also be considered, illustrating how, within our model, both critical slowing down and divergence of susceptibility occur at the critical point.

Paper 5 considered the same model as paper 4 but with the addition of an external input to all neurones in the system. Without the external input the model assumes a separation of timescale not realistic from a physiological perspective. We then considered how the model would perform close too, but not at, a critical bifurcation. By scaling the external input h as x/N we could investigate two scenarios where the system was pushed towards the critical regime. Firstly we considered the fixing of the network size (N) and the reduction of x. In this way the system was driven towards the critical point of the non-driven system and as expected we found the avalanche distribution was well approximated (over a limited range) by a power-law. Interestingly, whilst the distribution of inter-avalanche intervals were well approximated by a power-law for external input equal to $1/N$, as it was decreased (with network sized fixed) the distribution became more exponential in nature. Secondly we considered the case where the critical regime is approached via an increase in the network size. Again we found the system was pushed towards a critical regime (although not the same one as with no external input). Interestingly, however, whilst the avalanche distribution did not appear to become more scale-free as N increased, the system exhibited long-range temporal correlations in the inter-avalanche intervals. Thus we find that two important markers of criticality,

a scale-free like avalanche distribution and long-range temporal correlations may not occur simultaneously within our system (importantly we note that when considering a wide temporal scale of network activity, Poil et al. (2012) found long-range temporal correlations did occur simultaneously with power-law scaling in the avalanche distribution). We also discussed how the fact that *in-vivo* avalanche distributions may not be well approximated by power-laws (Dehghani et al., 2012) would not necessarily mean a system is not critical but is instead an expected result. We argued that when considered *in-vivo* and thus subject to external inputs the system should instead maximise functional benefits, illustrating this by showing the dynamic range is maximised when tuned (in the absence of external input) to criticality.

With regards to the work on criticality of papers 4 and 5, future research should study the effect of more complex network topologies. Changing connectivity can be utilised as another way to approach a critical bifurcation and again it would be interesting to see how the resultant behaviour compares to the different outcomes obtained from reducing external input. Further work should also aim to develop our understanding of the functional benefits (Shew and Plenz, 2013) that being tuned to criticality can provide and how these could firstly be predicted and then measured within the brain. Note that more complex network topologies may also allow some insight to be found from some of the motif-based approaches, common to epidemiology. As noted earlier, Droste et al. (2013) has attempted[1] to do just this, making use of a dynamic pairwise model, with the intent of gaining more analytical tractability, to study adaptive self-organised criticality (aSOC) in neural networks.

Finally whilst self-organised criticality is one explanation for the emergence of apparent power-laws and scale invariance in neural data, recent work by Moretti and Munoz (2013)[2], provides a much welcomed, highly original and intriguing perspective. Rather than operating at a critical point, they hypothesise that due to the complex hierarchical-modular architecture of cortical networks the brain operates in an extended region where critical behaviour is intrinsic. Thus the brain would not need to be tuned to a specific point rather it would need to operate in a broad region known as a Griffiths phase (arriving there possibly via self-organisation, adaption or evolution). Whilst Moretti and Munoz (2013) do consider the effect on the dynamic range of operating within this extended region, future work should consider whether other functional benefits are also generically maximised within this broad region.

[1] As noted earlier, the analysis is flawed. A differential equation given for the average degree of the network is incorrect. Later this means that what should be given as a non-linear system of equations is erroneously derived as linear, greatly simplifying the resultant analysis.

[2] To our knowledge currently only on arXiv.

Chapter 9

Bibliography

Albert, R. and Barabási, A.-L. (2002a). Statistical mechanics of complex networks. *Rev. Mod. Phys.*, 74:47–97.

Albert, R. and Barabási, A.-L. (2002b). Statistical mechanics of complex networks. *Rev. Mod. Phys.*, 74:47–97.

Allen, L. S. (2008). *Lecture Notes in Mathematics*, volume 1945, chapter Introduction to Stochastic Epidemic Models, pages 81–130. Springer Berlin Heidelberg.

Amari, S. and Misra, R. (1997). Closed-form expressions for distribution of sum of exponential random variables. *IEEE Transactions On Reliability*, 46:519–522.

Anderson, R. M., May, R. M., and Anderson, B. (1992). *Infectious diseases of humans: dynamics and control*, volume 28. Wiley Online Library.

Andersson, H. (1999). Epidemic models and social networks. *The Mathematical Scientist*, 24:128.

Bak, Tang, and Wiesenfeld (1987). Self-organized criticality: An explanation of the 1/f noise. *Phys Rev Lett*, 59(4):381–384.

Ball, F., Mollison, D., and Scalia-Tomba, G. (1997). Epidemics with two levels of mixing. *The Annals of Applied Probability*, pages 46–89.

Ball, F. and Neal, P. (2008). Network epidemic models with two levels of mixing. *Mathematical Biosciences*, 212(1):69 – 87.

Ball, F., Sirl, D., and Trapman, P. (2010). Analysis of a stochastic {SIR} epidemic on a random network incorporating household structure. *Mathematical Biosciences*, 224(2):53 – 73.

Bansal, S., Grenfell, B. T., and Meyers, L. A. (2007). When individual behaviour matters: homogeneous and network models in epidemiology. *Journal of The Royal Society Interface*, 4(16):879–891.

Barabási, A.-L. (2009). Scale-free networks: A decade and beyond. *Science*, 325(5939):412–413.

Barabási, A.-L. and Albert, R. (1999). Emergence of scaling in random networks. *science*, 286(5439):509–512.

Bauch, C. T. (2005). The spread of infectious diseases in spatially structured populations: An invasory pair approximation. *Mathematical Biosciences*, 198(2):217 – 237.

Beggs, J. M. (2006). Neuronal avalanche. *Scholarpedia*, 2(1):1344.

Beggs, J. M. and Plenz, D. (2003). Neuronal avalanches in neocortical circuits. *J Neurosci*, 23(35):11167–11177.

Beggs, J. M. and Plenz, D. (2004). Neuronal avalanches are diverse and precise activity patterns that are stable for many hours in cortical slice cultures. *J Neurosci*, 24(22):5216–29.

Beggs, J. M. and Timme, N. (2012). Being critical of criticality in the brain. *Frontiers in Physiology*, 3(163).

Ben-Ari, Y. (2002). Excitatory actions of gaba during development: the nature of the nurture. *Nat Rev Neurosci*, 3(9):728–39.

Benayoun, M., Cowan, J. D., van Drongelen, W., and Wallace, E. (2010). Avalanches in a stochastic model of spiking neurons. *PLoS Comput Biol*, 6(7):e1000846.

Berthouze, L., James, L. M., and Farmer, S. F. (2010). Human eeg shows long-range temporal correlations of oscillation amplitude in theta, alpha and beta bands across a wide age range. *Clin Neurophysiol*, 121(8):1187–97.

Boffetta, G., Carbone, V., Giuliani, P., Veltri, P., and Vulpiani, A. (1999). Power laws in solar flares: Self-organized criticality or turbulence? *Physical Review Letters*, 83(22):4662–4665.

Bonachela, J. A., de Franciscis, S., Torres, J. J., and Muñoz, M. A. (2010). Self-organization without conservation: are neuronal avalanches generically critical? *Journal of Statistical Mechanics: Theory and Experiment*, 2010(02):P02015.

Bonachela, J. A. and Muñoz, M. A. (2009). Self-organization without conservation: true or just apparent scale-invariance? *J. Stat. Mech.*, page P09009.

Borgs, C., Chayes, J. T., Kesten, H., and Spencer, J. (2001). The birth of the infinite cluster: Finite-size scaling in percolation. *Commun Math Phys*, 224(1):153–204.

Botcharova, M., Farmer, S. F., and Berthouze, L. (2013). A maximum likelihood based technique for validating detrended fluctuation analysis (ML-DFA). *arXiv:1306.5075*.

Brauer, F. and Castillo-Chavez, C. (2012). *Mathematical models in population biology and epidemiology*. Springer Science+ Business Media.

Brauer, F., Van den Driessche, P., and Wu, J. (2008). *Lecture Notes in Mathematical Epidemiology*. Springer.

Broder, A., Kumar, R., Maghoul, F., Raghavan, P., Rajagopalan, S., Stata, R., Tomkins, A., and Wiener, J. (2000). Graph structure in the web. *Computer Networks*, 33(1–6):309 – 320.

Buckley, C. L. and Nowotny, T. (2011). Multiscale model of an inhibitory network shows optimal properties near bifurcation. *Phys Rev Lett*, 106(23):238109.

Buice, M. A., Cowan, J. D., and Chow, C. C. (2009). Systematic fluctuation expansion for neural network activity equations. *Neural Computation*, 22(2):377–426.

Bullmore, E. and Sporns, O. (2009). Complex brain networks: graph theoretical analysis of structural and functional systems. *Nature Reviews Neuroscience*, 10(3):186 – 198.

Cannon, W. B. (1932). *The Wisdom of the Body (revised edition)*. New York, W. W. Norton and company.

Castiglioni, P., Parati, G., Di Rienzo, M., Carabalona, R., Cividjian, A., and Quintin, L. (2011). Scale exponents of blood pressure and heart rate during autonomic blockade as assessed by detrended fluctuation analysis. *J Physiol*, 589(Pt 2):355–69.

Cator, E., van de Bovenkamp, R., and Van Mieghem, P. (2013). Susceptible-infected-susceptible epidemics on networks with general infection and cure times. *Phys. Rev. E*, 87:062816.

Chan, D. Y. C., Hughes, B. D., Leong, A. S., and Reed, W. J. (2003). Stochastically evolving networks. *Phys. Rev. E*, 68:066124.

Cherubini, E., Gaiarsa, J. L., and Ben-Ari, Y. (1991). Gaba: an excitatory transmitter in early postnatal life. *Trends Neurosci*, 14(12):515–9.

Chialvo, D. R. (2010). Emergent complex neural dynamics. *Nat Phys*, 6(10):744–750.

Chialvo, R. (2004). Critical brain networks. *Physica A*, 340:756–765.

Clauset, A., Shalizi, C. R., and Newman, M. E. J. (2009). Power-law distributions in empirical data. *Siam Rev*, 51(4):661–703.

Danon, L., Ford, A. P., House, T., Jewell, C. P., Keeling, M. J., Roberts, G. O., Ross, J. V., and Vernon, M. C. (2011). Networks and the epidemiology of infectious disease. *Interdisciplinary Perspectives on Infectious Diseases*, 2011.

Deco, G., Senden, M., and Jirsa, V. (2012). How anatomy shapes dynamics: a semi-analytical study of the brain at rest by a simple spin model. *Front Comput Neurosci*, 6:68.

Dehghani, N., Hatsopoulos, N. G., Haga, Z. D., Parker, R., Greger, B., Halgren, E., Cash, S. S., and Destexhe, A. (2012). Avalanche analysis from multi-electrode ensemble recordings in cat, monkey and human cerebral cortex during wakefulness and sleep. *Frontiers in Physiology*, 3(302).

Demirel, G., Vazquez, F., Böhme, G. A., and Gross, T. (2013). Moment-closure approximations for discrete adaptive networks. *Physica D: Nonlinear Phenomena*, pages –.

Dichter, M. A. and Ayala, G. F. (1987). Cellular mechanisms of epilepsy: a status report. *Science*, 237(4811):157–164.

Diekmann, O., Heesterbeek, H., and Metz, H. (1995). *The legacy of Kermack and McKendrick*, pages 95–115. Cambridge University Press.

Diekmann, O. and Heesterbeek, J. (2000). *Mathematical Epidemiology of Infectious Diseases: Model Building, Analysis and Interpretation*. Wiley Series in Mathematical & Computational Biology. Wiley.

Diekmann, O., Heesterbeek, J., and Metz, J. (1990). On the definition and the computation of the basic reproduction ratio r 0 in models for infectious diseases in heterogeneous populations. *Journal of mathematical biology*, 28(4):365–382.

Dorogovtsev, S. (2010). *Lectures on Complex Networks*. Oxford University Press, Inc., New York, NY, USA.

Dorogovtsev, S. N. and Mendes, J. F. F. (2002). Evolution of networks. *Advances in Physics*, 51(4):1079–1187.

Droste, F., Do, A.-L., and Gross, T. (2013). Analytical investigation of self-organized criticality in neural networks. *Journal of The Royal Society Interface*, 10(78).

Eames, K. T. D. and Keeling, M. J. (2002). Modeling dynamic and network heterogeneities in the spread of sexually transmitted diseases. *Proceedings of the National Academy of Sciences*, 99(20):13330–13335.

Essam, J. W. (1980). Percolation theory. *Rep Prog Phys*, 43:833–912.

Expert, P., Lambiotte, R., Chialvo, D. R., Christensen, K., Jensen, H. J. J., Sharp, D. J., and Turkheimer, F. (2010). Self-similar correlation function in brain resting-state functional magnetic resonance imaging. *J R Soc Interface*.

Friedman, N., Ito, S., Brinkman, B. A. W., Shimono, M., DeVille, R. E. L., Dahmen, K. A., Beggs, J. M., and Butler, T. C. (2012). Universal critical dynamics in high resolution neuronal avalanche data. *Phys Rev Lett*, 108:208102.

Ganesh, A., Massoulie, L., and Towsley, D. (2005). The effect of network topology on the spread of epidemics. In *INFOCOM 2005. 24th Annual Joint Conference of the IEEE Computer and Communications Societies. Proceedings IEEE*, pages 1455–1466 vol. 2.

Gao, J., Hu, J., Tung, W.-W., Cao, Y., Sarshar, N., and Roychowdhury, V. P. (2006). Assessment of long-range correlation in time series: how to avoid pitfalls. *Phys Rev E Stat Nonlin Soft Matter Phys*, 73(1 Pt 2):016117.

Gillespie, D. T. (1977). Exact stochastic simulation of coupled chemical reactions. *The Journal of Physical Chemistry*, 81(25):2340–2361.

Gireesh, E. D. and Plenz, D. (2008). Neuronal avalanches organize as nested theta- and beta/gamma-oscillations during development of cortical layer 2/3. *P Natl Acad Sci USA*, 105(21):7576–81.

Gleeson, J. P. (2011). High-accuracy approximation of binary-state dynamics on networks. *Phys. Rev. Lett.*, 107:068701.

Greenfield, E. and Lecar, H. (2001). Mutual information in a dilute, asymmetric neural network model. *Phys. Rev. E*, 63:041905.

Grindrod, P. and Higham, D. J. (2010). Evolving graphs: dynamical models, inverse problems and propagation. *Proceedings of the Royal Society A: Mathematical, Physical and Engineering Science*, 466(2115):753–770.

Gross, T. and Blasius, B. (2008). Adaptive coevolutionary networks: a review. *Journal of The Royal Society Interface*, 5(20):259–271.

Gross, T., D'Lima, C. J. D., and Blasius, B. (2006). Epidemic dynamics on an adaptive network. *Phys. Rev. Lett.*, 96:208701.

Hadjichrysanthou, C., Broom, M., and Kiss, I. Z. (2012). Approximating evolutionary dynamics on networks using a neighbourhood configuration model. *Journal of Theoretical Biology*, 312(0):13 – 21.

Hagmann, P., Sporns, O., Madan, N., Cammoun, L., Pienaar, R., Wedeen, V. J., Meuli, R., Thiran, J.-P., and Grant, P. (2010). White matter maturation reshapes structural connectivity in the late developing human brain. *Proceedings of the National Academy of Sciences*.

Hahn, G., Petermann, T., Havenith, M. N., Yu, S., Singer, W., Plenz, D., and Nikolic, D. (2010). Neuronal avalanches in spontaneous activity in vivo. *Journal of Neurophysiology*.

Harris, T. E. (1963). *The theory of branching processes*. Berlin Göttingen Heidelberg: Springer Verlag.

Hartley, C., Berthouze, L., Mathieson, S. R., Boylan, G. B., Rennie, J. M., Marlow, N., and Farmer, S. F. (2012). Long-range temporal correlations in the eeg bursts of human preterm babies. *PLoS One*, 7(2):e31543.

Hartley, C., Taylor, T., Kiss, I., Farmer, S., and Berthouze, L. (2013). Identification of criticality in neuronal avalanches: Ii. a theoretical and empirical investigation of the driven case. *arXiv:1309.3535*.

Heffernan, J., Smith, R., and Wahl, L. (2005). Perspectives on the basic reproductive ratio. *Journal of The Royal Society Interface*, 2(4):281–293.

Hellwig, B. (2000). A quantitative analysis of the local connectivity between pyramidal neurons in layers 2/3 of the rat visual cortex. *Biol Cybern*, 82(2):111–121.

Ho, K. K., Moody, G. B., Peng, C. K., Mietus, J. E., Larson, M. G., Levy, D., and Goldberger, A. L. (1997). Predicting survival in heart failure case and control subjects by use of fully automated methods for deriving nonlinear and conventional indices of heart rate dynamics. *Circulation*, 96(3):842–8.

Holmes, G. L., Khazipov, R., and Ben-Ari, Y. (2002). New concepts in neonatal seizures. *Neuroreport*, 13(1):A3–8.

House, T. and Keeling, M. J. (2008). Deterministic epidemic models with explicit household structure. *Mathematical Biosciences*, 213(1):29 – 39.

House, T. and Keeling, M. J. (2010). The impact of contact tracing in clustered populations. *PLoS Comput Biol*, 6(3):e1000721.

House, T. and Keeling, M. J. (2011). Insights from unifying modern approximations to infections on networks. *Journal of The Royal Society Interface*, 8(54):67–73.

House, T., Ross, J. V., and Sirl, D. (2013). How big is an outbreak likely to be? methods for epidemic final-size calculation. *Proceedings of the Royal Society A: Mathematical, Physical and Engineering Science*, 469(2150).

Hu, K., Ivanov, P. C., Chen, Z., Carpena, P., and Stanley, H. E. (2001). Effect of trends on detrended fluctuation analysis. *Phys Rev E Stat Nonlin Soft Matter Phys*, 64(1 Pt 1):011114.

Huttenlocher, P. R. and Dabholkar, A. S. (1997). Regional differences in synaptogenesis in human cerebral cortex. *J Comp Neurol*, 387(2):167–78.

Jansen, V. A. A., Stollenwerk, N., Jensen, H. J., Ramsay, M. E., Edmunds, W. J., and Rhodes, C. J. (2003). Measles outbreaks in a population with declining vaccine uptake. *Science*, 301(5634):804.

Jensen, H. (1998). *Self-organized criticality: emergent complex behavior in physical and biological systems*. Cambridge, United Kingdom: Cambridge University Press.

Kaiser, M. and Hilgetag, C. C. (2010). Optimal hierarchical modular topologies for producing limited sustained activation of neural networks. *Front Neuroinform*, 4:8.

Keeling, M., Rand, D., and Morris, A. (1997). Correlation models for childhood epidemics. *Proceedings of the Royal Society of London. Series B: Biological Sciences*, 264(1385):1149–1156.

Keeling, M. J. (1999). The effects of local spatial structure on epidemiological invasions. *Proceedings: Biological Sciences*, 266(1421):859–867.

Keeling, M. J. and Eames, K. T. (2005). Networks and epidemic models. *Journal of The Royal Society Interface*, 2(4):295–307.

Kelso, J. A. S. (2008). Haken-kelso-bunz model. *Scholarpedia*, 3(10):1612.

Kenah, E. and Miller, J. C. (2011). Epidemic percolation networks, epidemic outcomes, and interventions. *Interdisciplinary Perspectives on Infectious Diseases*, 2011.

Kenah, E. and Robins, J. M. (2007). Second look at the spread of epidemics on networks. *Phys. Rev. E*, 76:036113.

Kermack, W. O. and McKendrick, A. G. (1927). A contribution to the mathematical theory of epidemics. *Proceedings of the Royal Society of London. Series A*, 115(772):700–721.

Kessler, D. A. (2008). Epidemic size in the sis model of endemic infections. *J Appl Probab*, 45(3):757–778.

Kinouchi, O. and Copelli, M. (2006). Optimal dynamical range of excitable networks at criticality. *Nat Phys*, 2(5):348–351.

Kiss, I. Z., Berthouze, L., Taylor, T. J., and Simon, P. L. (2012). Modelling approaches for simple dynamic networks and applications to disease transmission models. *Proceedings of the Royal Society A: Mathematical, Physical and Engineering Science*.

Klaus, A., Yu, S., and Plenz, D. (2011). Statistical analyses support power law distributions found in neuronal avalanches. *PLoS ONE*, 6(5):e19779.

Koch, C. and Segev, I. (1998). *Methods in Neuronal Modeling: From Ions to Networks*. A Bradford book. MIT Press.

Kossinets, G. and Watts, D. J. (2006). Empirical analysis of an evolving social network. *Science*, 311(5757):88–90.

Kuramoto, Y. (1984). *Chemical Oscillations, Waves, and Turbulence*. Springer-Verlag, New York, p. 164.

Larremore, D. B., Carpenter, M. Y., Ott, E., and Restrepo, J. G. (2012). Statistical properties of avalanches in networks. *Phys Rev E*, 85:066131.

Larremore, D. B., Shew, W. L., and Restrepo, J. G. (2011). Predicting criticality and dynamic range in complex networks: Effects of topology. *Phys Rev Lett*, 106:058101.

Levina, A., Herrmann, J. M., and Geisel, T. (2007). Dynamical synapses causing self-organized criticality in neural networks. *Nat Phys*, 3(12):857–860.

Li, J., Blakeley, D., and Smith, R. J. (2011). The failure of r0. *Comput Math Methods Med*, 2011:527610.

Li, J. and Brauer, F. (2008). Continuous-time age-structured models in population dynamics and epidemiology. In Brauer, F., Driessche, P., and Wu, J., editors, *Mathematical Epidemiology*, volume 1945 of *Lecture Notes in Mathematics*, pages 205–227. Springer Berlin Heidelberg.

Liljeros, F., Edling, C. R., and Amaral, L. A. (2003). Sexual networks: implications for the transmission of sexually transmitted infections. *Microbes and Infection*, 5(2):189 – 196.

Liljeros, F., Edling, C. R., Amaral, L. A. N., Stanley, H. E., and Aberg, Y. (2001). The web of human sexual contacts. *Nature*, 411(6840):907–908.

Lindquist, J., Ma, J., Driessche, P., and Willeboordse, F. (2011). Effective degree network disease models. *Journal of Mathematical Biology*, 62(2):143–164.

Linkenkaer-Hansen, K., Nikouline, V. V., Palva, J. M., and Ilmoniemi, R. J. (2001). Long-range temporal correlations and scaling behavior in human brain oscillations. *The Journal of Neuroscience*, 21(4):1370–1377.

Linkenkaer-Hansen, K., Nikulin, V. V., Palva, J. M., Kaila, K., and Ilmoniemi, R. J. (2004). Stimulus-induced change in long-range temporal correlations and scaling behaviour of sensorimotor oscillations. *Eur J Neurosci*, 19(1):203–11.

Lombardi, F., Herrmann, H. J., Perrone-Capano, C., Plenz, D., and de Arcangelis, L. (2012). Balance between excitation and inhibition controls the temporal organization of neuronal avalanches. *Phys Rev Lett*, 108(22):228703.

Low, N., Bender, N., Nartey, L., Shang, A., and Stephenson, J. M. (2009). Effectiveness of chlamydia screening: systematic review. *International Journal of Epidemiology*, 38(2):435–448.

Magnasco, M. O., Piro, O., and Cecchi, G. A. (2009). Self-tuned critical anti-hebbian networks. *Phys Rev Lett*, 102(25):258102.

Marceau, V., Noël, P.-A., Hébert-Dufresne, L., Allard, A., and Dubé, L. J. (2010). Adaptive networks: Coevolution of disease and topology. *Phys. Rev. E*, 82:036116.

Matsuda, H., Ogita, N., Sasaki, A., and Satō, K. (1992). Statistical mechanics of population. *Progress of Theoretical Physics*, 88(6):1035–1049.

McSharry, P. (2005, Last checked: 11 January 2011). Dfa matlab code found on the website of the systems analysis, modelling and prediction group, department of engineering sciences, university of oxford. available: http://www.eng.ox.ac.uk/samp/software/ cardiodynamics/dfa.m. *DFA Matlab code found on the website of the Systems analysis, modelling and prediction group, Department of Engineering Sciences, University of Oxford. Available: http://www.eng.ox.ac.uk/samp/software/ cardiodynamics/dfa.m.*

Meisel, C., Storch, A., Hallmeyer-Elgner, S., Bullmore, E., and Gross, T. (2012). Failure of adaptive self-organized criticality during epileptic seizure attacks. *PLoS Comput Biol*, 8(1):e1002312.

Meyers, L. A., Pourbohloul, B., Newman, M., Skowronski, D. M., and Brunham, R. C. (2005). Network theory and sars: predicting outbreak diversity. *Journal of Theoretical Biology*, 232(1):71 – 81.

Miller, J. (2011). A note on a paper by erik volz: Sir dynamics in random networks. *Journal of Mathematical Biology*, 62(3):349–358.

Miller, J. C., Slim, A. C., and Volz, E. M. (2012). Edge-based compartmental modelling for infectious disease spread. *Journal of The Royal Society Interface*, 9(70):890–906.

Milton, J. G. (2012). Neuronal avalanches, epileptic quakes and other transient forms of neurodynamics. *Eur J Neurosci*, 36(2):2156–2163.

Moretti, P. and Munoz, M. A. (2013). Brain architecture, griffiths phases, and the stretching of criticality. *arXiv:1308.6661v1.*

Nåsell, I. (1996). The quasi-stationary distribution of the closed endemic sis model. *Adv Appl Probab*, 28(3):895–932.

Newman, M. (2003a). The structure and function of complex networks. *SIAM Review*, 45(2):167–256.

Newman, M. (2010). *Networks: An Introduction*. Oxford University Press, Inc., New York, NY, USA.

Newman, M. E. J. (2002). Spread of epidemic disease on networks. *Phys. Rev. E*, 66:016128.

Newman, M. E. J. (2003b). Mixing patterns in networks. *Phys. Rev. E*, 67:026126.

Nikulin, V. V. and Brismar, T. (2004). Long-range temporal correlations in alpha and beta oscillations: effect of arousal level and test-retest reliability. *Clin Neurophysiol*, 115(8):1896–908.

Nikulin, V. V. and Brismar, T. (2005). Long-range temporal correlations in electroencephalographic oscillations: Relation to topography, frequency band, age and gender. *Neuroscience*, 130(2):549–58.

Olami, Z., Feder, H., and Christensen, K. (1992). Self-organized criticality in a continuous, nonconservative cellular automaton modeling earthquakes. *Phys Rev Lett*, 68(8):1244–1247.

Palva, J. M., Zhigalov, A., Hirvonen, J., Korhonen, O., Linkenkaer-Hansen, K., and Palva, S. (2013). Neuronal long-range temporal correlations and avalanche dynamics are correlated with behavioral scaling laws. *Proc Natl Acad Sci U S A*, 110(9):3585–90.

Peng, C. K., Buldyrev, S. V., Havlin, S., Simons, M., Stanley, H. E., and Goldberger, A. L. (1994). Mosaic organization of dna nucleotides. *Phys Rev E Stat Phys Plasmas Fluids Relat Interdiscip Topics*, 49(2):1685–9.

Peng, C. K., Havlin, S., Stanley, H. E., and Goldberger, A. L. (1995). Quantification of scaling exponents and crossover phenomena in nonstationary heartbeat time series. *Chaos*, 5(1):82–7.

Petermann, T., Thiagarajan, T. C., Lebedev, M. A., Nicolelis, M. A. L., Chialvo, D. R., and Plenz, D. (2009). Spontaneous cortical activity in awake monkeys composed of neuronal avalanches. *Proceedings of the National Academy of Sciences*, 106(37):15921–15926.

Plenz, D. and Chialvo, D. R. (2009). Scaling properties of neuronal avalanches are consistent with critical dynamics. *arXiv:0912.5369v1*.

Poil, S.-S., Hardstone, R., Mansvelder, H. D., and Linkenkaer-Hansen, K. (2012). Critical-state dynamics of avalanches and oscillations jointly emerge from balanced excitation/inhibition in neuronal networks. *J Neurosci*, 32(29):9817–9823.

Poil, S.-S., van Ooyen, A., and Linkenkaer-Hansen, K. (2008). Avalanche dynamics of human brain oscillations: relation to critical branching processes and temporal correlations. *Hum Brain Mapp*, 29(7):770–7.

Priesemann, V., Munk, M. H. J., and Wibral, M. (2009). Subsampling effects in neuronal avalanche distributions recorded in vivo. *BMC Neurosci*, 10:40.

Rämö, P., Kauffman, S., Kesseli, J., and Yli-Harja, O. (2007). Measures for information propagation in boolean networks. *Physica D: Nonlinear Phenomena*, 227(1):100–104.

Rand, D. (1999). Correlation equations and pair approximations for spatial ecologies. *Advanced ecological theory: principles and applications*, pages 100–142.

Read, J. M., Eames, K. T., and Edmunds, W. J. (2008). Dynamic social networks and the implications for the spread of infectious disease. *Journal of The Royal Society Interface*, 5(26):1001–1007.

Ribeiro, T. L. and Copelli, M. (2008). Deterministic excitable media under poisson drive: power law responses, spiral waves, and dynamic range. *Phys Rev E Stat Nonlin Soft Matter Phys*, 77(5 Pt 1):051911.

Ribeiro, T. L., Copelli, M., Caixeta, F., Belchior, H., Chialvo, D. R., Nicolelis, M. A. L., and Ribeiro, S. (2010). Spike avalanches exhibit universal dynamics across the sleep-wake cycle. *PLoS ONE*, 5(11):e14129.

Risau-Gusman, S. and Zanette, D. H. (2009). Contact switching as a control strategy for epidemic outbreaks. *Journal of Theoretical Biology*, 257(1):52 – 60.

Rivera, C., Voipio, J., Payne, J. A., Ruusuvuori, E., Lahtinen, H., Lamsa, K., Pirvola, U., Saarma, M., and Kaila, K. (1999). The k+/cl- co-transporter kcc2 renders gaba hyperpolarizing during neuronal maturation. *Nature*, 397(6716):251–5.

Roberts, M. (2007). The pluses and minuses of 0. *Journal of The Royal Society Interface*, 4(16):949–961.

Ross, S. M. (2010). *Introduction to probability models*. Academic Press, Amsterdam, 10th ed edition.

Roxin, A., Riecke, H., and Solla, S. (2004). Self-sustained activity in a small-world network of excitable neurons. *Phys Rev Lett*, 92(19):198101.

Rubinov, M., Sporns, O., Thivierge, J.-P., and Breakspear, M. (2011). Neurobiologically realistic determinants of self-organized criticality in networks of spiking neurons. *PLoS Comput Biol*, 7(6):e1002038.

Saramäki, J. and Kaski, K. (2005). Modelling development of epidemics with dynamic small-world networks. *Journal of Theoretical Biology*, 234(3):413–421.

Satō, K., Matsuda, H., and Sasaki, A. (1994). Pathogen invasion and host extinction in lattice structured populations. *Journal of Mathematical Biology*, 32(3):251–268.

Scheffer, M., Bascompte, J., Brock, W. A., Brovkin, V., Carpenter, S. R., Dakos, V., Held, H., van Nes, E. H., Rietkerk, M., and Sugihara, G. (2009). Early-warning signals for critical transitions. *Nature*, 461(7260):53–59.

Scheuer, E. (1988). Reliability of an m-out of-n system when component failure induces higher failure rates in survivors. *IEEE Transactions On Reliability*, 37:73–74.

Schwarzkopf, Y., Rákos, A., and Mukamel, D. (2010). Epidemic spreading in evolving networks. *Phys. Rev. E*, 82:036112.

Segev, R., Benveniste, M., Hulata, E., Cohen, N., Palevski, A., Kapon, E., Shapira, Y., and Ben-Jacob, E. (2002). Long term behavior of lithographically prepared in vitro neuronal networks. *Phys Rev Lett*, 88(11):118102.

Sethna, J. P., Dahmen, K. A., and Myers, C. R. (2001). Crackling noise. *Nature*, 410(6825):242–250.

Shadlen, M. N. and Newsome, W. T. (1994). Noise, neural codes and cortical organization. *Curr Opin Neurobiol*, 4:569–579.

Sharkey, K. (2008). Deterministic epidemiological models at the individual level. *Journal of Mathematical Biology*, 57(3):311–331.

Shew, W. L. and Plenz, D. (2013). The functional benefits of criticality in the cortex. *The Neuroscientist*, 19(1):88–100.

Shew, W. L., Yang, H., Petermann, T., Roy, R., and Plenz, D. (2009). Neuronal avalanches imply maximum dynamic range in cortical networks at criticality. *The Journal of Neuroscience*, 29(49):15595–15600.

Shew, W. L., Yang, H., Yu, S., Roy, R., and Plenz, D. (2011). Information capacity and transmission are maximized in balanced cortical networks with neuronal avalanches. *The Journal of Neuroscience*, 31(1):55–63.

Shriki, O., Alstott, J., Carver, F., Holroyd, T., Henson, R. N. A., Smith, M. L., Coppola, R., Bullmore, E., and Plenz, D. (2013). Neuronal avalanches in the resting meg of the human brain. *J Neurosci*, 33(16):7079–90.

Simon, P., Taylor, M., and Kiss, I. (2011). Exact epidemic models on graphs using graph-automorphism driven lumping. *Journal of Mathematical Biology*, 62(4):479–508.

Simon, P. L., Farkas, H., and Wittmann, M. (1999). Constructing global bifurcation diagrams by the parametric representation method. *Journal of Computational and Applied Mathematics*, 108(1–2):157 – 176.

Simon, P. L. and Kiss, I. Z. (2012). From exact stochastic to mean-field ode models: a new approach to prove convergence results. *IMA Journal of Applied Mathematics*.

Smit, D. J. A., de Geus, E. J. C., van de Nieuwenhuijzen, M. E., van Beijsterveldt, C. E. M., van Baal, G. C. M., Mansvelder, H. D., Boomsma, D. I., and Linkenkaer-Hansen, K.

(2011). Scale-free modulation of resting-state neuronal oscillations reflects prolonged brain maturation in humans. *J Neurosci*, 31(37):13128–36.

Sornette, D. (2006). *Critical phenomena in natural sciences (2nd edition)*. Springer Berlin Heidelberg New York.

Sporns, O. (2011a). The human connectome: a complex network. *Annals of the New York Academy of Sciences*, 1224(1):109–125.

Sporns, O. (2011b). The non-random brain: efficiency, economy, and complex dynamics. *Front Comput Neurosci*, 5:5.

Steyn-Ross, M. L., Steyn-Ross, D. A., Sleigh, J. W., and Whiting, D. R. (2003). Theoretical predictions for spatial covariance of the electroencephalographic signal during the anesthetic-induced phase transition: Increased correlation length and emergence of spatial self-organization. *Phys Rev E*, 68(2 Pt 1):021902.

Stollenwerk, N. and Jansen, V. A. (2007). Criticality in epidemiology. In Blasius, B., Stone, L., and Kurths, J., editors, *Complex Population Dynamics: Nonlinear Modelling in Ecology, Epidemiology and Genetics*, pages 159–188. World Scientific Publishing Company. World Scientific Lecture Notes in Complex Systems, vol 7.

Stollenwerk, N. and Jansen, V. A. A. (2003). Evolution towards criticality in an epidemiological model for meningococcal disease. *Physics Letters A*, 317(1–2):87–96.

Strogatz, S. H. (2001). Exploring complex networks. *Nature*, 410(6825):268–276.

Taqqu, M., Teverovsky, V., and Willinger, W. (1995). Estimators for long-range dependence: An empirical study. *Fractals*, 3(4):785–798.

Taylor, M., Simon, P., Green, D., House, T., and Kiss, I. (2012a). From markovian to pairwise epidemic models and the performance of moment closure approximations. *Journal of Mathematical Biology*, 64(6):1021–1042.

Taylor, M., Taylor, T. J., and Kiss, I. Z. (2012b). Epidemic threshold and control in a dynamic network. *Phys. Rev. E*, 85:016103.

Taylor, T., Hartley, C., Simon, P., Kiss, I., and Berthouze, L. (2013). Identification of criticality in neuronal avalanches: I. a theoretical investigation of the non-driven case. *The Journal of Mathematical Neuroscience*, 3(1):5.

Taylor, T. and Kiss, I. (2013). Interdependency and hierarchy of exact and approximate epidemic models on networks. *Journal of Mathematical Biology (in press)*.

Touboul, J. and Destexhe, A. (2010). Can power-law scaling and neuronal avalanches arise from stochastic dynamics? *PLoS ONE*, 5(2):e8982.

Toweill, D. L., Kovarik, W. D., Carr, R., Kaplan, D., Lai, S., Bratton, S., and Goldstein, B. (2003). Linear and nonlinear analysis of heart rate variability during propofol anesthesia for short-duration procedures in children. *Pediatr Crit Care Med*, 4(3):308–14.

Trapman, P. (2007). On analytical approaches to epidemics on networks. *Theoretical Population Biology*, 71(2):160 – 173.

Turrigiano, G. (2011). Too many cooks? intrinsic and synaptic homeostatic mechanisms in cortical circuit refinement. *Annu Rev Neurosci*, 34:89–103.

Van Kampen, N. G. (2007). *Stochastic Processes in Physics and Chemistry, Third Edition (North-Holland Personal Library)*. North Holland, 3 edition.

Van Mieghem, P. and van de Bovenkamp, R. (2013). Non-markovian infection spread dramatically alters the susceptible-infected-susceptible epidemic threshold in networks. *Phys. Rev. Lett.*, 110:108701.

Van Segbroeck, S., Santos, F. C., and Pacheco, J. M. (2010). Adaptive contact networks change effective disease infectiousness and dynamics. *PLoS Comput Biol*, 6(8):e1000895.

Vergu, E., Busson, H., and Ezanno, P. (2010). Impact of the infection period distribution on the epidemic spread in a metapopulation model. *PLoS ONE*, 5(2):e9371.

Vernon, M. C. and Keeling, M. J. (2009). Representing the uk's cattle herd as static and dynamic networks. *Proceedings of the Royal Society B: Biological Sciences*, 276(1656):469–476.

Volz, E. (2008). Sir dynamics in random networks with heterogeneous connectivity. *Journal of Mathematical Biology*, 56(3):293–310.

Volz, E. and Meyers, L. A. (2007). Susceptible–infected–recovered epidemics in dynamic contact networks. *Proceedings of the Royal Society B: Biological Sciences*, 274(1628):2925–2934.

Volz, E. and Meyers, L. A. (2009). Epidemic thresholds in dynamic contact networks. *Journal of The Royal Society Interface*, 6(32):233–241.

Volz, E. M., Miller, J. C., Galvani, A., and Ancel Meyers, L. (2011). Effects of heterogeneous and clustered contact patterns on infectious disease dynamics. *PLoS Comput Biol*, 7(6):e1002042.

Watts, D. J. and Strogatz, S. H. (1998). Collective dynamics of small-world networks. *Nature*, 393(6684):440–442.

Williams, A. H., O'Leary, T., and Marder, E. (2013). Homeostatic regulation of neuronal excitability. *Scholarpedia*, 8(1):1656.

Wilson, H. R. and Cowan, J. D. (1972). Excitatory and inhibitory interactions in localized populations of model neurons. *Biophysical journal*, 12(1):1–24.

Winterbach, W., Ridder, D., Wang, H. J., Reinders, M., and Mieghem, P. (2012). Do greedy assortativity optimization algorithms produce good results? *The European Physical Journal B*, 85(5):1–9.

Wissel, C. (1984). A universal law of the characteristic return time near thresholds. *Oecologia*, 65(1):101–107.

Zanette, D. H. and Risau-Gusmán, S. (2008). Infection spreading in a population with evolving contacts. *Journal of biological physics*, 34(1-2):135–148.

Ziff, R. M. (2011). Correction-to-scaling exponent for two-dimensional percolation. *Phys Rev E*, 83:020107.